UNIVERSITÉ CATHOLIQUE DE LOUVAIN

FACULTY OF SCIENCE

EARTH AND LIFE INSTITUTE

GEORGES LEMAÎTRE CENTRE FOR EARTH AND CLIMATE RESEARCH

Combining climate models with high- and low-resolution proxy records to reconstruct the Antarctic centennial temperature variability over the past two millennia

DOCTORAL DISSERTATION PRESENTED BY

Zhiqiang Lyu

IN PARTIAL FULFILLMENT OF THE

REQUIREMENTS FOR THE DEGREE OF

DOCTOR IN SCIENCES

THESIS COMMITTEE:

Prof. Hugues Goosse (Supervisor)	Université catholique de Louvain
Prof. Jacques Mahillon (Chair)	Université catholique de Louvain
Prof. Qiuzhen Yin	Université catholique de Louvain
Prof. Thierry Fichefet	Université catholique de Louvain
Dr. Liz Thomas	British Antarctic Survey
Dr. Didier Swingedouw	Université de Bordeaux

LOUVAIN-LA-NEUVE

Acknowledgements

After finishing the last sentence of my PhD thesis, many words of thanks are about to pile up. I know I could not have completed my PhD thesis without your help.

First, I would like to express my deepest appreciation to my PhD supervisor, Professor Hugues Goosse. Hugues, thanks for your guidance during my entire PhD. You have been always sharing your knowledge with me from the first day I arrived at the LLN to the last day I submit my thesis. As a student with no background in climate dynamics but with enthusiasm for paleoclimate, I know I have asked many “stupid” questions over the past four years, but you have been always patient and giving me suggestions and "extra" guidance in every discussion. Science is not always easy, but I really enjoyed every moment of working on this topic with you. The simple words “that’s life” always express your wisdom in dealing with difficulties. Both science and life are full of surprises, and thus keeping a calm and optimistic attitude toward them makes the magic happen.

I would also like to thank the jury members of my thesis committee: Thierry Fichefet, Qiuzhen Yin, Liz Thomas, and Didier Swingedouw. Thanks for taking the time to review my thesis and to provide valuable insight and suggestions in the completion of this thesis. Also, I would like to express my gratitude to the chairman of my thesis committee, Jacques Mahillon, for his organization and professional supervision of the defence.

Working at Mercator was a wonderful journey over the last four years. Thanks François and Pierre-Yves answering me many questions in using the server. Thanks Jeanne, my office roommate, for many interesting discussions about Belgian food, Chinese food and, of course, research related questions. Thanks Charles, Koffi, Marie, and Bianca for many nice conversations and relax moments during the working days. Special thanks to Quentin, who helped me with many technical problems in coding, data assimilation...as well as many interesting discussions about science and life. I would also like to thank my colleagues: Zhipeng Wu, Anqi Lyu, Qianqian Su, and Mingqiang Liang for sharing with me many knowledge about climate change in the last million years.

Some special words of gratitude go to my friends who have always been a major source of support: Pu Shi, He Zhang and Man Zhao, Pengzhi Zhao and Yijie Zhao, Fei Xu, Peng Wang, Chao Gao, and many friends that I have in Leuven and Louvain-La-Neuve Chinese basketball team. When things got a little frustrating, you were always there to listen and support me. I am so grateful and will always remember the time we spent together.

Last but not least, I would like to thank my parents. My parents have always worked hard, and have always been my role models. They support every choice I made and provided unconditional love and care in the past thirty years. I would not have made it this far without them. I would also like to express my gratitude to my wife, Siyao Du. We have lots of beautiful memories during past four years in Leuven. This is one of the best pieces in the picture of our lifes. I am truly grateful to Siyao for sticking by my side, even when I was irritable and frustrated. I think we have both learned a lot about life and strengthened our commitment and determination to each other!

Zhiqiang (志强)

Contents

Contents I

List of abbreviations II

1 Introduction 1

1.1 Physical Geography of Antarctica 2

1.2 Current Antarctic climate changes and possible mechanisms 3

1.3 Proxy data in Antarctica and proxy-based climate reconstructions 8

1.4 Antarctic climate changes in climate models 14

1.5 Combination of modeling results and proxy records using data assimilation 20

1.6 Objectives and outlines of this thesis 22

2. Comparison of observed borehole temperatures in Antarctica with simulations using a forward model driven by climate model outputs covering the past millennium 27

2.1 Introduction 29

2.2 Data and Methods 31

2.3 Results 38

2.4 Proposed metric of Antarctic climate for model validation 44

2.5 Conclusion 51

3. Spatial patterns of multi–centennial surface air temperature trends in Antarctica over 1–1000 CE: Insights from ice core records and modeling 53

3.1 Introduction 54

3.2 Data and Methods 56

3.3 Reconstructed and simulated SAT variations over the past two millennia. 61

3.4 Analysis of the reconstructions with data assimilation 66

3.5 Sensitivity of the reconstruction with data assimilation to the uncertainty of the records 79

3.6 Comparison to other terrestrial records over Antarctica 81

3.7 Conclusion 85

4. Widespread cooling over West Antarctica and adjacent seas over the past millennium 89

4.1 Introduction 90

4.2 Data and Methods 92

4.3 Results and Discussion 97

4.4 Conclusion 113
5. Conclusions and perspectives 115
5.1 Main achievements 115
5.2 General conclusions 119
5.3 Perspectives 120
A. Supplement to Chapter 2 123
A.1 Borehole forward model description 123
A.2 Supplementary Figures 125
A.3 Observed borehole temperature distribution at WAIS 131
A.4 Observed borehole temperature distribution at LARISSA 134
A.5 Observed borehole temperature distribution at Mill Island 135
A.6 Observed borehole temperature distribution at Styx. 136
B. Supplement to Chapter 3 139
B.1 Supplementary Tables 139
B.2 Supplementary Figures 144
C. Supplement to Chapter 4 151
C.1 Supplementary Figures 151
D. Particle-filter based data assimilation in paleoclimatology 157

Reference 159
List of publications related to the thesis 173

List of abbreviations

AIS	Antarctic Ice Sheet
AP	Antarctic Peninsula
ASL	Amundsen Sea Low
CE	Common Era
CESM	Community Earth System Model
CMIP	Coupled Model Intercomparison Project
CMIP5	Coupled Model Intercomparison Project Phase 5
CMIP6	Coupled Model Intercomparison Project Phase 6
DA	Data assimilation
DML	Dronning Maud Land
EA	East Antarctic Ice Sheet
ECMWF	Centre for Medium-Range Weather Forecasts
ENSO	El-Niño Southern Oscillation
ESM	Earth System Model
GCM	General Circulation Model
IPCC	Intergovernmental Panel on Climate Change
IPO	Interdecadal Pacific Oscillation
MB	Mass balance
NCAR	National Center for Atmospheric Research
NSIDC	National Snow and Ice Data Center
PMIP3	Paleoclimate Modelling Intercomparison Project Phase 3
RACMO	Regional Atmospheric Climate MOdel
SAM	Southern Annular Mode
SAT	Surface air temperature
SH	Southern Hemisphere
SMB	Surface mass balance
SST	Sea surface temperature
TRW	Tree-ring width
WA	West Antarctica
WAIS	West Antarctic Ice Sheet

1

Introduction

Based on the instrumental temperature data, global mean surface air temperature has been increasing since at least the 1880s. The warming rate is around 0.05 °C decade^{-1} over the twentieth century but it has accelerated to 0.15–0.20 °C decade^{-1} since the 1970s [Morice et al., 2021; Osborn et al., 2021]. Putting those recent changes on a longer perspective, our planet has not yet experienced such warming characterized by its near-global spatial consistency over at least the past 2000 years according to the current Sixth Assessment Report from Working Group I of the Intergovernmental Panel on Climate Change (IPCC) [IPCC, 2021].

In the framework of the current global warming, polar regions are of great concern because of their critical importance for the global sea level rise [e.g., The IMBIE Team, 2020], carbon cycle [e.g., Wadham et al., 2019], and large-scale atmospheric/oceanic circulation changes [e.g., Post et al., 2019; Timmermans and Marshall, 2020]. Moreover, polar regions have already expressed high sensitivity and vulnerability to global warming. For instance, West Antarctica experienced one of the most rapid increase in surface air temperature (SAT) of the planet from 1951 to 2000, more than twice as fast as the global average [Steig et al., 2009; Bromwich et al., 2013]. This amplified warming, combined with complex atmosphere-ocean-ice interactions in this region [e.g., Turner et al., 2016], could lead to large impacts on the mass balance of the Antarctic Ice Sheet and potentially to its stability [Etourneau et al., 2019; Verfaillie et al., 2022]. The Antarctic Ice Sheet is known to be the largest reservoir of fresh water on earth, thus becoming the largest potential source of global sea level rise. It is estimated to contribute to the sea level rise by 3 to 7 m by the year 2300 [Edwards et al., 2019], albeit the values remain highly uncertain [e.g., Pattyn and Morlighem, 2020].

Naturally occurring internal interactions between the atmosphere, ocean, land, and ice combined with the response to external forcings, such as orbital and solar variability, are responsible for climate variability from synoptic to multimillennial and longer time scales [e.g., Kunz and Laepple, 2021; Franzke al., 2020]. The climate variability at the multi-decadal and centennial time scales is particularly interesting because it occurs at the same time scale as anthropogenic climate change and may determine future changes in the coming decades and

centuries. If centennial variability is mainly forced by external influences on Earth's climate, then future changes may be predictable to the extent that future forcing trajectories can be known. If internally generated centennial variability is also large, then future changes will be strongly influenced by this internal variability too. As for Antarctica, such low-frequency variability is closely linked to the stability of the regional glaciers and the whole ice sheet mass balance [e.g., Etourneau et al., 2019]. In this thesis, we explore how to improve the reconstructions of centennial variability at high southern latitudes over the past two millennia by comparing and combining various sources of information derived from climate models and observations.

1.1 Physical geography of Antarctica

Antarctica is situated almost entirely south of the Antarctic Circle (66°33′49.1″) and is surrounded by the Southern Ocean (Fig. 1.1). Its unique position in the high latitudes of the Southern Hemisphere means that almost all of Antarctica has temperatures below freezing all year long. Snowfall is the main form of precipitation there and snow is transformed in ice through time. Nowadays, roughly 98% of the Antarctic continent is covered by the largest single mass of ice on Earth [Fretwell et al., 2013]. This ice mass is referred to as the Antarctic Ice Sheet (AIS), with an area of almost 14 million square kilometers and an average thickness of 2160 m [Fretwell et al., 2013].

The AIS is often divided into three main sectors: East Antarctica, West Antarctica, and the much smaller Antarctic Peninsula (AP). The physical geography of these three sectors is briefly introduced below.

- The Antarctic Peninsula is covered by a narrow rocky mountain range, like a finger pointing towards the tip of South America (Fig. 1.1). Those mountains reach more than 2,000 meters high and run north-south, forming a very effective barrier to the circumpolar winds. This topographic barrier is thus associated with strong Foehn winds over the western Antarctic Peninsula, raising air temperature there, and inducing melting of the snow and the ice shelves [e.g., Kirchgaessner et al., 2021]
- East Antarctica, lying on the east of the Transantarctic Mountains, constitutes the majority (two-thirds) of the Antarctic continent. Most of the East Antarctic coastline is adjacent to the Indian Ocean, and thus the coastal regions are largely influenced by marine air intrusions. The interior of East Antarctica is covered by the Antarctic Plateau, which ranges from 2,000 to 4,100 meters above sea level (Fig. 1.1). This large difference in altitude induces distinct climates between the coastal and interior regions [e.g., Ghilain et al., 2022].
- West Antarctica is situated west of the Transantarctic Mountains. It lies between the Ross Sea (partly covered by the Ross Ice Shelf), and the Weddell Sea (partly covered by the Filchner-Ronne Ice Shelf), and is bordered by the Pacific sector of the Southern

Ocean (Fig. 1.1). It is covered by the West Antarctic Ice Sheet (WAIS), flowing down from the Transantarctic Mountains. The relatively low altitude (850 m on average) allows frequent interactions with the surrounding seas.

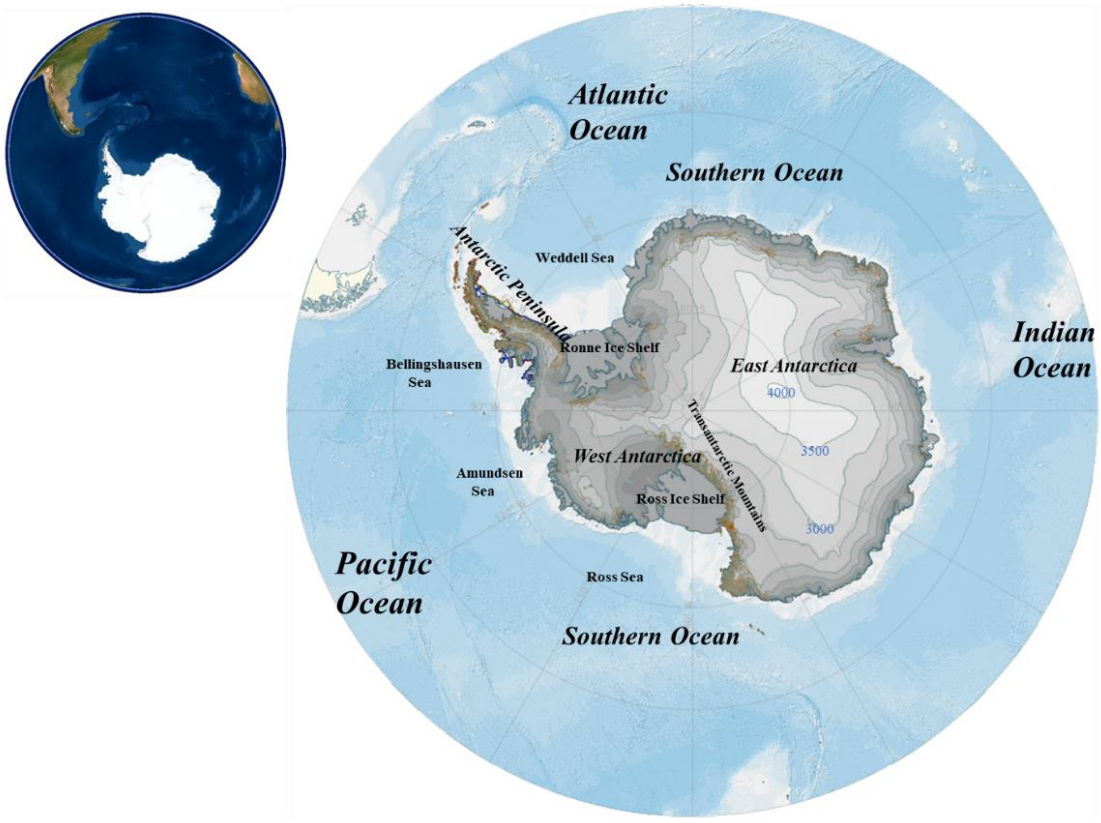

***Figure 1.1**: Location of Antarctica on the earth (left) and the sites mentioned in the manuscript. Background map from British Antarctic Survey Data (https://www.bas.ac.uk/data/our-data/maps/geological-maps/).*

1.2 Current Antarctic climate changes and possible mechanisms

The Antarctic climate is characterized by a strong coupling between the atmosphere, the ocean and the ice [Thompson and Solomon, 2002; Goosse et al., 2009; Fan et al., 2014]. One hallmark of the recent climate changes is the large spatial asymmetry for the recent trend in the surface air temperature between East and West Antarctica [Nicolas and Bromwich, 2014; Turner et al., 2020; Smith and Polvani, 2017; Jun et al., 2020]. Over 1979-2014 CE, a strong surface warming was observed over West Antarctica and the Antarctic Peninsula, in stark contrast with the insignificant cooling trend over East Antarctica (Fig. 1.2).

In addition to the changes over the continent, heterogeneous spatial trends are also observed over the ocean. Sea ice in the Amundsen–Bellingshausen Sea sector largely shrank since 1979, but in the Ross Sea sector, the sea ice expanded substantially during the same period [Hobbs et al., 2016; Parkinson, 2019]. Consistent with sea ice changes, the pattern of the sea surface temperature (SST) trend over the Southern Ocean shows warming in the southeast Indian Ocean sector, the Weddell Sea, and Bellingshausen and Amundsen Seas, while widespread cooling in the rest of the Southern Ocean [Fan et al., 2014].

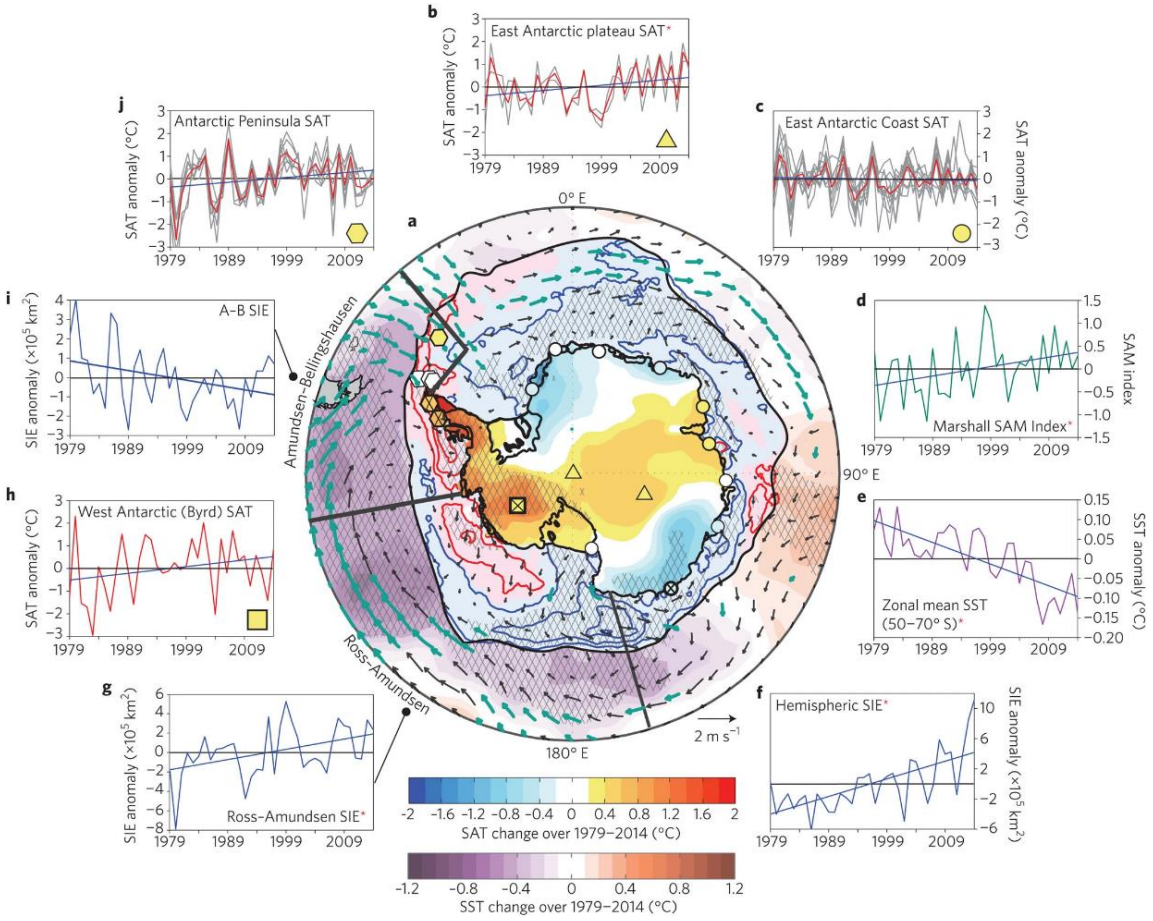

***Figure 1.2**: Spatial pattern of trend in annual mean surface air temperature (blue–red shading), sea ice concentration (red and blue contours denote negative and positive trends respectively), sea surface temperature (purple–red shading), and near-surface winds (vectors). The significant trends at the 95% level are shown with hatching and teal vectors. The surrounding small panels display the time series of station-based surface air temperature from the East Antarctic plateau (b), East Antarctic coast (c), West Antarctica (h), and Antarctic Peninsula (j), sea ice extent (SIE) over the Ross-Amundsen Sea sector (g; in $10^5 km^2$), the Amundsen-Bellingshausen Sea sector (i; in $10^5 km^2$), and the total Southern Ocean SIE (f), the SAM index (d; unitless), and zonal mean SST (e; in °C). Figure from Jones et al. [2016].*

Imprinted on these trends over past decades, large decadal variability has also been observed, for instance, in the surface air temperature. During the second half of the twentieth century, West Antarctica and the Antarctic Peninsula warmed twice faster than the global average, but in the first two decades of the twenty-first century, the temperature remains relatively stable, which may appear as a surprising reversal in the context of the global warming [Turner et al., 2016]. This halting warming is in contrast with the change at the South Pole, where a record-high warming trend was observed from 1989 to 2018 [Clem et al., 2020].

The Southern Ocean and Antarctic climate are strongly influenced by the extratropical Southern Hemisphere atmospheric circulation and teleconnections between the tropics and high southern latitudes. The strongest large-scale mode of atmospheric variability in the Southern Hemisphere is the Southern Annular Mode (SAM). A positive (negative) SAM phase is associated with an increased (decreased) pressure gradient between the polar circle (65 °S) and midlatitudes (40 °S) and with a strengthening (weakening) and shifting towards (away from) Antarctica of the Southern Hemisphere westerly winds (Fig. 1.3). The SAM has a broad influence on the SAT pattern over Antarctica, with a large-scale spatial asymmetry between East and West Antarctica. The geographical position of the Antarctic Peninsula extending northward into the circumpolar westerlies results in warming there, in particular through the Foehn effect [e.g., Kirchgaessner et al., 2021], and northerly meridional winds related to the SAM [e.g., Lefebvre et al., 2004; Marshall et al., 2011]. Concurrently, the positive SAM is characterized by stronger zonal flow, reducing meridional exchanges of warm air mass between the Antarctic interior and the midlatitude, thus broadly cooling East Antarctica.

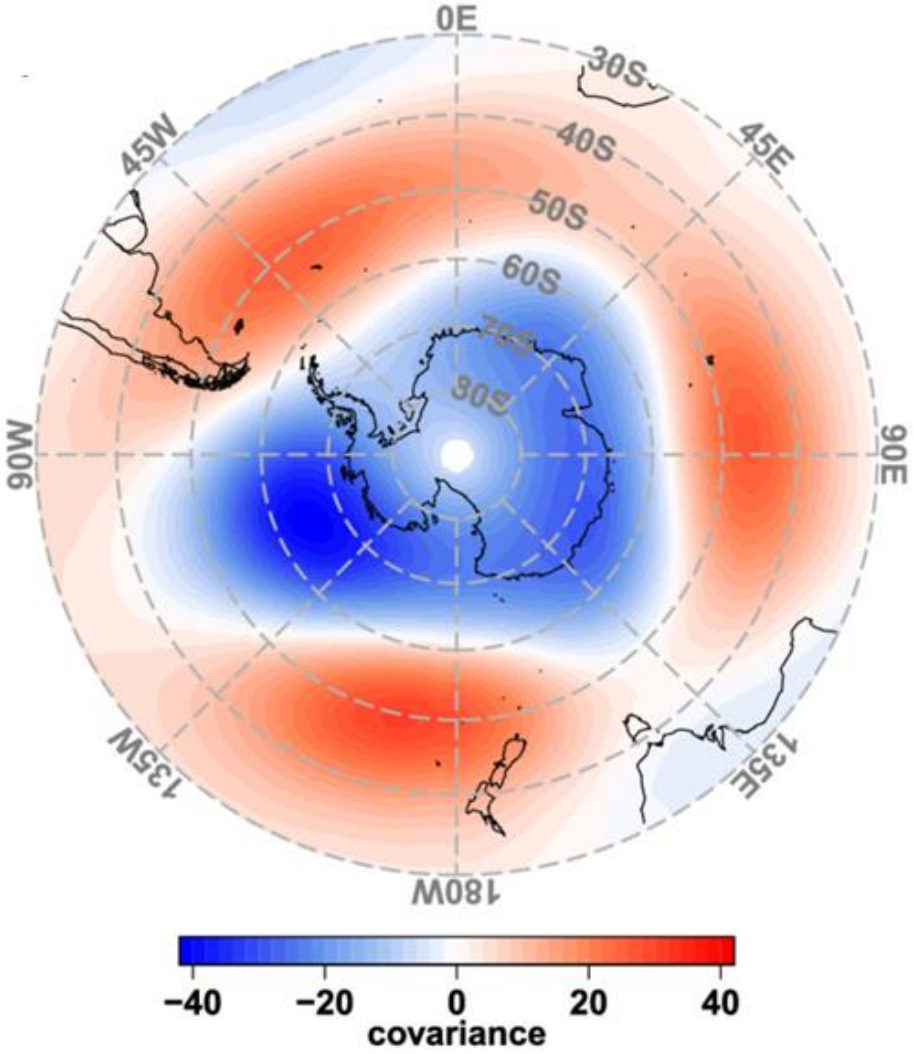

***Figure 1.3**: The SAM pattern in the ERA-Interim 500 hPa level. The shading denotes the covariance between the SAM index time series and 500 hPa geopotential height anomalies over 1981–2010.*

A semi-permanent low-pressure system (as shown in Fig. 1.3), referred to as the Amundsen Sea low (ASL), is present over the high-latitude South Pacific Sector of the Southern Ocean. The ASL tends to be deepened in the positive SAM phase, but its strength and position are also modulated by tropical sea surface temperature through Antarctic-tropical teleconnections [e.g., Turner et al., 2013; Raphael et al., 2016]. A deeper ASL induces stronger northern winds over the Antarctic Peninsula, the eastern part of West Antarctica, and the surrounding seas, resulting in a SAT increase and decreasing sea ice extent in the Amundsen-Bellingshausen Sea. Conversely, southerly winds caused by deepening ASL blow in West Antarctica and the Ross Sea region, leading to SAT decrease and sea ice expansion [Hosking et al., 2013].

The SAM index has displayed a positive trend since 1979 as evident in the SAM index time series in Fig. 1.2 d. This trend, particularly in summer, has been attributed to the reduction of stratospheric ozone and the increase in greenhouse gas concentration [Gillet and Fyfe, 2013]. Nevertheless, as an internal mode of variability of the atmosphere, the SAM index is also changing without any perturbations of external forcings [Thompson and Wallace, 2000], for instance because of tropical-extratropical teleconnections [Li et al., 2021].

In addition to the SAM, there are other climate modes known to influence temperature variability across the Antarctic continent. For instance, the two Pacific–South American patterns (PSA1 and PSA2) represent atmospheric Rossby wave trains of alternating circulation anomalies, which are initiated by anomalously deep tropical convection during El Niño–Southern Oscillation events (ENSO) and are directed toward West Antarctica and the Antarctic Peninsula [Mo and Higgins, 1998]. The positive phase of PSA1 is associated with anticyclonic wind anomalies in the South Pacific centered at ∼120° W, which has been linked to an anomalous cold southerly flow to the Antarctic Peninsula and a warm northerly flow to the Ross Ice Shelf and western West Antarctica [Marshall and Thompson, 2016]. The positive phase of the PSA2 corresponds to a shift of the anticyclonic anomaly westward to the Ross Sea, around 150° W. This pattern allows winds to transport more marine air masses along the western Ross Ice Shelf but simultaneously enhances katabatic flow along the eastern Ross Sea coast [Marshall and Thompson, 2016].

The recent climate variability over Antarctica is thus strongly influenced by the combined effects of a positive SAM trend, an intensification of the westerlies, and the teleconnections from the tropics [Li et al., 2021]. Recent studies have emphasized that low-frequency tropical variability, for instance, the Pacific Decadal Oscillation (PDO)/Interdecadal Pacific Oscillation [IPO; Meehl et al., 2016; Purich et al., 2016] and the Atlantic Multidecadal Oscillation [AMO, Li et al., 2014], may affect climate variability on decadal time scales over Antarctica. The IPO is an index that is defined as the leading empirical orthogonal functions (EOF) mode of decadal low-pass filtered SST variability over the entire Pacific, while AMO denotes an average over the entire North Atlantic basin of the linearly detrended SST yearly anomalies on which a 10-year running mean is applied, as proposed by Enfield et al. [2001]. Changes in the tropical ocean have been demonstrated to intensify the Southern Hemisphere westerly winds via both the AMO [Li et al., 2014]and the IPO [Meehl et al., 2016]. The IPO affects Antarctic atmospheric circulation through Rossby wave trains, with anomalies persisting for decades [Meehl et al., 2016; Purich, 2016]. The positive phase of the IPO favours weakened westerlies and an anomalous high pressure in the Amundsen/Bellingshausen seas. This disturbance originates from the central equatorial Pacific and propagates southwards through Rossby waves leading to changes in the ASL [Clem and Fogt, 2015]. Similarly, SST variability in the north and tropical Atlantic generates a stationary Rossby wave train that propagates to the Southern Ocean, and ultimately influences the atmospheric circulation around Antarctica. The positive (negative) phase of the AMO may intensify (weaken) the

westerlies and deepen (shallow) the ASL [Simpkins et al., 2016]. In fact, both the positive phase of the AMO since the late 1970s and the negative phase of the IPO beginning in the early 2000s have potentially contributed to the deepening of the ASL and intensification of the SAM, with a potential effect on the observed long-term increase of the total sea ice cover around the Antarctic before 2015 [Eayrs et al., 2022]. However, the short instrumental record makes it hard to understand climate variability on those time scales.

1.3 Proxy data in Antarctica and proxy-based climate reconstructions

Proxy records provide an invaluable tool to place the recent changes in a longer temporal context. Over the past few decades, many studies have proposed reconstructions of climate on global and regional scales, combining high (i.e., annual to sub-decadal) and low (decadal or longer time scales) temporal resolution records to estimate the climate variability over the past millennium [e.g., Jones et al., 2009; PAGES 2k Consortium, 2013; Neukom et al., 2014, 2019]. In this section, several proxy records over Antarctica that are commonly used for climate reconstruction are introduced, focusing on their ability to record high- and low-frequency climate variability, and presenting some of the key reconstructions based on those records.

1.3.1 Antarctic ice cores

Ice cores are cylinders of ice drilled from ice sheets and glaciers. They have become one of the golden standards in paleoclimate research, because of their high accuracy in dating, high time-resolution, and well-preserved paleoclimate information [e.g., Masson-Delmotte et al., 2013]. Water stable isotopic composition, primarily hydrogen and oxygen elements, is one of the main proxy records retrieved from ice cores. This proxy has been developed as an "isotopic thermometer", expressed as oxygen isotope ratios ($\delta^{18}O$) and deuterium isotope ratios [Jouzel et al., 2007; Masson-Delmotte et al., 2008].

The basis for paleoclimatic interpretations of the stable isotope content of water molecules is that the vapor pressure of $H_2{}^{16}O$ is higher than that of $HD^{16}O$ and $H_2{}^{18}O$. Thus, water evaporation produces a vapor that contains less deuterium (D) and ^{18}O than the initial water, while the remaining water is rich in deuterium and ^{18}O. This process is referred to as "isotopic fractionation". In contrast, when condensation occurs, the lower vapor pressure of $HD^{16}O$ and $H_2{}^{18}O$ induces a larger transfer of those molecules from the vapor state to the liquid state. As the air mass moves away from its source and releases water through precipitation, the remaining water becomes increasingly depleted in heavy isotopes. Since this isotopic fractionation process is inversely proportional to the temperature at which condensation occurs, the isotopic composition of precipitation is theoretically linked with local temperature.

The relationship between the water isotopic composition and temperature has been validated, in particular on long time scales (e.g., millennial time scales), from models [e.g., Jouzel et al., 2003] and observational evidence [e.g., Masson-Delmotte et al., 2008]. Nevertheless,

converting the stable isotopic signal from ice cores to paleotemperature is still a complex task due, for instance, to the changes in moisture origins and the intermittency of Antarctic precipitation [Masson-Delmotte et al., 2008; Sime et al., 2009] that could influence the isotopic composition of snowfalls and stratigraphic noise that could mask climate signals preserved in ice cores from interannual to multi-decadal scales [Münch et al., 2016].

To extract a reliable signal of past temperature changes in Antarctica from water isotopic records, previous studies mainly focused on two aspects: the combination of multiple ice core records from a given site or region and the finding of appropriate calibration methods for the relationship between water isotopic composite and surface air temperature [PAGES 2k Consortium, 2013; Stenni et al., 2017].

A first attempt to reconstruct SAT over the past millennium in Antarctica relies on seven standardized water stable isotope records [Goosse et al., 2012]. This study took advantage of a spatial isotope–temperature relationship for the last millennium to transfer the water isotope to surface air temperature. Then, within the coordinated efforts of the Past Global Change (PAGES)-2K Network project, 11 annual-resolution water isotopic records over Antarctica were selected to obtain the Antarctic SAT reconstruction spanning the past 2000 years, based on a statistical-based method referred to as composite-plus-scaling (CPS). Nevertheless, the very limited number of ice core water isotopic records in PAGES 2k Consortium [2013] does not allow for estimating changes on smaller spatial scales (Fig 1.4 a). Therefore, Stenni et al. [2017] further enlarged the database, collecting 112 high-resolution isotopic records. For the methodology, Stenni et al. [2017] used more complex like-CPS methods than the one used in PAGES 2k Consortium [2013], and implemented unweighted/weighted composite methods and model-based scaling for the regional $\delta^{18}O$–temperature relationships. The reconstructions consistently show a long-term cooling from 1-1900 CE over Antarctica, but Stenni et al. [2017] suggests clear regional variations. Some large centennial variabilities are also observed, for instance a significant warming over 1-500 CE in the Antarctic Plateau (Fig 1.4 a). However, it should be noted that some regional reconstructions of Stenni et al. [2017] rely simply on a few records (for instance three records over the Antarctic Plateau) with the temporal span extending the full past two millennia (Fig 1.4 a). The relatively small number of records may cause considerable uncertainty in climate reconstructions. For instance, a new climate record derived from ice-core water stable isotopes in East Antarctica suggests that the long-term cooling in East Antarctic Plateau from 1 to 1900 CE proposed by Stenni et al. [2017] is only robust between 550 and 1550 CE [An et al., 2021]. Therefore, confirmation of the robustness of these signals and understanding of the mechanisms remain necessary.

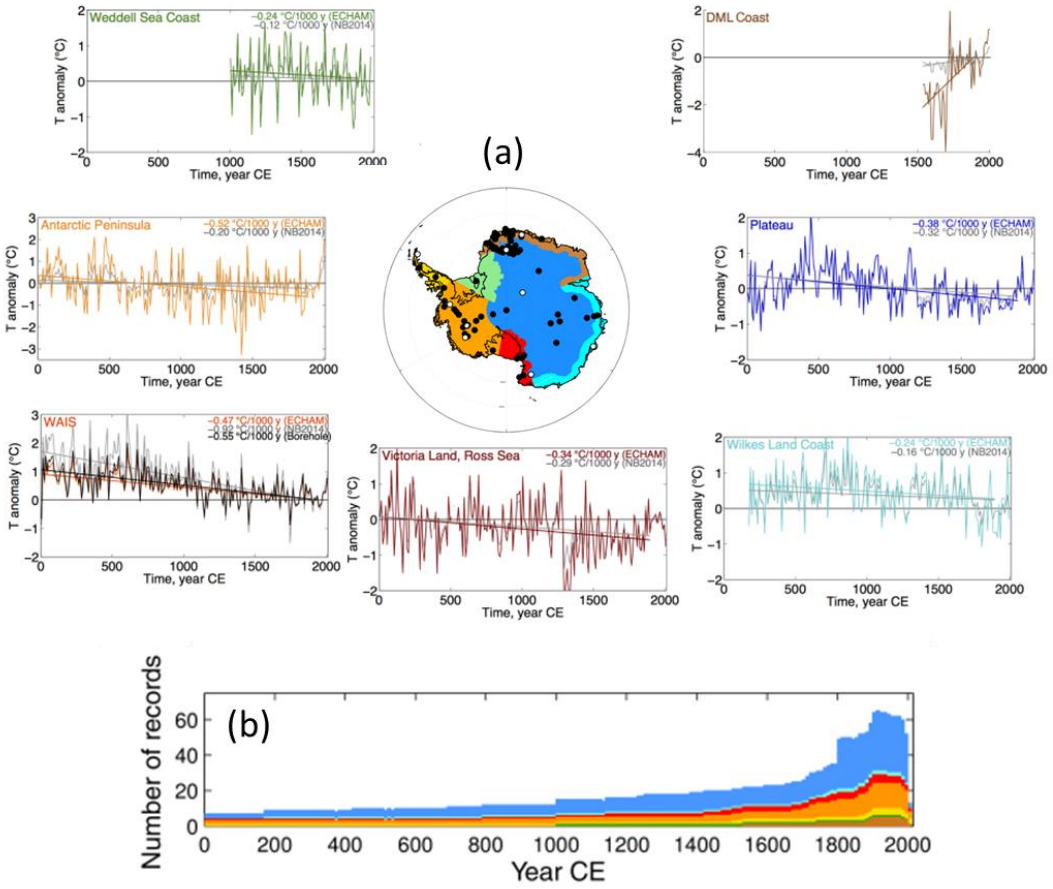

***Figure 1.4**: (a) Statistical-based Antarctic temperature reconstruction (T anomalies in ˚C, referenced to the 1900–1990 CE period) for the past 2000 years from Stenni et al. [2017]. The centre map shows the seven Antarctic regions selected for the regional reconstructions. The dots within this map show the site locations, and the white ones denote the sites that have been used in the previous continent-scale reconstructions [PAGES 2k Consortium, 2013]. (b) The temporal distribution of the records in Stenni et al. [2017]. The figure is modified from Stenni et al. [2017].*

Snow accumulation is another proxy that could be derived from ice cores, indicating the variability of paleo-precipitation (or snowfall) on interannual to millennial time scales. For the past 1000 years, a database containing 79 ice-core based snow accumulations has been recently developed, but most of them only cover several past centuries (only four covering the full past millennia from 1000-2000 CE as shown in Fig 1.5 i) [Thomas et al., 2017]. The corresponding snow accumulation reconstructions for several Antarctic regions show little consistency between them [Thomas et al., 2017, Fig 1.5 a-g], reminding us of the large spatial variability of snow accumulation and that a few records may not be enough to estimate accurately large-scale variability.

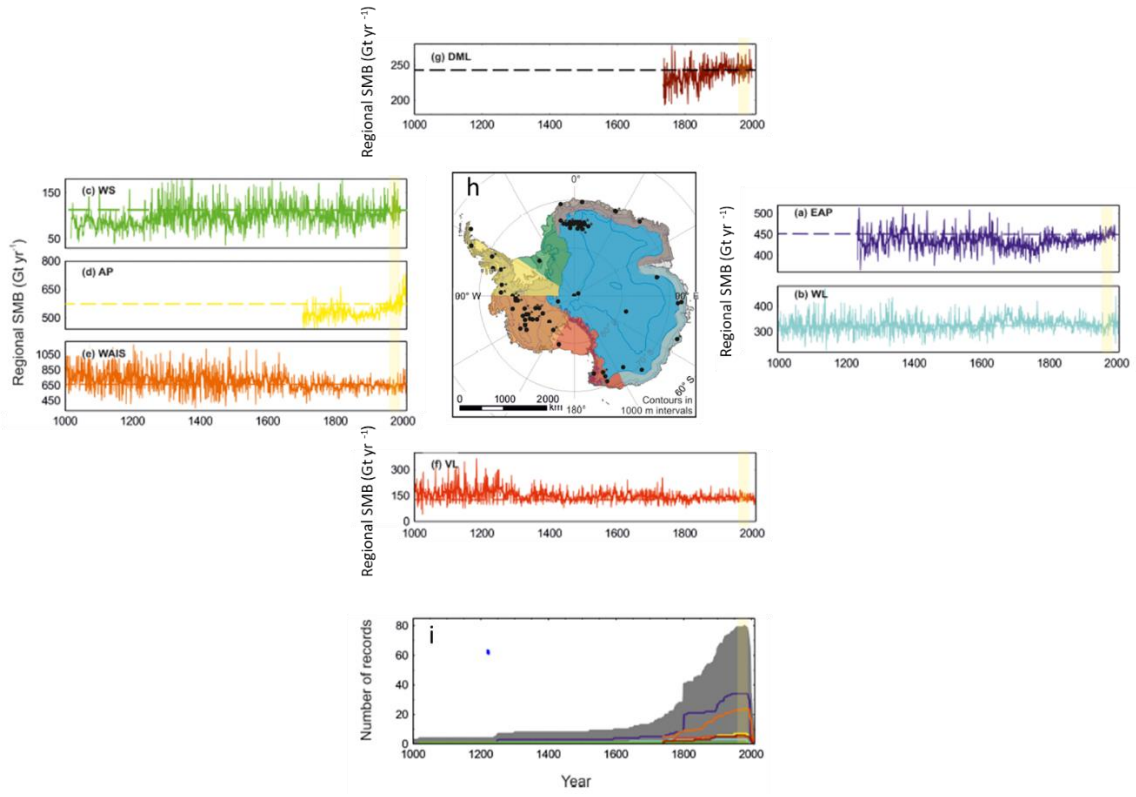

Figure 1.5*: Regional reconstruction of the surface mass balance (SMB) during the period 1000-2010 CE for (a–g) the East Antarctic Plateau (EAP, dark blue); Wilkes Land coast (WL, cyan), Weddell Sea coast (WS, green), Antarctic Peninsula (AP, yellow), West Antarctic Ice Sheet (WAIS, orange), Victoria Land (VL, red), and Dronning Maud Land (DML, brown). Panel (i) represents the temporal distribution of snow accumulation records (solid grey) and the number of records by region. The figure is modified from Thomas et al. [2017].*

Both the large-scale atmospheric circulation and thermodynamic processes (e.g., Clausius-Clapeyron relation) could be responsible for the variability of snow accumulation [Frieler et al., 2015; Fudge et al., 2016; Dalaiden et al., 2020]. Consequently, in addition to the reconstruction of surface mass balance [e.g., Medley and Thomas 2019; Thomas et al., 2017], there is great potential to perform reconstructions of surface air temperature and atmospheric circulation using snow accumulation. In particular, a recent study using data assimilation has suggested that snow accumulation may be a better proxy for past surface temperature than stable water isotopes [Dalaiden et al., 2020]. Furthermore, by combining ice core water isotopic and snow accumulation records, skillful reconstructions for some surface variables, e.g., sea ice, SAT, and atmospheric circulation at an interannual scale have been obtained for the past two centuries [Dalaiden et al., 2021; O'Connor et al., 2021].

Ice sheet borehole temperature corresponds to the temperature of the ice in a hole left after collecting an ice core (Fig. 1.6 a). It is always analyzed in conjunction with ice core studies. Since heat diffuses through the snow and ice, the signal related to the evolution of

surface air temperature propagates downward (Fig. 1.6 b) and ice sheet borehole temperature contains thus information about past surface temperatures [MacAyeal et al., 1991]. The biggest advantage of borehole temperature is that it provides an absolute temperature measurement, and is not a proxy that needs to be calibrated [e.g., Cuffey, 2007]. However, the time resolution and length of borehole-based surface temperature reconstructions are severely limited by the physics of the heat transfer process [Clow, 1992]. It is this physical constraint that allows recording low-frequency climate variability or long-term averaged temperatures., e.g., at a centennial or multi-centennial scale.

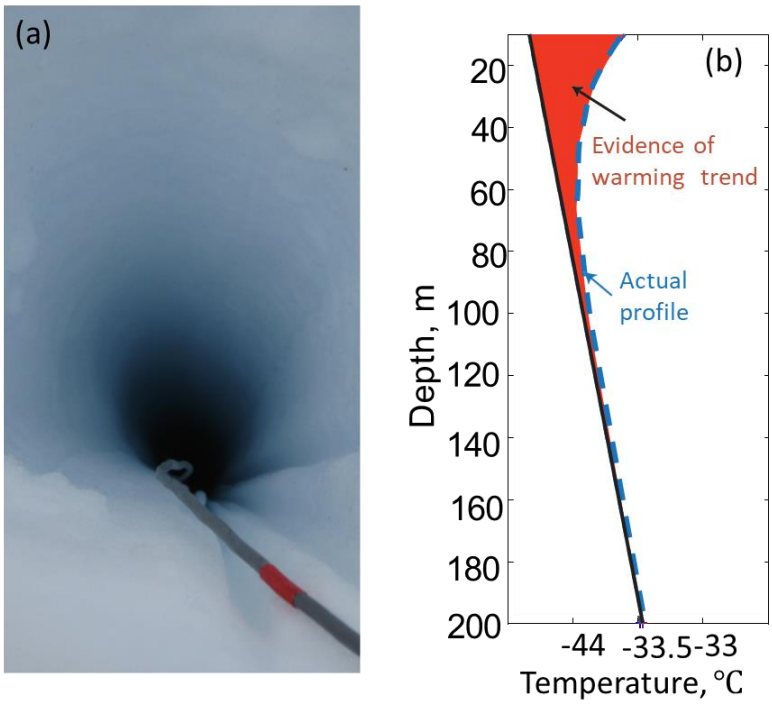

Figure 1.6*: (a) Ice borehole and its temperature; (b) Schematic illustration of the borehole temperature profile.*

Ice borehole reconstructions are based on a heat diffusion-advection process model and an inversion model [Cuffey and Paterson, 2010, Chapter 9]. The forward model could be different according to the specific conditions at the location of interest, but it generally considers heat and ice flow processes [Cuffey and Paterson, 2010, Chapter 9]. The goal of the inversion model is to find potential temperature histories that fit the measured ice borehole temperatures. However, since the diffusion process blurs the temperature history, there could be many potential temperature histories fitting the observations, which indicates large uncertainty in the reconstruction [e.g., Dahl-Jensen et al.,1998].

Over the past decades, several ice borehole temperatures-based reconstructions have provided valuable information on the SAT changes over Antarctica. For instance, the reconstruction from the borehole at the West Antarctic Ice Sheet (WAIS) Divide indicated that

the SAT in the 15th-19th centuries was about 0.5°C cooler than the average temperature of the past 1000 years and that the estimated warming over 1957-2007 was 0.15-0.3°C per decade, comparable to instrumental data [Orsi et al., 2012]. This reconstruction was used as a benchmark for adjusting the magnitude of temperature changes over the past millennium derived from isotopic records as Stenni et al. [2017].

1.3.2 Marine proxy records

Marine sediments in the Southern Ocean usually preserve a variety of surface condition-related deposits, from which a range of biological, chemical, and physical proxies can be extracted to reconstruct past sea surface temperatures (SST), primary productivity, ocean currents, and sea ice variations [Lamping et al., 2021, Thomas et al., 2019, Allen and Weich, 2022]. Compared to the continental proxy records with annual or nearly annual resolutions, marine proxy records retain in general lower-frequency signals because of their low sedimentation rate, although some tropical corals are also able to preserve SST information at the interannual time scale [Jones et al., 2001; Hetzinger et al., 2012]. Regarding the SST reconstructions for the Southern Ocean, in particular for those targeting the sub-Antarctic ocean (e.g., along the Southern Chilean coast), the alkenones-based reconstructions are the main records for estimating the SST over the past two millennia [e.g., Collins et al., 2018; Caniupán et al., 2014; Haddam et al., 2018]. Additionally, diatom-based proxy records in marine sediments are the primary means to estimate sea ice changes in the Antarctic marginal zone [Allen and Weich, 2022]. Therefore, in this thesis, we focus on these two types of proxy records and describe their main features below.

Alkenones are organic compounds preserved in marine sediments that can be the basis for a robust biogeochemical proxy for estimating SSTs or very near-surface (upper mixed layer) ocean temperatures in paleoceanography [Müller et al., 1998; Herbert, 2006]. Determining the seasonal signal included in alkenone records, which are typically calibrated to mean annual temperatures, is still an open question. Alkenone-based SST reconstruction records have been suggested to be influenced by the seasonal variation in alkenone production [e.g., Kim et al., 2006]. However, a recent study did not detect any seasonal bias from the samples in the high-latitude oceans [Tierney and Tingley, 2018]. The nonlinearity of alkenone response to SST is also an important issue for the calibration of the alkenone paleothermometer [e.g., Tierney and Tingley, 2018]. Until now, there are several alkenone-based SST reconstructions for the past two millennia in the mid-latitude Pacific sector of the Southern Ocean, in particular along the southern Chilean coast. They show consistent and significant centennial variability in this region, reflecting either multi-centennial internal variability (e.g., related to the SAM) or external forced response [e.g., Collins et al., 2019].

Diatoms are microscopic single-celled algae that inhabit a wide range of aquatic and sub-aquatic environments [e.g., Allen and Weich, 2022]. Since diatoms have different tolerances and preferences for sunlight, temperature, salinity, nutrient availability, etc., they usually

occupy certain conditions that could be beneficial to their production and export, such as the environment close to or within the sea ice [Crosta et al., 2005; Abram et al., 2013]. Accordingly, diatoms preserved in marine sediments offer excellent potential for reconstructing Antarctic sea-ice conditions. Currently, two general approaches using fossil diatom assemblages to reconstruct past sea ice conditions have been developed. The first is to use a type of diatom (e.g., Fragilaropsis curta and F. cylindrus) that is known to be associated with sea ice to identify qualitatively specific sea ice conditions [e.g., Etourneau et al., 2013; Allen and Weich, 2022]. The second is to link the quantitative sea-ice conditions to relative abundance of diatoms using statistical methods [e.g., Barbara, et al., 2013; Crosta et al., 2021].

With adequate chronological control and resolution of the marine sediments, particularly from the sites with high accumulation rates, the reconstructions based on sea ice related diatom have provided important information for the sea ice conditions over the past two millennia. For instance, a decadal-resolved diatom record located at Adélie Land coast has been used to reconstruct quantitatively the sea ice presence and to identify significant multi-decadal variability related to ENSO and SAM over the past two millennia [e.g., Crosta et al., 2021]. Even the qualitative reconstructions based on links between specific diatom taxa and their preferred environment suggest that the sea ice extent has experienced several centennial or multi-centennial expansion or retreat periods over the past centuries [Thomas et al., 2018].

1.4 Antarctic climate changes in climate models

Climate models are essential tools to better understand past climate variations by simulating the evolution of the key variables describing the climate system [e.g., Hegerl et al., 2007]. According to the complexity of model physics, current climate models can be grouped into three main categories. They range from 0-D or 1-D energy balance models (EBMs) that provide highly simplified and globally-averaged dynamics of the system [e.g., Mann et al., 2014] to general circulation models (GCMs) that have fully interactive atmospheric and oceanic components, being able to account for all the important properties of the system at current grid resolutions from 50 KM to 200 KM [e.g., Schmidt et al., 2011]. Such GCMs are also referred to as Earth system models (ESM) if they include more components, i.e., the terrestrial and marine carbon cycle, atmospheric chemistry, vegetation dynamics and ice sheets [e.g., Otto-Bliesner et al., 2015]. In the last decades, water isotope capabilities have been incorporated into all the components of some GCMs, such as isotope-enabled Community Earth System Model version 1 [iCESM1, Brady et al., 2019]. Between these two extremes, Earth System Models of Intermediate Complexity (EMICs) present more sophisticated atmospheric and oceanic components than EBMs but contain some simplification and parameterization of processes to improve computational efficiency [e.g., Goosse et al., 2010].

Within the framework of the Past Model Intercomparison Project Phase III [PMIP3; Otto-Bliesner et al., 2009] and the Coupled Model Intercomparison Project Phase V [CMIP5; Taylor et al., 2012], coordinated climate modelling activities (based on GCMs) have produced a series

of the simulations for different past periods. Regarding the Antarctic climate for the historical period (1850-2005 CE), the simulations performed with the PMIP3-CMIP5 models have been comprehensively evaluated by comparison with observational data, in particular for the changes since the 1950s. Climate simulations of the SAM response to rising atmospheric greenhouse gas levels and stratospheric ozone depletion over the last century compare reasonably well to observations and proxy data [Miller et al., 2006; Raphael and Holland, 2006; Swart and Fyfe, 2012; Gillett and Fyfe, 2013; Zheng et al., 2013]. However, the simulated spatially homogeneous warming over Antarctica disagrees with the observed West-East Antarctic asymmetry in the temperature trend [Jones et al., 2019; Klein et al., 2019; Jun et al., 2020]. Additionally, the CMIP5 models have generally been unable to reproduce the observed long-term sea ice extent increase since 1979, instead simulating ice loss over this period [e.g., Turner et al., 2013; Zunz et al., 2013]. It should be noted that those inconsistencies are smaller between the multi-model ensemble mean and the observations than for some individual simulations as the observed trends are not inconsistent within the available ensemble of simulations [Klein et al., 2019, Chemke and Polvani, 2020]. This suggests that the observed changes in those surface variables for past decades may not be attributed to the forced response, and natural climate variability may play a large role in some current climate changes in Antarctica [e.g., Jones et al., 2016; Turner et al., 2020; Jones et al., 2019; Previdi and Polvani, 2016].

In addition, there is also a suite of simulations for the past millennium (850-1850 CE) performed with CMIP5–PMIP3 models. Following the common protocols in the framework of the CMIP5–PMIP3 project, climate models are driven by forcing datasets that include volcanic aerosols, greenhouse gas concentrations, solar radiation associated with changes in orbital configuration and changes in solar output and anthropogenic land use. [Fig. 1.7; Schmidt et al., 2011]. For Antarctica, these simulations show a consistent millennia-scale cooling from 850-1850 CE [Fig. 1.8]. This long-term cooling trend is more due to the relatively cold period between the 15th and 19th centuries [Fig. 1.8, Klein et al., 2018] since the warming phase during the first centuries of the last millennium over Antarctica is not as significant as the one in the North Hemisphere [e.g., PAGES consortium, 2013]. This simulated temperature evolution has been evaluated by comparison with the ice core water isotope-based reconstructions using statistical methods derived from Stenni et al. [2017]. The result shows a good consistency between the reconstruction and simulations for the SAT trend during past millennia at the continental scale [Fig. 1.8, Klein et al., 2018].

However, obtaining unambiguous conclusions from the comparison between reconstructions and modeling results remains difficult. On the one hand, observations or proxy-based reconstructions are describing the real evolution of the system which can be considered as the realization of the climate system evolution that occurred among all possible ones. By comparison, a comprehensive climate model could theoretically achieve all the potential realizations, in particular through an ensemble of simulations [e.g., Otto-Bliesner et al., 2016],

if it was able to represent the real world in a satisfactory way. Therefore, the basic criteria for claiming consistency between simulations and reconstructions is that reconstructions should be within the range of the modeling results, when considering all the potential realizations [PAGES 2K-PMIP3 group, 2015]. This appears to be the case for the statistical-based Antarctic SAT reconstructions for the past millennium in Stenni et al. [2017] and the simulations with CMIP5–PMIP3 models (Fig. 1.8). However, several regional reconstructions, for instance over the Antarctic Plateau (Fig. 1.4), remain highly uncertain as they are strongly dependent on one or two $\delta^{18}O$ water isotope records covering the whole period [An et al., 2021]. In addition, due to computational constraints, it remains impossible to generate an ensemble using a comprehensive climate model (e.g., ESM) that contains a large number of members for the past two thousand years, in order to completely follow the observed time evolution of the climate system.

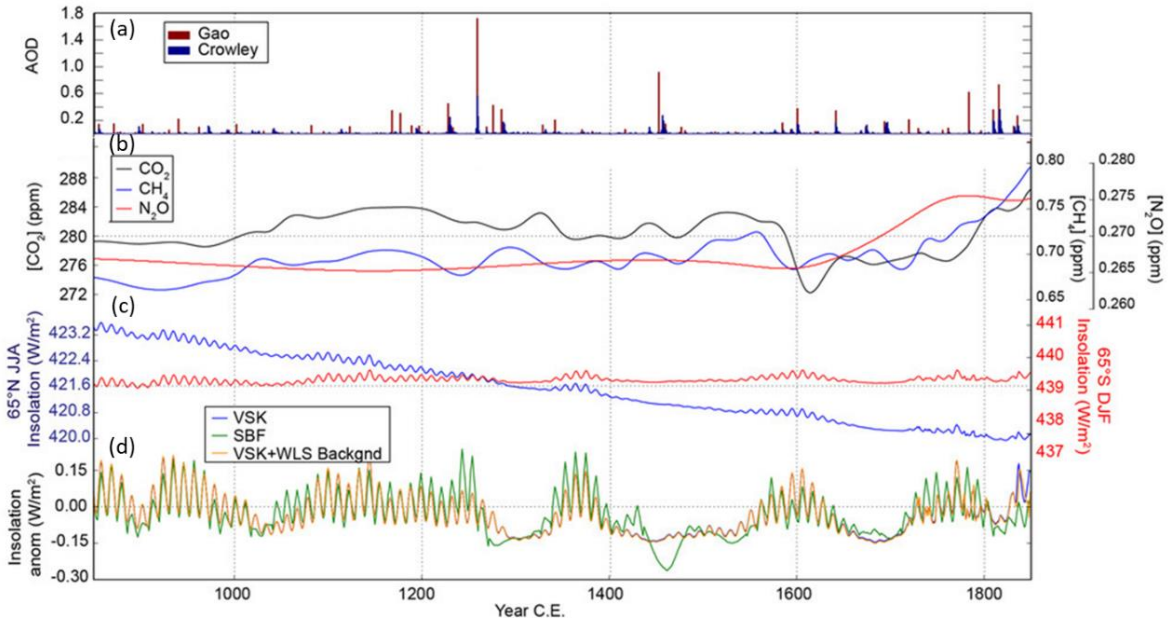

***Figure 1.7**: Climate forcings through the last millennium in the CMIP5 models. (a) Aerosol optical depth (AOD) from Crowley et al. [2008] (blue bars) and estimated from Gao et al. [2008] (red bars). (b) Concentrations of CO_2, CH_4, and N_2O [Gerber et al., 2003]. (c) Changes in insolation at 65°N in JJA (blue) and 65°S in December–February (DJF; red) were calculated from Berger [1978]. (d) Globally averaged insolation anomalies (relative to 950–1200 CE) for the solar forcing datasets (VSF from Vieira et al. [2011]; SBF from Steinhilber et al. [2009]; WLS from Wang et al. [2005]). The figure is modified from Atwood et al. [2016].*

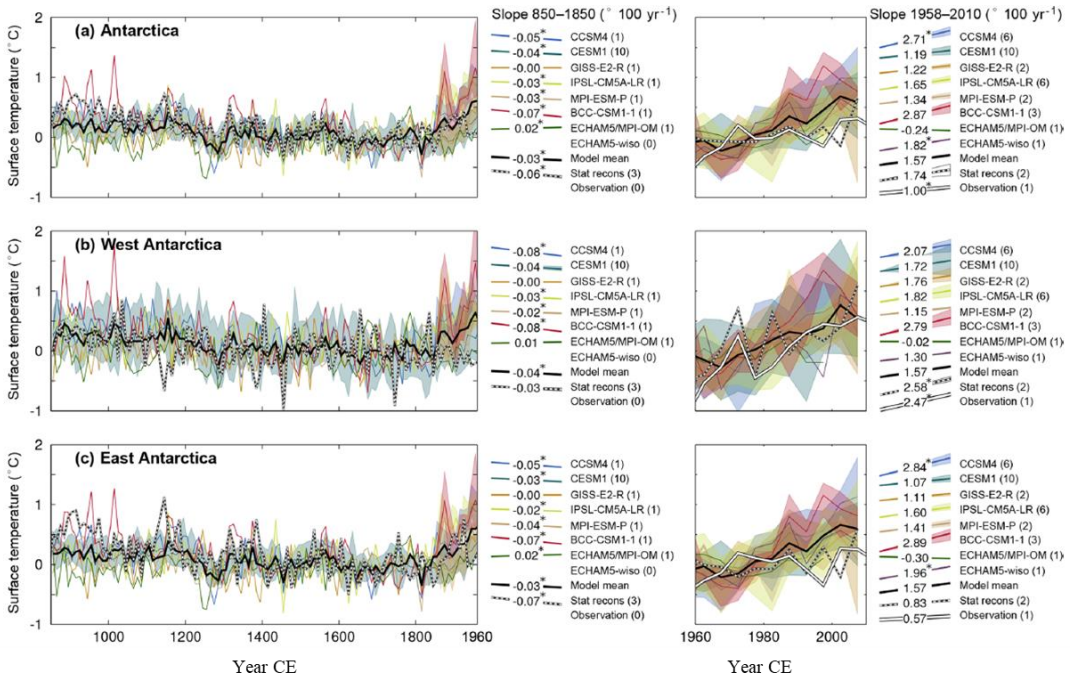

***Figure 1.8**: The simulated surface air temperature derived from the CMIP5–PMIP3 models (colorful lines) and the statistical-based reconstruction from Stenni et al. [2017] (dash lines) over the 850–2000 CE over (a) Antarctica, (b) West Antarctica, and (c) East Antarctica. The mean slopes (in degrees per century) over the 850–1850 and 1958–2010 CE periods are shown to the right of each panel. Figure from Klein et al. [2019].*

In addition to this analysis of temperature evolution in models and reconstructions, it is also instructive to compare their representations of the changes in SAM. According to the reconstructions, SAM displayed large centennial variability during the last millennium as evidenced in the paleoclimate proxies [Abram et al., 2014; Dätwyler et al., 2018]. For instance, a minimum in the SAM index (i.e., negative SAM) occurred during the 1400s, and a positive trend in the SAM (with superimposed interannual to century-scale variability) is evident since then. Although current climate model simulations reproduce well the observed positive trend in the SAM over the past decades, models are unable to reproduce the structure or magnitude of pre-industrial SAM trends that are reconstructed from proxies further back in time, [Abram et al., 2014]. Some studies argued that volcanic forcing or solar forcing plays a role in the SAM variations [Fogt et al., 2017], but the mechanisms responsible for the centennial variability of the SAM are still on debate.

Currently, the Paleoclimate Model Intercomparison Project has progressed into the phase CMIP6-PMIP4 [Eyring et al., 2016]. However, the corresponding simulations for the past millennium (and for the past two millennia) were still not publicly available at the time of our analysis. Recent studies show that CMIP6 models generally show a modest improvement in performance compared to the CMIP5 models in simulating the Antarctic climate over the past

decades [Roach et al., 2020; Bracegirdle et al., 2020; Mohrmann et al., 2021; Lee et al., 2021]. For instance, the simulated regional distribution of Antarctic sea ice by the CMIP6 models has slightly improved and the intermodel spread in mean sea ice quantities has decreased compared to CMIP5. Consequently, the results derived from the CMIP5 models are likely also valid for the CMIP6 models.

Throughout this thesis, the climate model results are mainly drawn from simulations performed with the iCESM1. Critical for our purpose, iCESM explicitly simulates the transport and transformation of stable water isotopes (e.g., $\delta^{18}O$ and δD) in all of the model components. This model has been shown to reproduce key features of climate and isotopes in the present day and paleoclimate observations [Brady et al., 2019]. Dalaiden et al. [2020] has evaluated its ability to simulate the present Antarctic climate by comparing it to the latest ECMWF's atmospheric reanalysis ERA5 [Hersbach et al., 2020], as shown in Fig. 1.9. Over the 1979–2005 CE period, the patterns of geopotential height at 500-hPa, the near surface air temperature and snow accumulation are well simulated in iCESM1. However, iCESM1 is not able to reproduce the high spatial variability of snow accumulation at a local scale, especially on the coast of Dronning Maud Land and the Ross Sea, because of its coarse horizontal spatial resolution. In addition, the precipitation-weighted $\delta^{18}O$ pattern over Antarctica captures well the general gradient between the coast (with the highest values, less negative) and the Plateau (with the lowest values, more negative).

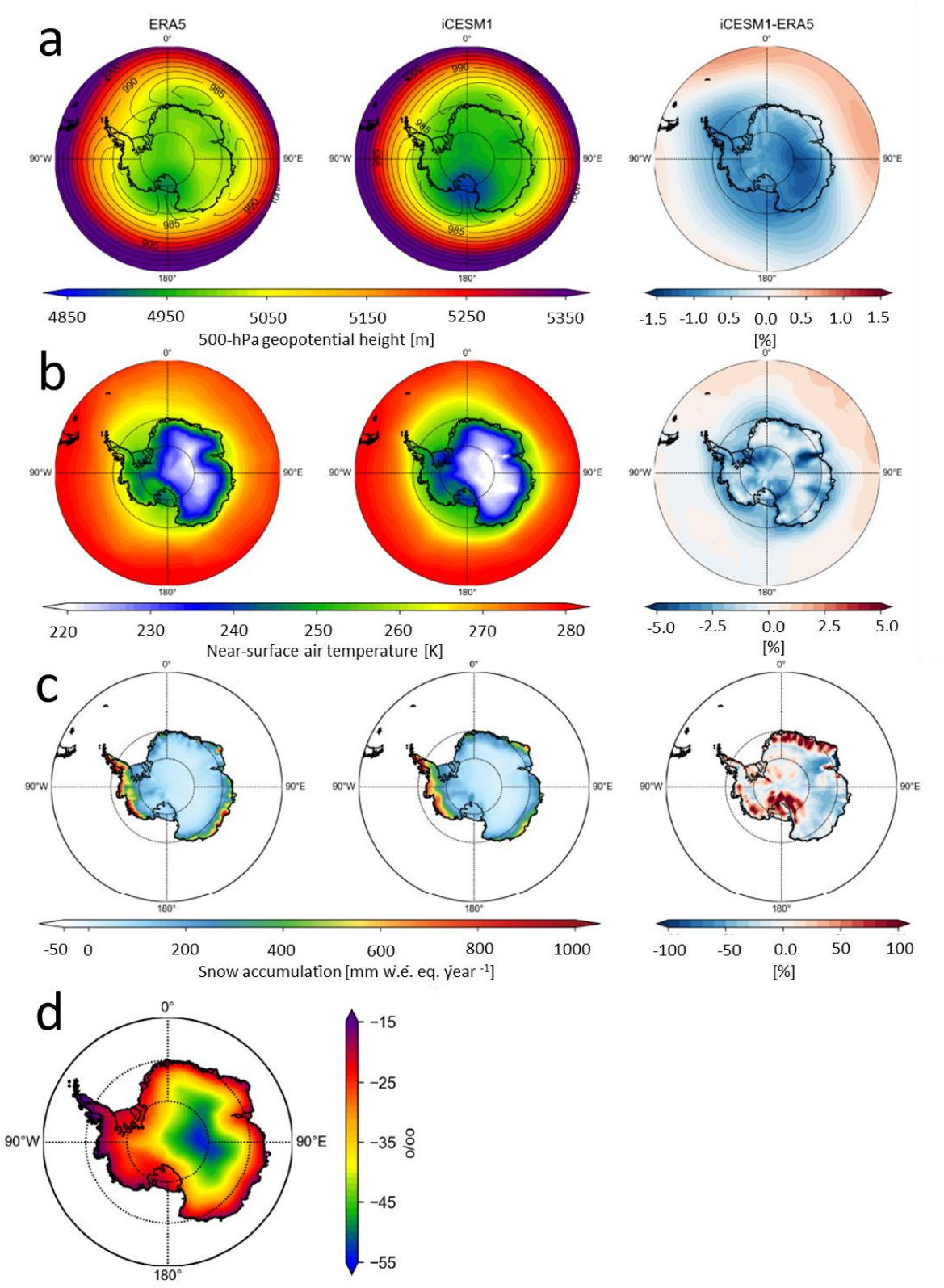

***Figure 1.9**: (a) Mean of 500-hPa geopotential height (m), (b) near-surface air temperature (K) and (c) snow accumulation (mm w.e. eq. year-1) from ERA5, and iCESM1, and the*

difference between iCESM1 and ERA5 (%) over the 1979–2005 period. For the 500-hPa geopotential height maps, contours represent the sea-level pressure (hPa). (d) Mean of precipitation-weighted ^{18}O (‰) from iCESM1 over the 1979–2005 CE period. Figure from Dalaiden et al. [2020].

1.5 Combination of modeling results and proxy records using data assimilation

Observations and modeling results are two complementary ways to study climate change. The optimal combination of modeling results and proxy records is potentially achieved by one approach, data assimilation (DA). This method is able to constrain climate models to follow the observed trajectory and provide a full spatial estimate for all variables simulated in climate models [e.g., Goosse et al., 2012; Hakim et al., 2016]. Therefore, it is very helpful to understand the mechanisms that might be responsible for the origin of the signals preserved in proxy records.

The basic state update equation of DA [e.g., Kalnay, 2003, chapter 5] is given by:

$$X_{\mathrm{a}} = X_{\mathrm{b}} + W(Y - H(X_{\mathrm{b}}))$$

In this equation, X_{b} is the prior (or "background") estimate of the state vector and X_{a} is the posterior (or "analysis") state vector. Vector Y denotes the observations (or proxies). $H(X_{\mathrm{b}})$ is referred to as an "observation operator", mapping X_{b} from the model state space to the observation space. W is a weight matrix determined by accounting for uncertainties in model results and observations.

Several methods are available to define the matrix W but the ones that have been applied in paleoclimatology over the past millennium are ensemble-based particle filters [e.g., Dubinkina and Goosse, 2013] and Kalman filters [Kalnay, 2003, Chapter 5]. The particle filter is based on a weighted mean across all ensemble members, and the weights are determined according to the closeness of each member to the available observations [van Leeuwen, 2009; Dubinkina and Goosse, 2013]. In this way, the particle-filters based DA method requires a large ensemble to provide a sufficiently good analogue to the observed state and thus particles with a large enough weight. However, when a few of particles close to the observation receive significant weights while others are discarded, one issue called particle degeneracy could occur, thus inducing the extra uncertainty for DA results. Such problems could be alleviated by reducing the degree of freedom such as performing appropriate time averaged or spatial filtering [Goosse et al., 2009; 2011; Mathiot et al., 2013]. In contrast, Kalman filters are more efficient with a limited number of ensemble numbers [Liu et al., 2017]. However, the particle-filters based DA method does not rely on any assumptions regarding the prior distribution of the prior, while Kalman filters assume that X_{b} and $H(X_{\mathrm{b}})$ are Gaussian-distributed and that their

errors are unbiased [van Leeuwen, 2009]. Consequently, particle-based data assimilation is applied in this thesis.

Data assimilation enables the propagation of information provided by proxy observations to other regions where proxy records are not available and is able to infer multiple climate fields consistent with available data and model physics at the same time. For instance, the assimilation of observed surface air temperature allows estimating the 500-hPa geopotential height by relying on the co-variance between the two variables in the model, as long as a co-variance between the assimilated variable and the analyzed variable exists. However, the covariance between climate variables could be non-stationary across different time scales [e.g., Steiger et al., 2014]. For instance, a two-timescale response to the strengthened westerlies has opposing effects on sea-ice cover. On interannual and shorter timescales, strengthened westerlies drive cooling and sea-ice expansion by advecting cold, surface mixed-layer waters northwards by the Ekman effect. On decadal to multidecadal timescales, this enhanced northward transport is thought to drive upwelling of warm, deep waters from below the mixed layer and lead to sea-ice reduction [Ferreira et al., 2015]. Therefore, it is essential to test the sensitivity of the reconstruction to the assimilation window (i.e., the temporal step in DA process) when applying data assimilation.

Some caveats and limitations of DA must be taken into account. Since DA uses a prior derived from the model states to fill in missing information from proxy records, the accuracy of DA-based reconstructions is limited by the ability of the models to reproduce real-world ocean and atmospheric circulation patterns. As a consequence, it is important to assess the performance of the model used in the data assimilation, at least for this thesis in simulating the near-surface climate over the Antarctic illustrated in Section 1.4. In addition, when the patterns present in the proxy data do not fit with the patterns produced by the models, the DA-based reconstruction represents an imperfect compromise between the conflicting sources of information that could smear out any real-world climate features [Mann, 2020]. Therefore, systematic validation of DA-based reconstructions against the independent proxy records is always necessary to ensure that the trade-off made by DA is reasonable.

There are two types of ensemble-based DA approaches applied in paleoclimatology [e.g., Matsikaris et al., 2015; Okazaki et al., 2021]. First, data assimilation can be used to update an ensemble of simulations at regular intervals (on-line data assimilation). In this process, the ensemble is generated sequentially and thus temporal consistency is ensured over the whole period. Another DA method is referred to as off-line data assimilation, which uses an existing ensemble of simulations as prior modeling results. It means that the prior is identical for all the time intervals and the reconstructed state at one time is not constrained by the previous ones. Therefore, the offline DA method using an existing ensemble of simulations allows to establish a DA scheme based on higher resolution GCMs or ESMs and thus larger ensemble size, while the on-line approach is currently achieved within EMICs or Linear Inverse Model

to achieve the balance between computer resources and generating sufficient ensemble members [e.g., Goosse, 2017; Perkins and Hakim, 2017]. The offline DA is fine for those states that can be considered independent of each other, but online data assimilation is more adapted if the slow component, such as the oceans, plays the dominant role in the state of the climate system [e.g., Goosse, 2017]. In other words, if the predictability of the variables of interest is shorter than the assimilation step, for instance for the interannual variations of atmospheric-related processes, an on-line technique would not outperform an off-line one [Matsikaris et al., 2015; Okazaki et al., 2021]. Consequently, particle-based offline data assimilation is applied in this thesis (the detailed mathematics related to this method in Supplementary D).

1.6 Objectives and outlines of this thesis

Characterizing Antarctic centennial climate fluctuations over the past two millennia is critical to understanding how the region may evolve with present human-induced climate change. To this end, the priority is to provide as reliable as possible reconstructions of past Antarctic climate variations. However, previous SAT reconstructions for Antarctica over the past two millennia based on ice-core water isotope records [i.e., Stenni et al., 2017] have demonstrated large uncertainties, in particular at the regional scales [Klein et al., 2019; An et al., 2021]. As a consequence, the physical processes ruling the Antarctic centennial temperature variability over the past two millennia are still unclear, and thus separating the contribution of internal versus forced variability is difficult.

Most of the ice-core water isotopic records used in Stenni et al. [2017] resolve high-frequency variations (i.e., at annual resolution). There are additional available ice core records with longer time coverage, such as those extending to the Holocene [e.g., Masson et al., 2000; Kaufman et al., 2020]. These records thereby are able to expand the spatial and temporal coverage over Antarctica, and in particular over the full Common Era, although with lower temporal resolutions (e.g., at decadal or multi-decadal time scale). They could potentially give us more information related to low-frequency processes in the climate system [e.g., Dee et al., 2017]. However, the main reason for not including those records in previous statistical-based reconstructions is the small overlap periods with instrumental data and thus a too short calibration period (e.g., 1979-2000) including a few data points at the low temporal resolutions of those records.

Such drawbacks shown in the statistical-based reconstructions could be overcome by data assimilation in paleoclimatology [e.g., Goosse et al., 2009; Widmann et al., 2010; Steiger et al., 2017; Hakim et al., 2016; Klein et al., 2019]. In particular, with the availability of the simulations performed with isotopic-enable GCMs (such as iCESM1), the current data assimilation version allows for achieving a direct comparison and combination between the modeled water isotopes and the observed ones [e.g., Steiger et al., 2017; Klein et al., 2019; Dalaiden et al., 2020]. The interest in the approach has been highlighted in a reconstruction of the regional SAT from the regional $\delta^{18}O$ composites of Stenni et al. [2017] with two isotope-

enabled climate models over the last two millennia [Klein et al., 2019]. Furthermore, since there is no need for calibration of the isotope-temperature relationship as for the statistical method, data assimilation allows combining additional water isotopic records with lower temporal resolutions and longer time coverage the during past two millennia over Antarctica.

Nevertheless, the number of $\delta^{18}O$ records is still limited and the recorded signals are too complex to faithfully capture the SAT over Antarctica for the past two millennia, and Klein et al. [2019] proposed to use additional climate-sensitive proxies, rather than simply relying on $\delta^{18}O$ records to estimate past temperature change. This is confirmed by Dalaiden et al., [2020]. Their results suggest that the reconstruction using the assimilation of both ice core snow accumulation and $\delta^{18}O$ data has higher skill than the one based on $\delta^{18}O$ records alone. In particular, the reconstruction of the surface climate state (e.g., surface air temperature, snow accumulation, and sea ice extent) in West Antarctica and surrounding seas is greatly improved by incorporating different records from recent compilations including $\delta^{18}O$ and snow accumulation, as well as the records in lower latitudes [Dalaiden et al, 2021; O'Connor et al., 2022].

In addition to those terrestrial records over Antarctica, there are some marine records reflecting the low-frequency changes in surface conditions of the Southern Ocean (e.g., sea surface temperature and sea ice) over the past two millennia [e.g., Crosta et al., 2021; Collins et al., 2018]. For instance, several alkenone sea surface temperature records from the Southern Chilean Coast suggest a clear cooling trend over the past millennium [Sepúlveda et al., 2009; Haddam et al., 2018; Caniupán et al., 2014; Collins et al., 2018]. This signal, however, does not fully coeval with the changes, in particular over West Antarctica as reconstructed by Stenni et al. [2017]. This difference between the Antarctic continent and the Southern Ocean may appear inconsistent with the expected strong interconnections in the Antarctic climate system as illustrated by close relationships between atmosphere and ocean (including sea ice) over the past decades [e.g., Goosse et al., 2005; Jones et al., 2016]. Therefore, understanding those signals preserved in marine records have the potential to inform on the past centennial-scale climate variability in Antarctica and the Southern Ocean during the Common Era by taking advantage of those links.

Although Klein et al. [2019] have assessed the compatibility between the reconstruction from Stenni et al. [2017] and the simulations performed with the PMIP3-CMIP5 models for seven regional means, the spatially heterogeneous nature of the Antarctic climate makes comparisons at smaller spatial scales also necessary. In this framework, borehole temperature measurements provide valuable reconstructions for some regional surface temperatures over the past two millennia in Antarctica [Barrett et al., 2009; Muto et al., 2011; Orsi et al., 2012; Zagorodnov et al., 2012; Roberts et al., 2013; Yang et al., 2018]. These independent long-term temperature records can thus give us important benchmarks for evaluating those modeling results, complementary to existing studies focused on other records. This has been done for some

regions of the world such as North America for which the performance of climate models over the last millennium, particularly in the aspect of the low-frequency surface temperature changes, has been assessed by the comparison with observed thermal profiles obtained from boreholes using a borehole forward model [Stevens et al., 2007; Gonzalez-Rouco et al., 2009]. Consequently, it would be very interesting to apply the same methodology to investigate the compatibility between modeling results and reconstructions based on borehole temperatures in Antarctica.

Finally, Klein et al. [2019] have focused their model-data comparison on the SAT over Antarctica during the past millennium. However, over the first millennia (1-1000 CE) the reconstruction from Stenni et al. [2017] also suggests large centennial variability, in particular, a significant asymmetry in SAT trends between East and West Antarctica. This potentially complex spatial structure of multi-centennial trends may differ significantly from that observed one between 1000 and 1850 CE, and thus may bring relevant information about the dynamics of the system.

In this thesis, our goal is to reconstruct the centennial variability of the Antarctic surface air temperature over the past two millennia and to understand the related physical processes by combining low and high-frequency records with climate model results using data assimilation. This joined use of different sources is needed as none is able alone to provide a complete picture of observed variations but, to our knowledge, it is the first time that it is applied to reconstruct Antarctic SAT over the past two millennia. Specifically, including here the low frequency records offers the ability to reproduce better the amplitude of the centennial variations. Furthermore, compared to previous reconstructions with data assimilation (e.g., Goosse et al. [2012]) focused on Antarctica, the longer time period covered allows for comparing the dynamics during the last millennium when forcing variations are larger and the first one where the forcing is more muted.

Therefore, to achieve this research goal, the thesis is divided into three chapters, each addressing a specific scientific question:

- Are current models able to reproduce the observed signals derived from borehole temperature over the past two millennia?
- Are there robust multi-centennial trends during the past two millennia observed in East and West Antarctica?
- Is there a coherent SAT evolution over Antarctica and surrounding seas over the past two millennia?

The main objective of Chapter 2 is to evaluate the GCMs' ability to reproduce the low-frequency SAT (multidecadal to centennial-scale) variability observed in borehole temperatures. To this end, we use the one-dimensional heat advection and diffusion model from Orsi et al. [2012] to simulate the propagation of the signal coming from the surface

temperature history into the subsurface of ice as borehole temperatures are exceptional at capturing low-frequency temperature variabilities. More specifically, four measured borehole temperatures in Antarctica and corresponding reconstructions are used to perform model–data comparisons using two different methods. The most straightforward way is to directly compare the surface temperature reconstructed from the borehole measurements with the surface-temperature time series simulated by the climate model at the grid cell closest to each site. However, due to the imposed-temporal smoothing on the time window of the reconstructions, which changes over time, the classical way of model-data comparison could be difficult [Beltrami et al., 2006; Harris and Gosnold, 1999]. Therefore, the alternative way is to compare the simulated subsurface borehole temperature with the observation by driving the forward model with climate model outputs. In this case, we analyze the temperature at a fixed time as a function of depth. The advantage of using a forward model is that the simulated subsurface temperature profile can be directly compared to the measured borehole temperature profile. Finally, some metrics derived from the corresponding reconstructions are proposed to be used more widely in model evaluation.

In Chapter 3, we aim to identify the robust low-frequency variability of the surface air temperature over Antarctica. In particular, we focus on the first millennia during which the proxy records show a clearly contrasted signal between East and West Antarctica at multi-centennial scale. We first present the general characteristics of the simulated SAT changes over the full Common Era in climate models and a comparison with several previous reconstructions, as until now no modeling study has been specifically devoted to the 1-1000 CE period. Since the flexible framework of data assimilation also makes it possible to combine high- and low-resolution isotope data, we then use this methodology to estimate the changes in surface air temperature over Antarctica over the past two millennia constrained by the ice core water isotope records with different temporal resolutions in order to identify robust signals.

While the analyses in Chapter 3 are specifically dedicated to the ice core records, in Chapter 4 we combine marine and terrestrial proxy records together using data assimilation to investigate the potential existence of a widespread cooling over West Antarctica and adjacent seas over the past millennium and the underlying mechanisms. We first study whether covariance relationship between several key climate variables (SAT, sea ice, and atmospheric circulation) in the DA process is timescale dependent. To achieve this, we compare two DA experiments that assimilate the same terrestrial proxy records but with the annual and decadal temporal resolutions. Then, to clarify the contributions of continental and marine records on the reconstructions, we separately perform two DA experiments: one assimilating the continental proxies and another assimilating continental and marine records. The assimilation of marine records is useful to have a stronger and more direct constraint on the evolution of the ocean-atmosphere coupled system. Both reconstructions are validated against independent sea ice-related marine records in order to identify which reconstruction is more faithful. Finally,

based on our reconstruction for multiple variables, we analyze the contribution of external forcing (e.g., volcanic forcing) and atmosphere internal processes on the long-term changes over the past millennium in West Antarctica.

The general conclusions, the main contributions as well as some perspectives of this thesis are discussed in Chapter 5.

2

Comparison of observed borehole temperatures in Antarctica with simulations using a forward model driven by climate model outputs covering the past millennium

Abstract

The reconstructed surface temperature time series from boreholes in Antarctica have significantly contributed to our understanding of multi-decadal and centennial temperature changes and thus provide a good way to evaluate the ability of climate models to reproduce low-frequency climate variability. However, up to now, there has not been any systematic model-data comparison based on temperature from boreholes at a regional or local scale in Antarctica. Here, we discuss two different ways to perform such a comparison using borehole measurements and the corresponding reconstructions of surface temperature at the West Antarctic Ice Sheet Divide (WAIS), Larissa, Mill Island and Styx Glacier in Antarctica. The standard approach is to compare the surface temperature simulated by the GCMs at the grid cell closest to each site with the reconstructions in the time domain derived from the borehole temperature observations. Although some characteristics of the reconstructions, for instance, the non-uniform smoothing, limit to some extent the model-data comparison, several robust features can be evaluated. In addition, a more direct model-data comparison based on the temperature measured in the boreholes is conducted using a forward model that simulates explicitly the subsurface temperature profiles when driven by the climate model outputs. This comparison in the depth domain is generally consistent with observations made in the time domain, but also provides information that cannot easily be inferred from the comparison in the time domain. The major results from these comparisons are used to derive metrics that can be applied for future model-data comparison. We also describe the spatial representativity of the sites chosen for the metrics. The long-term cooling trend in West Antarctica from 1000 to 1600 CE (-1.0 °C) is generally reproduced by the models, but often with a weaker amplitude. The 19th century cooling in the Antarctic Peninsula (-0.94 °C) is not reproduced by any of the GCMs, which tend to show warming instead. The trend over the last 50 years is generally well reproduced in West Antarctica and at Larissa (Antarctic Peninsula), but overestimated at other

This chapter is based on: Lyu, Z., Orsi, A. J., & Goosse, H. (2020). Comparison of observed borehole temperatures in Antarctica with simulations using a forward model driven by climate model outputs covering the past millennium. Climate of the Past, 16(4), 1411-1428. Supplementary materials are in Appendix A.

sites. The wide range of simulated trends indicates the importance of internal variability on the observed trends and shows the value of model-data comparison to investigate the response to forcings.

2.1 Introduction

Although most of the world has been steadily warming over the last few decades, the temperature trend in Antarctica is not homogeneous [Jones et al., 2016]. Several syntheses relying on instrumental air temperature records have shown a large recent warming over the Antarctic Peninsula (AP) and parts of West Antarctica, but the trend for the other parts of the Antarctic continent remains less clear [Chapman and Walsh, 2007; Nicolas and Bromwich, 2014; Steig et al., 2009; Turner et al., 2005]. It remains difficult to characterize the large interannual to multi-decadal variability at high southern latitudes because instrumental data are sparse, and limited to the last 60 years, at best. The mechanisms at the origin of recent changes are thus still uncertain [Goosse et al., 2012; Jones et al., 2016; Nicolas and Bromwich, 2014].

Proxy-based reconstructions offer the opportunity to place the recent temperature changes in a longer context. Thanks to their relatively good spatial coverage and high resolution, the reconstructions based on water stable isotopes derived from ice cores have provided important information on temperature variability during the past two millennia over Antarctica. They indicate a significant cooling trend during the preindustrial period across all Antarctic regions and confirm the strong spatial heterogeneity of the recent warming [Goosse et al., 2012; Schneider et al., 2006; Stenni et al., 2017]. However, the link between the isotope records and local climate is complicated, and this introduces significant uncertainties in the reconstructions [Stenni et al., 2017, Klein et al., 2019].

Borehole temperature observations provide another opportunity to reconstruct surface temperature and several studies have demonstrated their interest, particularly over Antarctica [e.g., Barrett et al., 2009; Muto et al., 2011; Orsi et al., 2012; Zagorodnov et al., 2012; Roberts et al., 2013; Yang et al., 2018]. The most significant advantage of borehole palaeothermometry is that temperature is directly measured with a thermistor calibrated in the laboratory. Therefore, the calibration is independent of the climate at the measurement site. Nevertheless, the characteristics of heat conduction that blur the surface temperature history make the reconstruction mathematically underdetermined: several temperature histories can result in the same borehole temperature profile, because diffusion will smooth out high frequency temperature variations. Consequently, the temperature history cannot be determined unequivocally. Several approaches have been proposed to overcome the problem, as synthesized by Orsi et al. [2012], for instance, the Bayesian Reversible Jump Markov chain Monte Carlo [Dahl-Jensen et al., 1999] and the generalized least-squares inversion [Muto et al., 2011; Orsi et al., 2012; Yang et al., 2018]. By applying these methods, the reconstructed temperature series have presented evidence of the existence of cold conditions corresponding to the Little Ice Age in West Antarctica from 1300 to 1800 CE [Orsi et al., 2012], as well as of a recent warming trend in West Antarctica [Barrett et al., 2009; Orsi et al., 2012; Yang et al., 2018], at some high elevation sites of East Antarctica [Muto et al., 2011; Roberts et al.,

2013] and over the AP [Zagorodnov et al., 2012], though the timing and magnitude vary between regions.

The reconstructed temperatures based on isotopic composition have been compared to the results of climate models. Most models display a relatively large and homogenous warming over Antarctica since 1850 CE, which is inconsistent with the signal inferred from the isotope records [Goosse et al., 2012; Klein et al., 2019; Stenni et al., 2017, Abram et al., 2016]. This disagreement may be due to the uncertainties in the reconstructions, or due to the biases in the climate models that may overestimate the response to greenhouse gas forcing or underestimate the natural climate variability in the region [Jones et al., 2016; Neukom et al., 2018]. However, a recent study assessing the link between isotope records from ice cores and regional climate over Antarctica using pseudoproxy and data assimilation experiments has not been able to identify any systematic bias in reconstructions on continental scale temperatures based on $\delta^{18}O$ [Klein et al., 2019].

Up to now, there were no systematic model-data comparison for temperature reconstructed from boreholes at a regional or local scale in Antarctica. This is, on the one hand, due to the characteristics of the inversion that imposes smoothing on a time window that increases as we go back in time and makes the comparison with the simulated surface temperature difficult [Beltrami et al., 2006; Harris and Gosnold, 1999]. Additionally, some reconstructions have an uncertainty range of the same magnitude as the full variability provided by the climate model results, which seriously limits the interest in model-data comparison.

As some of the difficulties in the comparison between the simulated surface temperature from climate model results and the reconstructions from boreholes come from the inversion procedure, comparing directly the observed profile with the one obtained using a one-dimensional heat advection and diffusion forward model can provide new insight. This approach is an example of the application of Proxy System Models (PSMs) that reproduce directly processes responsible for the signal recorded in the archive [Evans et al., 2013]. PSMs have been applied recently for several proxies, such as tree ring width or water-isotope in ice cores, corals, tree ring cellulose, and speleothem calcite [Evans et al., 2013; Dee et al., 2014]. The application of climate model outputs to drive a borehole temperature forward has demonstrated the strong coupling between near-surface air and ground temperature changes over decades to centuries [e.g., Beltrami et al., 2005; García-García et al., 2016; González-Rouco et al., 2003, 2006], and has also been used to validate climate model outputs [e.g., Beltrami et al., 2006; Stevens et al., 2008].

Nevertheless, using a PSM introduces some uncertainties that must be taken into account. A critical point for borehole temperature is the potential influence of long-term climate changes, such as glacial to inter-glacial cycles, which is difficult to estimate [Orsi et al., 2012, Rath et al., 2012]. In addition, the simulated subsurface temperature profiles in Antarctica are sensitive to model parameters and inputs, such as snow accumulation, ice thickness,

geothermal heat flow, and the physical properties of ice or ground, which may have significant uncertainties.

Previous studies using forward models driven by climate model outputs were focused on ground temperature [e.g., Beltrami et al., 2005; García-García et al., 2016; González-Rouco et al., 2003, 2006] and not on boreholes obtained in the ice. Here, we will fill in this gap by simulating directly subsurface temperature for the publicly available borehole profiles covering the past centuries in Antarctica, using the one-dimensional heat advection and diffusion forward model of Orsi et al. [2012]. Our goal is to provide a protocol for evaluating the climate model ability to reproduce observed low-frequency (multi-decadal to centennial scale) variability. We will analyze two model-data comparison methods to identify the potential advantages and drawbacks of each approach. The easiest way is to directly compare the surface temperature reconstructed from the borehole measurements with the surface temperature time series simulated by the climate model at the grid cell closest to each site. The second way is to compare the simulated subsurface borehole temperature with the observation by driving the forward model with climate model outputs. In this case, we analyze the temperature at a fixed time as a function of depth. For simplicity, we will later refer to those two methods as a comparison in the time domain and depth domain, respectively.

This study is organized as follows. The borehole temperature observations, the climate model results, the forward model and the sensitivity of the results to key parameters of the forward model are briefly described in Section 2.2. Section 2.3 presents the comparison of simulated and reconstructed surface air temperatures, and the comparisons of simulated and observed borehole temperature profiles. Some metrics of the Antarctic climate for model validation are proposed and discussed in Section 2.4. Conclusions are given in Section 2.5.

2.2 Data and methods

2.2.1 Borehole temperature observations and reconstructed surface temperature

The data used in this study include measured temperature in four boreholes in Antarctica. We refer to them as ‘WAIS’, ‘Larissa’, ‘Mill Island’, and ‘Styx’ respectively. Fig. 2.1 and Table 2.1 provide their locations and corresponding references. The borehole temperature profiles were sampled in January 2008 and January 2009 (WAIS), December-February 2009/10 (Larissa), the summer of 2009/10 (Mill Island), and the summer of 2014/15 (Styx). As shown in Fig. 2.1 (in red rectangles), the borehole temperature is affected by the seasonal cycle in the upper 15 meters [Bodri, et al., 2011, Chap. 1], which is not adequate for the reconstruction of annual mean surface temperature. Consequently, only the depth under 15 meters is used to reconstruct the surface temperature history and to compare it with simulated borehole temperature profiles.

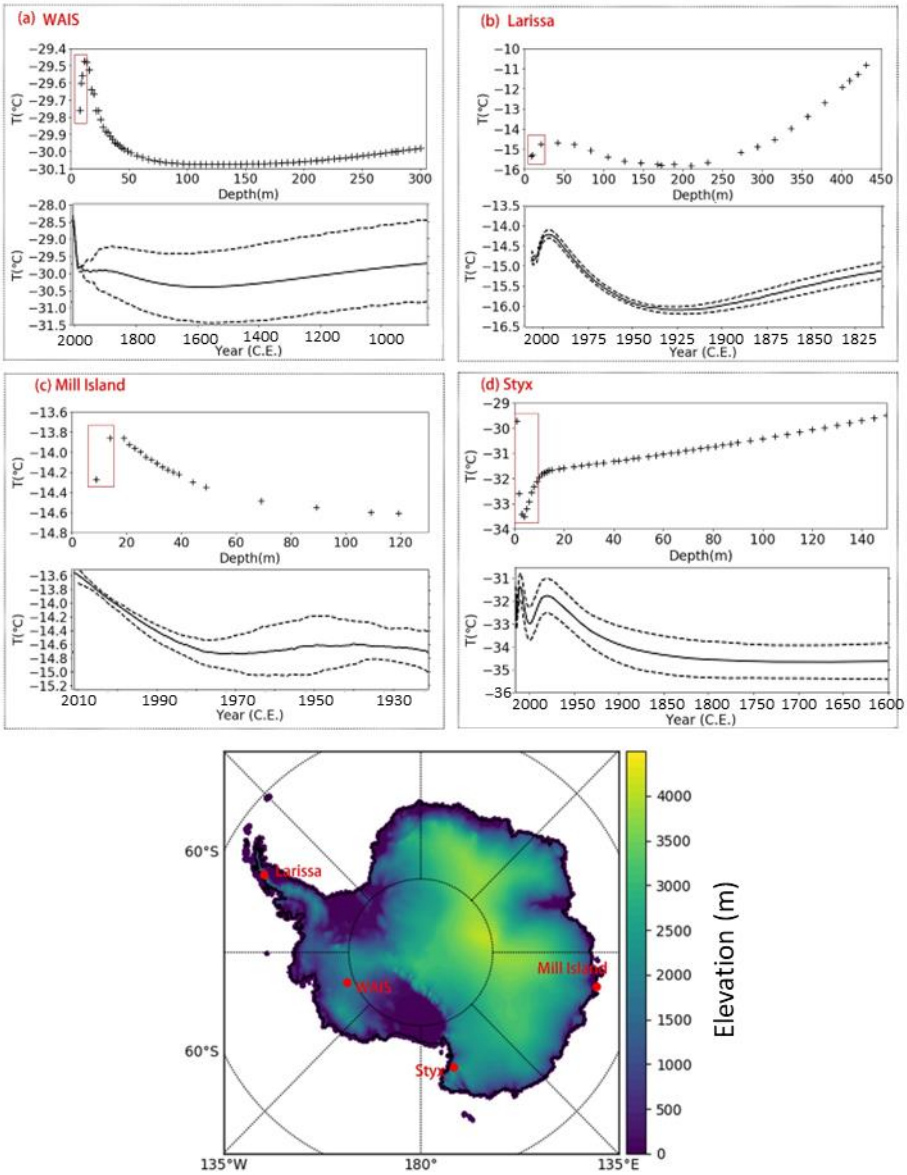

Figure 2.1*: The observed borehole profiles and corresponding surface temperature reconstructions at the four sites in Antarctica. The symbols (+) show the measured borehole temperature. The dashed lines represent the reconstructed uncertainty and the thick black lines are the mean reconstructed temperature. In (a), (b), (c), and (d), the red rectangles represent the borehole temperatures that are influenced by the seasonal cycle. The bottom panel shows the location of these four boreholes and their corresponding elevation over Antarctica.*

Table 2.1*: Location of the four boreholes. The elevation is in meters above sea level (m a.s.l.). Depth is in meters (m).*

Region	Referenced Name	Latitude	Longitude	Depth (m)	Elevation (m a.s.l)	Reference
West Antarctica	WAIS	79°28′S	112°05′W	3400	1766	Orsi et al. [2012]
Antarctic Peninsula	Larissa	66°02′S	64°04′W	447.73	1975.5	Zagorodnov et al. [2012]
East Antarctica	Mill Island	65°33′25.84″S	100°47′11.44″E	500	503	Roberts et al., [2013]
Western Coast of the Ross Sea	Styx	73°51.10′S	163°41.22″E	550	1623	Yang et al., [2018]

The temperature reconstructions and their uncertainty estimates for the four boreholes are shown in Fig. 2.1. For WAIS, Mill Island, and Styx, the reconstructed surface temperature series (Fig. 2.1 a, c, d) are computed using a generalized least-squares algorithm [e.g., Orsi et al., 2012]. For Larissa, the surface temperature is recovered by the Tikhonov regularization algorithm [Zagorodnov et al., 2012]. This method has been proved to be valid for inverse problems such as the reconstructions based on borehole temperature observations, and the details of this method are explained in Nagornov et al. [2001, 2006]. Since the temperature reconstructions are sensitive to the technique used, when we drive the borehole temperature model selected in this study by the published reconstructed temperature histories and compare them to the observed borehole temperature, differences are found. They are likely attributed to the different methodologies and hypotheses. However, they are relatively small (Fig. A6), suggesting that they do not have a major impact on the conclusions.

2.2.2 Climate model simulations

The simulated surface air temperatures used in this study (Table 2.2) are extracted from general climate model (GCM) simulations covering the past millennium performed in the framework of the third phase of the Past Model Intercomparison Project [PMIP3; Otto-Bliesner et al., 2009] and the fifth phase of the Coupled Model Intercomparison Project [CMIP5; Taylor et al., 2012]. These simulations cover the period 850-1850 CE (referred to as the past1000 experiment in CMIP/PMIP nomenclature) and the years 1850-2005 CE (historical period). For the majority of the models, the simulations start thus in 850 CE and finish in 2005 CE. However, for two of the models, CESM1-CAM5 and MPI-ESM-P, the historical simulations covering 1851-2005 CE were performed independently of the simulations covering 850-1850 CE. In order to obtain results over the full millennium, we adopt the approach from Klein and

Goosse [2018] and merge the first ensemble members (r1i1p1) of the past1000 experiment with the corresponding ensemble members of the historical experiment. Although not continuous, there is no large discrepancy in 1850 CE between the two merged simulations [e.g., Klein and Goosse, 2018].

These simulations are driven by natural (orbital, solar irradiance, volcanic) and anthropogenic (well-mixed greenhouse gases, ozone, aerosols, land use/land cover) forcings [Schmidt et al., 2011, 2012]. Note that, BCC-CSM1-1 and IPSL-CM5A-LR ignore the impact of land use/land cover, and IPSL-CM5A-LR does not consider any variations in aerosols and tropospheric ozone. Further description of the simulations and the forcing can be found, for instance, in Klein et al. [2016]. For CESM1-CAM5, it produces 12 different simulations with the same physics and same input forcings but slightly different initial conditions in the model. Therefore, the differences between ensemble members attributable to the process internal to climate system provide an estimate of the internal variability. For CCSM4, GISSE2-R, IPSL-CM5A-LR, MPI-ESM-P and BCC-CSM1-1, there is only one simulation available. In addition, although we can obtain the simulated surface mass balance (SMB) from these models [e.g., Dalaiden et al., 2020], we do not use it here and keep the observed accumulation rate in the forward model since biases in the simulation of SMB may affect our conclusions and the focus here is on the simulated temperature evolution.

Table 2.2*: Climate model simulations used to drive the forward model.*

Name	**Model resolution (lat × lon)**	**Number of simulations for 850-1850**	**Number of simulations for 1850-2005**	**Reference**
CESM1-CAM5	96 × 144	12	12	Otto-Bliesner et al., (2016)
GISS-E2-R	90 × 144	1	1	Schmidt et al. [2014]
IPSL-CM5A-LR	96 × 96	1	1	Dufresne et al. [2013]
MPI-ESM-P	96 × 192	1	1	Stevens et al. [2013]
CCSM4	192 × 288	1	1	Gent et al. [2011]
BCC-CSM1-1	64 × 128	1	1	Wu et al. [2014]

2.2.3 The forward model description

The forward model used herein to simulate the propagation of the signal coming from the surface temperature history into the subsurface is based on the one-dimensional heat and ice flow equation [Alley and Koci, 1990]:

$$\rho c_p \frac{\partial T}{\partial t} = \frac{\partial}{\partial z}\left(k \frac{\partial T}{\partial z}\right) - \rho c_p w \frac{\partial T}{\partial z} + Q \qquad (1)$$

where T is the temperature, t is the time, c_p is the heat capacity, ρ is the density of firn/ice, z is the depth, w is the downward velocity of the firn/ice, Q is the heat production term. In the Eq. 1, the term on the left side represents the change in heat content. On the right side, the first term corresponds to the rate of temperature change due to conduction based on the Fourier's law. Ice moving vertically (z-direction) with downward velocity, w, conveys a heat flux ρcpwT across a plane of unit area, oriented perpendicular to z, which is accounted for in the heat transfer by advection shown as the second term. The third term, Q, consists of two parts: (1) ice deformation [Cuffey and Ocean Sea 2010, Chap. 9, Eq. 9.30] and (2) firn compaction [Cuffey and Paterson, 2010, Chap. 9, Eq. 9.33]. Important model parameters are obtained from the references given in Table 2.1, and they are summarized in Table 2.3. A detailed description of the model is available in the supplement material.

Table 2.3 *Optimal parameters used to simulate subsurface temperature profile in the forward model driven by the reconstruction for each site: (a) WAIS; (b) Larissa; (c) Mill Island; (d) Styx.*

Site	**Surface temperature for steady state (℃)**	**Accumulation rate (m/second)**	**Temperature (T) at bottom (℃)**	**T gradient at bottom (℃/m)**	**Ice thickness (m)**
WAIS	-29.73	6.97×10^{-9}	-4.685	0.0256	3400
Larissa	-16	4.147×10^{-8}	-10.2	-0.04	447.73
Mill Island	-14.6	4.53×10^{-8}	-14.6	0	500
Styx	-32.5	2.6985×10^{-9}	-20.5	0.022	550

2.2.4 Sensitivity of subsurface temperature to model parameters

According to the original studies describing the records and the surface temperature reconstructions, the various parameters in the forward model have effects of different magnitudes on the results for the different sites. Consequently, in order to assess the uncertainty in the model-data comparison related to the parameters of the forward model, we perform a series of sensitivity experiments on the parameters which have been shown to have the largest effects on each of the borehole profiles shown in Fig. 2.2.

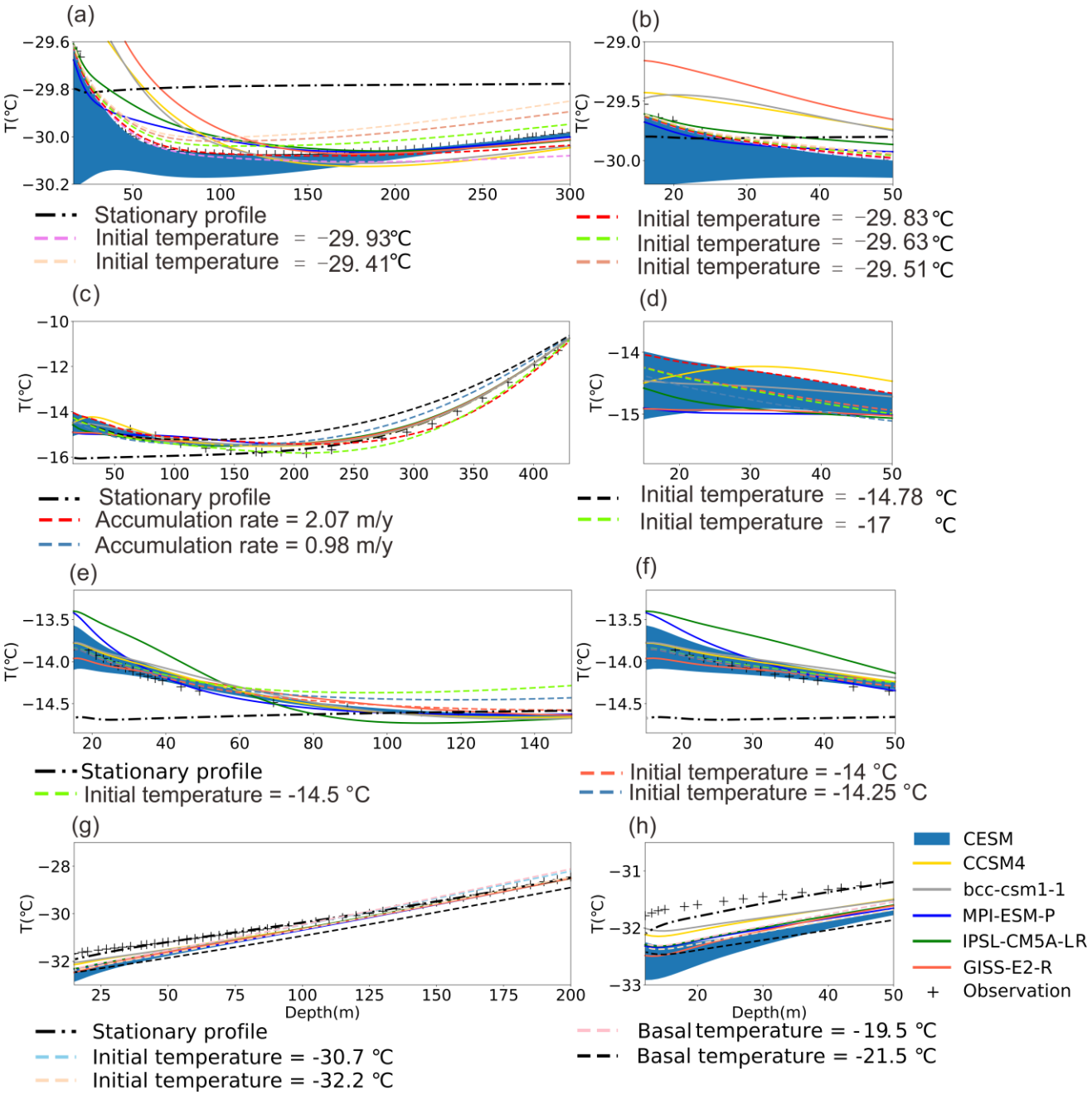

***Figure 2.2**: Comparison of borehole temperature profile outputs for the forward model driven by GCM surface temperature time series with optimal parameters (solid lines), and sensitivity tests using the temperature history of one CESM member (dashed lines) at each site. (a) WAIS: 15-300 m; (b) WAIS: 15-50 m; (c) Larissa: 15-430 m; (d) Larissa:15-50 m; (e) Mill Island:15-150 m; (f) Mill Island:15-50 m; (g) Styx:15-200 m; (h) Styx:15-50 m. The shaded area represents the simulated subsurface temperature ensemble driven by CESM using optimal parameters. The thick dash-dot line denotes the stationary profile at each site.*

At WAIS-Divide, the spread of the sensitivity tests is lower than the spread in the simulated borehole profiles driven by different climate model results (solid lines in colour in Fig. 2.2 a and b). However, the initial temperature derived from a steady state profile has an influence on the slope of the profile in the deeper part and on the depth of the temperature minimum, contributing to the uncertainty in the intensity of the pre-1900 cooling trend and the timing of the temperature minimum.

At Larissa, the effect of the bottom boundary conditions is important in setting up the temperature gradient from the bottom to 300 m, and therefore, we will not interpret that segment of the data in terms of climate. It is also evident in Fig. 2.2 c that the different temperature histories produce a very similar depth profile over that interval.

At Mill Island, the borehole profile is shallow and covers only a fraction of the full thickness of the ice sheet. At sites with such a deep ice sheet and with a high accumulation rate, the optimal surface temperature history was found to be essentially independent of the location of the imposed bottom boundary condition for depths in excess of 180 m below the surface [Roberts et al., 2013]. Consequently, here we modelled the temperature by assuming a zero heat flux bottom boundary. Although the initial temperature has an influence on the slope of the profile deeper than 120 m, this sensitivity is weak at the depth shallower than 80 m, and the borehole profile is dominated by the surface temperature history.

At Styx, the bottom boundary condition is adjusted to reproduce the slope of the temperature profile in the deeper part (100-200 m). The simulated borehole profiles driven by GCMs (solid lines in Fig. 2.2 e) show the large deviation in the top 100 m compared to the stationary temperature profile, which suggests that there is climate information stored in the upper part of the profile. Meanwhile, At depths below 50 m, the effect of boundary conditions is weaker than the differences in the temperature histories from the different models, which implies that the borehole temperature data can be used to discriminate between temperature histories provided by the different models.

The internal variability also has a significant impact on the shape of the simulated borehole profiles. At these four sites, the range of simulations driven by the CESM ensemble is much larger than the range of the different sensitivity tests in the top of 50 m (shown as the shaded area in Fig. 2.4 b, d, f, and h). This confirms that internal variability is a dominant source of uncertainty in a model-data comparison, at least in the top 50 m. For the deeper part of WAIS, as the shape of subsurface temperature profiles is influenced by the parameters of the forward model, the evaluation of the long-term cooling trend is more uncertain.

2.3 Results

3.1 Comparison between the simulated temperature and reconstructions

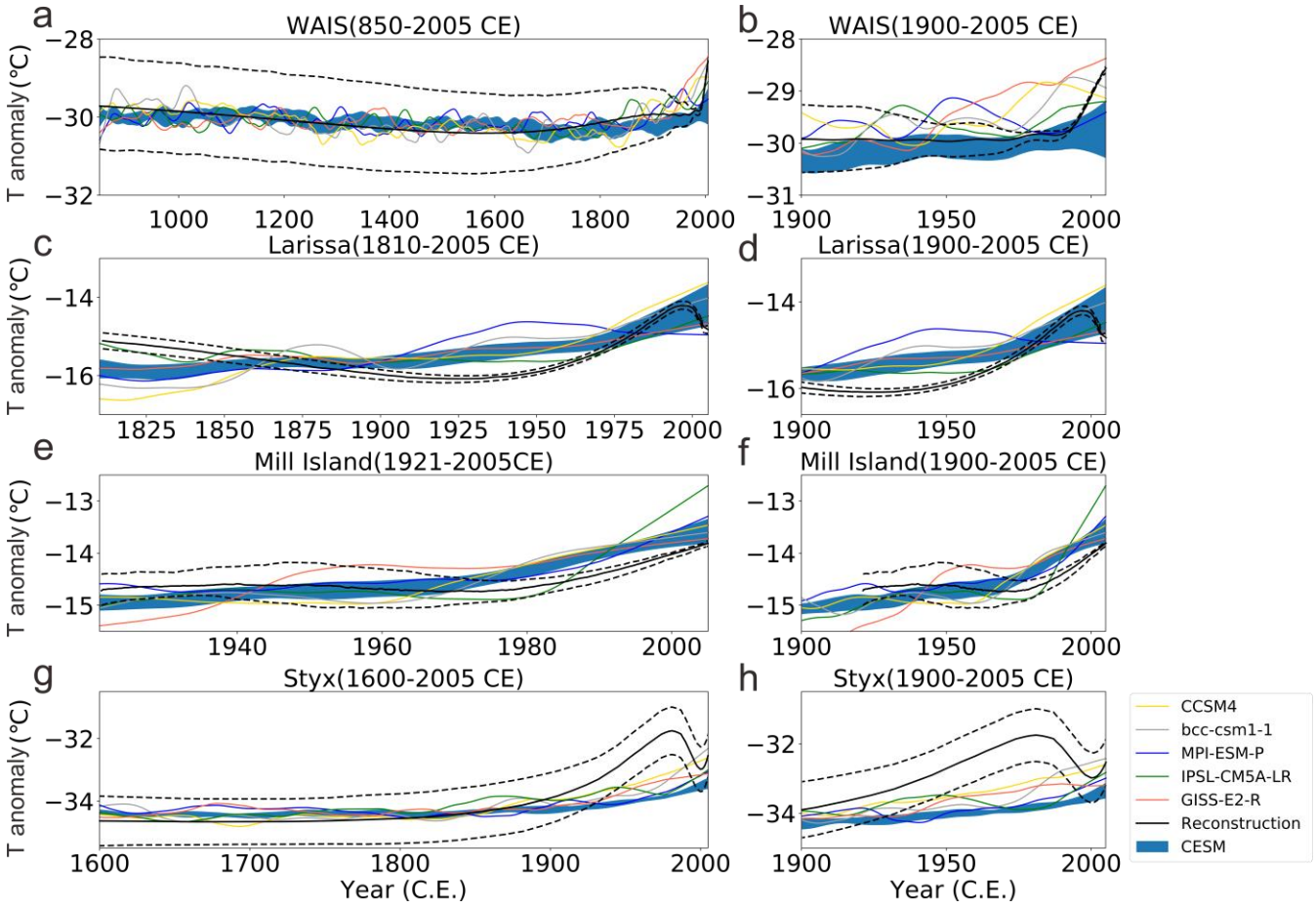

***Figure 2.3**: Comparison between reconstructed surface temperature series from boreholes and the climate model outputs at the grid cell closest to each borehole site. The borehole reconstructions are in black and their uncertainty ranges are given by the dashed lines. Colour lines correspond to the climate model results. The shaded area represents the mean ±1 standard deviation of the CESM model ensemble. For the left column, a 50-year Lowess smoothing has been applied for the WAIS and Styx time series; Larissa and Mill Island are smoothed using 10-year and 3-year windows respectively. The time series in the right column is smoothed using 3-year from 1900 to 2005 CE.*

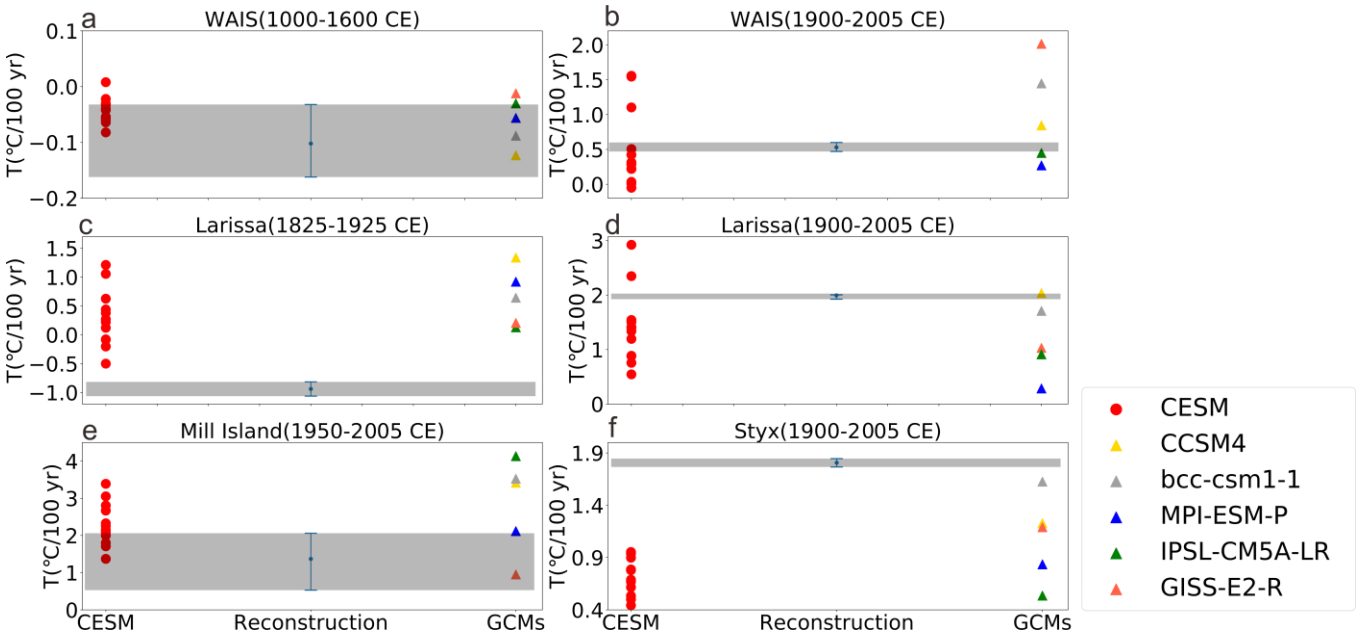

***Figure 2.4**: Linear trends for the four boreholes over different periods: (a) WAIS: 1000 to 1600 CE; (b) WAIS: 1900 to 2005 CE; (c) Larissa: 1825 to 1925 CE; (d) Larissa: 1900 to 2005 CE; (e) Mill Island: 1950 to 2005 CE; (f) Styx: 1900 to 2005 CE.*

Figure 2.3 displays the comparisons between climate model results and temperature reconstructions from the boreholes. The simulated temperatures displayed in Fig. 2.3 come directly from the surface temperature calculated by the climate model, based on its own dynamics and the forcing applied as discussed in Section 2.2. In order to ensure that the climate model results have the same mean over the reference period (which is the whole period derived from the reconstruction) as the reconstruction, we applied a very simple, constant correction to remove the mean bias of the climate model results as shown in Fig. 2.3. Due to the nature of physical diffusion, the heat propagation acts similarly as a low-pass filter. The reconstructions thus suffer from an attenuation of high frequency temperature variability that becomes stronger as time goes back [Beltrami et al., 2006; Harris and Gosnold, 1999]. For instance, in the reconstructed surface temperature of Styx, the point corresponding to 1800 CE in the curve may represent an average temperature between around 1600 CE and 1900 CE, while in 1900 CE it corresponds to an average over around 200 years. This characteristic complicates the model-data comparison. Therefore, in order to facilitate the comparison between the reconstruction and climate model results, we use variable smoothing to mimic the characteristic as much as possible. Since the reconstructions have much wider ranges than those from the climate model results, the basic compatibility between the model and data will not be changed due to various smoothing. Nevertheless, Fig. 2.3 must be interpreted carefully because of this inhomogeneous smoothing.

Because of the internal variability of the system, a single simulation without error bound is not expected to reproduce well all the characteristics of the observed variations. The difference can be large, in particular at the local level [e.g., Goosse et al., 2005], but the observations should correspond to a credible member of an ensemble of simulations. Ensuring this compatibility can be achieved using various techniques but the first step is to simply check if the reconstruction is within the range provided by the ensemble [e.g., PAGES2k-PMIP, 2015].

Considering the large uncertainty range in these reconstructions, the climate models are visually able to reproduce the general characteristics of reconstructed temperature variability, particularly the long-term cooling during the last millennium and the recent warming (Fig. 2.3 and 2.4). Nevertheless, disagreements have also been identified.

The first major feature in the data is this long-term cooling trend, visible at the WAIS-Divide and Larissa sites. At Larissa, the borehole temperature reconstruction gives a cooling trend of -0.94 $\pm$ 0.12 °C/century from 1825 to 1925 CE [Zagorodnov et al., 2012]. None of the models is able to reproduce this observation, and instead, they all show a warming trend of comparable magnitude (Fig. 2.3 c and 2.4 c). At WAIS-Divide, the borehole temperature inversion also shows a long-term cooling trend, from 1000 CE to about 1600 CE, with a magnitude of -0.10 $\pm$ 0.07 °C/century (Fig. 2.3 a). The large uncertainty in the long-term trend is principally due to the uncertainty in the initial surface temperature [Fig. 2.2 a; Orsi et al., 2012, their Fig. 3]. The quantitative comparison between the trend of reconstructions and climate model outputs (Fig. 2.4 a) indicates that the simulations generally show a cooling trend over 1000-1600 CE, in agreement with previous studies [e.g., Goosse et al. 2012, Abram et al. 2016, Klein et al. 2019]. The amplitude of the trend is lower, particularly for GISS (-0.01 °C/century) and IPSL (-0.03 °C/century) models, but most remain within the lower end of the reconstructed uncertainty range. This long-term cooling trend is a feature of the Antarctic climate that is visible in many other ice core records [Stenni et al., 2017]. A recent compilation of PAGES Antarctica 2k datasets calculated a trend of -0.26 to -0.4 °C/1000 years for the period 0-1900 CE for the Antarctic continental average [Stenni et al., 2017]. In the high latitudes of the Southern Hemisphere, the origin of this millennial-scale cooling is currently not well understood, but an intermediate complexity model has shown a multi-millennial cooling in summer because of a delayed response to the decrease in local spring insolation [Renssen et al., 2005] with also a potential influence of volcanic forcing [Goosse et al. 2012, Abram et al. 2016, Stenni et al. 2017].

A second feature of the data is a warming trend in the twentieth century, which started at different times in the different records. Styx shows an early warming trend from 1900 to 1980 CE, and general stabilization of the temperature afterward (Fig. 2.3 h). This signal is consistent with the data from weather stations, and ice core isotope-derived records [Yang et al., 2018]. Models tend to show the opposite timing, with nearly no trend from 1900 to 1960 CE, and a late warming trend that differs in amplitude between models. Overall, the simulated warming

of the 20th century is about half of what is observed (Fig. 2.4 f), with bcc (1.63 °C/century) and CCSM4 (1.23 °C/century) having the largest trends, closest to the observations (1.81 °C/century).

Larissa shows a temperature minimum in the 1940s, followed by a steady warming trend until around 1995. The magnitude of the 20th century trend is 1.99 °C/century. Most models reproduce the timing of the warming reasonably well, with the exception of MPI, which shows an early warming, but no trend in 1940-2005, and GISS, which has a very muted trend. If the trend present in the other models is too low, it seems rather due to a lack of cooling in the preceding century, than because of errors in the latest decades.

Mill Island shows a late warming trend starting in the 1980s. Models tend to overestimate this trend (Fig. 2.4 e), in particular IPSL, bcc and CCSM4. Similarly to Mill Island, WAIS-Divide also shows a positive trend over the period 1900-present that intensifies after 1980. The amplitude of the 20th century warming (0.53 °C/century) is well simulated, but the start of the trend occurs sometimes too early, with the exception of CESM, bcc and IPSL, which show a late warming trend (Fig. 2.3 b).

Overall, for WAIS (Fig. 2.4 b) and Larissa (Fig. 2.4 d), the reconstructed trends lie in the CESM ensemble range, suggesting many apparent model disagreements for those sites can be due to internal variability. For Styx (Fig. 2.4 f) and Mill Island (Fig. 2.4 e), the reconstructed trends are larger than the spread of the CESM ensemble, which means the disagreements are not only due to internal climate variability but are related to a systematic climate model bias in this region.

However, as stated above, borehole temperature reconstructions are “underdetermined”, which means that there are many possible temperature histories that can fit the data (a more detailed explanation of “underdetermined” is given in the Introduction). The next step is to determine if the differences between simulated and reconstructed time series can be discriminated when analyzing observed and simulated temperature profiles.

2.3.2 Comparison of the simulated subsurface temperature with observation

The simulated subsurface temperature profile is the result of the superposition of two components: (1) the initial temperature profile that incorporates the effects of basal heat flux and vertical advection due to ice accumulation; (2) the subsurface temperature deviations arising from the surface temperature variability. Since the initial temperature profile for each borehole is obtained by driving the forward model with the optimal parameters obtained from the original publications (see Section 2.4), the differences among the simulated borehole profiles for each location are caused only by the changes in the upper boundary, i.e., in the climate model outputs. The simulated subsurface temperature profiles for each borehole are displayed in Fig. 2.5.

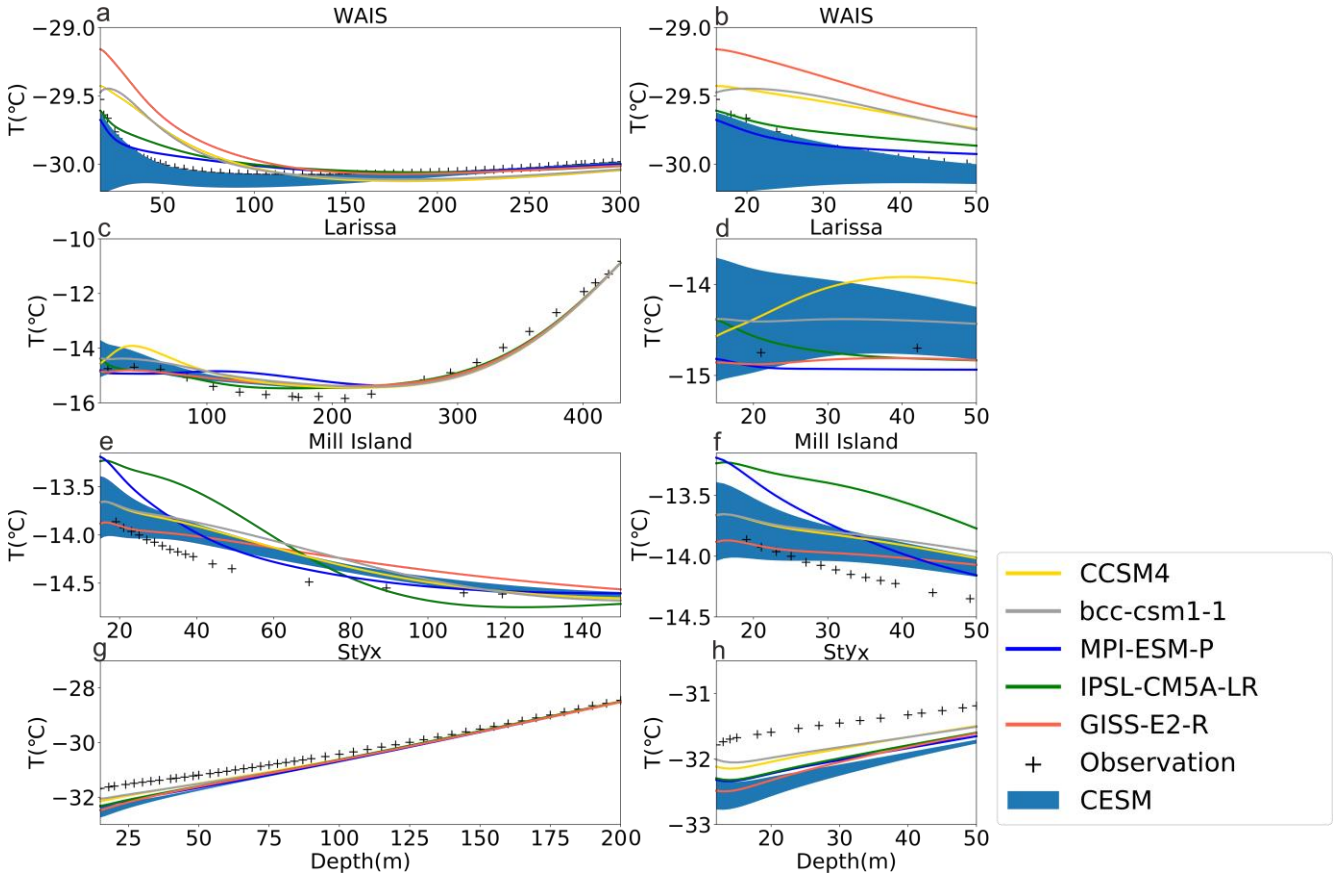

***Figure 2.5**: Comparisons between simulated subsurface temperature and measurements for: (a) WAIS: 15-300 m; (b) WAIS: 15-50 m; (c) Larissa: 15-430 m; (d) Larissa:15-50 m; (e) Mill Island:15-150 m; (f) Mill Island:15-50 m; (g) Styx:15-200 m; (h) Styx:15-50 m. The shaded area represents the simulated subsurface temperature ensemble driven by the CESM ensemble. The right panel is a zoom over the upper 50m for each borehole.*

As previous studies shown [e.g., Bodri, Louise, and Vladimir Cermak, 2011, Chap. 2], a 'U' shape subsurface temperature profile is direct evidence of past climate change with a minimum that separates the deeper warming trend due to geothermal heating and the shallower warming trend related to a recent temperature increase [Orsi et al., 2012; Stevens et al., 2008]. Among these four sites, WAIS and Larissa have such characteristics of a 'U' shape. For Mill Island, this is less clear but a significant breaking point in each simulated subsurface temperature profile reflects the surface temperature warming over recent decades. For Styx, such a break does not seem to be present at all and the slope does increase with depth.

Aided by these key properties, we can identify a link between the interpretation in the depth domain and in the time domain. The analysis of the simulated and observed temperature profile confirms the main conclusion obtained in Section 2.3.1, in particular the agreement between the model and data on the general tendencies, characterized by a long-term cooling trend over the last millennium and the recent warming. For the deeper part of the profile, the simulated

temperature profiles driven by MPI, IPSL, and GISS at WAIS almost coincide with the corresponding observation, but they fail to reproduce the depth of the temperature minimum around 120 m in the data. This is consistent with the fact that IPSL and MPI are at the edge of the reconstructed cooling trend of the last millennium and GISS presents a significant underestimation of this trend (Fig. 2.4 a). On the other hand, the CESM ensemble follows the borehole temperature profile (shaded area in Fig. 2.5 a), and can also reproduce the magnitude of the cooling trend for some of the members (Fig. 2.4 a). Specifically, the minima in the simulated profiles driven by MPI, IPSL, GISS, and CESM are -30.06 ℃, -30.06 ℃, -30.07 ℃, and a range of -30.8 ℃ to -30.17 ℃ respectively, which is very close to the minimum of -30.08 ℃ in the observation.

At Larissa, the bottom (270-450 m) of the profile is controlled by boundary conditions (Fig. 2.2 c), and contains no climate information, as demonstrated by the fact that all curves are on top of each other in Fig. 2.5 c. Additionally, no simulation has a pronounced inflection point around 170 m as shown in the observations. These characteristics are perfectly consistent with the lack of a cooling trend from the mid~19th century to the early 20th century in the simulations (Fig. 2.3 c). We conclude from this that the cooling trend of 1825-1925 CE is a robust feature in the data that can be used to benchmark climate models.

For the recent warming, we see some significant discrepancies among the simulated subsurface temperature profiles driven by different climate models at the four boreholes in the depth domain that are consistent with the signal analyzed in the time domain. For WAIS, in the uppermost part, the simulated subsurface temperature profiles driven by GISS, CCSM4, and bcc display significantly higher temperatures than those in the observations, while IPSL and MPI-simulated profiles are close to the observations (Fig. 2.5 b). This is in perfect agreement with the too high temperatures in models compared to the reconstructions in the second half of the 20th century (Fig. 2.3 b).

For Larissa, all simulated profiles display an increasing temperature toward the surface as in observations but with different magnitudes and shapes (Fig. 2.5 c). The temperature in the simulation driven by the MPI displays a relatively rapid increase until around 100 m and then is constant, which is consistent with the near constant temperature from 1940-2005 CE (Fig. 2.3 d). For the ones driven by CCSM4 and bcc, they are warmer than the observations between the depth of 15 to 50 m, which reflects the consistently larger temperature shown in Fig. 2.3 d. The IPSL-simulated subsurface temperature profile displays the largest similarity to the observations, whilst the simulations performed with CESM can cover almost all the observations in the shallow zone.

For Mill Island, the simulated subsurface temperatures are larger than observations above 50 m, confirming the too large warming trend deduced from the analysis of surface temperature. In particular, the IPSL model has the largest warming trend (Fig. 2.3 e and 2.3 f)

and also has the warmest temperature profile (Fig. 2.5 e and f), followed by MPI. For Styx, the main discrepancies occur over the shallow depths, between 15 to 60 m, where all the simulations depict colder conditions compared with observations (Fig. 2.5 g and h), as for the surface temperature over the recent decades on Fig. 2.3.

We also find in the depth domain some signals that are not obvious in the time domain. In particular, for WAIS, one of the CESM runs matches the warming trend of the top 100 m, while in the time domain, the CESM ensemble is significantly colder than the reconstruction over recent decades. The CESM outputs generally follow the data in the deeper part of the profile (200-300 m), and have an even steeper slope between 100 and 200 m (Fig. 2.5), while in the time domain, the cooling trend is underestimated (Fig. 2.4 a). In addition, for WAIS, the simulated subsurface temperature profiles driven by CCSM4 and bcc in the deeper part of the profile are colder than observations, but the warming trend starts deeper, at about 200 m against 120 m in the observations. This seems puzzling because, in the time domain, the cooling trend continues until 1800 CE for CCSM4 (Fig. 2.2 a, yellow). However, the larger warming in the last 100 years is probably shifting the temperature minimum downwards. This example shows that it is difficult to pinpoint the date corresponding to a temperature minimum in the depth profile, because it depends on the respective speed of warming and cooling before and after. At Mill Island, in the deeper part (around 140 to 100 m) of the profile, the simulated subsurface temperature profile driven by IPSL, is very different from the other ones, with a slightly decreasing temperature and a colder climate than observations. However, in the time domain, the difference compared to other time series for IPSL was much less clear (Fig. 2.3 e) but the consistency between these two domains still exists, and especially the temperature minimum in 1980 CE might correspond to the deeper part (around 100 m) in the depth domain.

The comparison between the analyses in the two domains appears thus complementary and instructive as it illustrates that the interpretation may be easier in one case or the other. It also shows the observations can help to evaluate the models by comparing different borehole temperature profiles driven by different climate model results with the corresponding observations. In particular, the analysis of the simulated temperature profiles confirms that the CESM ensemble can reproduce the multi-decadal and centennial climate variability at WAIS.

2.4 Proposed metric of Antarctic climate for model validation

In this section, we use the results of the previous section to describe a few metrics that can be used easily to evaluate the next generation of climate model simulations [e.g., PMIP4-CMIP6, Jungclaus et al., 2017], and investigate the spatial representativity of the records.

2.4.1 Metric 1: last millennium cooling at WAIS Divide

Of the four records presented here, WAIS-Divide has the longest retrievable history. We propose here to use the temperature trend of the period of 1000 to 1600 CE as a metric, with a

magnitude of -0.102 ± 0.07 ℃/century (Fig. 2.4 a). The end of the cooling trend is not clearly defined by the data, due to the complex time-varying smoothing of the borehole temperature record, but 1600 CE seems to be safely in the cold interval [see Orsi et al., 2012, for details]. The start of the period is more open, and we chose 1000 CE to be compatible with the last millennium simulations. External evidence from a compilation of water isotope records indicates that the cooling trend extended likely from 0 to 1900 CE in many parts of Antarctica [Stenni et al., 2017]. It is a robust feature of the Antarctic climate of the last 2 ka, and the WAIS-Divide record is unique in providing a clear quantification of the temperature trend.

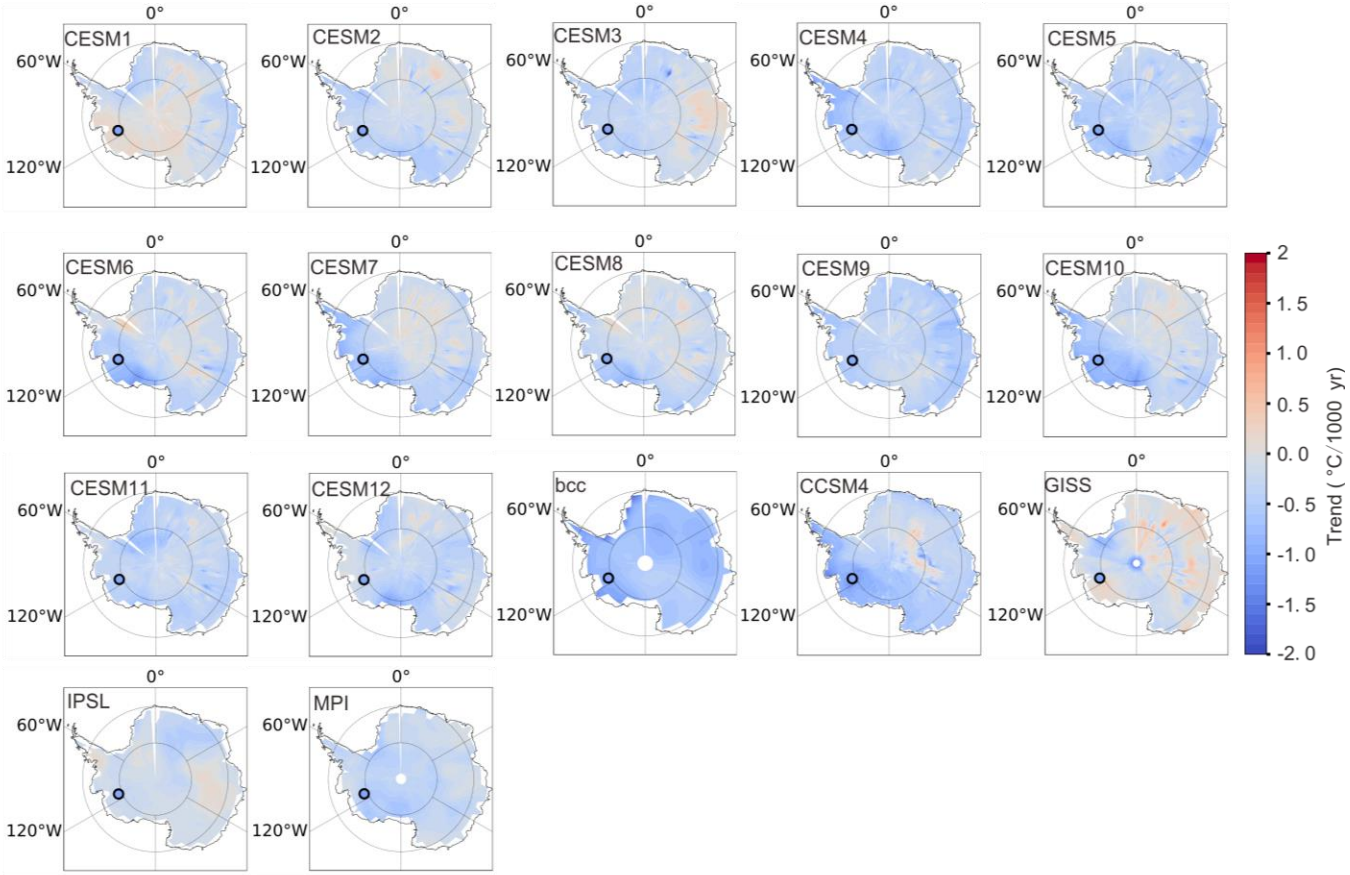

***Figure 2.6**: The simulated (blue-red shading area) and observed (circle) surface temperature trend from 1000 to 1600 CE in Antarctica.*

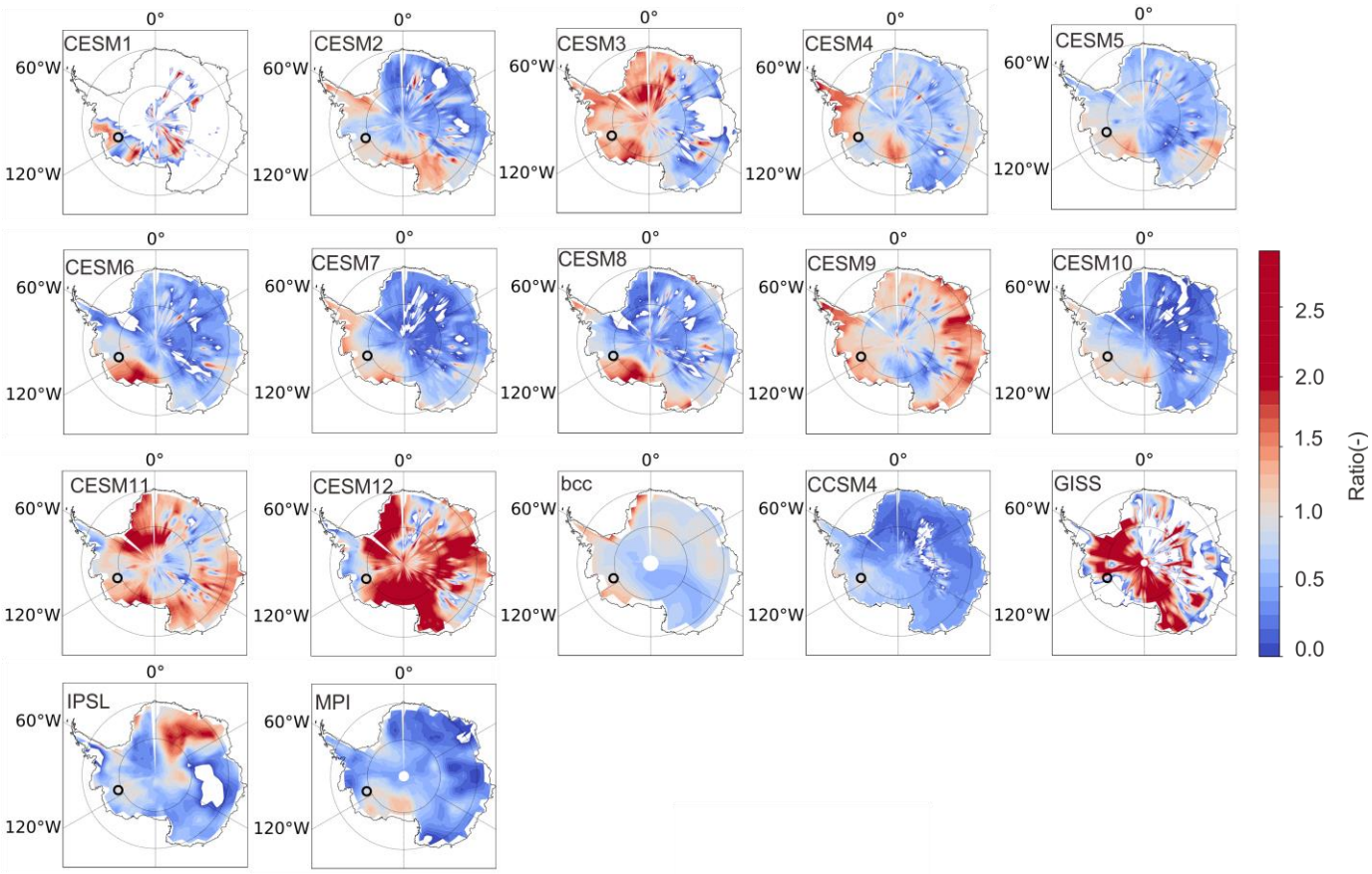

***Figure 2.7**: The ratio of the surface temperature trend (blue-red shading area) from 1000 to 1600 CE between other grid cells in Antarctica and WAIS-Divide. The black circle denotes the location of the WAIS-Divide.*

In Fig. 2.6, we show the 1000 to 1600 CE surface temperature trend at WAIS-Divide and other sites in Antarctica from the model output. Visually, for most simulations, the cooling at the grid cell of WAIS-Divide is similar to the one obtained at many locations in West Antarctica. Only the first member of CESM and GISS show a small warming trend in West Antarctica. The large spatial coherence of the trend indicates that, although we are making a single point comparison, it represents a signal common to a large part of the continent. It is also important to estimate the magnitude of the trend at WAIS compared to other regions. To do so, we calculate the ratio of the trend of surface temperature from 1000 to 1600 CE at any location with the one at WAIS-Divide (Fig. 2.7). Except the first member of CESM, if the value is greater than 1 (shown in red tones), it means that the trend at the grid cell is larger than that at WAIS-Divide; if the value lies between 0 and 1 (shown in blue tones), it means that the trend at the grid cell is less than that observed at WAIS-Divide. Negative values (i.e., a trend of a different sign compared to WAIS) are not shown and the corresponding region is blank. Since the goal of Fig. 2.7 is to show the intensity of cooling at WAIS compared with other points in Antarctica, the first member of CESM 1, which shows a warming trend close

to zero at WAIS, is not very meaningful but it is still included for completeness. 75% models show WAIS displays a larger cooling from 1000 to 1600 CE than other locations in Antarctica (shown in blue) but with a magnitude similar to other grid cells in West Antarctica. This is consistent with the reconstruction of Stenni et al. [2017] which shows the largest cooling in this region over the period 0-1900 CE [Stenni et al., 2017]. The spatial patterns of the trends (Fig. 2.7) are different between models, but also within the CESM ensembles, showing that the changes in Antarctica are strongly influenced by internal variability, even at century timescale. Future work including more sites, or using water isotopes and the Antarctica-2K database will help constrain the spatial pattern of this trend.

2.4.2 Metric 2: nineteenth century cooling at Larissa

The second metric is the surface temperature trend over the period from 1825 to 1925 CE at Larissa, with a magnitude of -0.94 ± 0.12 ℃/century. Fig. 2.8 shows the spatial correlation between the temperature from 1825 to 1925 CE at Larissa and other grid cells for each climate model. As there are no significant differences between each member in the CESM ensemble (see the Fig. A1), only one member CESM1 is presented in Fig. 2.8. Despite the correlation coefficient decreasing with the distance from the Larissa, the values are higher than 0.6, at least around Larissa, showing that this metric is representative of part of the AP region, and not extremely site-specific.

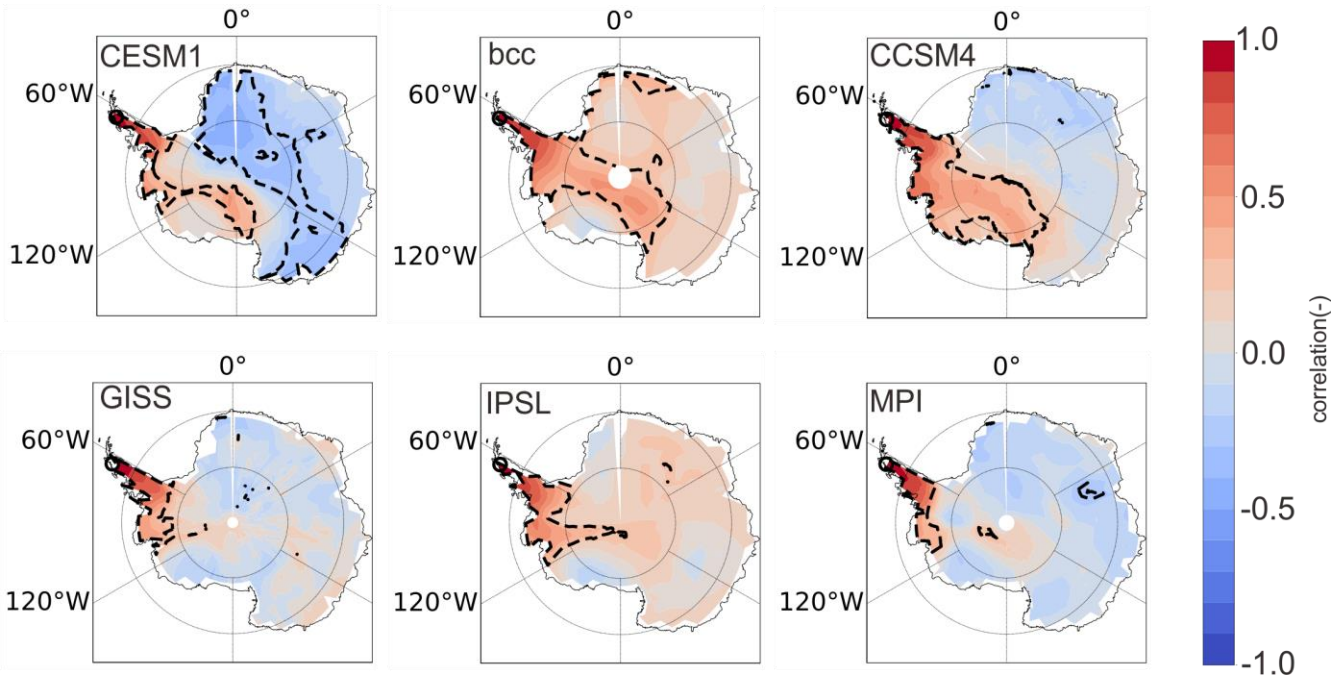

***Figure 2.8**: The correlation map (blue-red shading area) showing the relationship between the temperature from 1825 to 1925 CE at Larissa and other grid cells in Antarctica for each climate model. The black dotted contour lines show a significant correlation at the 99 % significant level.*

None of the models is able to capture the observed temperature trend from 1825 to 1925 CE (Fig. 2.9). Overall, models are showing a warming trend (largest for CCSM4, MPI and BCC), contradicting the observations, as highlighted already in Fig. 2.4 c. Only four members of CESM (CESM1, 7, 8, and 9) show a cooling trend over AP, but their magnitudes are still less than the observed one.

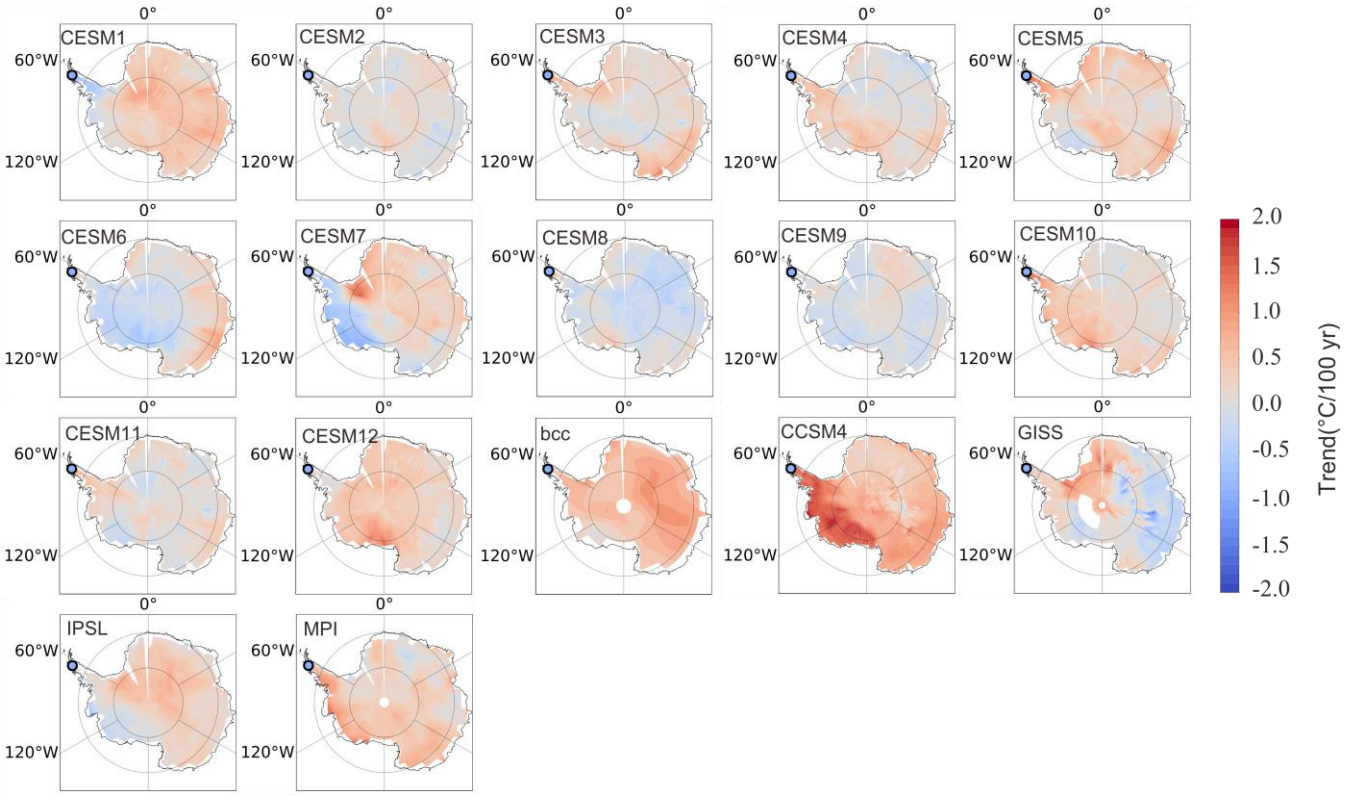

***Figure 2.9**: The simulated (blue-red shading area) and observed (circle) surface temperature trend from 1825 to 1925 CE.*

The 19th century is a time period when the Northern Hemisphere has started warming, whereas Southern Hemisphere records [Neukom et al., 2014], and specifically Antarctica, show no general warming trend [Stenni et al., 2017]. Models tend to overestimate the interhemispheric synchronicity [Neukom et al., 2014], and show a warming trend also in Antarctica, possibly in response to the anthropogenic forcing. This metric is thus an important tool for future research to evaluate whether the model data mismatch is due to internal variability (which will be investigated with more ensembles of the same model), or to an overestimated sensitivity to the anthropogenic forcing.

2.4.3 Metric 3: recent warming trend

The warming trend of the last 50 years is one of the clearest features of the observations. Here we propose a metric of the warming trend from 1950 to 2005 CE at each of the four sites, to investigate whether model can reproduce these features.

First we look at the spatial correlation of the temperature between each site and other grid cells for all GCMs (Fig. 2.10). Only one member of CESM1 is presented in Fig. 2.10 since no significant difference is observed between each member in CESM ensemble (see in the Fig. A2-A5). The correlation is calculated on annual data for 1950 to 2005 CE. It is clear that each of our borehole temperature sites gives information about different sectors of Antarctica. Generally speaking, WAIS is representative of the West-Antarctic continent, with a more pronounced dipole between WAIS and the Weddell Sea sector in MPI, and to a lesser extent CESM and GISS. Larissa is representative of the AP as a whole, and from this resolution of climate model results, there is no evidence of a dipole between both sides of the Transantarctic mountains. Similar to WAIS, MPI has the strongest expression of a dipole between the AP and East Antarctica, a feature that is weaker but also present in GISS. Mill Island is generally representative of the Wilkes Land sector of East Antarctica, with the largest spatial homogeneity for BCC and IPSL (Fig. 2.10 c). Finally, for Styx, the models with the largest spatial homogeneity (BCC and IPSL) show a strong correlation between Victoria Land and the rest of East Antarctica.

Figure 2.11 shows the surface temperature trend from 1950 to 2005 CE. The strong warming trend at Larissa is underestimated in all the models except the CESM ensemble (Fig. 2.11 b). Additionally, three out of twelve CESM simulations indicate cooling in West Antarctica, which is coherent with the hypothesis that part of the observed warming is due to unforced variability and that models are not expected to match this trend perfectly. The warming at Mill Island is relatively well reproduced. However, none of the models can reproduce the muted recent warming seen at Styx. The lower spatial representativity of this site (Fig. 2.10) leads us to interpret this as local processes missing in low resolution GCMs, such as the influence of topography on katabatic wind forcing, rather than a large scale failure of models to represent reality.

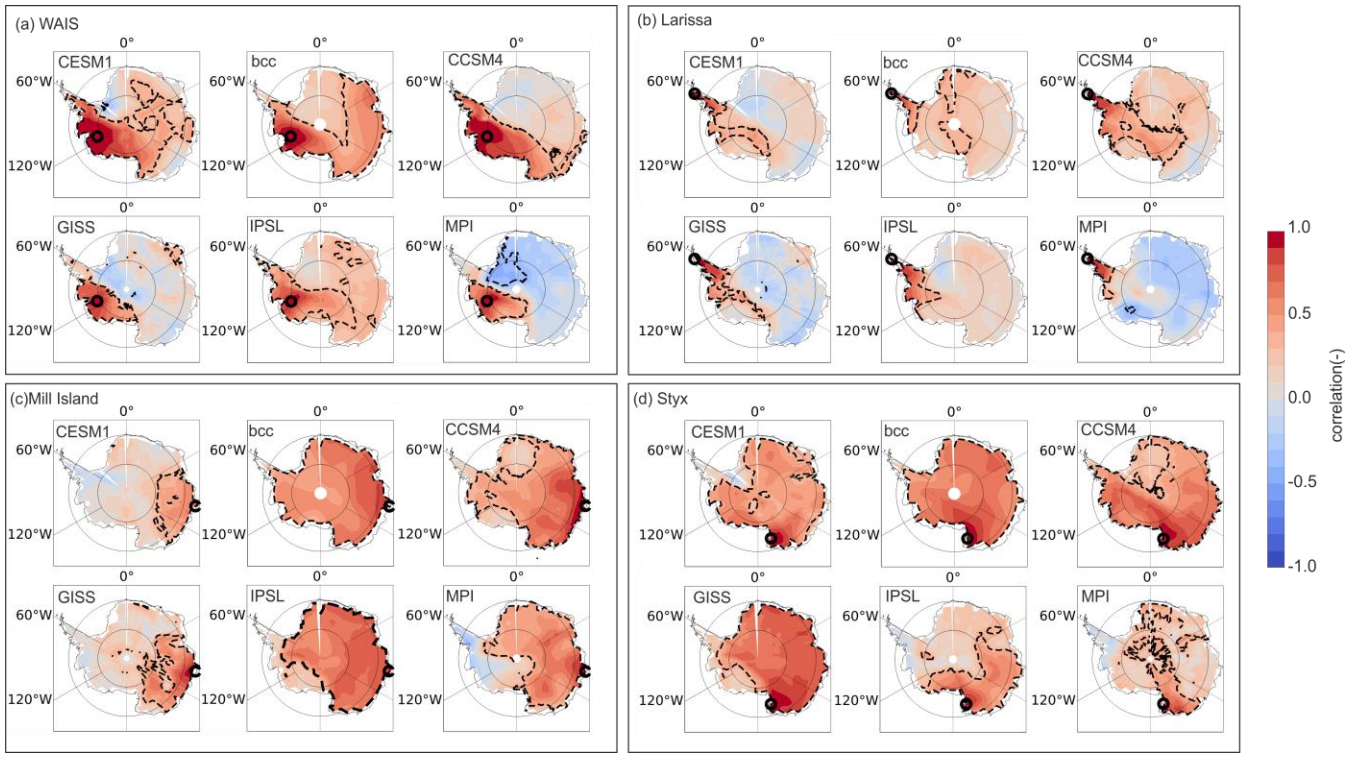

***Figure 2.10**: The correlation map showing the relationship between the temperature from 1950 to 2005 CE at WAIS (a), Larissa (b), Mill Island (c), Styx (d) and other grid cells for each climate models. The red dashed contour lines show a significant correlation at the 99 % significant level.*

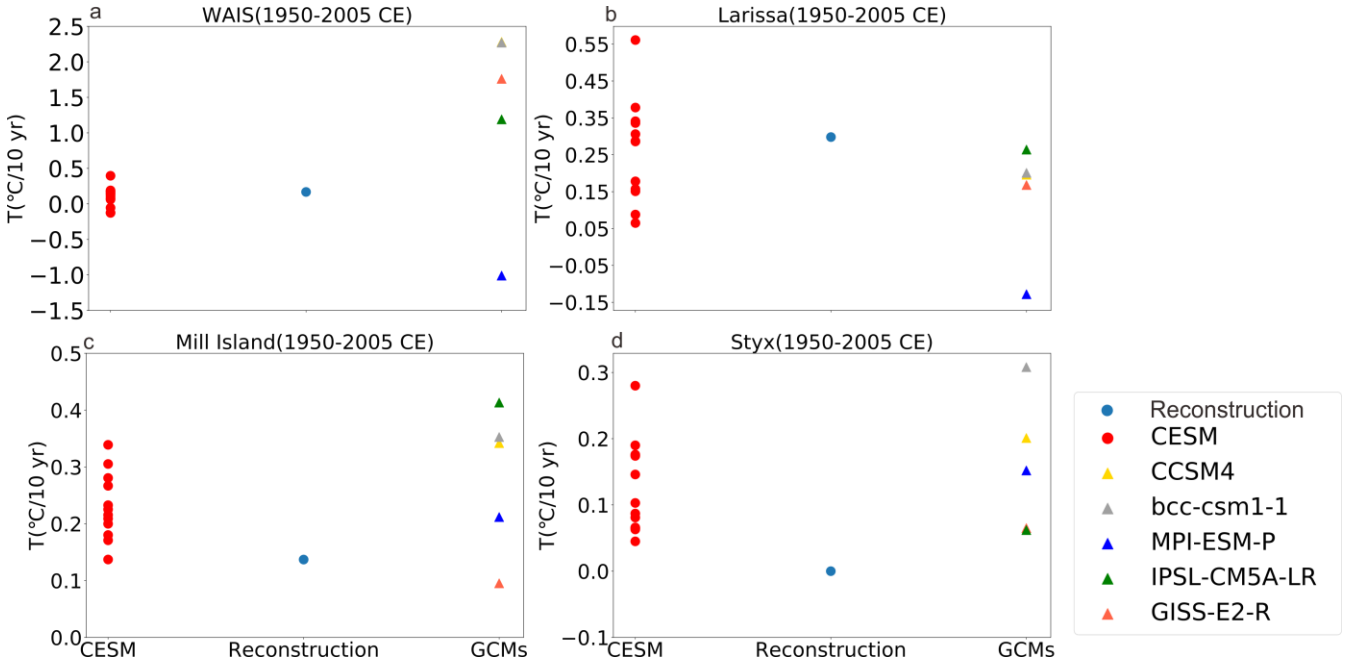

***Figure 2.11**: Linear trends for the four boreholes from 1950 to 2005 CE: (a) WAIS; (b) Larissa; (c) Mill Island; (d) Styx.*

2.5 Conclusion

In this study, we test two complementary ways to evaluate the climate model performance using borehole temperature observations. The standard way is to compare the reconstruction of surface temperature with simulated values in the time domain. The successful application here of a forward model driven with climate model results provides an additional way to jointly analyze model results and borehole temperature measurements. In contrast to the model-data comparison in the time domain, the forward model allows us to reproduce the subsurface temperature profile and compare it directly with the measured borehole temperature profile.

The comparison of the surface temperature time series is simpler and more straightforward but it is limited by the different resolutions of the reconstructions and climate model results. Nevertheless, some robust conclusions can be derived from this model-data comparison that is confirmed by the direct analyses of the temperature profiles as a function of the depth. For instance, the long-term cooling trend over the last millennium observed at WAIS is relatively well reproduced in all models but with a weaker amplitude, which means the model maybe miss some feedback or low-frequency internal variability. Most simulations agree with data on a recent warming but the magnitude and timing vary a lot between models for the four sites. The large variability of the trends over the 20th century within the CESM ensemble for WAIS and Larissa suggests that many apparent model disagreements for those sites can be due to internal variability while the disagreement for Styx and Mill Island may be related to local processes not captured by global models.

The comparison of the model output and data in the depth domain is useful because the borehole temperature inversion is an under-determined problem, and many different temperature histories could fit the data equally well. The comparison of the temperature profiles confirms the conclusions found in the time domain, and validates the significance of some of the differences found. Some features are however difficult to interpret, such as the depth of the temperature minimum at the WAIS Divide site. This points to the complexity of the interpretation of the borehole profiles, and the complementary use of the analyses in the depth and time domain.

Finally, some metrics derived from the corresponding reconstructions are proposed to be used more widely in model evaluation. The metrics used are demonstrated to be generally representative of a large spatial area, although they are calculated at a specific site. The results confirm that no models can reproduce the cooling during the 19th over the AP and a stabilization of the temperature over the last 50-years in northern Victoria Land. Nevertheless, these models can capture the larger long-term cooling from 1000 to 1600 CE in West Antarctica, and the recent 50-years warming in West Antarctica and the AP. This work brings quantitative tools to evaluate models and better simulate the Antarctic climate and its response to forcings.

3

Spatial patterns of multi–centennial surface air temperature trends in Antarctica over 1–1000 CE: Insights from ice core records and modeling

Abstract

The spatial pattern of Antarctic surface air temperature variability on multi-decadal to multi-centennial time scales is poorly known because of the short instrumental records, the relatively small number of high-resolution paleoclimate observations, and biases in climate models. Here, changes in surface air temperature over Antarctica are reconstructed over the past two millennia using data assimilation constrained by different ice core water isotope records in order to identify robust signals. The comparison between previous statistically based temperature reconstructions and simulations covering the full Common Era driven by natural and anthropogenic forcings shows major discrepancies occurring in the period 1-1000 CE over East Antarctica, with the reconstructions displaying a warming over 1-500 CE that is not reproduced by the simulations. This suggests that the trends in the first millennium deduced from the statistically based reconstructions are unlikely to be entirely forced by external forcings. Our reconstructions show the high sensitivity of the multi-centennial temperature trend in Antarctica and its spatial distribution to selection of the records for the reconstructions, especially during 1-500 CE. A robust cooling over Antarctica during 501-1000 CE has been obtained in three data assimilation–based reconstructions with a larger magnitude in the WAIS than elsewhere over Antarctica, in agreement with previous estimates but with the larger changes than simulated in climate models. The reconstructions for atmospheric circulation indicate the pattern of temperature changes over 501-1000 CE is related to the positive trend of Southern Annular Mode and the deepening of the Amundsen Sea Low. This confirms the role of internal variability in the temperature trends on multi-centennial scales.

Lyu, Z., Goosse, H., Dalaiden, Q., Klein, F., Shi, F., Wagner, S., & Braconnot, P. (2021). Spatial patterns of multi–centennial surface air temperature trends in Antarctica over 1–1000 CE: Insights from ice core records and modeling. Quaternary Science Reviews, 271, 107205. Supplementary materials are in Appendix B.

3.1 Introduction

Changes in surface air temperature (SAT) over Antarctica during the past decades are characterized by a spatially heterogeneous pattern. A general cooling is observed in many regions of East Antarctica that contrasts with the large warming in the Antarctic Peninsula (AP) and the West Antarctica Ice Sheet (WAIS) [e.g., Marshall et al., 2013; Smith and Polvani 2017; Jones et al., 2019]. This spatial pattern is influenced by changes in atmospheric circulation, particularly by the positive trend of the Southern Annular Mode (SAM), a dominant mode of atmospheric variability associated with opposing pressure anomalies over middle and high southern latitudes and thus changes in the intensity of the westerly winds over the Southern Ocean [Marshall 2003]. However, the short instrumental records in Antarctica, with the majority of the observations starting after the International Geophysical Year of 1957/58 [e.g., Bromwich and Fogt, 2004], limit our knowledge of multi-decadal to centennial climate changes and their underlying mechanisms.

In order to put the recent changes into a long-term context, previous studies have reconstructed Antarctic SAT over the past thousand years at the regional and continental scales on the basis of ice core water stable isotope records [Goosse et al., 2012; PAGES 2k Consortium, 2013; Stenni et al., 2017; Klein et al., 2019]. Different methods and observational networks have been used. For instance, Goosse et al. [2012] proposed a simple averaging of seven ice core water stable isotope records to calculate a composite representing Antarctic SAT. PAGES 2k Consortium [2013] utilized a composite-plus-scaling approach based on eleven ice core isotopic records to reconstruct Antarctic SAT during the past two thousand years. Stenni et al. [2017] based their reconstructions on an expanded ice core water isotopic database including 112 records and applied three different statistically based methods to estimate past Antarctic SAT changes at regional scales. Klein et al. [2019] provided a data assimilation-based SAT reconstruction over Antarctica by directly assimilating the regional composite $\delta^{18}O$ of Stenni et al. [2017]. All these reconstructions consistently show a general cooling from 850 CE to 1850 CE over Antarctica. Furthermore, model-data comparisons suggested that an increase in the frequency of major volcanic events during this period could explain this long-term cooling over the second millennium [Goosse et al., 2012; PAGES 2k Consortium, 2013].

Although these studies have provided SAT reconstructions covering the past two millennia over Antarctica [e.g., PAGES 2k Consortium, 2013; Stenni et al., 2017; Klein et al., 2019], few of them focus on changes in the Antarctic SAT during the first millennium, as noticed also for other regions [e.g., Esper and Büntgen 2021]. In addition, no modeling study has been specifically devoted to the 1-1000 CE period up to now. Compared to the ice core records covering the past millennium, a smaller number of data is available during 1-1000 CE [nine records in the database of Stenni et al., 2017]. Furthermore, they display contrasted signals. For instance, the $\delta^{18}O$ signal from Plateau Remote, an ice core located in the interior of the Antarctic Plateau, has a large positive linear trend during the first five centuries, while the

record in West Antarctica (e.g., at WDC06A) shows no significant change (or even a low negative trend) superimposed on large centennial variability during this period [e.g., Steig et al., 2013]. The signals from these individual records have left an evident fingerprint on the regional composite of $\delta^{18}O$ and the corresponding reconstructed SAT provided by Stenni et al. [2017] that shows a large warming during 1-500 CE in East Antarctica. Accordingly, the statistically based reconstructions present a significant east-west asymmetry in SAT trends during 1-500 CE. The signal appears more homogenous between 501 to 1000 CE with an overall cooling of Antarctica, albeit more pronounced in West Antarctica.

Consequently, we only have a very fragmentary knowledge of the changes in the SAT during the first millennium. Yet, the potentially complex spatial structure of multi-centennial trends inferred from the existing studies may be substantially different from the one observed between 1000 and 1850 CE and thus may bring relevant information on the dynamics of the system. In this study, we aim to understand better the signals included in ice core $\delta^{18}O$ records over the first millennium of the Common Era and, in particular, to determine the differences in SAT evolution between East and West Antarctica on multi-centennial scales. To identify the most robust signals and investigate the underlying mechanisms, we will first quantify similarities and differences between simulations in climate models and the reconstructed Antarctic SAT over the past two millennia, and then perform a spatial reconstruction of SAT changes using a data assimilation approach that combines the available ice core water isotope records from Antarctica with the information of the physics of the system derived from climate models.

Many previous studies have successfully applied data assimilation to estimate past climate states [Goosse et al., 2010; Widmann et al., 2010; Steiger et al., 2018]. We follow the same approach as Klein et al. [2019] and Dalaiden et al. [2020], using results from an isotopic-enabled model so that the $\delta^{18}O$ records can be directly compared to the simulated $\delta^{18}O$ in the process of data assimilation. A distinct advantage is that the $\delta^{18}O$-temperature relationship can vary with time as a function of the conditions and the link is physically consistent. In contrast, the statistically based reconstructions must rely on a short calibration period (e.g., the past decades) to infer the covariances between $\delta^{18}O$ and SAT that will be applied to estimate SAT changes over the past two millennia [Stenni et al., 2017]. This can have a clear influence on the skill of those reconstructions as the covariances between $\delta^{18}O$ and SAT can display large variations over the past millennium among different Antarctica regions [Klein et al., 2019].

The paper is organized as follows. Section 3.2 describes the methodology, including the climate model simulations (Section 3.2.1), the data (Section 3.2.2), the data assimilation technique (Section 3.2.3), and the experimental design (Section 3.2.4). The general characteristics of the simulated SAT changes over the full Common Era in climate models and a comparison with data are shown in Section 3.3. The reconstructions of $\delta^{18}O$ and SAT obtained by data assimilation are presented in Section 3.4.1 and 3.4.2, respectively, and the

corresponding mechanisms are analyzed in Section 3.4.3. Results from sensitivity experiments are discussed in Section 3.5, and the robustness of our results is assessed in Section 3.6 by comparison with independent proxies over Antarctica. Finally, conclusions are given in Section 3.7.

3.2 Data and methods

3.2.1 Climate model simulations

The climate model simulations selected for this study are divided into two categories according to their time span. We will refer to them as corresponding to (1) the full pre-industrial Common Era (1-1850 CE); and (2) the pre-industrial past millennium (850-1850 CE). The latter category mainly contains simulations performed with general circulation models (GCMs) in the framework of the Paleoclimate Modeling Intercomparison Project Phase 3-Coupled Modelling Intercomparison Projects 5 (PMIP3-CMIP5 models). They are driven by natural (orbital, volcanic, and solar) and anthropogenic (greenhouse gases, land use, aerosol) forcings [Schmidt et al., 2012, Taylor et al., 2012]. The list of selected models with some key characteristics is provided in the supplementary material (Table B.1). In addition, a simulation covering the past millennium (850-1850 CE) performed with an isotope-enabled general circulation model (iGCM), iCESM1 [Brady et al., 2019], is also used here. This simulation is driven by the same transient external forcing as those for PMIP3. Cavitte et al. [2020] have evaluated the iCESM1 simulations of Antarctic SAT, precipitation, and atmospheric circulation for 1979-2000 CE against the latest version of the Regional Atmospheric Climate Model [RACMO2.3p2, hereafter RACMO, van Wessem et al., 2018], showing good agreement. The precipitation-weighted $\delta^{18}O$ pattern under the present-day condition in iCESM underestimates the spatial variability of $\delta^{18}O$ for most of the ice sheet surface compared to ice core records [Cavitte et al., 2020], but this bias is small, justifying the use of this model here (see Section 3.2.3).

For climate model simulations covering the full pre-industrial Common Era, we collected three simulations performed with GCMs: CESM1 [Zhong et al., 2018], MPI-ESM-P [Stevens et al., 2013], and IPSL-TR6A-MR [Braconnot et al., 2019], as well as an ensemble of simulations performed with Earth System Model (ESM) of intermediate complexity LOVECLIM [Shi et al., 2021]. These simulations are chosen because they were available at the time of the analysis. The MPI-ESM-P simulation does not follow the PMIP4 protocol [Jungclaus et al., 2017] because it was launched before the definition of this protocol. The main difference is in the volcanic forcing as the volcanic forcing driving the MPI-ESM-P simulation is based on the sulfate data set of Sigl et al. [2013] with Crowley and Unterman's algorithm [Crowley and Unterman., 2013], while PMIP4-CMIP6 protocol uses the latest volcanic reconstruction of Toohey and Sigl [2017]. This difference does not induce major changes in the 500-year SAT trends over Antarctica compared to other simulations performed with GCMs driven by PMIP4-CMIP6 protocol (see details in Section 3.3). The simulation spanning the past two millennia

performed with CESM1 uses the same configuration as for the CESM Last Millennium Ensemble [Otto-Bliesner et al., 2016] and is forced following PMIP4 recommendations [Jungclaus et al., 2017]. IPSL-TR6A-MR is the version of the IPSL Earth System Model (ESM) that includes interactive dynamical vegetation and carbon cycle [Braconnot et al., 2019]. Since it was initially used to study the climate-vegetation dynamics over Mid-Holocene, it uses the PMIP4-CMIP6 forcings for the Holocene, which includes only the changes in the astronomical parameters and trace gases. One portion of the simulation spanning 1 to 1850 CE is analyzed in this study.

As an Earth System model of intermediate complexity (EMIC), LOVECLIM has a simpler representation of physical processes and a coarser resolution than GCMs [Goosse et al., 2010]. It thus runs much faster than GCMs, so that a large ensemble of simulations can be performed to explore internal variability [70 members in this study, Shi et al., 2021]. LOVECLIM has been used to analyze the Antarctic SAT changes over the past millennium, showing a good agreement with the ice core water isotopic records for the long–term cooling during 850-1850 CE [Goosse et al., 2012]. Here, the forcings follow the latest PMIP4-CMIP6 protocol too.

3.2.2 Data used in data assimilation and for independent validation.

In this study, three sets of ice core $\delta^{18}O$ data are employed, corresponding to three groups of experiments with data assimilation (Table 3.1). The first set is the same as the one used in the Last Millennium Climate Reanalysis project (referred to as LMR hereafter) [Tardif et al., 2019] for a direct comparison with their results. According to the LMR specific criterions, only the records in the PAGES 2k 2017 database [PAGES 2k Consortium, 2017] with sub-annual to annual resolutions are selected to be assimilated [Tardif et al., 2019]. This consists of five records covering (almost completely) the period 1-1000 CE, which is the focus of the present study: Plateau Remote (1), Law Dome (2), DML (3), WDC06A (4), and James Ross Island (5). The general information about those cores has been listed in Table B.2, and their locations are shown in Fig. 3.1.

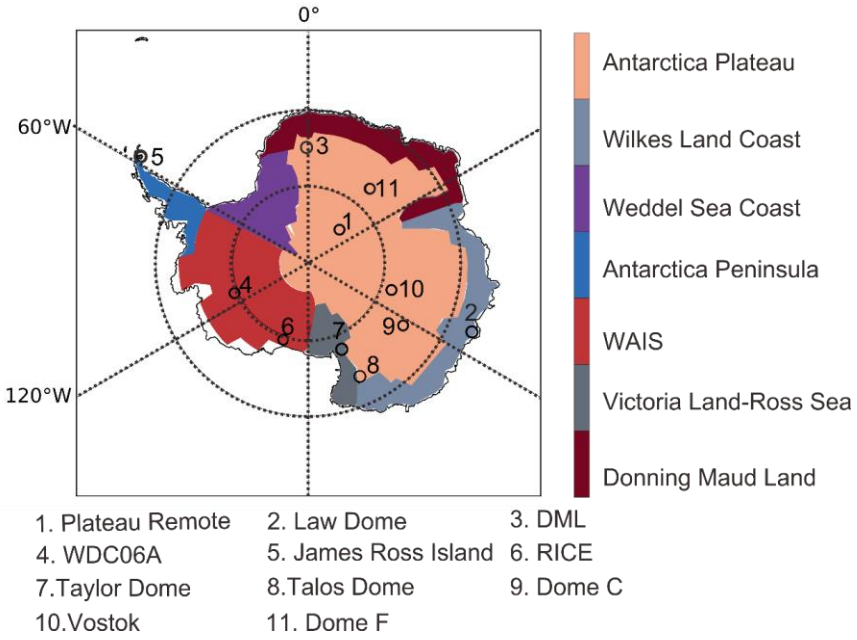

Figure 3.1: *Antarctic regions and the geographical locations of ice core water isotopic records used in this study.*

The second data set is derived from the database of Stenni et al. [2017]. It contains 112 records, but only nine cover almost completely the CE: Plateau Remote (1), Law Dome (2), DML (3), WDC06A (4), James Ross Island (5), RICE (6), Taylor Dome (7), Talos Dome (8), and Dome C (9) (Fig. 3.1).

The third data set is obtained by adding two low time-resolution ice core records from a database of Holocene paleotemperature records [Kaufman et al., 2020] to the ones of Stenni et al. [2017]. These records are named Vostok (10) and Dome F (11), having a time resolution of 35 years and 20 years, respectively. These data are linearly interpolated to the same annual average as the ones in the database of Stenni et al. [2017].

We have also collected 17 additional proxies (Table B.3). Those records are not used for the data assimilation nor in previous reconstructions, so they can provide an independent assessment of the reconstructions. These data are selected according to the following criteria:

1. The proxy is derived from Antarctic terrestrial records.
2. The minimum mean sample resolution for each proxy is at least one observation every 200 years.
3. The records cover the period (or nearly) 1-1000 CE.

We follow the interpretation of those paleoclimatic records proposed in their original publications. For the time series not available in public databases, we have used WebPlotDigitizer (https://automeris.io/WebPlotDigitizer/) to digitize the plots from the

original publication to obtain the data displayed in our analyses. General information for these proxies is listed in the supplementary Table B.3.

3.2.3 Data assimilation method

The goal of data assimilation is to obtain an optimal estimate of past climate by combining observational data (ice core $\delta^{18}O$ data here) and climate model simulations. There are two types of applications of data assimilation in paleoclimatology, based on the way the model ensemble is generated: offline and online methods. The online method corresponds to an ensemble generated sequentially as the transient simulation is running, constrained by available proxies at each assimilation step. The information brought by the records can thus be propagated forward in time through the model. Therefore, it is well adapted to studies that focus on relatively slow processes like the one controlled by ocean dynamics because of the large inertia of the ocean [e.g., Goosse et al., 2017]. However, the main limitation of the online method is the computational cost of running the ensemble simulations. A sufficiently large ensemble is required in data assimilation, and running tens to hundreds of simulations over the past 2000 years is prohibitive for high complexity models such as isotope-enabled GCMs.

In contrast to the online method, the offline method generates an ensemble of model states from existing simulations [e.g., Hakim et al., 2016; Steiger et al., 2018]. If the contribution of external forcing to climate evolution can be considered weak compared to internal variability, the model states could be chosen from any time step in the simulation. In this context, the number of states included in the ensemble for each time step can reach several hundreds or even thousands, depending on the length of the simulations. In this study, as we will focus on the role of atmospheric processes with a relatively short memory, we employ an offline method as in the large majority of recent studies applying data assimilation over the past millennia [Hakim et al., 2016; Steiger et al., 2018, Tardif et al., 2019, Klein et al., 2019, Dalaiden et al., 2020].

The data assimilation method is based on a particle filter. The details of the implementation are described in Dubinkina et al. [2011]. In the procedure, the likelihood of each member of the ensemble of model states (also called particle) is computed each year by comparing the particle with the proxy-based reconstructions used as constraints, taking into account the data uncertainties. A weight is given to each particle depending on this likelihood. When all the particles are given the weights, the mean reconstruction for this time step is completed as a weighted average of the particles.

3.2.4 Experimental design

In this study, data assimilation is employed to reconstruct $\delta^{18}O$, SAT, and atmospheric circulation. As mentioned in Section 3.2.2, three different sets of $\delta^{18}O$ records are used to constrain the model during the data assimilation process, corresponding to three experiments: ASSIM-LMR, ASSIM-STENNI, and ASSIM-ALL (Table 3.1). A 5-year Lowess smoothing

is applied to reduce the noise induced by non-climatic processes before performing the data assimilation experiments [Stenni et al., 2017]. The model results used to produce the ensemble come from three simulations covering the past 1000 years (850-1850 CE) performed with iCESM1. The time step for data assimilation is one year, so that up to 3003 (3*1001) annual mean climate state (also called the "prior" in the data assimilation) can be obtained from three simulations of iCESM1.

Table 3.1: *Descriptions of the experiments.*

Name of experiment	Description
ASSIM-LMR	Five records (B32DML05, Plateau Remote, Law Dome, James Ross Island, and WDC06A) with standard errors are assimilated.
ASSIM-STENNI	All records in the database of Stenni et al. (2017) with standard error are assimilated.
ASSIM-ALL	All records of Stenni et al. (2017) database and two lower resolution records, VOSTOK and Dome F, are assimilated.

Uncertainty in the observed data is key to determining the likelihood of each particle in the data assimilation process. In this study, we argue that the uncertainties arise mainly from the representativeness error of the $\delta^{18}O$ time series as the model and data do not represent variations occurring at the same scales. This error is estimated as described in Dalaiden et al. [2021]. We first linearly interpolate iCESM1 outputs onto a grid with 27 km. Then, we spatially average the iCESM1 outputs over a 500 km grid, which is the grid used for the comparison with proxy records. Next, we calculate the errors which are defined by the standard deviation of the difference between the average of the annual mean $\delta^{18}O$ time series for those available records in the 27 km grid cells and the average within the 500 km grid cells. Note that the time series used to calculate the difference are the anomalies referenced over 850–1850 CE. Since some local scale processes are not correctly simulated in iCESM1, leading to the underestimated spatial variability of $\delta^{18}O$ [Cavitte et al., 2020], the estimated errors are finally multiplied by a factor of 3 [Dalaiden et al. 2021]. Besides, associated with the 5-year Lowess smoothing for the data, the corresponding uncertainties are divided by the square root of the length of the smoothing (i.e., $\sqrt{5}$). We refer it to as "standard error" hereafter on each data.

To compare our results with available statistically based reconstructions, the regions selected in this study are identical to those defined in Stenni et al. [2017]. On the sub–continental scales, they include East and West Antarctica. East Antarctica contains the Antarctic Plateau, Wilkes Land coast, Weddell Sea coast, Victoria Land coast–Ross Sea, and Dronning Maud Land coast. West Antarctica includes Antarctic Peninsula and West Antarctic Ice Sheet (Fig. 3.1).

3.3 Reconstructed and simulated SAT variations over the past two millennia

As our study is on the basis of model results, it is important to first determine similarities and identify discrepancies between simulations and reconstructions of Antarctic SAT over the past two millennia. Fig. 3.2 confirms that the multi-centennial trends in the average of three statistically based reconstructions of Stenni et al. [2017] over the past millennia (–0.08 and –0.03 °C per century during 1001-1500 CE and 1501-1850 CE, respectively) are well within the range of the PMIP3/CMIP5 simulations (from –0.13 to 0 °C per century during 1001-1500 CE and from –0.11 to 0.03 °C per century during 1501-1850 CE), as shown in PAGES2k Consortium [2013] and Klein et al. [2019]. Simulations covering the full CE performed with LOVECLIM, CESM1, and MPI-ESM-P display cooling trends over this period as well. This general agreement between most of the simulations and statistically based reconstruction is consistent with the hypothesis that the cooling trend has an origin in the external forcings, particularly the volcanic forcing [Goosse et al., 2012; PAGES 2k Consortium, 2013].

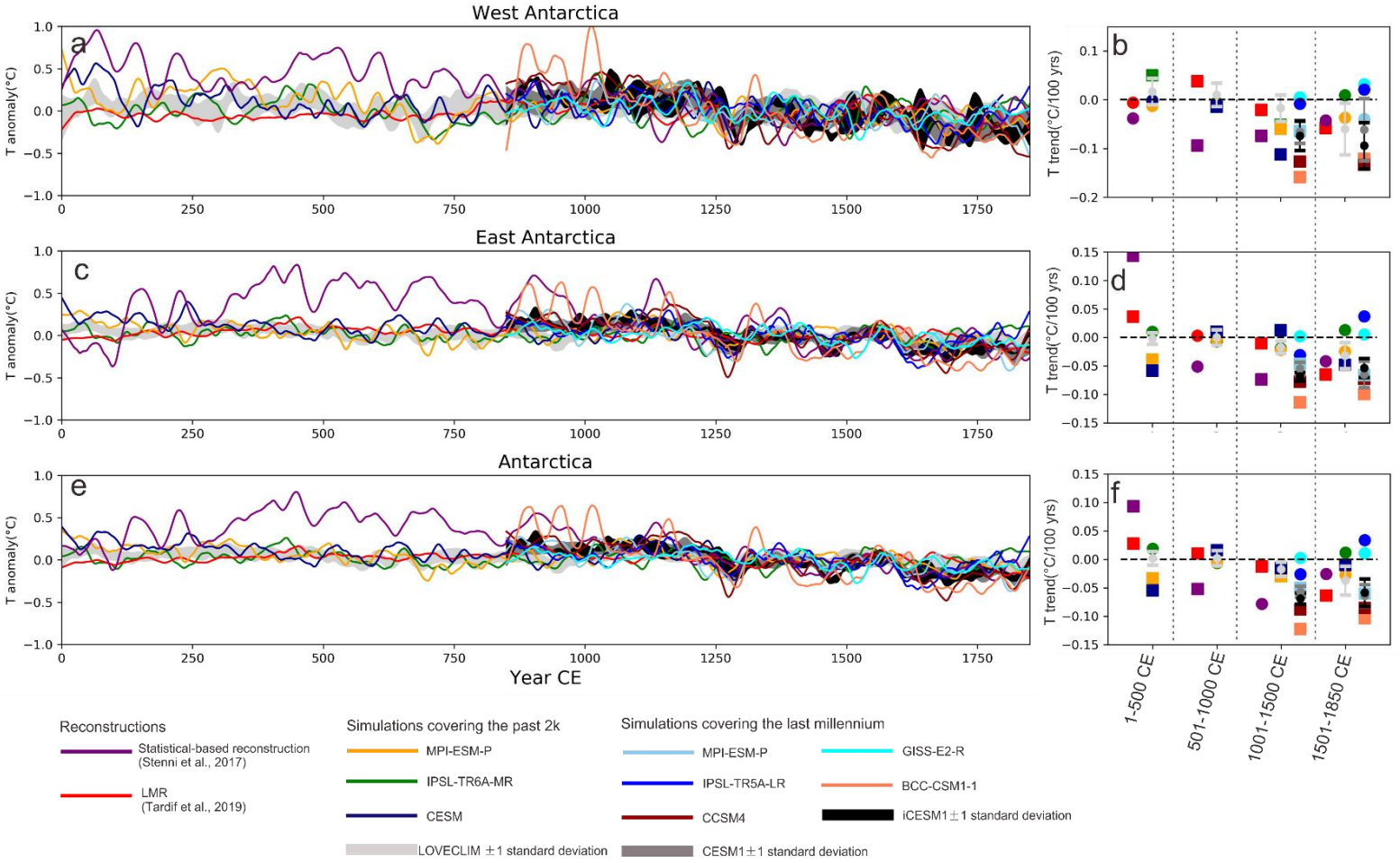

Figure 3.2: *Comparison of the reconstruction of Stenni et al. [2017] (in purple) and LMR (Tardif et al., 2019, in red) with annual mean SAT anomaly simulated in the models covering the entire CE (LOVECLIM ±1 standard deviation in light-*

grey shading, MPI-ESM-P in orange, IPSL-TR6A-MR in green, CESM1 in blue), and the last millennium (MPI-ESM-P in light blue, IPSL-TR5A-LR in dark blue, CCSM4 in dark red, BCC-CSM1-1 in orange, GISS-E2-R in aqua, CESM1 ±1 standard deviation in dark-grey shading, iCESM1 in black shading) over (a) West Antarctica, (c) East Antarctica, and (e) Antarctica. A 50-year Lowess smoothing has been applied to the time series for a, c, and e. The reference period is over 1000-1800 CE. The 500-year trends in the simulations and reconstructions are shown in the right panels, and they share the same color as the time series. The statistically significant trend (p value<0.1) is illustrated using the square in b, d, and f.

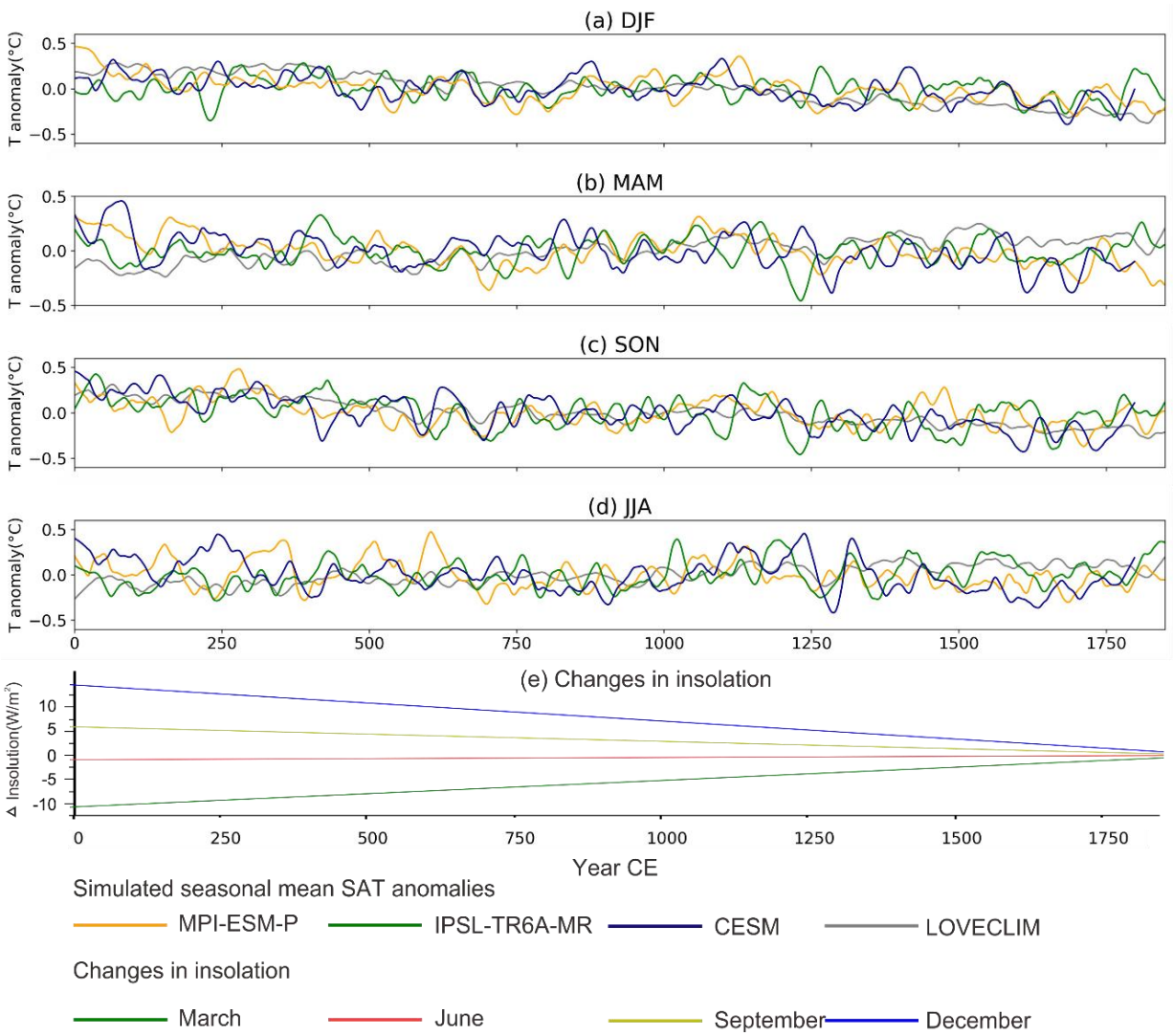

Figure 3.3: *Simulated seasonal mean SAT anomalies over Antarctica in LOVECLIM (in light grey), MPI-ESM-P (in orange), IPSL-CM5A-MR (in green), and CESM1 (in blue) for December-January-February (a), March-April-May (b), June-July-August (c), September-October-November (d). A 50-year Lowess smoothing has been applied to these time series, and the reference period is over 1-1800 CE. The change in insolation is shown in e for March (in green), June (in red), September (in yellow), and December (in blue) at 65 °S relative to 2000 CE from Berger et al. [1978].*

The differences between the reconstruction of Stenni et al. [2017] and simulations are much larger in the first than in the second millennium. The reconstruction of Stenni et al. [2017] shows a significant overall warming in the Antarctic continent during 1-500 CE, explained mainly by the observed warming in East Antarctica, followed by a cooling trend over 501-1000 CE. In contrast, neither the ensemble of LOVECLIM nor the individual simulations of CESM1, IPSL-TR6A-MR, and MPI-ESM-P simulate significant multi-centennial SAT trends

at continental or sub-continental scales. During 1-500 CE, CESM1 and MPI-ESM-P show a small cooling in East Antarctica, which is the opposite of the statistically based reconstruction. During 501-1000 CE, the close to zero trends in all simulations are also different with the significant cooling in the reconstruction. Therefore, while both the data and models are consistent in the past millennium, we observe an apparent model–data discrepancy in the first millennium.

Some studies have argued that solar forcing may play a major role in multi-centennial SAT trends [e.g., Anchukaitis et al., 2017; Lüning et al., 2019; An et al., 2021]. However, the solar forcing used within the PMIP4 framework [Jungclaus et al., 2017] does not show any trend similar to those in the SAT reconstruction of Stenni et al. [2017] (Fig. B.1). Furthermore, the SAT response to solar forcing is generally considered relatively weak and difficult to detect [e.g., Schurer et al., 2013]. Low-frequency changes in volcanic forcing are also less pronounced in the first millennium than in the second [Bradley et al., 2016, Jungclaus et al., 2017, Fig. B.1]. Several large tropical volcanic eruptions occurred in the last millennium, while only a few large eruptions occurred with long periods of volcanic quiescence in the first millennium. These relatively minor changes in the forcing therefore had most likely not a very strong impact on SAT, especially over the high southern latitudes and they were most likely masked by the presence of internal climatic processes. This could explain why the models do not display a common trend in the first millennium, as is the case for the second millennium. Consequently, it seems reasonable to assume that the evolution of Antarctic SAT in the first millennium is unlikely to be driven by external forcings and may be related to internal variability. However, the warming over 1-500 CE in East Antarctica (0.14 °C per century, p value < 0.1) reflected in the statistically based reconstruction of Stenni et al. [2017] is far beyond the ensemble range of LOVECLIM simulations (from –0.01 to 0.01 °C per century) or other model simulations. The much lower amplitude of simulated multi-centennial SAT changes compared to the statistically based reconstruction may be due to the weak internal variability in the models, an argument that has also been used to explain some model-data discrepancies in other regions during the past millennium [PAGES 2k Consortium, 2013; Neukom et al., 2014; Ljungqvist et al., 2019].

An alternative explanation is related to the uncertainties in the statistically based reconstruction. First, because ice core $\delta^{18}O$ observations record information when precipitation occurs, the reconstruction may be seasonally biased and does not faithfully reflect annual means. Although the current observations suggest that the season with the highest precipitation across most of Antarctica is the austral winter [Marshall 2009; Palerme et al., 2017], it is difficult to link isotope ice core data to specific seasons as the actual seasonal distribution of past precipitation (which determines the isotope signal) is unknown. Nevertheless, estimates of potential biases can be obtained by analyzing seasonal SAT evolution in the simulations over the past two millennia. Consistent with variations in insolation associated with astronomical forcings, the SAT in the simulations is characterized by a long-term trend for

each season in the first millennium (Fig. 3.3). This monotonous trend does not correspond to the multi-centennial variations shown for East Antarctica and Antarctica in the statistically based reconstruction. The cooling simulated in summer (DJF; from –0.04 to 0 °C per century during 1-500 CE in different models) could explain the trend in the reconstruction for West Antarctica (–0.04 °C per century during 1-500 CE), but there is no clear maximum in precipitation for this season in the current estimate for the ice core locations, nor changes in precipitation in the simulations that could explain a temporal bias toward this season (not shown). Therefore, the seasonality in ice cores alone cannot completely explain the 0.5 °C warming within 500 years during the first millennian. This is consistent with a recent analysis focused on interglacials [Bova et al. 2021]. Besides, the noise in ice cores associated with precipitation intermittency and diffusion process may also smear the climatic signals at the centennial (or multi-centennial) scale. This is particularly critical for the ice cores extracted from low accumulation areas (for instance the East Antarctic Plateau) [Casado et al., 2020; Münch and Laepple, 2018].

A second potential explanation of the model-data discrepancies is that the magnitude of the 500-year trend over the first millennium inferred from the statistically based reconstruction of Stenni et al. [2017] is overestimated because of the small number of records and the uncertainties in those records. For instance, recent pseudo-proxy experiments have found that the statistical methods can provide reconstructions with unrealistic variances in some Antarctic subregions (e.g., Antarctic Plateau) when the calibration period is very short [Klein et al., 2019]. Those uncertainties related to the reconstructions are investigated in Sections 3.4 and 3.5.

3.4 Analysis of the reconstructions with data assimilation

3.4.1 Data assimilation of $\delta^{18}O$

Visually, most of the $\delta^{18}O$ time series reconstructed in ASSIM-LMR, ASSIM-STENNI, and ASSIM-ALL follow reasonably well the individual ice core $\delta^{18}O$ measurements used as constraints in each experiment, as expected (Fig. 3.4). However, there are some exceptions. For instance, for the period 1-500 CE, the correlation coefficients between the observed and the reconstructed $\delta^{18}O$ at EDC Dome C in ASSIM-STENNI and at Dome F in ASSIM-ALL are only 0.26 and 0.29, respectively. During the period 501-1000 CE, the correlation coefficient at RICE in ASSIM-ALL is only 0.31 (Table 3.2). Additionally, the variability in the reconstructions is lower than that observed at most of the sites.

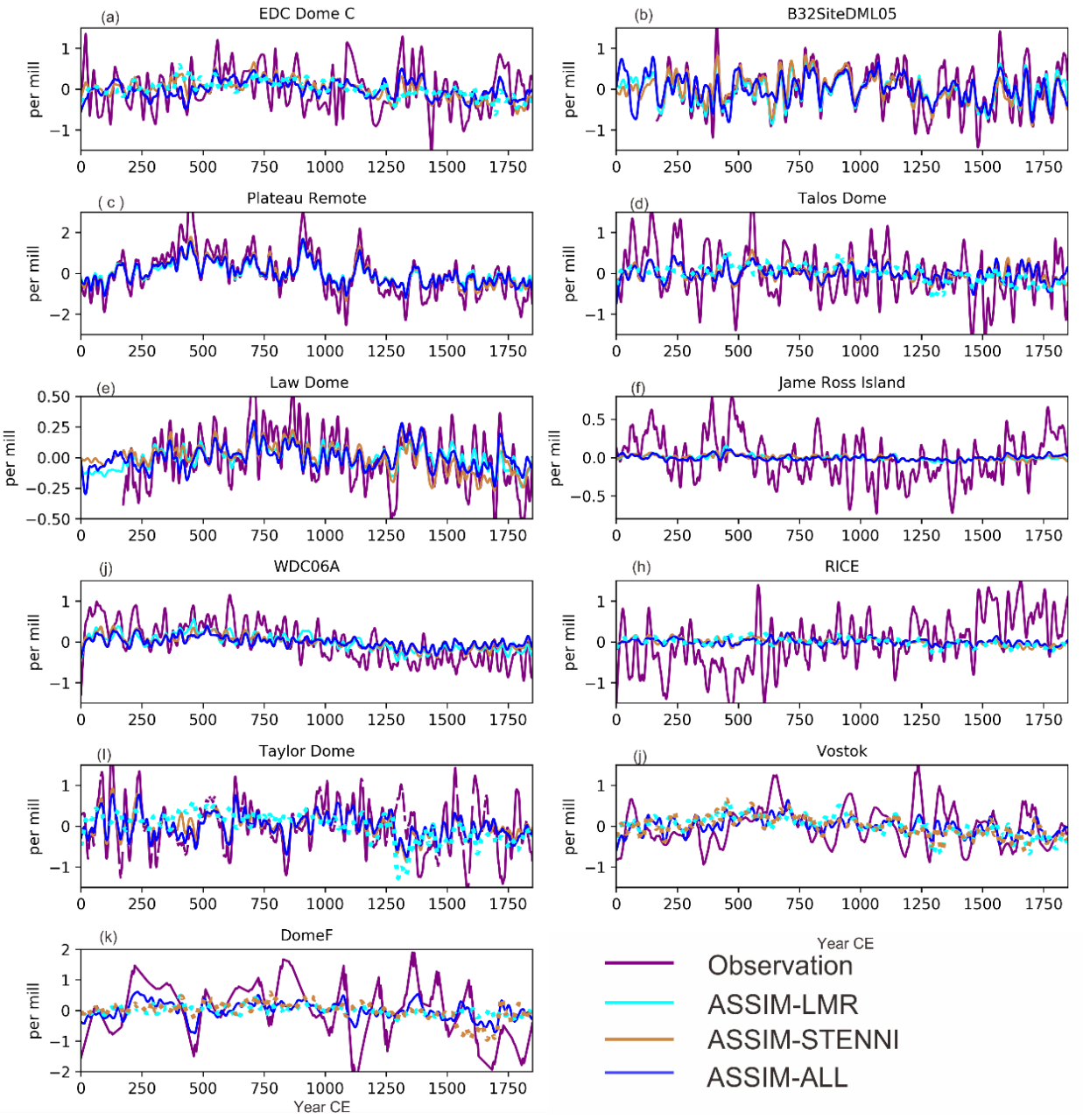

Figure 3.4: *Comparison of the $\delta^{18}O$ measurements covering the entire CE (in purple) with the reconstructed $\delta^{18}O$ in three data assimilation experiments (ASSIM-LMR in cyan, ASSIM-STENNI in brown, ASSIM-ALL in blue). The time series are shown as 10-year averages. The non-assimilated series (dotted lines) generally show poor agreement with the reconstructions (see Table 3.2).*

Table 3.2: *Correlation coefficients between $\delta^{18}O$ reconstructed in ASSIM-LMR, ASSIM-STENNI, and ASSIM-ALL, and $\delta^{18}O$ observations (10-year mean). The statistically significant (P value < 0.1) correlations are present using bold font. The correlations for the records that are not assimilated are shown in italics.*

Ice core	1-500 CE			501-1000 CE		
	ASSIM-LMR	ASSIM-STENNI	ASSIM-ALL	ASSIM-LMR	ASSIM-STENNI	ASSIM-ALL
EDC Dome C	*-0.05*	0.26	0.38	*-0.02*	0.36	**0.48**
B32SiteDML05	**0.98**	**0.98**	**0.71**	**0.99**	**0.99**	**0.78**
Plateau Remote	**0.97**	**0.98**	**0.96**	**0.97**	**0.98**	**0.98**
Talos Dome	*0.11*	**0.69**	**0.57**	*0.00*	**0.69**	**0.59**
Law Dome	**0.91**	**0.68**	**0.80**	**0.96**	**0.91**	**0.89**
James Ross Island	0.39	**0.60**	**0.56**	**0.53**	**0.50**	**0.42**
WDC06A	**0.62**	**0.58**	**0.44**	**0.55**	**0.43**	**0.40**
RICE	*-0.14*	**0.43**	**0.41**	*-0.31*	0.39	0.31
Taylor Dome	*-0.06*	**0.87**	**0.90**	*-0.22*	**0.91**	**0.92**
Vostok	*0.04*	*-0.03*	**0.87**	*-0.07*	*0.19*	0.40
DomeF	*0.00*	*-0.13*	0.29	*-0.06*	*-0.13*	0.38

The goal of data assimilation is to find an optimal estimate, taking into account all the available information and its uncertainties. The apparent discrepancies between the data assimilation-based reconstructions and some measurements may be related first to the estimated errors of the records. In our methodology, smaller errors imply stronger constraints, leading to reconstructions in better agreement with observations. By contrast, if the error associated with one record is large, it is legitimate that the reconstructions diverge substantially from it in order to better match with other observations. For instance, the signal to noise ratio (referred to as SNR defined as the ratio of the standard deviation of the time series over 1-1000 CE used in the data assimilation process to the "standard error" applied for the corresponding record (Table B.4)) for B32SiteDML05 is 11.79, much larger than the SNR for EDC Dome C and Dome F with the value of 0.55 and 1.18, respectively. This explains why the correlation between three data assimilation-based reconstructions and the observation is much higher at B32SiteDML05 than at EDC Dome C and Dome F when all the data are assimilated (Table 3.2). Secondly, the variability of $\delta^{18}O$ simulated by iCESM1 (and thus of the prior) also affects the agreement between the data assimilation–based reconstructions and observations. The variability at James Ross Island (standard deviation = 0.19 ‰) and RICE (standard deviation = 0.52 ‰) deduced from iCESM1 are much smaller than the one inferred from the observation (1.06 ‰ and 1.50 ‰ at James Ross Island and RICE, respectively). This implies that there are a few possibilities to find particles in agreement with the observations and explains why the variability is underestimated in the reconstructions compared to RICE and James Ross Island records.

The three data assimilation-based reconstructions capture well the 500-year trend inferred from most of the records assimilated in the corresponding experiments (Table 3.3). The exceptions are the observed negative trend during 1-500 CE at the WDC06A site and the positive trend during 501-1000 CE at the RICE site. The discrepancy at the WDC06A site may be due to the relatively low SNR (1.80) for this site inducing a small constraint on the model. Regarding the RICE site, the difference between the observed and reconstructed trends may result from the local or regional conditions. Indeed, the RICE record is characterized by a trend during 501-1000 CE opposite to the surrounding records (i.e., opposite to the negative trends shown at the Taylor Dome and Talos Dome). Therefore, even though the assimilation process is carried out on a grid scale, the large-scale coherence imposed by the model results induces a general cooling in the region and the data assimilation-based reconstructions are not able to reproduce the specific condition recorded at RICE.

Table 3.3: *Trend analysis of the period 1-500 CE and 501-1000 CE for $\delta^{18}O$ measurement and $\delta^{18}O$ reconstructed in ASSIM-LMR, ASSIM-STENNI, and ASSIM-ALL. Trends are calculated based on linear regression and are expressed in per mile per century units. The statically significant (p value < 0.1) trend is shown using bold font. The trends in the records that are not assimilated are shown in italics.*

	Trends over 1-500 CE				Trends over 501-1000 CE			
	Observation	ASSIM-LMR	ASSIM-STENNI	ASSIM-ALL	Observation	ASSIM-LMR	ASSIM-STENNI	ASSIM-ALL
Site	‰/100yrs (p)	‰/100yrs (p)	‰/100yrs (p)	‰/100yrs (p)	‰/100yrs (p)	‰/100yrs (p)	‰/100yrs (p)	‰/100yrs (p)
EDC Dome C	-0.03(0.60)	***0.06(0.00)***	**0.05(0.03)**	-0.02(0.48)	**-0.13(0.01)**	*0.00(0.47)*	0.03(0.24)	**-0.06(0.01)**
B32SiteDML05	-0.17(0.18)	-0.11(0.35)	-0.11(0.34)	-0.14(0.15)	0.02(0.66)	0.02(0.47)	0.02(0.64)	0.05(0.26)
Plateau Remote	**0.58(0.00)**	**0.26(0.00)**	**0.30(0.00)**	**0.28(0.00)**	-0.04(0.71)	-0.02(0.62)	-0.03(0.65)	-0.02(0.74)
Talos Dome	-0.11(0.12)	***0.03(0.07)***	-0.02(0.33)	-0.01(0.80)	**-0.13(0.03)**	*0.00(0.98)*	**-0.06(0.00)**	**-0.03(0.10)**
Law Dome	0.08(0.20)	0.02(0.35)	0.03(0.11)	0.02(0.34)	0.02(0.48)	0.01(0.63)	0.01(0.57)	-0.01(0.62)
James Ross Island	0.02(0.55)	**0.01(0.01)**	0.01(0.29)	0.01(0.48)	-0.04(0.20)	**-0.01(0.06)**	-0.01(0.46)	-0.01(0.55)
WDC06A	-0.03(0.52)	**0.04(0.03)**	0.00(0.87)	0.01(0.71)	**-0.12(0.00)**	**-0.03(0.08)**	**-0.06(0.00)**	**-0.04(0.01)**
RICE	**-0.12(0.08)**	*0.01(0.20)*	-0.02(0.15)	**-0.02(0.04)**	0.08(0.33)	*-0.01(0.24)*	**-0.03(0.02)**	**-0.02(0.10)**
Taylor Dome	**-0.14(0.10)**	***0.03(0.08)***	-0.05(0.25)	**-0.08(0.06)**	-0.06(0.40)	*-0.03(0.17)*	**-0.06(0.09)**	-0.05(0.19)
Vostok	-0.02(0.67)	***0.08(0.00)***	***0.07(0.01)***	**0.04(0.10)**	**-0.08(0.04)**	*-0.02(0.39)*	***-0.06(0.01)***	**-0.07(0.00)**
Dome F	0.07(0.37)	*0.03(0.11)*	*0.01(0.50)*	0.02(0.56)	0.02(0.73)	*0.00(0.95)*	*0.01(0.73)*	0.03(0.27)

It is also instructive to investigate the correlation coefficients and the 500-year trends for the records that are not assimilated. The low correlation coefficients, with values close to zero for most non-assimilated sites, imply a weak linear relationship between the reconstructions and those observations. This low agreement for independent data indicates that the data assimilation-based reconstructions are generally not able to provide local information at decadal scales, likely because the observation network is too sparse. At longer time scales, ASSIM-STENNI reproduces well the sign of 500-year trend for the non-assimilated records at Vostok and Dome F, except for the weak non-significant 1-500 CE trend at Vostok (that is also the case in ASSIM-ALL even though this record is assimilated). This suggests that the model dynamics can propagate the dominant low frequency signal brought by the assimilated proxy-based reconstructions toward the locations where no data is assimilated. However, the number of records is too small to obtain robust conclusions for this experiment. By contrast, ASSIM-LMR does not capture the reconstructed trend in the majority of the cases for the non-assimilated records. This may indicate that the relatively low number of records assimilated in the reconstruction of ASSIM-LMR (five records) limits the reconstruction skill, and that this reconstruction should be taken with caution.

After this evaluation of each record, the next step is to assess the reconstruction skills at the regional and continental scales. For this purpose, we use the regional composite of $\delta^{18}O$ from Stenni et al. (2017). Note that the reconstructions for Dronning Maud Land and the Weddell Sea coast are not discussed here as the composites in these two regions do not cover the first millennium.

As expected, among the three reconstructions, the agreement with the statistically based regional $\delta^{18}O$ composite is the best for ASSIM-STENNI as they are based on the same data. Over 1-500 CE, the correlation coefficients between the time series are higher than 0.6 for all the regions except for the WAIS and West Antarctica (Fig. 3.5). Although only five records are assimilated in ASSIM-LMR, the correlation coefficients with the statistically based regional $\delta^{18}O$ composite over 1-500 CE for the Antarctic Plateau are only slightly smaller than in ASSIM-STENNI. This indicates that EDC Dome C and Talos Dome, which are not assimilated in ASSIM-LMR but assimilated in ASSIM-STENNI, have a little impact at the regional scale for the Antarctic Plateau. By contrast, the two additional records in ASSIM-ALL (Vostok and Dome F) significantly affect the reconstructed $\delta^{18}O$ variations in Antarctic Plateau, with the lowest correlation coefficients among the experiments. However, this is not the case for the period 501-1000 CE as the correlations between the three experiments are very close for the Antarctic Plateau (and for subregions of East Antarctica).

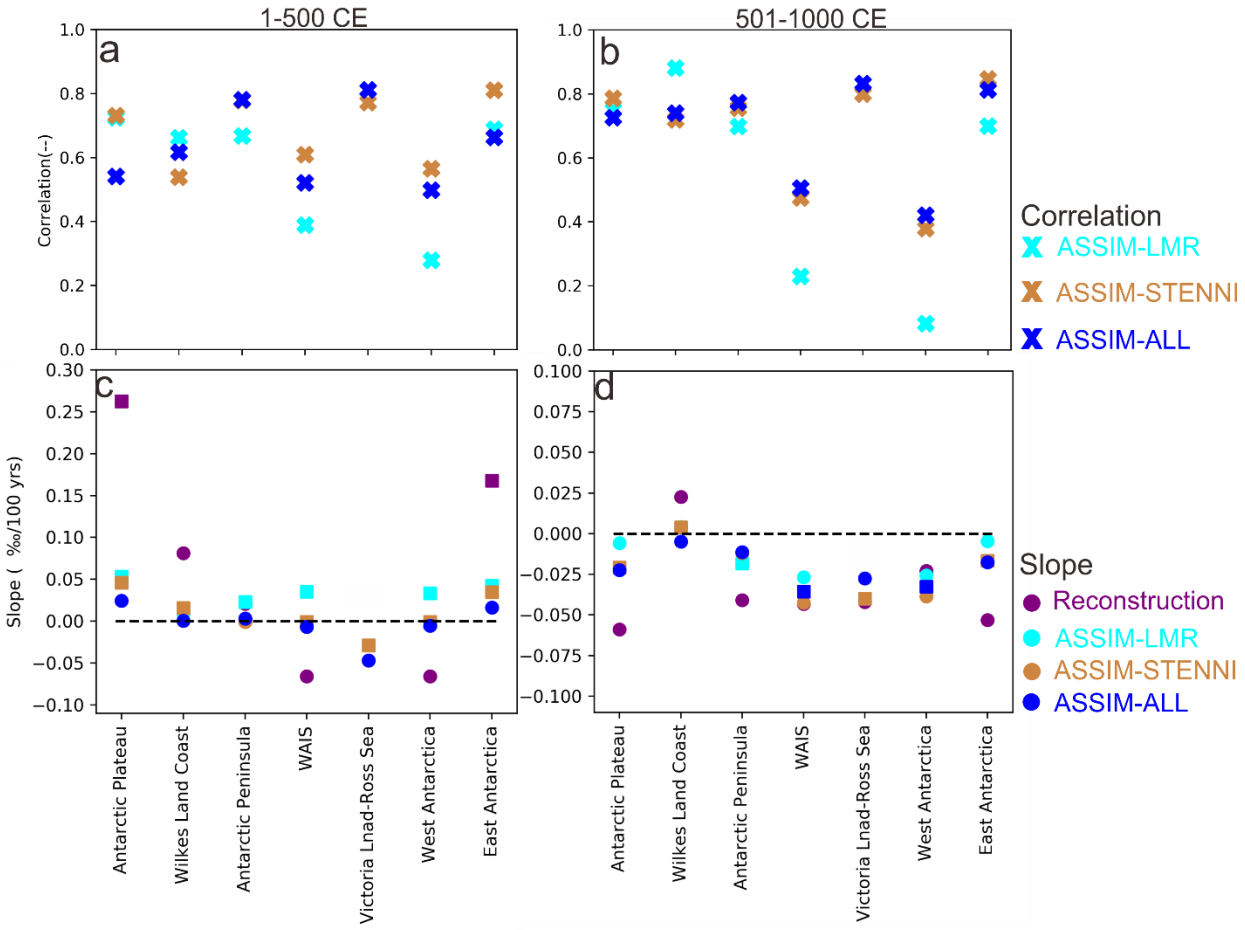

Figure 3.5: *Correlation coefficients (a, b) between the statistical-based composite $\delta^{18}O$ (Stenni et al. 2017) and data assimilation-based $\delta^{18}O$ in three reconstructions (ASSIM-LMR in the cyan, ASSIM-STENNI in the brown, ASSIM-ALL in the blue), and their trends over 1-500 CE (c) and 501-1000 CE (d). The statistically significant trend (p value<0.1) is illustrated using the square in c and d.*

Regarding the 500-year trends of the regional $\delta^{18}O$, the ASSIM-LMR presents significant positive linear trends in the WAIS and West Antarctica (0.04 ‰ per century and 0.03 ‰ per century respectively at $p < 0.1$) over 1-500 CE. During this period, the trends deduced from ASSIM-STENNI and ASSIM-ALL are negative but insignificant, consistent with the ones derived from Stenni et al. [2017]. The three reconstructions reproduce the positive trends in East Antarctica during 1-500 CE. During 501-1000 CE, the trends for most of the regions over Antarctica reconstructed in the three reconstructions have the same sign as in the statistically based reconstruction, except the Wilkes Land coast, where ASSIM-ALL shows a very weak negative trend in contrast with the positive observed one.

3.4.2 Reconstruction of surface air temperature

The comparison in Fig. 3.2 has shown that the simulations are not able to reproduce the large warming during 1-500 CE in East Antarctica and the cooling during 501-1000 in West Antarctica estimated by Stenni et al. [2017]. Indeed, three data assimilation-based SAT reconstructions in this study also show differences in this aspect (Fig. 3.6). During 1-500 CE, ASSIM-LMR and ASSIM-STENNI display statistically significant warming over East Antarctica (0.02 and 0.03 °C per century at $p < 0.1$, Fig. B.2), consistent with LMR (0.04 °C per century at $p < 0.1$), but much smaller than the statistically based reconstruction of Stenni et al. [2017] (0.14 °C per century at $p < 0.1$). However, this large-scale regional warming does not seem robust as the trend becomes very close to zero when assimilating more records (Vostok and Dome F) located in East Antarctica, as shown in ASSIM-ALL (0.00 °C per century at p value > 0.1). For West Antarctica, the data assimilation-based reconstructions, with the trend of 0.05, 0.01, 0.00 °C per century during 1-500 CE for ASSIM-LMR, ASSIM-STENNI, and ASSIM-ALL, respectively, do not show a similarity to the LMR (–0.01 °C per century at $p > 0.1$) and the statistically based reconstruction (–0.04 °C per century at $p > 0.1$).

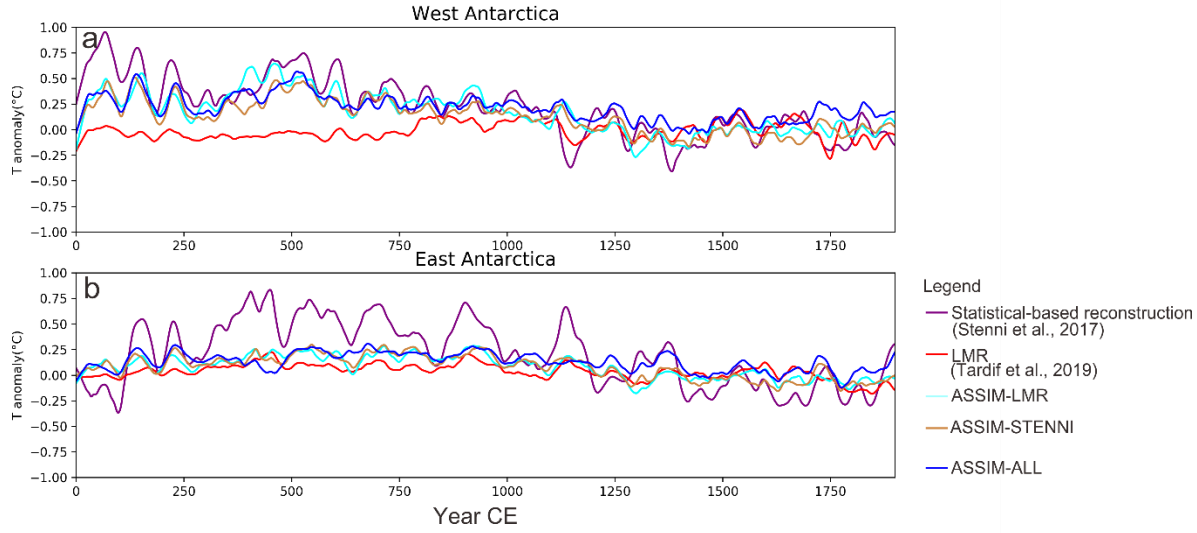

Figure 3.6: *Surface temperature anomalies (a for West Antarctica; b for East Antarctica) in the average of three statistical-based reconstructions [Stenni et al., 2017, in purple], in LMR [Tardif et al., 2019, in red], and in the three data-assimilation based reconstructions (ASSIM-LMR in cyan, ASSIM-STENNI in brown, ASSIM-ALL in blue). A 31-year Lowess smooth has been applied to the time series to see the long-term trend. The reference period is over 1000-1800 CE.*

Over 501-1000 CE, the linear trend in SAT for East Antarctica shows a common weak cooling (–0.01 °C per century for ASSIM-STENNI and ASSIM-ALL at $p < 0.1$, but at $p > 0.1$ for ASSIM-LMR), consistent with the sign of the trend in the reconstruction of Stenni et al. [2017] (–0.05 °C per century at $p < 0.1$) but with smaller magnitude. The significant cooling over

West Antarctica inferred from the statistically based reconstruction (–0.09 °C per century at $p < 0.1$) is also reproduced by our three experiments (–0.04, –0.05, and –0.04°C per century at $p < 0.1$ simulated in ASSIM-LMR, ASSIM-STENNI, and ASSIM-ALL, respectively). In contrast with the cooling deduced from the statistically based reconstruction and the three data assimilation-based reconstructions, the LMR shows significant warming (0.04 °C per century at $p<0.1$) during 501-1000 CE over West Antarctica. One possible explanation lies in a weak constraint in the LMR provided by the WDC06A record, as shown by the weak linear relationship with the measurement at WDC06A (correlation coefficient = 0.2). In the LMR, data errors are estimated using a statistical proxy system model, whose calibration relies on a sufficient overlap with the calibration data. The poor fit of proxies to the calibration data (e.g., Steig et al. [2013] show a correlation between the $\delta^{18}O$ at WDC06A and the SAT at Byrd Station of only 0.48) leads then to small weights of proxies in the LMR [Tardif et al., 2019].

Investigating the spatial distribution of the reconstructed SAT changes is also informative (Fig. 3.7). Although the temperature trends averaged over East Antarctica are similar (Fig. B.2 c) in the three experiments over 1-500 CE, the regions where a warming area is reconstructed are different (Fig. 3.7 a, c, and e). Significant warming is reconstructed nearly everywhere in East Antarctica in ASSIM-LMR (Fig. 3.7 a), but the regions shrink in ASSIM-STENNI and ASSIM-ALL (i.e., no significant warming around Victoria Land Fig. 3.7 c and e). Additionally, cooling is observed in the ASSIM-ALL and ASSIM-STENNI on the eastern Amundsen Sea coast and the western Ross Sea coast, in contrast with the ASSIM-LMR.

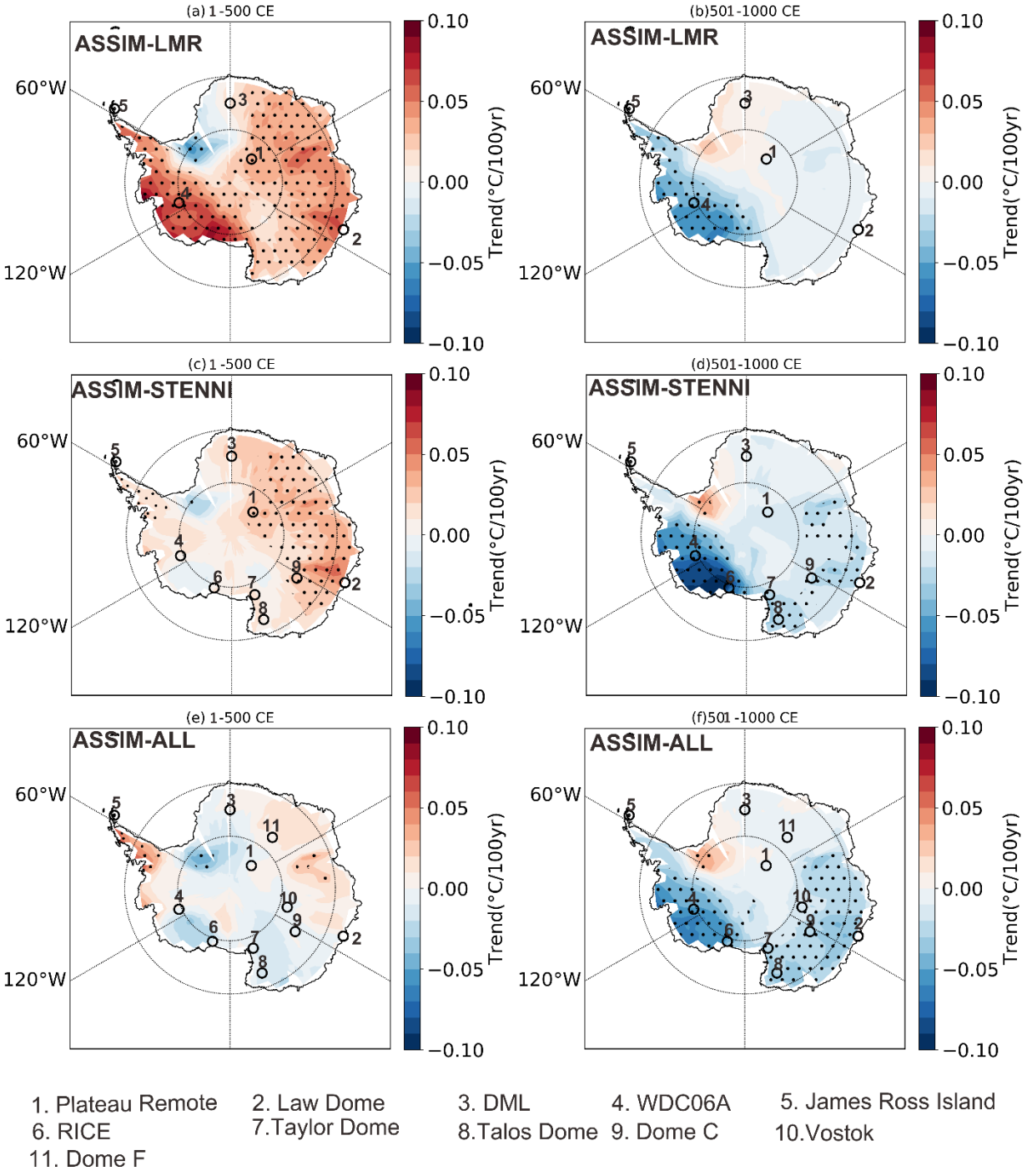

Figure 3.7: *Spatial patterns of temperature trend over 1-500 and 501-1000 CE reconstructed in ASSIM-LMR (a, b), ASSIM-STENNI (c, d), ASSIM-ALL (e, f). The position of the data assimilated in each experiment is marked by circles. The dotted area represents regions where the trend is significant at the $p < 0.1$ level.*

Over 501-1000 CE, the spatial patterns of 500-year SAT trends derived from ASSIM-LMR, ASSIM-STENNI, and ASSIM-ALL (Fig. 3.7 b, d, and f) illustrate a common signal with a statistically significant cooling over the WAIS and most of East Antarctica except in the southern Weddell Sea region. While there are minor differences in the magnitude of the cooling between the three experiments, the larger cooling over the WAIS than elsewhere in Antarctica is robust.

3.4.3 Atmospheric circulation responsible for reconstructed spatial patterns of the SAT trend

As mentioned in the Introduction, the SAM is the primary mode of atmospheric variability in the extratropical Southern Hemisphere [Marshall, 2003]. A positive (negative) SAM phase is associated with an increase (decrease) in the pressure gradient between Antarctica and midlatitudes and a strengthening (weakening) of the westerlies. The associated circulation changes have a strong influence on SAT in Antarctica, and it has been argued that positive trends in the SAM index have contributed to the contrast SAT changes between cooling in East Antarctica and warming in the AP over the past decades [Marshall, 2007; Marshall and Bracegirdle, 2015; Thompson and Solomon, 2002].

To estimate the evolution of SAM in our reconstructions, we have calculated the SAM index, as defined by Gong and Wang [1999], based on the difference of the normalized zonal mean 10-year average 500 hPa geopotential height between 40 °S and 65 °S. Except for a weak negative trend in the SAM during 1-500 CE in ASSIM-LMR, all the other trends are positive, with the trends during 501-1000 CE in ASSIM-STENNI (0.47 per century, p value = 0.03) and ASSIM-ALL (0.44 per century, p-value = 0.00) being statistically significant (Fig. B.3 a). A congruence analysis [Thompson et al., 2000] is then used to determine SAM contribution to the SAT trends. This is done by first detrending the time series of reconstructed SAT for each grid cell and linearly regressing the detrended SAT onto the detrended SAM index. We then multiply the regression coefficients by the SAM trend to obtain the SAM–congruent trends. For the reconstructions with positive SAM trends (i.e., during 1-500 CE in ASSIM-STENNI (Fig. B.4 c) and ASSIM-ALL (Fig. B.4 e) and during 501-1000 CE in three reconstructions (Fig. B.4 b, d, f)), the patterns of SAM–congruent trends show general cooling over Antarctica and warming in AP. In particular, for the reconstructions presenting significant trends in SAM, the SAM–congruent trends during 501-1000 CE over Antarctica are –0.023 °C per century and –0.017 °C per century in the ASSIM-STENNI (Fig. B.4 d) and ASSIM-ALL (Fig. B.4 f), respectively, which is almost identical to the SAT trend in ASSIM-STENNI and ASSIM-ALL (–0.020 °C per century and –0.018 °C per century).

The Amundsen Sea Low (ASL) is a climatological low–pressure system centered around 120°E, 68°S. Its variations, which are not independent to the ones of SAM, strongly influence the climate of the WAIS and the AP [Raphael et al., 2016, Hosking et al., 2013]. Over 1-500 CE, there is no common signal of the geopotential height trends in the ASL region in three

reconstructions. In ASSIM– LMR, the trends in geopotential height display a dipole pattern with an increase centered roughly over the AP and a decrease in the north of the Ross Sea (Fig. 3.8 a). In ASSIM-STENNI and ASSIM-ALL, the geopotential decreases in the whole Pacific sector of the Southern Ocean with a maximum trend around 120°W but the changes are significant only in ASSIM-ALL (Fig. 3.8 c, e). Over 501-1000 CE, the deepening ASL is consistent among three reconstructions (Fig. 3.8 b, d, and f).

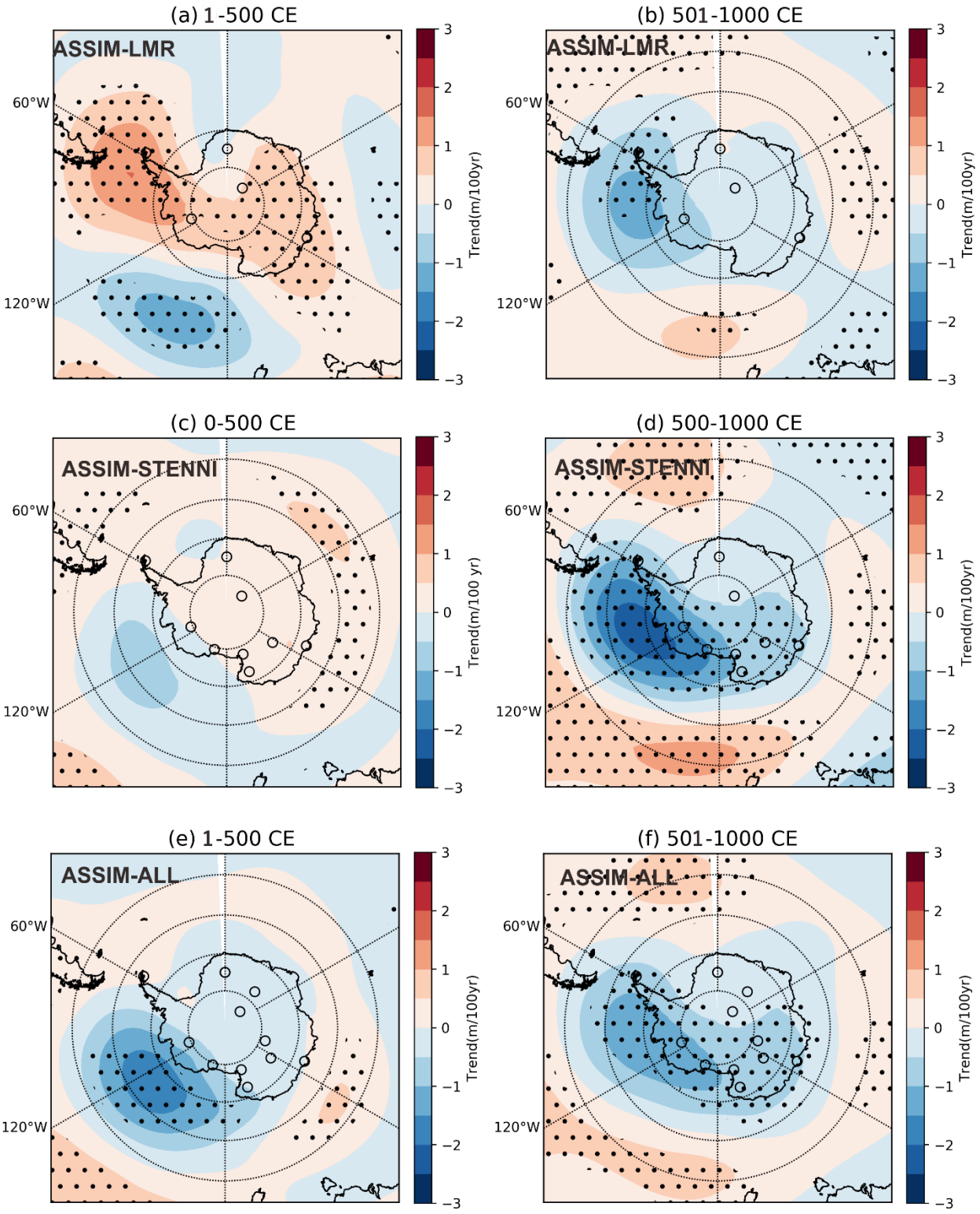

Figure 3.8: *Same as Fig. 3.7 but for spatial patterns of 500 hPa geopotential height trend (m/century).*

In order to quantitatively describe the changes in ASL, we calculate the ASL index by first calculating the 10–year average 500–hPa geopotential height over the region defined as 170° E to 70°W, 60°S to 75°S [Turner 2013, Hosking et al., 2013], and then normalized it (zero mean and unity standard deviation) over the first millennia. Consistent with the negative anomalies over the ASL region in Fig. 3.8, the changes in the ASL index show the negative trend during 1-500 CE in ASSIM-STENNI (–0.06 per century at p value > 0.1) and ASSIM-ALL (–0.21 per century at p value < 0.1) and during 501-1000 CE in three reconstructions (–0.10, –0.26, and –0.17 per century at p value < 0.1 in ASSIM-LMR, ASSIM-STENNI, and ASSIM-ALL, respectively) (Fig. B.3 b). The ASL-congruent trends in three reconstructions indicate the larger cooling in western WAIS than elsewhere in Antarctica (Fig. B.5). For instance, the ASL-congruent trend over 501-1000 CE in the WAIS is –0.044 °C per century in ASSIM-STENNI and –0.028 °C per century in ASSIM-ALL, explaining 80 % of the trend in ASSIM-STENNI (–0.055 °C per century) and 67 % of the trend in ASSIM-ALL (–0.042 °C per century).

However, the attribution of warming over East Antarctica during 1-500 CE in the three reconstructions is still not clear. It is well known that the SAM could impact the SAT over East Antarctica [e.g., Marshall and Thompson 2016]. However, we do not find a clear large-scale circulation pattern over 1-500 CE common in ASSIM-LMR, ASSIM-STENNI and ASSIM-ALL to explain the warming over East Antarctica. Nevertheless, we find that the northerly winds from the South Atlantic Ocean, penetrate the interior of the Antarctica Plateau, directly reach the site of Plateau Remote and potentially induce warming there in ASSIM-LMR and ASSIM-STENNI (Fig. B.6). In ASSIM-ALL, the weak positive SAM trend during 1-500 CE would be related to cooling in East Antarctica, not with a warming there. Note that this result should be taken with caution as the different circulation patterns over 1-500 CE reconstructed in three experiments indicate the sensitivity of the changes to the records assimilated.

3.5 Sensitivity of the reconstruction with data assimilation to the uncertainty of the records

The error of the data is a key parameter in the data assimilation process to determine the effective weight given to the information provided by each record. It has thus a direct impact on the local agreement between reconstruction and data. The results presented in Section 3.4.1 have shown that when using standard errors obtained by the methodology described in section 3.2, the reconstructions do not follow some of the records well. For instance, in ASSIM-LMR, the correlation coefficient between the reconstructed $\delta^{18}O$ with the observation at WDC06A during 1-500 CE is 0.62, smaller than the one obtained at Plateau Remote (0.97). This is consistent with larger SNR at Plateau Remote (3.58) than at WDC06A (1.80).

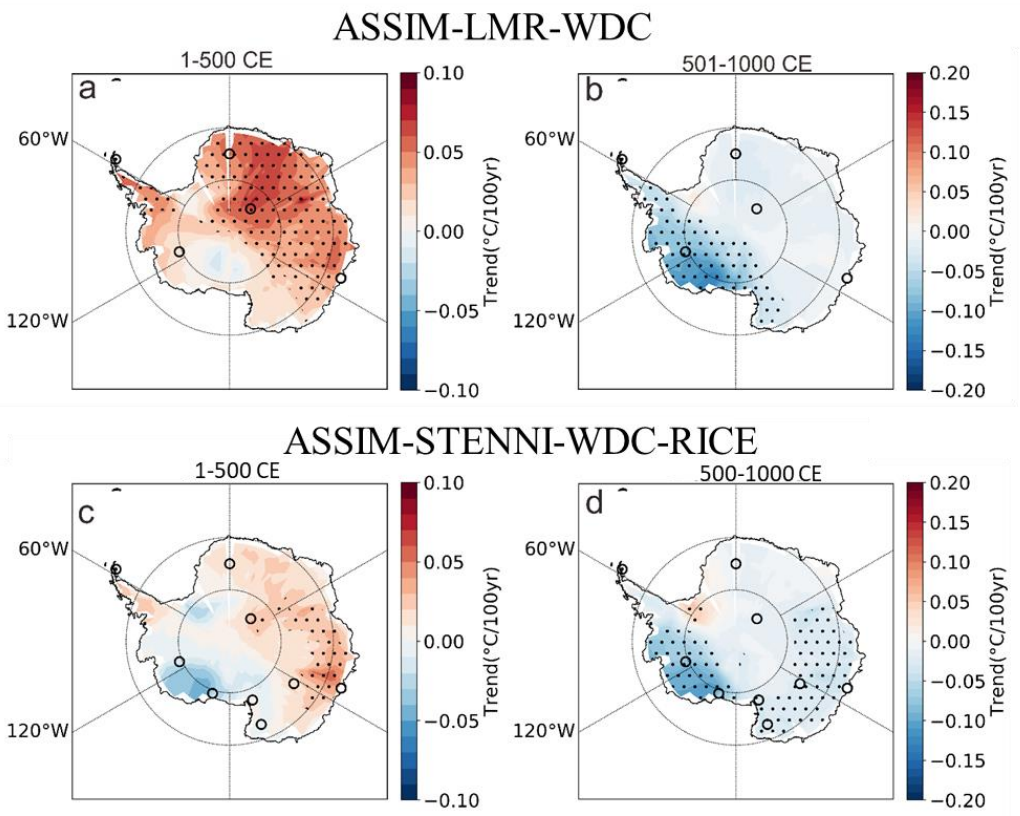

Figure 3.9: *Spatial patterns of temperature trend over 1-500 and 501-1000 CE reconstructed in ASSIM-LMR–WDC (a, b), and ASSIM-STENNI–WDC-RICE (c, d). The position of the data assimilated in each experiment is marked by circles. The dotted area represents regions where the trend is significant at the p<0.1 level.*

Previous studies have indicated that the ice core water isotopic signal at WDC06A is probably a good indicator of regional SAT for the WAIS [Steig et al., 2013; Stenni et al., 2017]. Several records at WDC06, like the borehole temperature and the snow accumulation record, are consistent with each other in the long–term trend over the past millennium [Orsi et al., 2012]. In contrast, RICE, another record in WAIS, may be affected by air mass from the eastern Ross Sea [Emanuelsson et al., 2017], thus reflecting more local signals. Since the changes in WDC06A appear more representative of large-scale variations, more weights have been given to WDC06A compared to RICE in the statistically based reconstructions of Stenni et al. [2017].

In order to test the influence of the way the climatic information brought by in WDC06A and RICE is taken into account in the reconstructions, we have first launched a sensitivity experiment in which the standard error of WDC06A has been decreased by 90% (ASSIM-LMR–WDC). For the other records, the experimental design is the same as that of ASSIM-LMR. As expected, due to a much stronger constraint on this record, the $\delta^{18}O$ observation at WDC06A is nearly perfectly reproduced in ASSIM-LMR-WDC, with a correlation coefficient of 0.98 for 1-1000 CE. However, the area–averaged SAT trend in the WAIS over 1-500 CE

still presents weak warming in contrast to the cooling displayed in Stenni et al. [2017]. This warming is distributed almost throughout the whole WAIS (Fig. 3.9 a), but with smaller magnitudes than in ASSIM-LMR. During the 501-1000 CE period, the spatial pattern of SAT trends seems very similar to ASSIM-LMR, with larger cooling in the WAIS than elsewhere in Antarctica (Fig. 3.9 b).

In the second sensitivity experiment, the errors in WDC06A and RICE have been reduced by 50%, and the experimental design is the same as in ASSIM-STENNI for the other records (ASSIM-STENNI-WDC-RICE, Fig. 3.9 c and d). In contrast to ASSIM-STENNI and ASSIM-ALL, the trend of SAT in the WAIS during 1-500 CE is negative in ASSIM-STENNI-WDC-RICE (–0.01 °C per century), consistent with the sign of statistically based reconstructions in Stenni et al. [2017]. The cooling over the WAIS is mainly located in the western part of the Amundsen Sea coast region, resembling the pattern shown in ASSIM-ALL. In addition, the circulation patterns for both periods are also very similar to those in ASSIM-ALL and ASSIM-STENNI (Fig. B.7).

These two sensitivity experiments, ASSIM-LMR, ASSIM-ALL, and ASSIM-STENNI, show that the spatial pattern of the trends reconstructed over the WAIS for the period 1-500 CE is complex, with likely a dipole between the eastern and western parts of the region. The magnitude of the changes is very sensitive to the way each record is included (or not) in the assimilation process. Furthermore, the local signal at the proxy location is not necessarily representative of larger scale averages. This implies that the mean trend over the region over 1-500 CE is very uncertain.

3.6 Comparison to other terrestrial records over Antarctica

The time series of publicly available proxies derived from lake sediments, peat banks, and ice cores are mainly distributed in the AP, WAIS coast, Wilkes Land coast, and Dronning Maud Land (Fig. 3.10). Therefore, comparisons of our reconstructions with these proxies will focus on these regions.

In the AP, moss accumulation rates (Fig. 3.10 A) and biological productivity (Fig. 3.10 B) derived from peat banks (cores) have been used as indicators of SAT based on its strong correlation with meteorological temperature records [Charman et al., 2018]. These proxies show a generally positive tendency during 1-500 CE, followed by a significant decrease over 501-1000 CE. This is consistent with the warming in the first five centuries, followed by the 500–year cooling shown in three data assimilation–based reconstructions. In addition, a biomarker proxy (Glycerol Dialkyl Glycerol Tetraether, GDGT, Fig. 3.10 C) obtained from lake sediment in a sub-Antarctic island close to the AP also suggests a large decrease in summer temperature since 500 CE [Roberts et al., 2017].

The spatial pattern of SAT trends in the WAIS during 1-500 CE reconstructed in our experiments depends on the records and the errors applied in the data assimilation. A cooling

area distributed in the western WAIS along the Amundsen Sea coast is observed in the experiments that both assimilate WDC06A and RICE, although its magnitude is influenced by the errors estimated for these records. Since there are only a few climate records available for comparison in the WAIS, we collect the proxies extracted from the ice cores, from which we use isotopic measurements (WDC06A and RICE). Snow accumulation data in Antarctica have been used as an SAT proxy because of the generally good correlation between the two variables [Dalaiden et al., 2020]. Here, the snow accumulation (Fig. 3.10 F) and borehole temperature inversion (Fig. 3.10 G) at WDC06A are consistent with the data assimilation–based SAT reconstructions with the cooling during 501-1000 CE. However, the large uncertainties in the borehole temperature reconstruction [Orsi et al., 2012] and the large centennial variability of the snow accumulation [Fudge et al., 2016] in the first five centuries make it challenging to present clear trends at WDC06A. The only information coming from a different location, the Siple Dome, shows positive multi-centennial trends expressed by the melt frequency record [Fig. 3.10 D, Das et al., 2018], which indicates long–term warming in contrast to all the other records. Long–term warming in the first millennia is also reflected in the positive trend in the snow accumulation record at RICE (Fig. 3.10 E). This is potentially related to sea ice effects in the Ross Sea [Bertler et al., 2018].

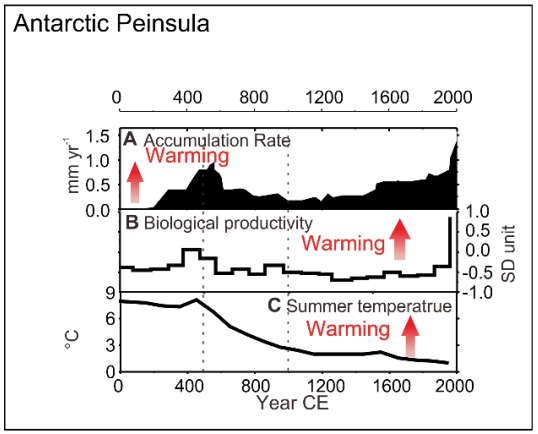

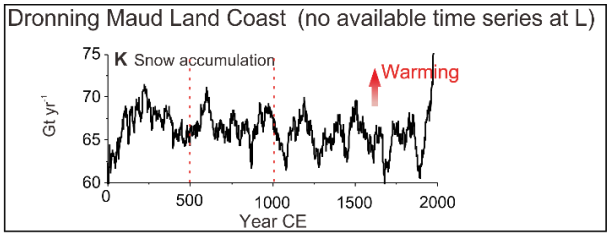

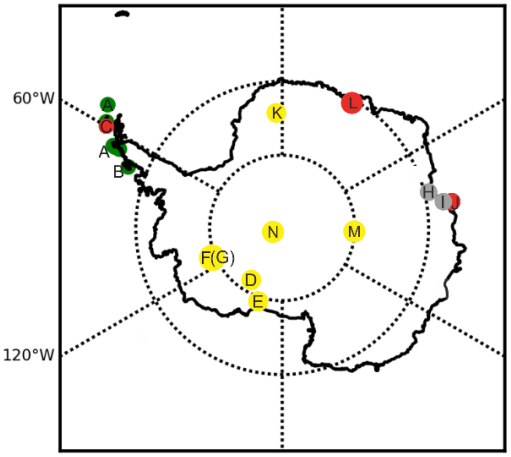

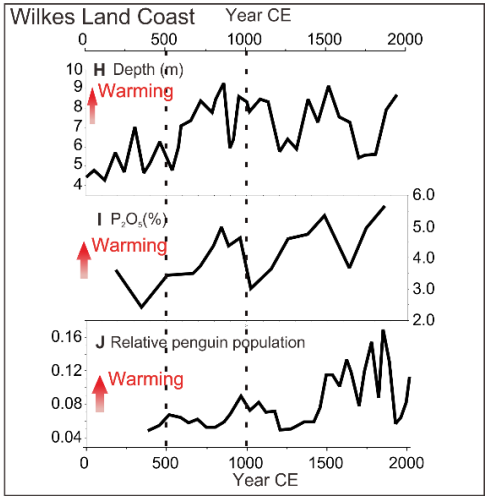

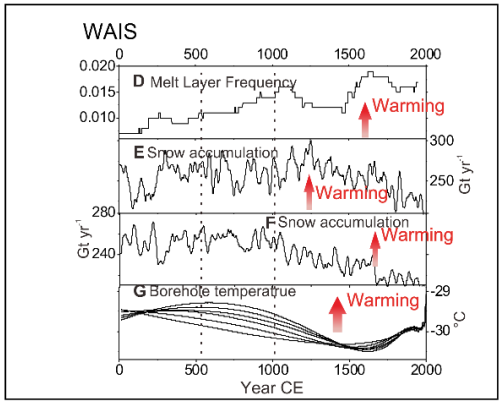

Lake core Peat core Ice core
Other proxes

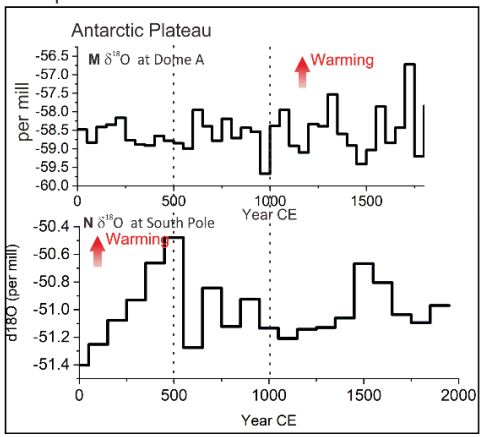

Figure 3.10: *Additional proxies from terrestrial records over Antarctica. The colored dots refer to the position of the different proxies. A moss accumulation in AP [Stelling et al., 2018]; B biological productivity [Charman et al., 2018]; C GDGTs [Roberts et al., 2017]; D melt layer frequency at Siple Dome [Das et al., 2008]; E snow accumulation at RICE [Bertler et al., 2018]; F snow accumulation at WDC06A [Fudge et al., 2016]; G borehole temperature at WDC06A [Orsi et al., 2012; H diatom [Verleyen et al., 2004]; I element concentrations [Huang et al., 2011]; J geochemical element [Gao et al., 2019]; K snow accumulation at B40 [Medley et al., 2018]; L fossil pigments, sedimentological and geochemical proxies [Tavernier et al., 2014, no available time series]; M water stable isotope record ($\delta^{18}O$) at Dome A [An et al., 2021]; N water stable isotope record ($\delta^{18}O$) at the South Pole [Steig et al., 2021].*

Proxies in East Antarctica are mainly distributed in coastal areas. On the Wilkes Land coast, the reconstructed lake depth using diatom from lacustrine sediments (Fig. 3.10 H) shows a significant increasing trend over the first millennium [Verleyen et al., 2004]. This indicates a tendency to more humid and warm conditions around Prydz bay (Fig. 3.10 H) in contrast to our reconstructions, in particular for the period 501-1000 CE. In the Vestfold Hills (Fig. 3.10 I) near Prydz bay, Huang et al. [2011] have observed an increase in the penguin population based on the Phosphorus concentration (Fig. 3.10 I) during 501-1000 CE. However, Gao et al. [2019] suggest a more stable population (Fig. 3.10 J), which is more consistent with our three reconstructions of SAT changes. It is noted that the factors that affect the penguin populations may be dependent on the food chain rather than the climate [Gao et al., 2019]. This is thus difficult to derive strong conclusions from the comparison with our reconstructions.

Some evidence of the warming over 1-500 CE is also found in Dronning Maud Land. The lake sediments in Lützow Holm Bay show a clear shift from marine to lacustrine conditions during 2120–1500 cal yr BP, with seasonal sea ice free coastal areas occurring in the region [Tavernier et al., 2014; no available time series in Fig. 3.10 L]. In addition, the snowfall accumulation record (Fig. 3.10 K) in western Queen Maud Land presents a positive trend during around 1–300 CE [Medley et al., 2018], also reflecting a warming trend consistent with our reconstructions.

In the Antarctic Plateau, no trend during 1-500 CE is reflected in the water stable isotope $\delta^{18}O$ record at Dome A [Fig. 3.10 M; An et al., 2021], consistent with the reconstruction in ASSIM-ALL. However, another $\delta^{18}O$ record at South Pole [Fig. 3.10 N; Steig et al., 2021] shows a significant increase during 1-500 CE, similar to the reconstruction in ASSIM-LMR and ASSIM-STENNI. Accordingly, it is still hard to assess the robustness of three reconstructions during 1-500 CE. Nevertheless, these independent water stable isotope $\delta^{18}O$ records at Dome A and the South Pole have shown a negative trend during 501-1000 CE. This is in agreement with the robust cooling during 501-1000 CE in our reconstructions. Unfortunately, due to the lack of terrestrial proxy in Victoria Land, we still are not able to evaluate the SAT changes in this region where the main discrepancies between the three experiments occur during the 1-500 CE.

3.7 Conclusion

Three different ice core $\delta^{18}O$ databases are assimilated in the different experiments (ASSIM-LMR, ASSIM-STENNI, and ASSIM-ALL) to reconstruct Antarctic SAT over the first millennium. The signals reconstructed in three experiments are generally consistent with the $\delta^{18}O$ observations, with a few exceptions at the local scale. The three reconstructions and two additional sensitivity experiments show that the spatial pattern of SAT trend over 1-500 CE is quite sensitive to the choice of data and errors used in the data assimilation procedure. The mean cooling in West Antarctica derived from the statistically based reconstructions is reproduced only when assimilating the same records as Stenni et al. [2017] and using relatively

low uncertainties at WDC06A and RICE. Over East Antarctica, the warming inferred from the reconstructions of Stenni et al. [2017] over 1-500 CE is reproduced in the experiment ASSIM-LMR and ASSIM-STENNI, but not in ASSIM-ALL that assimilates the largest number of records in the Antarctica Plateau. This indicates that the Plateau Remote record, which displays a large positive trend, has a large impact on the reconstruction in East Antarctica in ASSIM-LMR and ASSIM-STENNI as only a few records are available, but this influence decreases when there are more records in East Antarctica leading to a very weak trend in ASSIM-ALL. Nevertheless, we still find common warming in the AP during the period 1-500 CE in the three reconstructions, consistent with other terrestrial proxies. Although significant differences in the spatial distribution of SAT change during 1-500 CE are observed among three reconstructions, it is difficult to rank the credibility of these reconstructions based on independent data due to the limited number of proxies available. Still, our reconstructions are provided as three hypotheses of the spatial distribution of 500-year SAT change over Antarctica, which could be tested when new reconstructions would be available in the future.

In contrast, during 501-1000 CE, a robust signal has been obtained in the three data assimilation–based reconstructions with general cooling over continental Antarctica. This cooling occurs with a larger magnitude in the WAIS than elsewhere over Antarctica. The cooling in Antarctic Plateau has an agreement with the latest composite based on seven ice core $\delta^{18}O$ records in Antarctic Plateau provided by An et al. [2021]. Compared to the relatively complex spatial pattern during 1-500 CE, the pattern during the second half of the first millennium seems to be more robust and spatially homogeneous over Antarctica. The relatively similar results in our reconstructions indicate that adding more records in the data assimilation procedure is not modifying the large-scale pattern, likely because of a relatively homogeneous signal archived in records.

In agreement with the PMIP3-CMIP5 simulations, the simulations covering the full CE are able to reproduce the cooling in Antarctica over the past millennium. However, they fail to capture the multi-centennial changes in the first millennia derived from the statistically based reconstructions, in particular for East Antarctica. Similar discrepancies, but weaker in magnitude, are also observed between existing simulations and the reconstructions presented here. For instance, SAT in East Antarctica increases significantly during 1-500 CE (0.02 and 0.03 °C per century at $p < 0.1$ in ASSIM-LMR and ASSIM-STENNI and 0.00 per century at $p > 0.1$ in ASSIM-ALL), which is beyond the range or at the edge of the simulations (from –0.01 to 0.01 °C per century). The cooling during 501-1000 CE in West Antarctica in three reconstructions (–0.04 °C per century in ASSIM-LMR and ASSIM-ALL, –0.05 °C per century in ASSIM-STENNI; p value < 0.1) is also larger than in models (from –0.01 to 0.03 °C per century). The differences in the 500–year trends between the simulations and our reconstructions are smaller than the simulations and the statistically based reconstructions. Nevertheless, we conclude that the selected models have likely a too weak internal variability that may play the dominant role in the multi-centennial trends in the first millennium.

Atmospheric circulation associated with SAT changes has also been reconstructed in our three experiments. Consistent with the complex and uncertain SAT pattern over 1-500 CE, the reconstructed atmospheric circulations in our three reconstructions do not display a robust large-scale pattern during this period. The warming over East Antarctica reconstructed in ASSIM-ALL and ASSIM-STENNI might be related to more northerly inflow, but there is no clear atmospheric circulation pattern explaining this potential temperature increase at this stage. Nevertheless, the deepening of the ASL during 1-500 CE may be related to the cooling in western WAIS shown in ASSIM-STENNI and ASSIM-ALL. During 501-1000 CE, a positive SAM phase with deepening ASL is common in the three reconstructions. The trends in these atmospheric circulation changes have almost entirely explained the origin of SAT pattern shown in our reconstructions. This suggests that the 500-year SAT trend over Antarctica, at least during 501-1000 CE, arises from changes in atmospheric circulation, likely related to the internal variability of the climate system.

4

Widespread cooling over West Antarctica and adjacent seas over the past millennium

Abstract

Instrumental observations have highlighted strong inter-connections in the Antarctic climate system between the atmosphere, ocean and sea ice over past decades. In this study, our goal is to take advantage of those links to reconstruct past climate changes over West Antarctica and surrounding seas, by combining marine and terrestrial records with climate modeling results using data assimilation. By comparing two data assimilation experiments that use the same terrestrial proxy records with annual and decadal temporal resolutions, we confirm that the covariance relationship between several key climate variables (surface air temperature, sea ice, and atmospheric circulation) used in the data assimilation is timescale dependent. An assimilation step of 10 years appears as a good compromise in our experiments. We then found that the contributions of continental and marine records on the reconstructions are clarified by two separate data assimilation experiments: one using the continental proxies only and another one using both continental and marine records. Our results suggest that the latter assimilation is useful to have a stronger and more direct constrain of the evolution of the ocean-atmosphere coupled system, and is more faithful as suggested by the validation against independent sea ice-related marine records. Based on our reconstruction for multiple variables covering the past two millennia, we confirm a widespread cooling trend occurred over West Antarctica and surrounding seas over the period 900-1800 CE. This reconciles the inconsistency between some existing reconstructions and climate model results, in particular over the Antarctic Peninsula. This cooling could be explained by a direct thermodynamic response to volcanic forcing over the period. This result has highlighted that West Antarctica and surrounding seas are sensitive to the external forcings at this time scale, especially to the volcanic forcing, and the temperature evolution there is coherent with global changes at the centennial scale over the past millennium.

4.1 Introduction

Over the past decades, the West Antarctic climate has experienced pronounced interannual and decadal variations, with for instance a remarkable warming twice as fast as the global one from the 1970s to the 1990s followed by a pause or a cooling in the first two decades of the 21st century [Turner et al., 2016; Turner et al., 2020; Steig et al., 2009]. Many studies have attributed this change to the combined effects of the depleted stratospheric ozone, increased greenhouse gas concentrations [Thompson et al., 2002; Marshall et al., 2004], and internal variability, in particular related to tropical-high-latitude atmospheric teleconnections [Ding et al., 2011; Clem et al., 2021; Li et al., 2021], and atmospheric-sea ice interactions [Turner et al., 2016]. However, the too short instrumental records limit our ability to fully estimate the contribution of the respective forcings compared with the internal variability, especially at decadal to centennial scales [Jones et al., 2016; Clem et al., 2021].

The past millennia offer the possibility to gain insight into natural decadal- to centennial-scale changes that cannot be discerned from instrumental data. To this end, surface air temperature (SAT) for West Antarctica has been reconstructed from proxy data, mainly using borehole temperature [e.g., Orsi et al., 2012], water isotopic records from ice cores [e.g., Stenni et al., 2017], and climate model simulations [e.g., Klein et al., 2019]. Nevertheless, clear differences have been obtained between the various proxy-based reconstructions, as well as between reconstructions and modeling results. As a consequence, the past SAT changes over West Antarctica are still relatively uncertain, especially the magnitude of a potential multi-centennial cooling trend over the past millennium that is sometimes referred to as the transition from a relatively mild Medieval Climate Anomaly (MCA) to a colder Little Ice Age (LIA), in particular for some regions of the Northern Hemisphere [Bradley et al., 2003; Mann et al., 2009].

Among all existing proxy-based temperature reconstructions, Stenni et al. [2017] presents probably the most extensive one. On the basis of 112 ice-core water isotopic records, they provide SAT reconstructions for seven Antarctic regions over the past two millennia, including two regions for West Antarctica: the Antarctic Peninsula (AP) and the West Antarctica Ice Sheet (WAIS). While a pronounced cooling over the past millennium is reconstructed for the WAIS, as for many other regions of the world [PAGES 2k Consortium, 2013; McGregor et al., 2015], the trend is much weaker in the AP. However, the weak multi-centennial variability in the AP climate reconstructed by Stenni et al. [2017] seems inconsistent with the glacial advance that occurred there from 1550 CE to 1860 CE [Simms et al., 2021]. Additionally, Lüning et al. [2019] found that non-ice temperature sensitive records (mainly lake and marine sediments) suggest a generally warm MCA and cold LIA in the AP. The sea ice-related diatom records from marine sediments also suggest a heavier sea ice cover in the eastern AP since 1300 CE [Barbara et al., 2016]. Finally, the simulations performed in the framework of the Past Model Intercomparison Project [PMIP3, Otto-Bliesner et al., 2009] and the fifth phase of

the Coupled Model Intercomparison Project [CMIP5; Taylor et al., 2012] show a significant and widespread cooling over West Antarctica during the pre-industrial past millennium [Klein et al., 2019; Silvestri et al., 2021], which also disagrees with the reconstruction in Stenni et al. [2017] for the AP.

Studies based on reconstructions and model simulations have suggested that solar and volcanic forcings are the main drivers of the cooling trend over West Antarctica during the past millennium [e.g., Orsi et al., 2012; Goosse et al., 2012]. At the first order, the response to this forcing is expected to give a relatively homogenous cooling over the region due to a reduced radiative forcing. However, large-scale modes of variability such as the Southern Annular mode (SAM, the primary pattern of climate variability in the extra-tropical Southern Hemisphere characterized by opposing pressure and temperature anomalies over the middle and high southern latitudes), or changes in the Amundsen Sea Low (ASL, a climatological low-pressure system centered in the Amundsen Sea) can also modulate the surface climate at multi-decadal time scale [Lyu et al., 2021; Dalaiden et al., 2021]. For instance, the latter could induce temperature changes of different magnitude or even sign in West Antarctica, as a function of modifications of its location associated with changes in wind direction and intensity [e.g., Hosking et al., 2013; Dalaiden et al., 2021]. Describing precisely the pattern of past temperature changes is thus essential to identify the relative contribution of a direct radiative forcing and circulation changes.

In this framework, the goal of the present study is to investigate the potential existence of a widespread cooling over West Antarctica and adjacent seas over the past millennium and to identify the underlying mechanisms. Our analysis will be mainly based on the data assimilation (DA) method that combines observational data and model results to reconstruct the state of the climate system [e.g., Hakim et al., 2016]. Previous offline DA-based reconstructions [Dalaiden et al., 2021; O'Connor et al., 2022] assimilated annual-resolved continental data to obtain atmospheric states and oceanic conditions (in particular sea ice). However, the covariance between atmospheric and oceanic variables could be non-stationary across different time scales. For instance, the response of sea ice and oceanic temperatures in the Southern Ocean to stronger westerly winds includes a several-years long cooling and sea ice expansion due to the induced northward transport of cold Antarctic surface waters, potentially followed at the decadal scale by a warming due to the upwelling of Circumpolar Deep Waters [Ferreira et al., 2015]. In contrast to previous studies, we here assimilated five marine proxies in order to have a stronger and more direct constraint of the evolution of the ocean-atmosphere coupled system. We examined the sensitivity of our results to the temporal resolution (annual and decadal) of the assimilated data and the selection of the proxies to test the robustness of our results and for a comparison with earlier studies.

4.2 Data and methods

4.2.1 Proxy records

For the continental proxy records with the annual temporal resolution, we rely on ice-core based snow accumulation and water isotope ($\delta^{18}O$) data synthesized in Thomas et al. [2017] and Stenni et al. [2017]. As we are interested in long-term changes and to avoid the issues related to a changing number of records, data located in West Antarctica and having a time span covering the full (or almost full) Common Era (1-2000 CE) are selected. This corresponds to five $\delta^{18}O$ records and two snow accumulation records (as shown $\delta^{18}O$-DA and SN-DA in Fig. 4.1). In addition to the continental proxy records, we use four well-constrained multi-decadal Alkenone-based SST reconstructions off the southern Chilean coast (SST-DA in Fig. 4.1) and one quantitative reconstruction of sea ice presence off the coast of Adelie Land in Antarctica (SIP-DA in Fig. 4.1). They all cover the period 1-1800 CE. Previous studies argued that the Alkenone-based SST reconstructions could have a small bias toward the spring (and/or) summer blooming season [e.g., Tierney and Tingley, 2018]. Therefore, we test the sensitivity of the DA-based reconstructions to the seasonality of these SST reconstructions, as described in Section 4.3.2. In addition, several multi-decadal marine diatom records associated with qualitative sea ice changes in the AP and Ross Sea coast (SI-Valid in Fig. 4.1) are used to evaluate our results (see details in Section 4.3.2) as assimilating directly those qualitative records is difficult. Detailed information about these records is provided in Table 4.1.

It is still a challenge for current paleoclimate DA techniques to incorporate proxies across an arbitrary range of time resolutions [Steiger et al., 2017]. Therefore, in addition to the tests at annual resolution using only high-resolution records, we have selected a single uniform timescale of 10 years to fuse the low-resolution marine records and high-resolution continental records together. Specifically, a 10-year bin average is applied for the annual-scaled continental proxies, while we use linear interpolation to obtain a pseudo-decadal resolution for the multi-decadal marine records.

In addition to those proxy records covering the past two millennia, another set of data is used in the validation (see detailed in Section 4.2.4). These data are the same as the ones used in Dalaiden et al. [2021], thus including all ice-core based annual-resolved records from the database of Stenni et al. [2017] and Thomas et al. [2017] as well as tree-ring width records located in the Southern Hemisphere from PAGES 2K database [2017]. It should be noted that, in contrast to Dalaiden et al. [2021] that used the ice-core data over the whole Antarctic continent, we use only those located in WA (including 34 snow accumulation records and 20 $\delta^{18}O$ records shown in Fig. C.1).

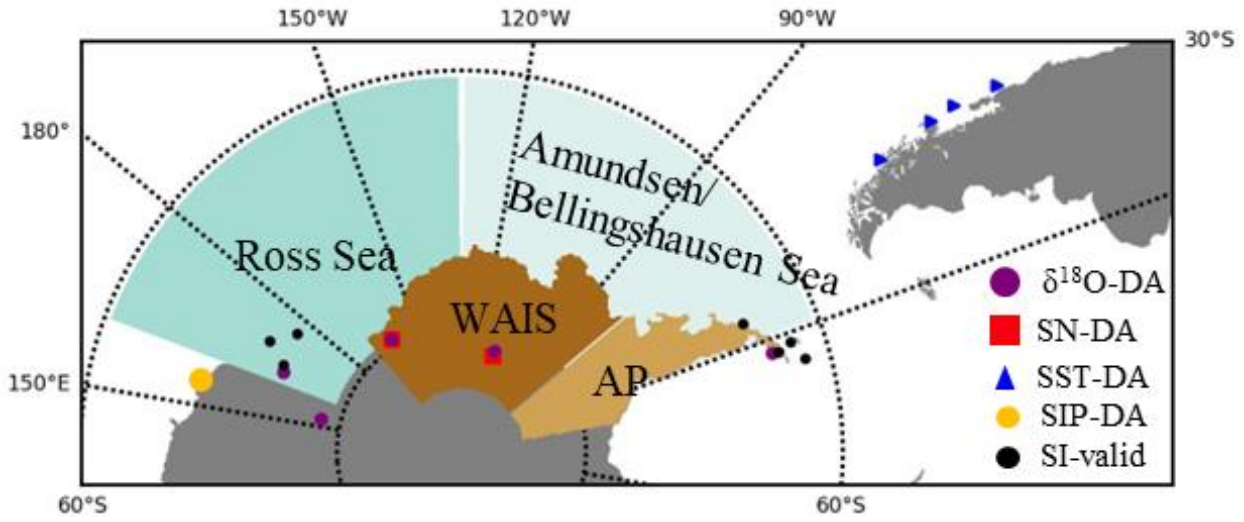

***Figure 4.1**: Locations of the proxy records covering the past two millennia used in this study. The symbols of blue triangle (SST-DA), yellow circle (SIP-DA), purple circle (δ^{18}O-DA), and red rectangular (SN-DA, almost overlapping with the δ^{18}O-DA) represent the locations of four SST reconstructions, one reconstruction of sea ice persistence, three precipitation-weighted δ^{18}O records and two snow accumulation records, respectively. The black triangles (SI-Valid) refer to qualitative data used for the validation of our results. The green shading area in the Southern Ocean denotes two zones with regional-scaled sea ice extent (i.e., at least 15% of the ocean surface covered by sea ice) following the definition of Parkinson [2019]: the Bellingshausen/Amundsen Sea zone (130°W-60°E, light green) and the Ross Sea zone (160°E-130°W, dark green). The brown shading area in Antarctica represents two climate regions investigated in this study including the Antarctic Peninsula (AP, 70 -74°S, 60°W - 80 °W, light brown) and the West Antarctic Ice Sheet (WAIS, north of 85°S, 60°W-170°W, dark brown) followed Stenni et al. [2017].*

***Table 4.1:** (a) Description of the proxy records covering the past two millennia used for the DA experiments. (b) Description of the proxy records used for the validation.*

Name	Location	Proxy type	Reference
GeoB3313-1	Southern Chilean coast	Alkenone	Lamy et al.,2002
MD07-3093	Southern Chilean coast	Alkenone	Collins et al., 2019
MD07-3088	Southern Chilean coast	Alkenone	Haddam et al.,2018
MD07-3124	Southern Chilean coast	Alkenone	Caniupán et al., 2014
James Ross Island	Antarctic Peninsula	δ^{18}O	Mulvaney et al., 2012
WDC06A	West Antarctic Ice Sheet	δ^{18}O	Steig et al., 2013
RICE	West Antarctic Ice Sheet	δ^{18}O	Bertler et al., 2018
Taylor Dome	Ross Sea coast	δ^{18}O	Steig et al., 2000
TALDICE-Talos Dome	Ross Sea coast	δ^{18}O	Stenni et al., 2011
RICE	West Antarctic Ice Sheet	Snow accumulation	Winstrup et al., 2019
WAIS 2014	West Antarctic Ice Sheet	Snow accumulation	Banta et al., 2008

IODPU 1357B	Adelie Land coast	Marine diatom	Crosta et al., 2021
Name	Location	Proxy type	Reference
GEBRA2	Antarctic Peninsula coast	Marine diatom	Bárcena et al., 1998
GEBRA1	Antarctic Peninsula coast	Marine diatom	Bárcena et al., 1998
A3	Antarctic Peninsula coast	Marine diatom	Bárcena et al., 2002
A6	Antarctic Peninsula coast	Marine diatom	Bárcena et al., 2002
JPC38	Antarctic Peninsula coast	Marine diatom	Barbara et al., 2016
JPC10	Antarctic Peninsula coast	Marine diatom	Etourneau et al., 2013
JPC127	Antarctic Peninsula coast	Marine diatom	Christ et al., 2015
Wood Bay (WB)	Ross Sea coast	Marine diatom	Mezgec et al., 2017
Cape Hallett (CH)	Ross Sea coast	Marine diatom	Mezgec et al., 2017
Joides Basin (JB)	Ross Sea coast	Marine diatom	Mezgec et al., 2017

4.2.2 Climate model simulations

As in some recent studies [e.g., Dalaiden et al., 2021; O'Connor et al., 2021], three simulations performed with the isotope-enabled Community Earth System Model version 1 [iCESM1, Brady et al., 2019; Stevenson et al., 2019] are selected here. iCESM1 is a coupled atmosphere-ocean-sea ice model that includes atmosphere and land components with a ~2° resolution and an ocean component with a ~1° resolution. The transient simulations are run from 850 to 1850 CE driven by the estimated solar, volcanic, greenhouse gases, aerosols, land-use, and orbital forcings. Three simulations were given identical forcings but slightly differed in the initial atmospheric state; this difference was sufficient to generate simulations with different internal ocean-atmosphere variability and therefore different time trajectories [Brady et al., 2019]. One of the main advantages of using an isotope-enabled model is the possibility to make a direct comparison with the proxy records. The modeling results have been fully evaluated for Antarctica. While some biases are present, in particular at a local scale, the simulations represent well the current climate from 1979-2005 CE for near-surface air temperature, snow accumulation, the mean state of Antarctic sea-ice extent, and geopotential height at 500-hPa, which are the variables investigated here [Dalaiden et al., 2021].

4.2.3 A particle-filter based offline data assimilation method

To estimate the state of the climate system, we apply here an ensemble-based offline data assimilation approach, similar to many previous studies [e.g., Hakim et al., 2016; Steiger et al., 2018; Klein et al., 2019], using a particle filter method as described by Dubinkina et al. [2011]. The ensemble of model states is derived from the three simulations performed with iCESM1 for the period 850-1850 CE. As two different temporal assimilation windows of 1-year and 10 years are applied in the DA experiments, this provides ensembles with 3003 (=1001 × 3) and 300 (= 100 × 3) members or particles, respectively, referred to as prior distributions. For a specific year or decade, each particle in the ensemble is compared with the

data to determine its likelihood for this period, taking the data uncertainty into account. The particles with high similarity to the data receive a higher weight while the ones having large differences with observations receive a lower weight. When the weight of each particle for that given year or decade is obtained, a weighted mean of the model states is calculated and provided as the mean reconstruction. The uncertainty of the DA-based reconstruction can then be given by the standard deviation of the weighted ensemble. Relying on the covariance relationship between climatic variables as represented in the prior model, the weights spread thus the information to reconstruct any simulated variables, even though they are not directly constrained by the proxy data. Here, the variables we estimate are sea ice concentration, sea level pressure, and surface air temperature.

The comparison between the modeling results and the continental proxy records is based on a spatial grid coarser than the initial modeling grid as this help reduce the effect of the inability of the model to reproduce some local feature and the small-scale noise in the records. Specifically, we follow the same strategy as Dalaiden et al. [2021] by computing composites including all the records located within 500 km × 500 km cells, and by linearly interpolating the initial prior modeling grid onto the 500 km regular grid. For the snow accumulation records, each original time series is first normalized for 1941-1990 CE and then all the series within a 500 km × 500 km grid cell are averaged. Those mean time series are finally calibrated to share the same mean and variance as the snow accumulation reconstruction of Medley and Thomas [2019] for the same boxes over the 1941–1990 period. The $\delta^{18}O$ composite for each grid cell is calculated by averaging the anomalies of $\delta^{18}O$ records over the 1941–1990 CE. Its calculation does not require the initial normalization because of the less dependence of $\delta^{18}O$ on the spatial distribution compared to the snow accumulation records.

Estimation of an error associated with the data is a key step in data assimilation as errors determine the strength of the constraint provided by each data. In this study, we follow the method of Dalaiden et al. [2021] to define the error for the ice-core based $\delta^{18}O$ and snow accumulation. Despite the spatial averaging of the records over 500 km × 500 km cells, ice core composites preserve climatic information at spatial scales that are smaller than the spatial resolution of iCESM1. A large fraction of the observation error for the composites of $\delta^{18}O$ or snow accumulation could thus arise from their spatial representativity. To evaluate the magnitude of this term, we select a simulation with a high spatial resolution of 27 km performed with the latest version of the polar-oriented Regional Atmospheric Climate MOdel (RACMO2.3p2, hereafter RACMO) [van Wessem et al., 2018]. We calculate the standard deviation of the differences between the average of the annual mean snow accumulation time series using only the original RACMO grid cell (~27 km) where ice core records are available and the "true" average over the continental part of 500 km × 500 km cells. This standard deviation is then used as the error of the snow accumulation records. The same method was used to calculate the error in the $\delta^{18}O$ records. Since no water isotope is generated by RACMO, a finer model is obtained by linear interpolation of iCESM1 to the RACMO grid for the years

1950-2005. For the error of the 10-year averaged data, we take the smoothing of the time series into account by dividing the error given at the interannual scale mentioned above with a factor of $\sqrt{10}$ (as classically done for instance in PAGES 2K-PMIP Group. 2015).

For the SST reconstructions, we choose an error of 0.5 °C. We deliberately select a value smaller than generally suggested in the literature [e.g., Collins et al., 2019] to obtain a strong constraint and have a clear contrast between the DA experiments that include or not those reconstructions.

4.2.4 Experimental design

To study the sensitivity of the results to the temporal (annual and decadal) resolution of the assimilated data, two DA experiments are performed for the past two centuries as the more available proxy records over this period than longer periods. These two experiments are similar to Dalaiden et al. [2021], including using the same ice-core based $\delta^{18}O$ and snow accumulation records (only for those located in West Antarctica), as well as tree ring width records in the South Hemisphere (Fig. C.1 and Table 4.2). The two experiments are referred to as ASSIM-P200-1yr at the annual resolution and ASSIM-P200-10yr at the decadal resolution.

For the experiments covering the past two millennia, we assimilate the continental proxy records and the marine records (i.e., Southern Ocean SST reconstructions) as introduced in Section 4.2.1 (Fig. 4.1). To further clarify the contributions of continental and marine records on the reconstructions, we separately perform two DA experiments. In the first one, we assimilate only the continental proxies (ASSIM-P2000-CON), while we assimilate all the records (ASSIM-P2000-ALL) in the second one. In addition, to test the sensitivity of the DA-based reconstructions to the seasonality of SST reconstructions, we perform the experiment, ASSIM-P2000-DJF, similar to ASSIM-P2000-ALL, but we use the summer SST (the mean over December, January, and February) as prior modeling results and we assume that the reconstructed SST represents summer conditions instead of annual mean. All experiments have been listed in Table 4.2.

Table 4.2: *Description of the DA experiments.*

Name	Assimilated proxy records	Temporal resolution	Temporal span
ASSIM-P200-1yr	20 ice-core based $\delta^{18}O$ and 34 snow accumulation records in West Antarctica and 6 tree ring width records (Fig. C.1)	1 year	1800-2000 CE
ASSIM-P200-10yr	20 ice-core based $\delta^{18}O$ and 34 snow accumulation records in West Antarctica and 6 tree ring width records (Fig. C.1)	10 years	1800-2000 CE
ASSIM-P2000-CON	Five Ice-core based $\delta^{18}O$ and two snow accumulation records in West Antarctica (Fig. 4.1)	10 years	1-2000 CE

ASSIM-P2000-ALL	Five Ice-core based $\delta^{18}O$ and two snow accumulation records in West Antarctica and five SST reconstructions (Fig. 4.1)	10 years	1-2000 CE
ASSIM-P2000-DJF	Same as ASSIM-P2000-ALL but considering that SST reconstructions represent summer conditions	10 years	1-2000 CE

The comparisons mentioned above are quantitively achieved by the computation of two statistical metrics. The first is the Pearson correlation coefficient (r value) and the related P-value. The second is the coefficient of efficiency (CE value):

$$CE = 1 - \sum_{i=1}^{n} \frac{(x_i - y_i)^2}{(x_i - \bar{x})^2}$$

where x_i is the "true" time series, $\bar{x}$ is the mean of the "true" time series over a reference period; y_i is the reconstructed time series. This metric is used in Section 4.3.1. The upper limit of CE is 1, which means that two time series have the same variations of both the amplitude and the timing, while negative CE values result from a bias between the two datasets, in either the mean or amplitude of the variability.

In our analyses, the SAM index is defined as the normalized difference in mean sea-level pressure between the 40° and 65° South bands [Gong and Wang, 1999]. The ASL index is defined as the normalized mean of the sea level pressure from 75°S to 60°S and 170°E to 70°W [Fogt et al., 2012; Hosking et al., 2013]. For the regional-scaled sea ice extent (i.e., at least 15% of the ocean surface covered by ice, Fig. 4.1), we follow the geographical definition of Parkinson [2019] and divide the ocean off West Antarctica into two zones: the Bellingshausen/Amundsen Sea zone (130°W-60°E) and the Ross Sea zone (160°E-130°W). The definition of the climate regions (Fig. 4.1), i.e., the AP (70 -74°S, 60°W - 80 °W) and the WAIS (north of 85°S, 60°W-170°W), follows the ones in Stenni et al. [2017].

4.3 Results and discussion

4.3.1 Evaluation of the skill of the reconstructions over the past 200 years

Since all the previous DA experiments were performed at annual resolution, we first assessed the sensitivity of the results to the temporal resolution (annual and decadal) of the assimilated observations. ASSIM-P200-1yr and ASSIM-P200-10yr show consistent results with high and statistically significant correlation coefficients between them and positive CE values for SAT over the AP ($r = 0.89$ at $p < 0.05$, $CE = 0.77$) and WAIS ($r = 0.86$ at $p < 0.05$, $CE = 0.72$), the SAM (0.94 at $p < 0.05$, $CE = 0.64$) and ASL index (0.92 at $p < 0.05$, $CE = 0.64$) over past two centuries (Fig. 4.2). The correlation coefficients between the local SAT and SLP time series are also high and significant at many locations in the domain (Fig. 4.3 a and b).

For the SIE, the two experiments also display clear similarity in the Bellingshausen/Amundsen sector ($r = 0.73$ at $p < 0.05$, CE = 0.48). However, the two experiments display larger differences in the SIE integrated over the Ross Sea sector, with a relatively small correlation coefficient ($r = 0.44$ at $p < 0.05$) and negative CE value (-0.03). The spatial distribution shows that the low correlations are mainly found on the northern edge of the Ross Sea and close to the coast of the western part of the Amundsen Sea (Fig. 4.3 c), where the correlation coefficients between the two experiments are not significant.

The results seem thus not very sensitive to the resolution of the records except for sea ice concentration in some regions. This discrepancy for sea ice might be related to the time scale-dependent covariance between the variables. To illustrate this point, we calculate correlation coefficients, which can be seen as the covariance normalized by the product of the standard deviations, between SIE, SAT, and the ASL. To avoid the influence of the trend related to the global warming over the past century, we calculate correlation coefficients based on the detrended time series (i.e., removing the linear trend of the time series denoted by r_d). Since the above discrepancy is mainly observed in the Ross Sea sector, the average of climate variables used for calculating the correlation coefficients is made over this region (160°E-130°W, 50°S -70°S).

Significant negative correlation coefficients are found between the ASL and SIE in the Ross Sea sector ($r = -0.88$ at $p < 0.05$; $r_d = -0.92$ at $p < 0.05$) in ASSIM-P200-1yr (Fig. 4.4). This highlights a strong control of the ASL on the SIE over the Ross Sea sector through atmospheric processes at the interannual scale, as proposed in several previous studies [e.g., Hosking et al., 2013; Raphael and Hobbs, 2014; Raphael et al., 2019, Dalaiden et al., 2022]. For instance, a deeper ASL results in stronger cold southerly winds transporting sea ice off the Ross Sea, thus leading to a larger regional SIE. In contrast, ASSIM-P200-10yr shows a non-significant correlation coefficient of 0.09, although the correlation based on the detrended time series is still negative ($r_d = -0.44$ at $p < 0.05$) but much smaller than ASSIM-P200-1yr.

The next step is to investigate the changes in the oceanic temperature at 100 m and 500 m, considering that the ocean could be responsible for this timescale dependence because of its large thermal inertia and slower time response to perturbations compared to the atmosphere. In ASSIM-P200-10yr, the SIE in the Ross Sea sector is negatively correlated to oceanic temperature at both 100 m ($r = -0.74$ at $p < 0.05$; $r_d = -0.37$ at $p < 0.05$) and 500 m ($r = -0.66$ at $p < 0.05$; $r_d = -0.26$ at $p > 0.05$). However, in ASSIM-P200-1yr, the significant negative correlation only occurs between the SIE and oceanic temperature at 100 m ($r = -0.51$ at $p < 0.05$; $r_d = -0.70$ at $p < 0.05$), while an insignificant positive correlation coefficient is obtained between the SIE and oceanic temperature at 500 m ($r = 0.29$ at $p > 0.05$; $r_d = 0.44$ at $p < 0.05$). In other words, an increase in SIE in the Ross Sea is associated with a cooling of the water column up to 500 m in ASSIM-P200-10yr while the cooling is restricted to the upper layers in ASSIMP200-1yr.

This can be interpreted as that, on the interannual timescale, only the upper ocean interacts with the surface while the deeper ocean can play an important role on the decadal timescale. Ferreira et al. [2015] proposed that the SO response to winds could be timescale-dependent; an atmospheric pattern similar to a positive SAM triggers short-term cooling at interannual scale by the horizontal Ekman drift, followed by the slower warming around Antarctica induced by Ekman upwelling of warmer water. Such a mechanism may induce different covariances between the variables as a function of the time scale. Our results are consistent with the hypothesis of a strong role of the upwelling of deeper waters on longer timescales [e.g., Ferreira et al., 2015]. However, this correlation analysis does not provide a causality link, and this is not our purpose here to go deeper in the physical mechanism. This also confirms that the co-variability between state variables in the system is very important in the DA process and that the validity of the model-derived covariance must be evaluated carefully for each application, especially when reconstructing sea ice or other oceanic variables [Tardif et al., 2014, 2015; Steiger et al., 2016]. Due to the absence of long-term sea ice observations over the past two centuries [e.g., Vorrath et al., 2020], it is impossible to assess which of the reconstruction ASSIM-P200-1yr or ASSIM-P200-10yr is more faithful. Nevertheless, in order to better integrate the role of ocean on the low-frequency variability of the system, it seems reasonable to perform assimilation here using a 10-year assimilation window.

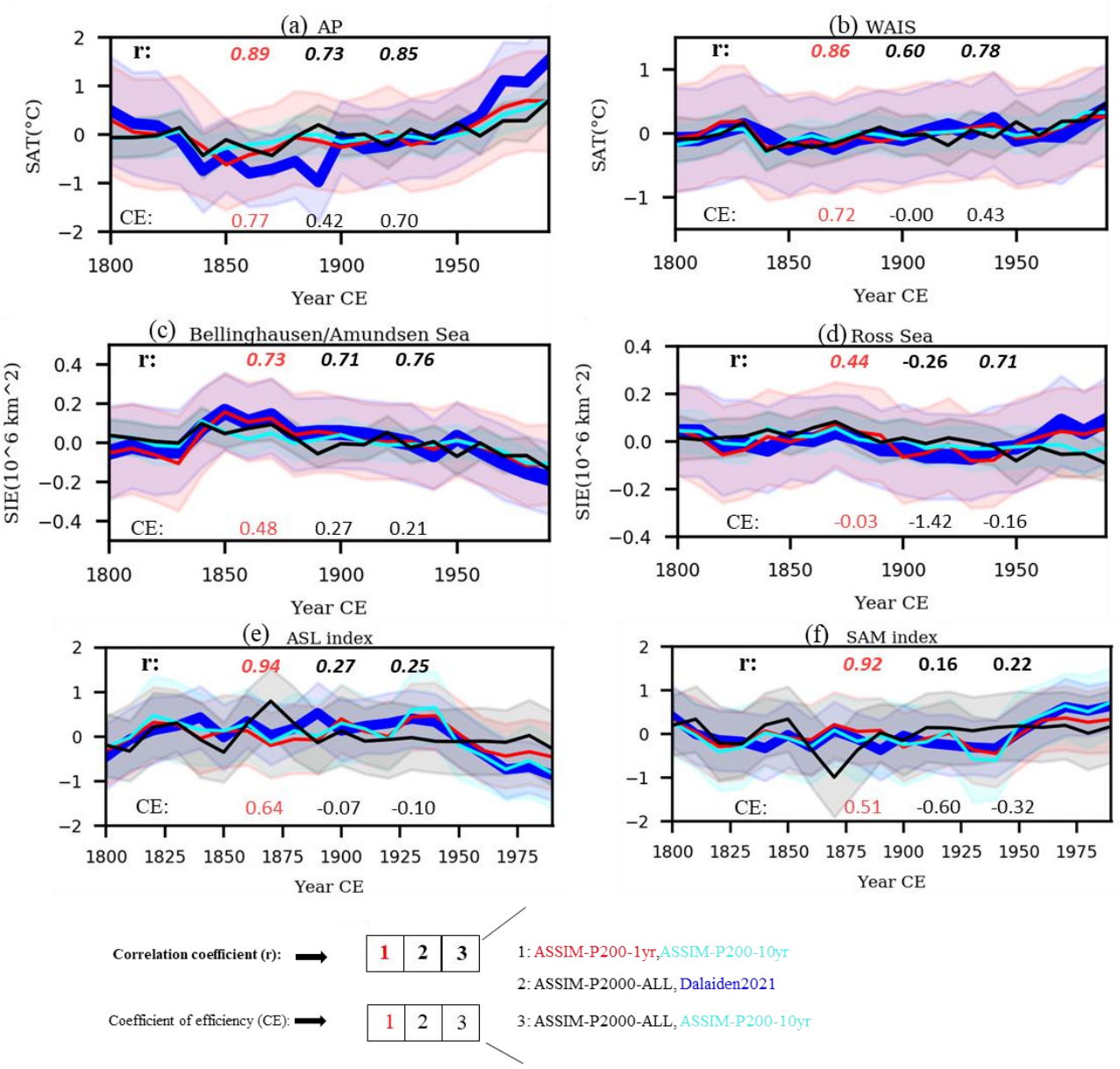

***Figure 4.2**: Comparisons for the surface air temperature (SAT) over the Antarctic Peninsula (AP, a) and the West Antarctic Ice Sheet (WAIS, b), for the sea ice extent integrated in the Bellingshausen/Amundsen sea sector (c) and the Ross Sea sector (d), and for the Amundsen Sea Low index (ASL, e) and the Southern Annual Mode index (SAM, f), over the past two centuries, between various reconstructions from this study, i.e., ASSIM-P200-1yr (red), ASSIM-P200-10yr (cyan), ASSIM-P2000-ALL (black), and from Dalaiden et al. (2021, blue). All quantities are expressed in anomalies (relative to the 1800–2000 CE period). Shaded areas represent ±1 standard deviation of the DA-based reconstructions. Correlation coefficients (r) between different reconstructions are shown in bold (the statistically significant ones at $p < 0.05$ is shown in italic font) and above the time series in each panel, while the others below the time series represent the values of coefficient of efficiency (CE).*

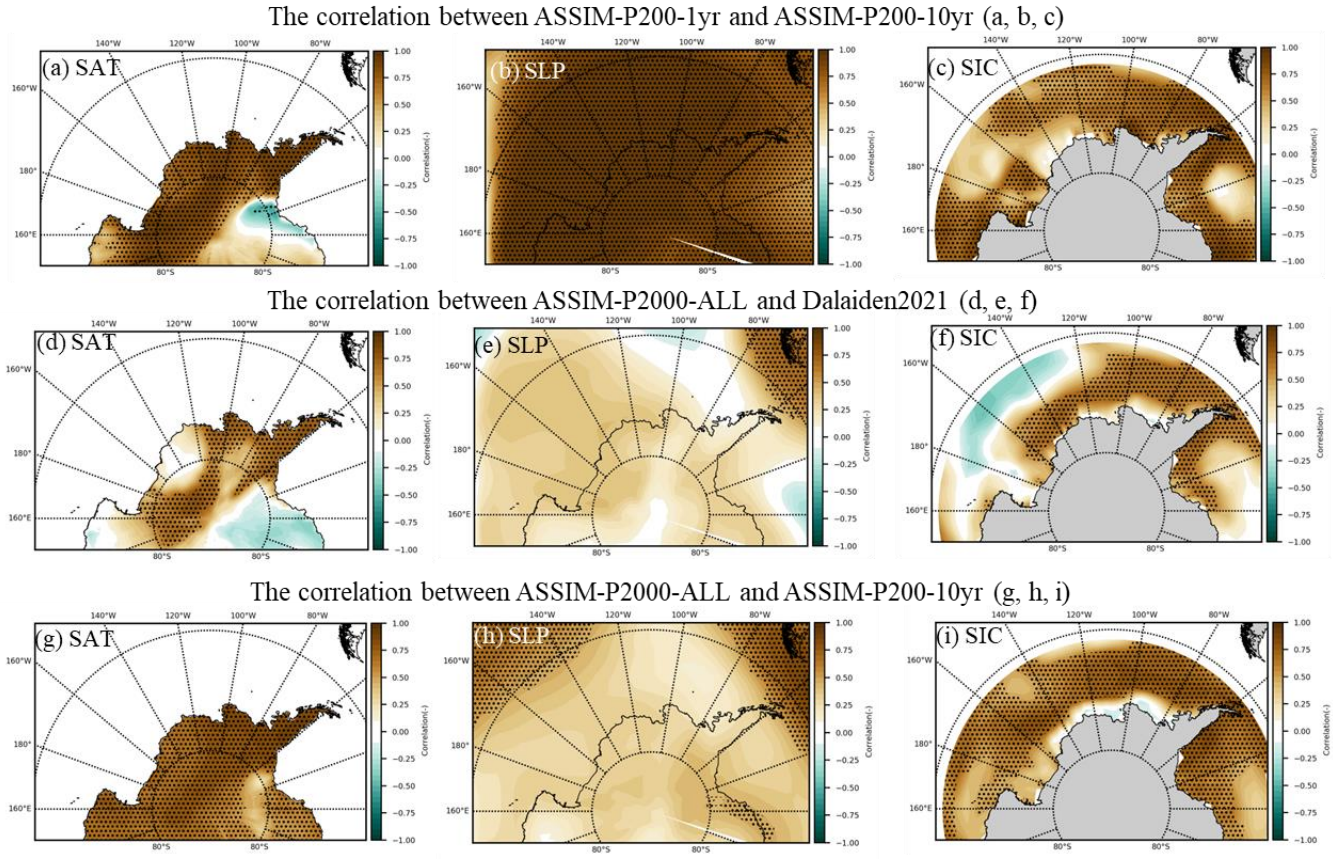

***Figure 4.3**: Spatial patterns of the correlation coefficients for the surface air temperature (SAT), sea level pressure (SLP), and sea ice concentration (SIC) between ASSIM-P200-1yr and ASSIM-P200-10yr (a, b, c), between ASSIM-P2000-ALL and the reconstruction from Dalaiden et al. [2021] (d, e, f), and between ASSIM-P2000-ALL and ASSIM-P200-10yr (g, h, i). The area with stippling indicates the correlation coefficients at a 95 % confidence level (p < 0.05).*

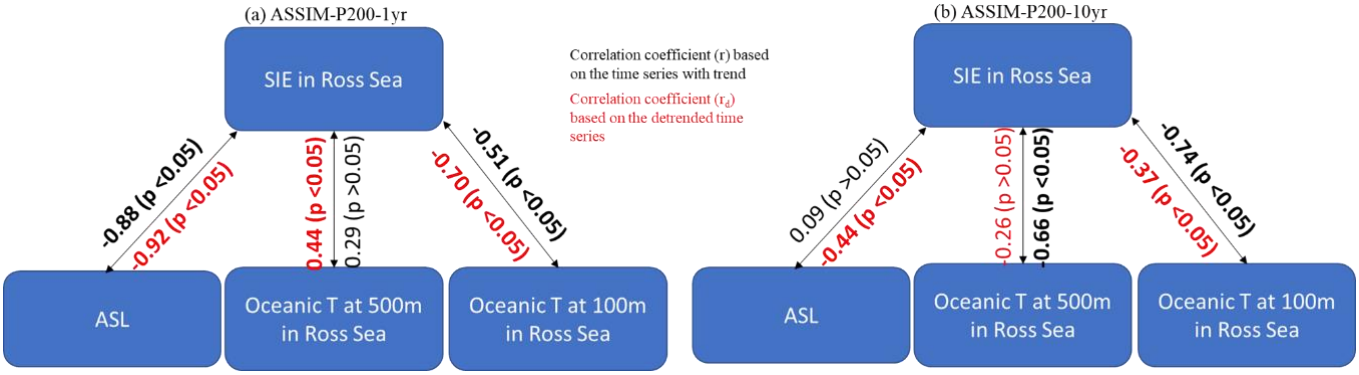

***Figure 4.4**: The correlation coefficients between sea-ice extent (SIE) in the Ross Sea sector and ASL, the subsurface oceanic temperature at 100 m and 500 m (their time series are shown*

in Fig. C.2), respectively, presented in the reconstructions of ASSIM-P200-1yr (a) and ASSIM-P200-10yr (b).

Ideally, our reconstruction covering the past 2000 years should be evaluated compared to observations but because of the decadal resolution of ASSIM-P2000-ALL and the short observations covering the past 2-3 decades, the remaining degrees of freedom (only 2 or 3 if observations are averaged using 10 years) is too limited. Alternatively, we decided to compare ASSIM-P2000-ALL to the reconstruction of Dalaiden et al. [2021] which has proved to provide skillful reconstructions of atmospheric circulation, sea ice concentration, and SAT over the past 200 years in the West Antarctic Sector. Dalaiden et al. [2021] assimilated the same records as in ASSIM-P200-1yr, using the same methodology but with additional records from East Antarctica. Dalaiden et al. [2021] and ASSIM-P200-1yr are thus very similar in West Antarctica (see the comparison between Dalaiden et al. [2021] and ASSIM-P200-1yr in Fig. C.3). In addition, the comparison between ASSIM-P2000-ALL and ASSIM-P200-10yr is involved here to evaluate the contribution of the number of proxies. It may also be useful to remind here that no marine record is assimilated in ASSIM-P2000-ALL over the period 1800-2000 CE and thus there is no difference for this period between ASSIM-P2000-ALL and ASSIM-P2000-CON.

For the spatial SAT reconstructions (Fig. 4.3 d), ASSIM-P2000-ALL is significantly correlated with Dalaiden et al. [2021] over the AP ($r=0.73$ at $p<0.05$; CE = 0.42 for the mean of the sub-region, Fig. 4.2 a). Over the WAIS, however, some small zones with non-significant correlations are observed in the western and center of the region. This could be due to the poor performance of ASSIM-P2000-ALL in the reconstruction of the atmospheric circulation (Fig. 4.3 e), in particular for the SAM (Fig. 4.2 f) and ASL index (Fig. 4.2 e). This leads to a CE value close to zero for the mean over WAIS but a significant correlation coefficient (0.60 at $p < 0.05$) indicates that ASSIM-P2000-ALL is able to capture the general signal over the past two centuries over the WAIS reconstructed in Dalaiden et al. [2021]. When compared to ASSIM-P200-10y, ASSIM-P2000-ALL displays remarkable consistency in West Antarctica (Fig. 4.3 g). The correlation coefficients between ASSIM-P2000-ALL and ASSIM-P200-10y are 0.85 ($p < 0.05$) over the AP, and 0.78 ($p < 0.05$) over the WAIS. The positive CE values indicate that the magnitude of the decadal variability is similar between both reconstructions. This suggests that the differences between ASSIM-P2000-ALL and Dalaiden et al. [2021] are due to the temporal resolution rather than the number of records.

ASSIM-P2000-ALL correlates very well with Dalaiden et al. [2021] for the SIC in the Bellingshausen/Amundsen Sea, but in the Ross Sea, there are large areas with negative correlation coefficients. By contrast, ASSIM-P200-10yr and ASSIM-P2000-ALL show a good agreement over almost the full high-latitude Pacific sector of the Southern Ocean (Fig. 4.3 i), indicating again a role of the time resolution in the differences between ASSIM-P2000-ALL and Dalaiden et al. [2021]. Regarding the performance of the reconstructed SIE integrated over

Bellingshausen/Amundsen Sea, ASSIM-P2000-ALL seems skillful when comparing to Dalaiden et al. (2021) ($r = 0.71$ at $p < 0.05$, CE = 0.27) and ASSIM-P200-10yr ($r = 0.76$ at $p < 0.05$, CE = 0.21) (Fig. 4.2 c). For the reconstruction of the SIE over the Ross Sea, ASSIM-P2000-ALL shows negative CE values when compared to Dalaiden et al. [2021] (-1.42) and ASSIM-P200-10yr (-0.16) (Fig. 4.2 d). Nevertheless, the high correlation coefficient between ASSIM-P2000-ALL and ASSIM-P200-10yr (0.71 at $p < 0.05$) indicates that the assimilation of only a few records in ASSIM-P2000-ALL is able to capture the general tendency of the SIE over the Ross Sea for past two centuries, even though the magnitude of the changes might be less trustable than in ASSIM-P200-10yr.

For the SLP over West Antarctica and its surrounding seas in the Southern Ocean, ASSIM-P2000-ALL correlates positively, but not significantly, with both Dalaiden et al. [2021] and ASSIM-P200-10yr (Fig. 4.3 e and h). This suggests that the number of records included in ASSIM-P2000-ALL might be too low and that the reconstruction for this variable should be taken with caution.

4.3.2 Surface temperature and sea ice changes in West Antarctica and its surrounding seas over the past two millennia

The evolution of SAT and SIE in the West Antarctic sector over the past two millennia from ASSIM-P2000-ALL and ASSIM-P2000-CON are displayed in Fig. 4.5. Both experiments appear quite similar, in particular during the first millennium. There are relatively small centennial fluctuations in the SAT and SIE over the years 1-400 CE. Subsequently, the warmest period over the first millennium is observed during 450-550 CE and is followed by a significant cooling until 1000 CE over the WAIS and AP. This is consistent with the previous reconstructions of Lyu et al. [2021] that focus on multi-centennial trends in the SAT over Antarctica during the first millennium. This implies that the assimilation of the marine records in ASSIM-P2000-ALL brings additional constraints for the first millennium compatible with the one in ASSIM-P2000-CON. This also confirms the robust SAT reconstruction of Lyu et al. [2021] for the first millennium over West Antarctica. In contrast to the evolution over the first millennium, we observe large centennial or multi-centennial fluctuations in the SIE and SAT for the second millennium (i.e., 850-1850 CE), with larger amplitude changes in ASSIM-P2000-ALL compared to ASSIM-P2000-CON. Accordingly, we focus on this period in the remaining part of the study. In particular, we observe significant differences in mean SAT and SIE between the 1400-1800 CE and 900-1300 CE periods. These two multi-centennial epochs are brought in phase with the LIA and MCA in the North Hemisphere [Mann et al., 2009], respectively, although different time schemes have historically been defined in the literature [Neukom et al., 2019]. Furthermore, the SAT and SIE reconstructions in ASSIM-P2000-ALL have good agreement with the ones in the sensitivity experiment (with correlations larger than 0.7 at $p < 0.05$) when the assimilated SST reconstructions are considered to represent summer temperatures, rather than annual ones (Fig. C.4). This implies that although SST

reconstructions are assumed to provide information only for summer, DA remains able to reconstruct the changes in the annual mean, albeit with a smaller magnitude.

For the SAT over the AP, a long-term MCA-LIA cooling is present in both ASSIM-P2000-ALL and ASSIM-P2000-CON but appears much larger in ASSIM-P2000-ALL (0.42 °C) than in ASSIM-P2000-CON (0.08 °C). Over the WAIS, the difference between the two reconstructions is smaller, although the cooling observed in ASSIM-P2000-ALL (0.27 °C) is still twice as large as the cooling in ASSIM-P2000-CON (0.13 °C). Consistent with the regional cooling in the West Antarctic sector, the SIE displays an expansion of 0.12 10^6 km^2 in the Bellingshausen/Amundsen Sea during the LIA relative to the MCA in ASSIM-P2000-ALL and of 0.03 10^6 km^2 in ASSIM-P2000-CON. In the Ross Sea, we observe a smaller difference in the evolution in SIE from the MCA to LIA in both reconstructions, with ASSIM-P2000-ALL and ASSIM-P2000-CON displaying an SIE increase of 0.05 10^6 km^2 and 0.02 10^6 km^2, respectively.

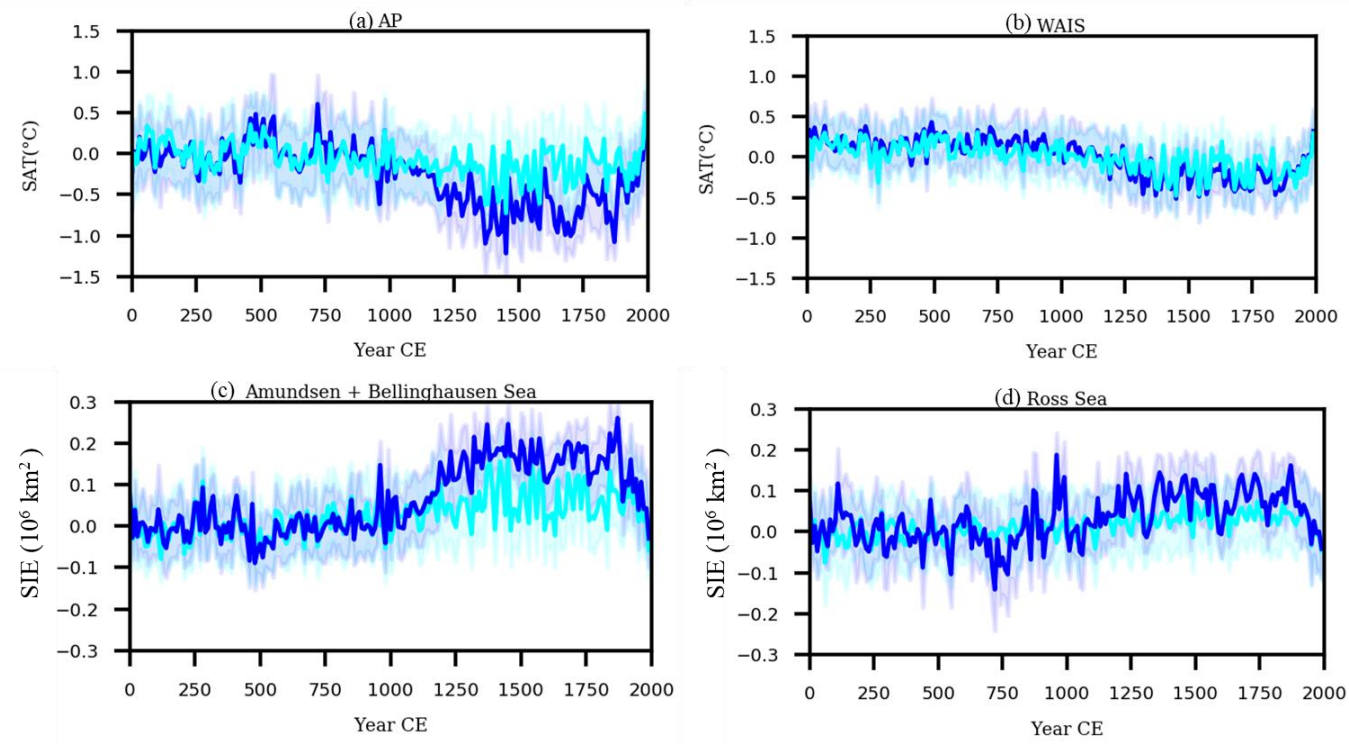

Figure 4.5. *The surface air temperature (SAT) anomalies (in °C relative to 1-2000 CE) over the Antarctic Peninsula (AP, a) and the West Antarctic Ice Sheet (WAIS, b), and the sea ice extent (SIE) anomalies (in 10^6 km^2 relative to 1-2000 CE) integrated over the Amundsen/Bellingshausen Sea sector (c) and the Ross Sea sector (d) derived from the ASSIM-P2000-ALL (blue) and ASSIM-P2000-CON (cyan) reconstructions. The shaded areas represent ±1 standard deviation of the DA-based reconstructions.*

To understand the differences between the reconstructions, it is instructive to compare them to the four SST reconstructions located on the southern Chilean coast that we assimilate in ASSIM-P2000-CON but not in ASSIM-P2000-ALL. As expected, the SST reconstructions from ASSIM-P2000-ALL show high correlation coefficients with the original ones, indicating the effective roles of the DA process in the reconstruction (Fig. 4.6). Interestingly, even though ASSIM-P2000-CON does not directly assimilate the SST reconstructions, the correlation coefficients between the DA-based reconstruction and the SST reconstructions remain significant and close to 0.5. This implies that the information provided by the continental proxy records assimilated in ASSIM-P2000-CON is consistent with the one of the SST reconstructions, especially for the long-term cooling trend over the last millennium.

Nevertheless, a visual comparison of the time series in Fig. 4.6 clearly reveals that our SST reconstructions underestimate the centennial variability compared to the original reconstructions, regardless of whether those SST reconstructions are assimilated. This potential underestimation of the variability is a common issue for DA reconstructions [e.g., Tardif et al., 2019]. However, this is likely here due to a more general problem of climate models underestimating the variance at the local scale compared to marine proxies [e.g., McGregor et al., 2015]. On the one hand, the model (i.e., iCESM1 in this study) is unable to reproduce the small-scale signal included in the proxy records. On the other hand, the SST reconstructions could also contain non-climatic information, and could suffer from methodological uncertainties (e.g., on the transfer function from the proxy to SST reconstructions). As a consequence, the model ensemble (i.e., the prior) does not include states that present large enough anomalies compared to the data. The filter selects the particles that have a strong signal at the location of the proxies but this is still significantly different compared to the one provided by the SST reconstructions. Nevertheless, one of the consequences of assimilating the marine proxy records is to amplify the variability locally in ASSIM-P2000-ALL at the location where marine proxies are available (even though it does not reach the one of the reconstructions) but also at larger scales, explaining the larger changes in the temperature over WAIS and the AP and the larger SIC increase between the MCA and the LIA in the Bellingshausen/Amundsen Sea in this experiment.

The comparison to independent reconstructions based on diatoms extracted from marine sediments is also useful to evaluate the relative performance of ASSIM-P2000-CON and ASSIM-P2000-ALL (Fig. 4.7). The high abundance of sea ice sensitive diatom records normally reflects sea ice expansion or persistent sea ice presence during that period [Crosta et al., 2020]. Most of the sea-ice related diatom records around the AP coast (5/7, including GEBRA-1, GEBRA-2, JPC127, JPC38, and JPC10) display a common signal with a clear sea-ice increase over the past millennium. The SIC at the locations of these five diatom records reconstructed in ASSIM-P2000-ALL appears to follow the increasing trend better than the reconstructions in ASSIM-P2000-CON, as evidenced by the higher correlation coefficients

between the diatom records and ASSIM-P2000-ALL (on average 0.52 at $p < 0.05$) than with ASSIM-P2000-CON (on average 0.27 at $p < 0.05$).

We have found inconsistencies between our reconstructions and the two remaining records located in the Bransfield Basin (referred to as A3 and A6). In contrast to our reconstructions for the regions, the A3 and A6 records display no significant trend for the past millennium, so that the correlations between our reconstructions and these two records are close to zero. A3 and A6 are also inconsistent with the other diatom records, in particular with the GEBRA-1 which is also located in the Bransfield Channel, east of A3 and A6. This highlights the complexity of the local dynamics in this region and of the interpretation of diatom records. In the case of A3 and A6, the sea ice information preserved in the sediments might have been affected by the seasonality of sea ice conditions and (or) the upwelling of deep warm water [Barcena et al., 1998] in the western Bransfield Strait, which could have masked the large-scale climatic signal shown in other records.

We have also compared our reconstructions to three marine diatom records in the western Ross Sea. Over the past two millennia, the SIC derived from ASSIM-P2000-ALL at three proxy sites positively correlate with the original records, although the values are relatively small (between 0.20 and 0.26). The correlation coefficients between ASSIM-P2000-CON and those proxy records are lower and are even negative for two of them (0.0 in the third one). The original study describing these three diatom records has identified the important role of katabatic winds and latent-heat polynyas on the coastal sea ice in this region [Mezgec et al., 2017]. The general circulation model used in the DA process is however unable to simulate and capture those small-scale coupled ocean-atmosphere processes, which may explain the relatively poor agreement between our reconstructions and proxy records in the Ross Sea region.

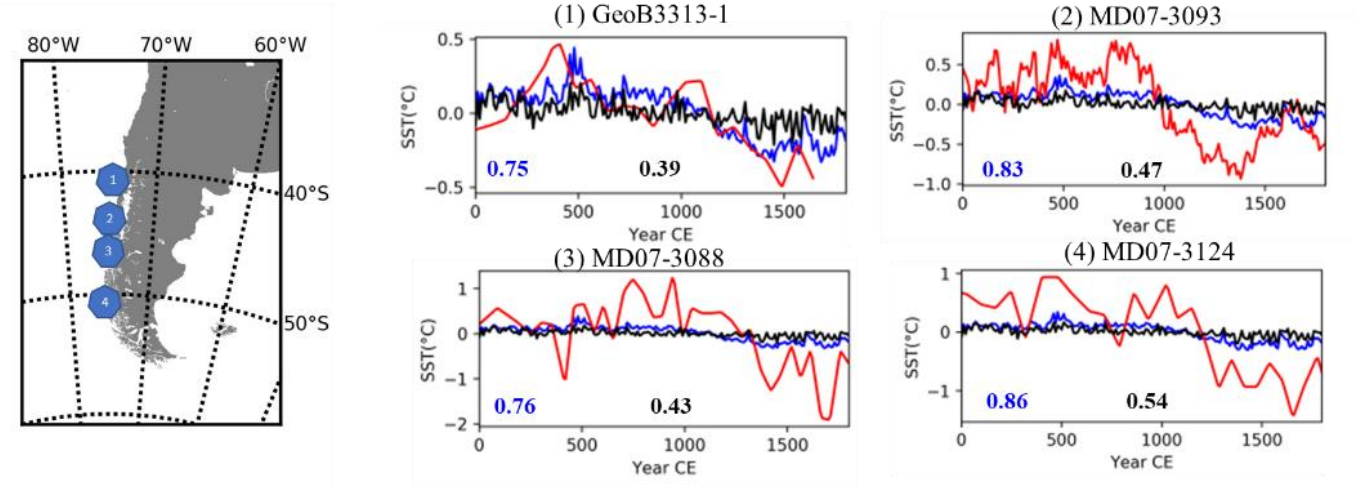

***Figure 4.6**: Comparison between the original SST reconstructions (anomalies over 1-1800 CE) (red) derived from the marine records located at the southern Chilean coast (as shown in the left map) and the reconstructions from ASSIM-P2000-ALL (blue) and ASSIM-P2000-CON (black). These four records are assimilated in ASSIM-P2000-ALL, but not in ASSIM-P2000-CON. The numbers within each subplot correspond to the correlation coefficients between the original SST reconstructions and ASSIM-P2000-ALL (blue) and ASSIM-P2000-CON (black).*

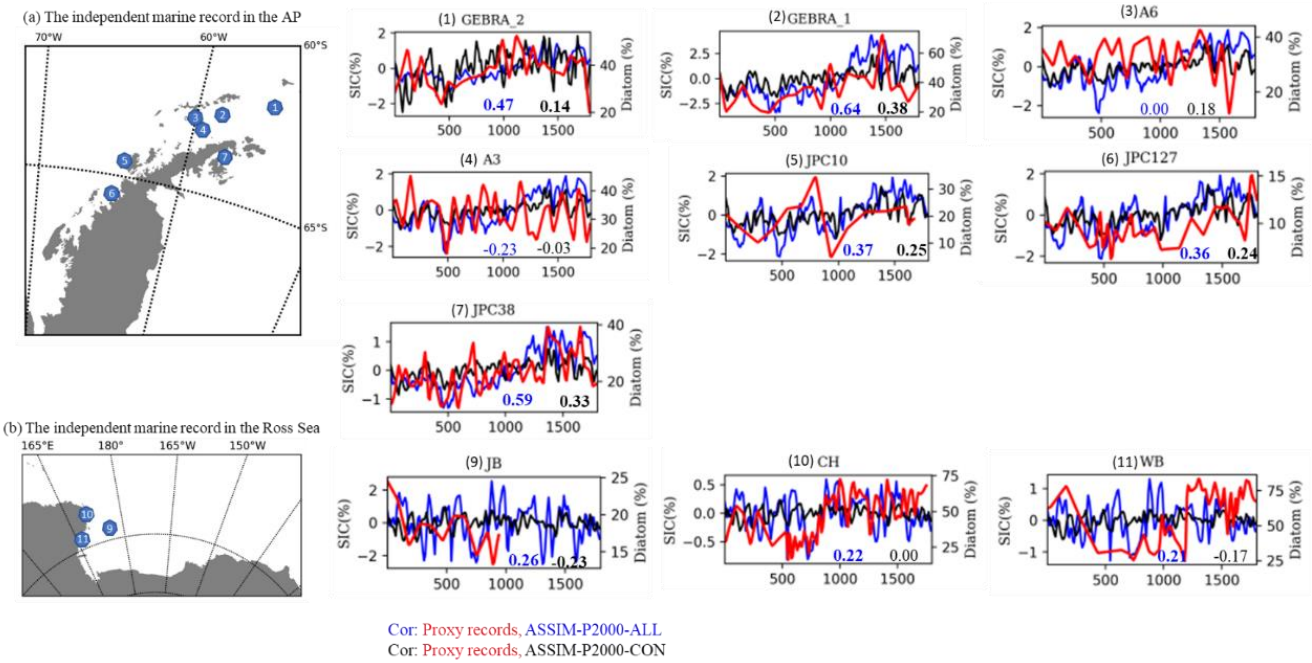

***Figure 4.7**: Same as Fig. 6, but for the independent marine diatom records in the Antarctica Peninsula (AP, a) and the Ross Sea (b).*

4.3.3 Is there a widespread cooling over WA and adjacent seas for the past millennium?

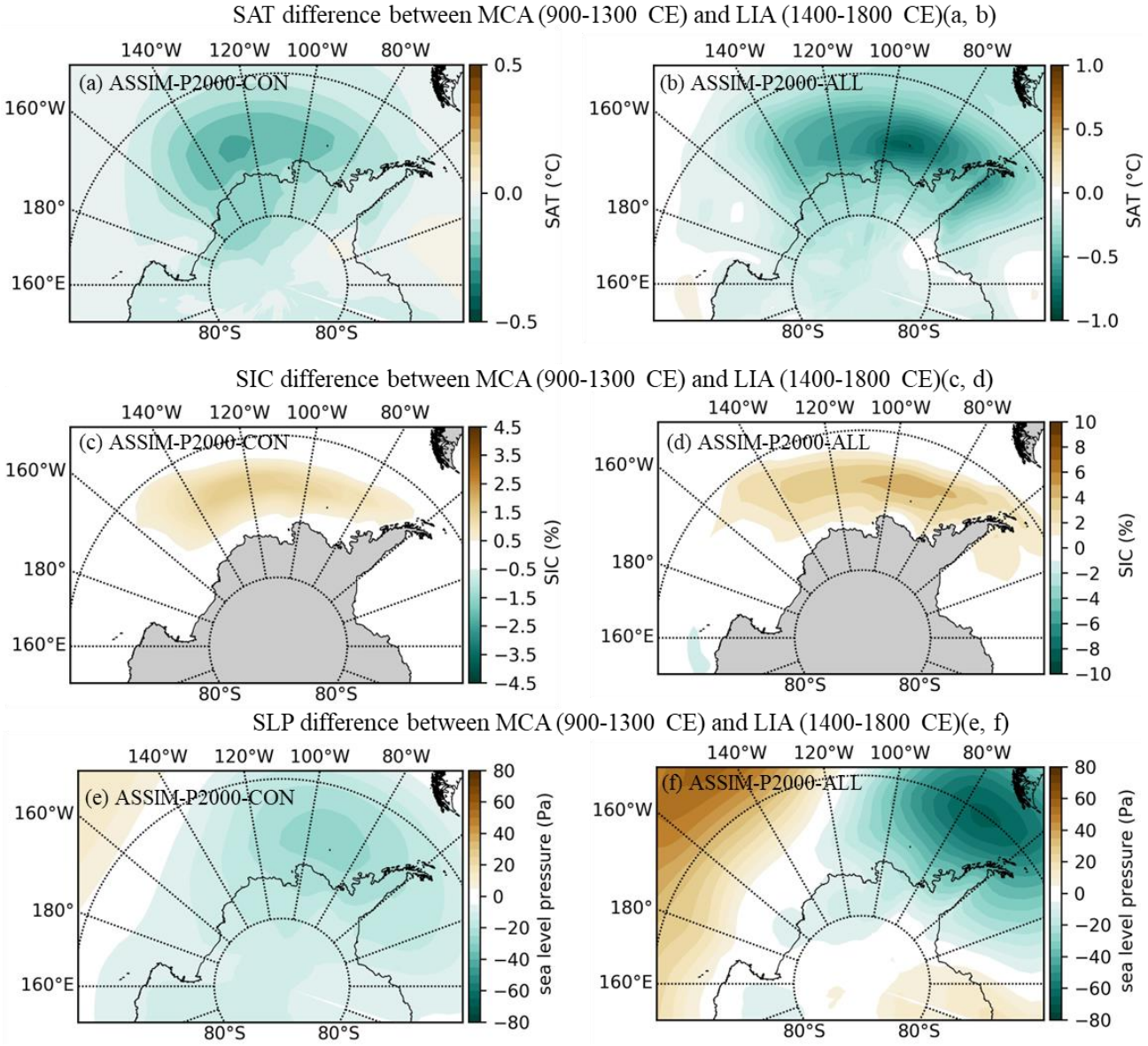

***Figure 4.8**: Spatial patterns of the LIA (1400-1800 CE)-MCA (900-1300 CE) difference in the SAT (a, b), SIC (c, d), and SLP (e, f) derived from ASSIM-P2000-CON and ASSIM-P2000-ALL. Note, the color bar is independent for each subplot to make the pattern visually readable.*

Here we investigate the spatial distribution of several key variables (i.e., sea ice concentration (SIC), sea level pressure (SLP), and surface air temperature (SAT)) to examine whether there is a widespread cooling over West Antarctica and adjacent seas for the past millennium in our two reconstructions and the potential associated mechanisms (Fig. 4.8). Compared to a relatively localized cooling zone in the western WAIS shown in the ASSIM-P2000-CON reconstruction (Fig. 4.8 a), more extensive and intense cooling over West Antarctica is observed in ASSIM-P2000-ALL. The largest cooling occurs in the western Amundsen Sea in

ASSIM-P2000-CON and in the eastern Amundsen Sea in ASSIM-P2000-ALL. The SIC pattern is consistent with the one of SAT, with a broader and higher SIC increase over the Pacific sector of the high latitudes of the Southern Ocean in ASSIM-P2000-ALL than in ASSIM-P2000-CON.

The reconstructed changes of the atmospheric circulation exhibit clear differences between the two experiments, but both display a decrease in SLP over the Bellingshausen Sea between the MCA and the LIA, with an eastward shift and a deepening of the low-pressure system in the ASSIM-P2000-ALL compared to ASSIM-P2000-CON. Despite these strong differences between the reconstructions in magnitude and patterns of the SLP changes and the low skill of our reconstruction for this variable over the past 200 years (Fig. 4.3), it is still instructive to analyze the impact of those SLP changes on the temperature over this region as the reconstructions provide an internally consistent dataset. Specifically, as the ASL is known to be a major contributor to the variability in the region, we have performed a congruence analysis to identify the contribution of the ASL to the changes in the SAT during the LIA-MCA transition. This methodology is same as the one used in previous studies, e.g., Thompson et al. [2020] and Jones et al. [2019]. We first derived the ASL index from our reconstructions and then perform a linear regression between the ASL index and the SAT for each grid cell after removing linear trends over 900-1800 CE period. We finally multiplied the SAT sensitivities derived from the regression by the trends in the ASL index over 900-1800 CE to estimate the ASL-congruent SAT changes. In both reconstructions, the SAT congruent trend shows a small cooling over the WAIS but signals of different signs over the AP (Fig. 4.9). Nevertheless, the values are relatively low indicating that the ASL plays a relatively small role in the cooling trend in our reconstructions.

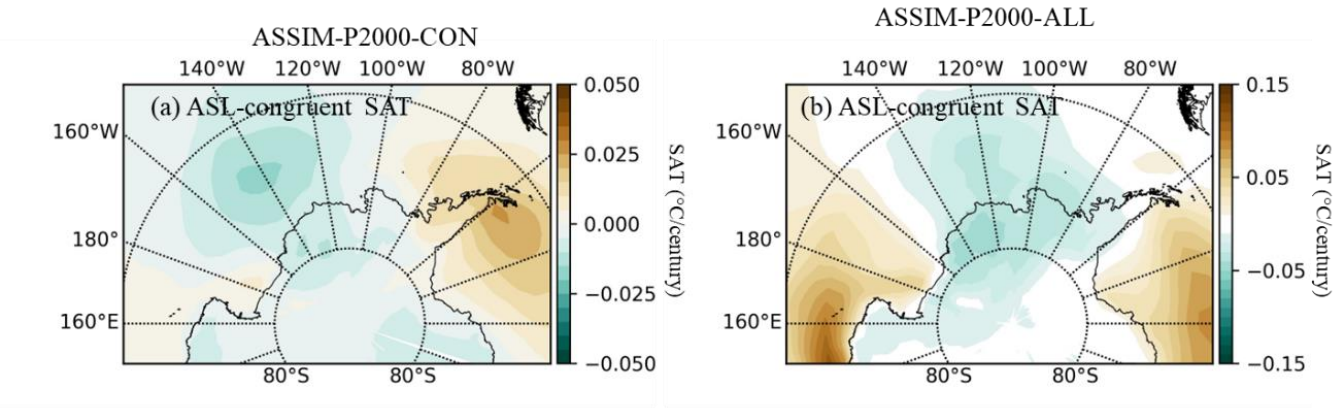

Figure 4.9. *Spatial patterns for the ASL-congruent trend in the SAT derived from ASSIM-P2000-CON (a) and ASSIM-P2000-ALL (b). Note, the color bar is independent for each subplot to make the pattern visually readable.*

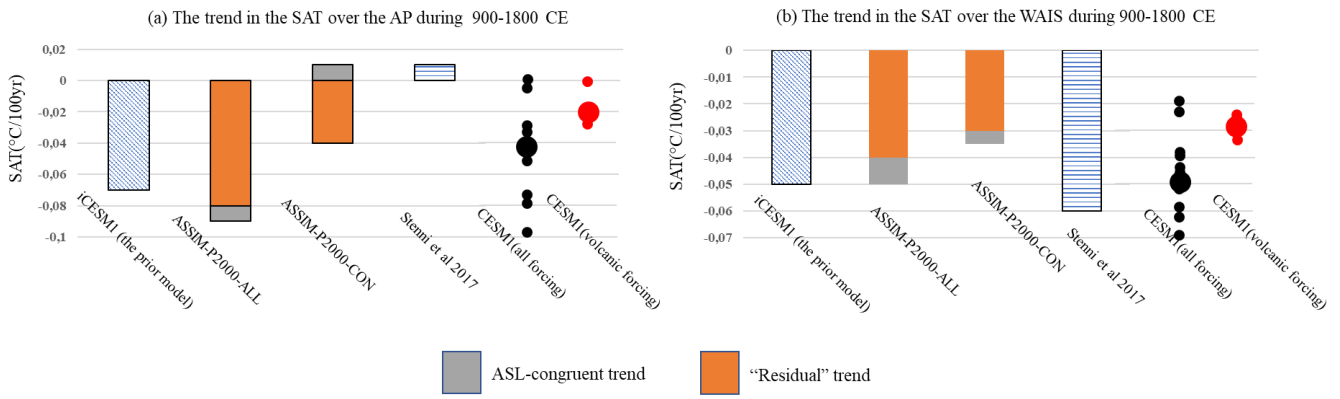

Figure 4.10. *The area-weighted mean of ASL-congruent and "residual" trend in the SAT from ASSIM-P2000-ALL, ASSIM-P2000-CON, and the trend from iCESM1 and CESM1 (including all forced simulations and volcanic-forced simulations) over the AP (a) and WAIS (b).*

The general cooling in West Antarctica and adjacent seas obtained in our reconstructions between the LIA and the MCA is consistent with the iCESM1 ensemble mean (Fig. 4.10) as well as with other simulations performed with climate models (e.g., LOVECLIM in Goosse et al., 2012, models in PMIP3/CMIP5 as shown in Klein et al., 2019). The magnitude of the changes in iCESM1 is actually very close to the one ASSIM-P2000-ALL, the reconstruction that appears the most faithful for the long-term trend over the past millennium as shown in Section 4.3.2, and larger than in ASSIM-P2000-CON, in particular over the AP. This suggests that the widespread cooling over West Antarctica and the Pacific sector of the Southern Ocean in ASSIM-P2000-ALL is driven by external forcings and corresponds to a standard response to the decrease in the global radiative forcing between the two periods. Goosse et al. [2012] and Phipps et al. [2013] suggests that volcanic forcing is the main contributor to this cooling trend over Antarctica and Southern Hemisphere for the last millennium. Here we confirm this conclusion by examining the simulations driven by all forcings and by only the volcanic forcing performed with the CESM1 [Fig. C.5, Otto-Bliesner et al., 2016]. Over 900-1800 CE, the ensemble mean of CESM1 driven by all the forcings shows a significant cooling trend with -0.04 °C/100yr in the AP and -0.05 °C/100yr in the WAIS. More than 50 % of this cooling trend is obtained in the simulations conducted using only the volcanic forcing, with -0.02 °C/100 yr in the AP and -0.03 °C/100 yr in the WAIS, highlighting the dominant influence of this forcing on the widespread MCA-LIA cooling over West Antarctica and the surrounding seas.

Our ASSIM-P2000-ALL and ASSIM-P2000-CON reconstructions agree also relatively well with the one of Stenni et al. [2017] in WAIS, which also displays a significant cooling there (-0.06 °C/100yr at $p < 0.05$). However, the slight warming of 0.01 °C/100yr (at $p > 0.05$) in the AP present in the Stenni et al. [2017] reconstruction contrasts with the cooling present in both our reconstructions. Assimilating the same continental proxy records as in ASSIM-P2000-CON but with annual resolution (Fig. C.6) reproduces the weak warming shown in Stenni et

al. [2017] because of a larger contribution of the changes in the ASL (ASL-congruent trend 0.02 °C/100 yr). However, this additional experiment shows less agreement with the independent sea-ice proxy records than ASSIM-P2000-CON and ASSIM-P2000-ALL, indicating that it is likely not able to reproduce the centennial variability in the AP region.

Since our reconstructions and the one of Stenni et al. [2017] only include one high-resolution $\delta^{18}O$ record covering the past two millennia in the AP from the ice core collected on the James Ross Island (JRI), it is interesting to investigate how this record constrains our reconstructions. The correlation between the original $\delta^{18}O$ record and the reconstructed one from ASSIM-P2000-CON (0.86, $p < 0.05$) is much higher than the correlation with ASSIM-P2000-ALL (0.46, $p < 0.05$) over the last two millennia. Furthermore, ASSIM-P2000-ALL displays a negative trend of -0.24 per mill/century ($p<0.05$) in the $\delta^{18}O$ at JRI over 900-1800 CE, while ASSIM-P2000-CON has no trend (0.00 per mill/century, $p>0.05$) and the original $\delta^{18}O$ has a positive one (0.3 per mill/century, $p<0.05$, Fig. C.6), consistent with the reconstruction of Stenni et al. (2017) which is based on this record. There are also large differences between both reconstructions in the trend of the snow accumulation at JRI, with -44.8 Gt year^{-1} per century ($p<0.05$) in ASSIM-P2000-ALL and 14.7 Gt year^{-1} per century ($p<0.05$) in ASSIM-P2000-CON (Fig. C.6). This confirms that the reconstruction in ASSIM-P2000-ALL is much less controlled by the JRI record because of the additional large-scale information provided by the marine data, while ASSIM-P2000-ALL and especially Stenni et al. [2017] reconstruction critically depend on this single record.

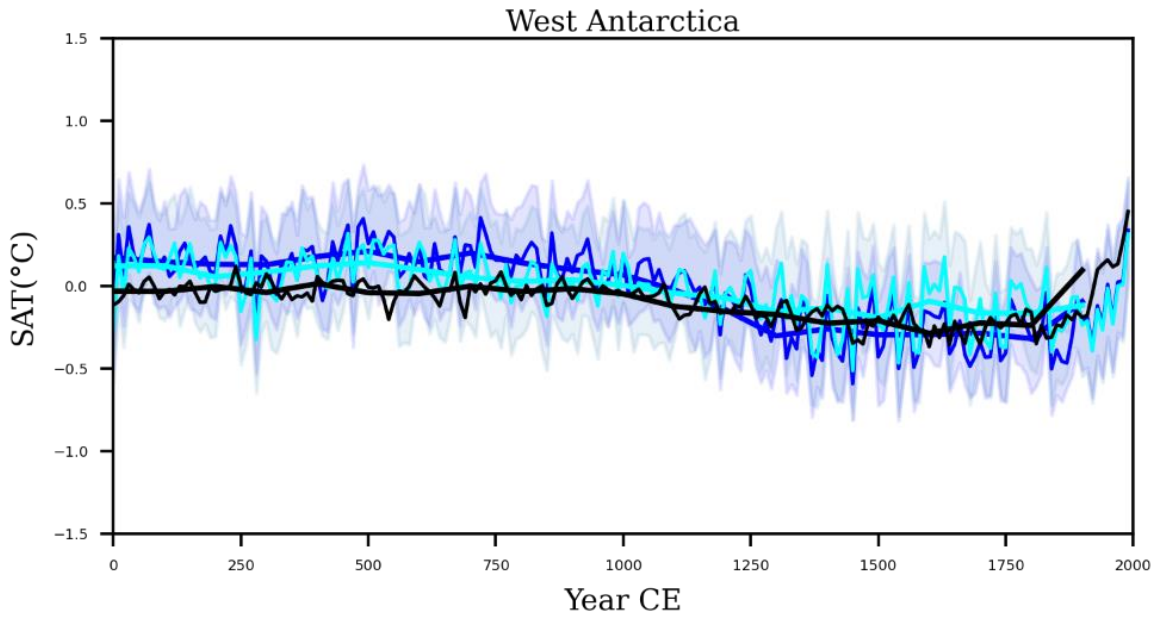

Figure 4.11. *The time series for the global-scale temperature from Neukom et al. [2019] (black) and the reconstructed SAT over West Antarctica in ASSIM-P2000-ALL (blue) and*

ASSIM-P2000-CON (cyan). The thin line denotes the 10-year averaged time series, while the thick line represents the 100-years averaged time series.

As there has been some debate about the temperature trends over the past millennium, the synchronicity between regions or even the existence of a transition between warmer and colder periods such as the MCA and the LIA [Neukom et al., 2019; PAGES2K-PMIP 2015], we examine the relationship between our reconstructions for the 10-year averaged SAT over West Antarctica and the global SAT reconstructions of Neukom et al. [2019] over the past millennium (850-1850 CE) (Fig. C.7). The results show that the global SAT correlates much better with the reconstructions in ASSIM-P2000-ALL (0.65 at zero lag) than with ASSIM-P2000-CON (0.35 at zero lag). It is sometimes argued that the Antarctic response to forcings may lag significantly behind the global one [e.g., Abram et al., 2017], but this does not seem the case for West Antarctica as the maximum correlation between the ASSIM-P2000-ALL and global SAT occurs for a lag of 20 years only (global temperature leading). By contrast, when we compute the same metrics but with the detrended time series, we find a poor relationship between our reconstructions and the global SAT. In addition, we also make a comparison of the recent warming between the reconstructions. The global reconstruction shows a warming trend starting around 1800 based on the 100-year averaged time series, which is very close to the one in ASSIM-P2000-ALL with a warming starting around the same time (Fig. 4.11). This suggests that the synchrony between the global-averaged signal in Neukom et al. [2019] and the one over West Antarctica in ASSIM-P2000-ALL exists not only for the cooling over the past millennium related to the dominant role of the volcanism forcing, but also for the recent warming at centennial scale. This confirms that the centennial-scaled temperature evolution over West Antarctica is coherent with global changes over the full past millennium.

However, the MCA–LIA temperature difference given by the global reconstruction is -0.16 °C, much smaller than the one over West Antarctica in ASSIM-P2000-ALL which reaches -0.31 °C. Additionally, the warming trend over the 20th century over West Antarctica in ASSIM-P2000-ALL is 0.60 °C/century, which is slightly larger than the global warming trend of 0.52 °C/century. We have to remind again that there is no assimilation of the marine records during 1800-2000 CE, and hereby the magnitude of this trend over the 20th century over West Antarctica is likely to be underestimated based on the validation against Dalaiden et al. [2020] mentioned in Section 4.3.1. These differences between the amplitude of the variations between global-mean and WAIS could be interpreted as a moderate polar amplification of temperature changes, applied here for the Southern Hemisphere [Pithan and Mauritsen, 2014; Manable and Wetherald, 1975; Goosse et al., 2018]. For instance, the expanded sea ice over the Bellingshausen/Amundsen Sea during the LIA would enhance surface albedo and thus amplify the initial cooling by surface albedo feedback.

The analyses of the trend over the past millennium have highlighted the role of external forcing. Previous studies have proposed that unforced internal climate variability is also responsible for a large fraction of the changes [Goosse et al., 2012; Wang et al., 2017; Lyu et al., 2021], inducing complex patterns of cooling and warming for different periods. This explains the lack of coherence between global and West Antarctic temperatures for the detrended series over the past millennium. Additionally, as the external forcing, i.e., volcanism, is weaker during the first millennium, internal variability is likely dominant for this period. This is why no clear synchronous changes between West Antarctic temperature and global temperatures over the first millennium are found in our reconstructions.

4.4 Conclusion

In this paper, we have studied the climate variability over the past millennium in West Antarctica and surrounding seas by estimating several key climate variables (SAT, sea ice, and atmospheric circulation) using an offline DA method constrained by both continental and marine proxies. This method allows for generating internally consistent climate fields by considering the covariance (including spatial covariance and covariance between each variable field) contained in prior modeling results.

Considering the dominant role of the covariance relationship between variables in the DA process and its timescale dependence [Kunz and Laepple, 2021; Franzke et al., 2020], we have compared two DA experiments that assimilate the same proxy records but with annual and decadal temporal resolutions (i.e., ASSIM-P200-1yr and ASSIM-P200-10yr). We confirm the existence of changes in covariance across time scales in our region of interest and show its impact on the reconstruction for some variables. For instance, previous studies [e.g., Hosking et al., 2013, Raphael et al., 2019] and ASSIM-P200-1yr have shown that the sea ice evolution in the Ross Sea over the past two centuries is highly correlated with the Amundsen Sea Low at inter-annual scale. Our experiment ASSIM-P200-10yr, however, indicates that both variables have a more complex link at the decadal scale, especially when considering the trend over the past two centuries, and the sub-surface oceanic temperature seems to have a larger contribution to the sea ice variations in the Ross Sea region on those longer timescales. In this framework, the assimilation of continental and marine records at a uniform temporal resolution of 10 years provides a good compromise to combine the available low- and high-frequency records.

Our reconstructions covering the past two millennia (ASSIM-P2000-ALL and ASSIM-P2000-CON) reproduce well the main characteristics of reconstructions performed over the past two centuries using a denser network of shorter time proxy series (Dalaiden et al., 2021 and ASSIM-P200-10yr) over their common period. Some inconsistencies, for instance in the atmospheric circulation and sea ice concentration in some parts of the Ross Sea, remain but the good agreement in terms of temporal and spatial variability of SAT and sea ice between ASSIM-P2000-ALL and ASSIM-P200-10yr suggests that assimilating only a few records in

those long reconstruction still provide valuable information for the decadal scale and longer climate variability over West Antarctica. Additionally, the comparison with independent sea ice-related marine records confirms a good skill in long-term variations, in particular when both continental and marine records are assimilated in ASSIM-P2000-ALL.

According to our reconstruction ASSIM-P2000-ALL, a widespread cooling trend occurred over West Antarctica and surrounding seas over the period 900-1800, which could be interpreted as the equivalent of the so-called transition between the MCA and LIA in the region. While the cooling over the WAIS is also present in many other reconstructions, Stenni et al. [2017] reconstruction based on the JRI record does not display a cooling trend over the AP. It seems thus that including additional records in our reconstruction and taking advantage of the spatial covariance using a data assimilation framework gives less weight to the single JRI record. This cooling over the AP present in ASSIM-P2000-ALL is also consistent with several independent records [Lüning et al., 2019; Simms et al., 2021]. ASSIM-P2000-ALL provides thus likely a more faithful estimate of the large-scale changes of the SAT in the AP region, but additional long records for the region would be extremely useful to confirm this hypothesis [e.g., Rowell et al., 2022].

This widespread cooling trend over the pre-industrial past millennium is also consistent with the climate modeling results which suggest that the cooling could be explained by a simple thermodynamic response to the radiative forcing evolution over the period. Analyzing ensembles of simulations driven by all the natural and anthropogenic forcings and an ensemble driven by only the volcanic forcing indicates a dominant contribution of the latter to the cooling trend. Furthermore, the temperature over West Antarctica are well correlated with the global mean surface temperature that has been shown to be strongly influenced by volcanic forcing [PAGES 2k Consortium, 2019; Schurer et al., 2014]. The global-scale radiative forcing change appears thus to be responsible also for the multi-century cooling in West Antarctica. By contrast, higher frequency variations are controlled by regional processes as the correlation between the global mean and Antarctic temperature becomes very low for detrended time series.

5

Conclusion and Perspectives

5.1 Main achievements

Understanding the recent climate changes in Antarctica requires to put its large interannual to multi-decadal variability into a longer context. The reconstructions of surface air temperature in Antarctica based on ice-core water isotopic records have provided series covering the last two millennia [PAGES, 2013; Goosse et al., 2015; Stenni et al., 2017; Klein et al., 2019; An et al., 2021]. In particular, the advancements in the collection, synthesis, and calibration of the ice core data have led to considerable progress in estimating the Antarctic climate variability over the past two millennia. However, uncertainties are still large at regional scales [Klein et al., 2019; An et al., 2021], and this hampers our understanding of the physical mechanisms responsible for the centennial climate variability. Therefore, the work presented in this thesis was dedicated to better reconstructing the Antarctic SAT for the past two millennia in a dynamically meaningful and physically plausible way. Unlike some previous studies that mainly rely on one single type of proxy record, such as ice core water isotopic records, we have combined different proxy records and climate model results in complement to the information preserved in water isotopic records in order to identify the robust signals of centennial climate variability. The goal has been achieved by establishing three chapters corresponding to three sub-questions. The main conclusions are synthesized below.

5.1.1 Are current climate models able to reproduce the observed signals derived from borehole temperature over the past two millennia?

The reconstructions from the observed borehole temperature in Antarctica have greatly contributed to our knowledge of the low-frequency surface air temperature changes on multi-decadal to centennial scales [e.g., Barrett et al., 2009; Muto et al., 2011; Orsi et al., 2012; Zagorodnov et al., 2012; Roberts et al., 2013; Yang et al., 2018]. The centennial-scale temperature change over the last millennium simulated with PMIP3-CMIP5 models, however, has hitherto not been systematically benchmarked against those borehole-temperature based reconstructions. In Chapter 2, we performed such comparisons by two complementary ways using borehole measurements and the corresponding reconstructions of surface temperature at four sites, respectively located in the Antarctic Peninsula, West Antarctic Ice Sheet, western coast of the Ross Sea, and Wilkes Land Coast.

The most simple and straightforward comparison was made between the reconstructed surface temperature time series from boreholes and modeling results. Due to the non-uniform smoothing of the signal and the large uncertainties reflected in the borehole temperature reconstructions, the comparison is limited when using the annual-resolved time series from the modeling results. It indicates that the long-term cooling trend in West Antarctica from 1000 to 1600 CE and the recent warming at those four sites are generally reproduced by those general climate models (GCMs), although its magnitude varies between models, highlighting the large roles of internal climate variability. However, no model is able to reproduce the cooling trend at the site located on the Antarctic Peninsula during the 19th century, yet our data assimilation-based reconstructions in Chapter 4 have reproduced it. This indicates that the model-data comparison is not straightforward, in particular for specific observed changes due to internal variability. This also highlights that, for those climate changes caused by internal variability, constraining the climate model to follow observations within their uncertainties is a plausible approach to investigate the specific hypotheses regarding the role of large-scale climate dynamics in explaining the paleo-observations.

Then, by using the simulated SAT as an upper boundary condition, a one-dimensional heat advection and diffusion forward model, developed by Orsi et al. [2012], was driven to simulate the under-ground thermal regime at each site. The comparison of the temperature profiles is more easily interpreted that the one from the depth domain. Note, here we assumed that Antarctic SAT changes are strongly coupled to ground surface temperature (GST) changes and transferred to the subsurface by thermal conduction. This SAT–GST relationship at multi-decadal scale during the last millennium has been evaluated by Camilo et al. [2018] which suggests that land cover changes in terrestrial regions are the main driver for locally and regionally decoupling between SAT and GST. Therefore, our hypothesis remains plausible because the four sites in Antarctica are always covered with snowfall according to the descriptions in the original papers.

Finally, we have evaluated the spatial representativeness of the metrics regarding the surface temperatures derived from the borehole reconstructions in the climate models.

Those metrics are demonstrated to be generally representative of a large spatial area, although they are calculated at a specific site. Consequently, they are proposed to be used more widely in model-data comparisons.

5.1.2 Are there robust multi-centennial trends during the past two millennia observed in East and West Antarctica?

The results in Chapter 2 have indicated that current GCMs are able to generally reproduce the SAT reconstructions derived from the measured borehole temperatures in Antarctica. However, borehole temperature-based reconstructions have a very low temporal resolution, in particular for the period during the first millennium (e.g., Orsi et al. [2011]). This makes the model-data comparison difficult, even in the depth domain as we did in Chapter 2. Therefore, an additional model-data comparison spanning the full CE has been achieved in Chapter 3.

To this end, we have quantified the similarities and differences between climate model simulations and the reconstructed Antarctic SAT over the past two millennia for 500-year trends. We have also performed several SAT reconstructions using a data assimilation approach. It allows to diagnose the impact of adding a particular proxy record or set of proxy records to the data assimilation product and to combine the available high and low frequency ice core water isotope records from Antarctica with the information derived from climate models.

Our results have indicated that the simulations fail to capture the multi-centennial changes in the first millennia derived from the existing statistically-based reconstructions, in particular for East Antarctica. Similar discrepancies are also observed between simulations and the data-assimilation based reconstructions presented in Chapter 3, although the magnitude of the difference is much smaller. This suggests that the trends in the first millennium deduced from the statistically based reconstructions are unlikely to be entirely forced by external forcings.

Our reconstructions have highlighted the complexity of the 500-year temperature trends and their spatial distributions in Antarctica, especially during 1-500 CE, and their high sensitivity to the selection of the records for the reconstructions. Nevertheless, our reconstructions have identified a common cooling over Antarctica during 501-1000 CE, with a larger magnitude in the WAIS than elsewhere over Antarctica. Additionally, the analysis of the atmospheric circulation in the reconstructions has indicated that a positive trend of the Southern Annular Mode and a deepening of the Amundsen Sea Low are responsible for the pattern of temperature changes over 501-1000 CE. In contrast to the past millennium, especially between the 13th century and the 19th century, only a few large eruptions occur in the first millennium, with long periods of volcanic quiescence. In the absence of a dominant signal due to the forcing, our results have thus highlighted the role of internal climate variability in the temperature trends on multi-centennial scales over the first millennium. It is likely that on such long time scales, oceanic dynamics play a strong

role, but the ocean processes that could drive such low-frequency variability in the Southern Ocean are still under debate [e.g., Zhang et al., 2021].

5.1.3 Is there a coherent SAT evolution over Antarctica and surrounding seas over the past two millennia?

In Chapter 4, we have achieved the combination of continental and marine proxy records with climate model results using an offline DA method to investigate the climate variability over the past two millennia in West Antarctica and surrounding seas. Based on this, we have reconstructed several key climate variables (SAT, sea ice, and atmospheric circulation) over the past two millennia in this region. According to this reconstruction, the assimilation of marine records in Chapter 4 brings additional constraints for the first millennia that are compatible with the reconstructions presented in Chapter 3. This confirms the robust SAT reconstruction present in this chapter for the first millennium over West Antarctica.

The first conclusion of Chapter 4 is that the covariance relationship between variables, which is the basis for the DA method to reconstruct the variable of interest using the observations, is time-scale dependent, in particular the one between sea ice and winds. Consequently, we suggest that a uniform temporal resolution of 10 years can provide a good compromise when assimilating the available low-frequency marine records and high-frequency continental records. Our reconstructions covering the past two millennia have confirmed a widespread cooling trend occurred over West Antarctica and surrounding seas over the period 900-1800 CE, which is inconsistent with Stenni et al. [2017] reconstruction based on the James Ross Island (JRI) record that does not display a cooling trend over the AP. This suggests that incorporating additional records in our DA-based reconstructions has allowed giving less weight to the single JRI record due to the effect of the spatial covariance, and JRI record may be representative of the proxy-scale (or local) changes, rather than the whole AP. Indeed, the reconstructions in Chapter 4 reconcile the inconsistency between some existing reconstructions and climate model results. In particular, this cooling could be explained by a simple thermodynamic response to the radiative forcing evolution over the period. Furthermore, the temperatures in west Antarctica are well correlated with the global mean temperature that has been shown to be strongly influenced by volcanic forcing.

5.2 General conclusions

This thesis has confirmed that the current climate models are able in general to reproduce the observed SAT variability at the centennial scale during the last millennium over West Antarctica [Chapter 2 and 4], while the models still have trouble to capture the changes over the first millennium, even when constraining the model using the proxy records by data assimilation [Chapter 3]. One potential reason for the different performance of the climate models regarding the simulation of the temperature changes over the first and second millennium could be due to the different mechanisms responsible for the centennial SAT variability during both periods. During the first millennium with weak external forcings, in particular a weaker volcanic activity, internal processes play a large role in the SAT changes. However, the models may not represent well the natural variability in Antarctica and the Southern Ocean. For instance, current climate models are still not able to reproduce the same magnitude of pre-industrial centennial SAM variability as reconstructed from the proxy records [e.g., Abram et al., 2014]. In contrast, during the past millennium when the external forcing due to volcanic eruptions dominates the centennial SAT variability, the climate models correctly simulate the magnitude of the forced response and thus capture the changes at least in West Antarctica. The internal oceanic variability or some feedback mechanisms between ocean and atmosphere could be responsible for this low-frequency natural variability during the first millennium [e.g., Zhang et al., 2021]. Unfortunately, we do not have much specific information about the changes in oceanic near-surface or deep circulation for the past millennia.

Additionally, the uncertainty in the SAT reconstructions due to the limited number of the proxy records spanning the full Common Era in Antarctica has been quantified by using different sets of proxy records in the data assimilation [Chapter 3 and 4]. As a result, one of the key messages here is that one should be extremely careful when using the reconstructed SAT (1) during the first millennium when a steep decline in the quality and quantity of available climate proxy records [Chapter 3] (2) for the regions with a few proxy records available such as the Antarctic Plateau [Chapter 3] and Antarctic Peninsula [Chapter 4]. Our reconstructions also highlighted the improvement in capturing the low-frequency climate variability, which could be achieved by incorporating the proxy records, such as the SST reconstructions based on marine sediments, with having a unique advantage in recording the slower process compared to the “standard” high frequency proxy records. In this aspect, data assimilation has been demonstrated to be particularly appropriate to provide a framework combining different temporal-resolution proxy records through Chapters 3 and 4.

5.3 Perspectives

Our results have highlighted the role of internal variability in explaining some of the observed centennial variations, focusing on the winds, but it would be interesting to explore further the mechanisms at the origin of this variability. For instance, while winds are well known to display strong variations inducing large interannual variability, what are the processes explaining the centennial changes in atmospheric forcing and their impact on the temperature? Considering the long-term memory of the ocean, it could integrate the high frequency atmospheric forcing leading to low frequency variability and feeding back on the atmosphere. Alternatively, the origin of the variability could be the ocean itself, in particular the deep ocean circulation [Petro et al., 2016; Zhang et al., 2021]. Many studies have suggested that an increased upwelling of deep waters, which are relatively warm with respect to the surface waters, could lead to SST warming and sea ice retreat [e.g., Menviel et al., 2015; Etourneau et al., 2013; Shevenell et al., 2011]. This might then change the meridional temperature gradient between mid and high latitudes, which is a key player in controlling the variability of the winds [Varma et al., 2011, 2012; Lamy et al., 2010]. In general, answering these questions would require obtaining specific information regarding oceanic variables at the surface but also in the deep ocean. As a result, online data assimilation, i.e., updating the ensemble at each time step so that all elements of the climate system have a consistent evolution [Goosse, 2017; Perkins and Hakim, 2017], is an interesting option for future development in order to complement the results obtained using the offline data assimilation in this thesis.

In this thesis, compared to previous reconstructions, we have increased the number of proxy records selected to cover the past 2000 years over Antarctica by incorporating several different types of proxy records. However, those having a quantitative interpretation for a specific physical variable such as temperature or precipitation, directly comparable to the simulated climate variables from climate models, and thus being able to be used in data assimilation, are still too few, especially in the ocean. This is also prominent in East Antarctica, considering the complex spatial pattern for the multi-centennial SAT trend there [Chapter 3]. This leads to reconstructions of the atmospheric circulations over West Antarctica and surrounding seas being less skillful over the past two millennia compared to the past two hundred years [Chapter 4]. Obtaining more annual snow accumulation and water isotope records from ice cores would be an ideal way to solve this issue, but it is also an expensive and challenging way due to the harsh natural environment in Antarctica, as well as the low snow-accumulation rate in East Antarctica. Utilizing all the available records, such as the low frequency $\delta^{18}O$ records, marine proxy-based SST reconstructions, peat records, glacial evidence, etc., is thus very important to provide insights into past climate evolutions. We have used some of those records in this thesis, with for instance several diatom-based sea ice proxies with temporal resolutions of the order of decades to a century selected as qualitative validation of the reconstructions. This could be further expanded in the future. Diatom transfer functions have been proposed and perform well in coastal regions of Adelie Land [Crosta et al., 2021]. Such a method is able to reconstruct quantitively the mean annual length of the sea-ice duration that can be used in data

assimilation. In addition, the chemical composition of ice cores, in particular, sea salts (e.g., Na^+), have been used to estimate the past atmospheric circulation [e.g., Legrand and Mayewski, 1997; Mayewski et al., 2017] and sea ice changes [e.g., Abram et al., 2013]. In particular, within the framework of the CLIVASH2k project, a new compilation of the chemical composition of existing ice cores is being carried out. Therefore, incorporating them into data assimilation would be very useful for better reconstructing the Antarctic centennial climate variability.

Since currently only one ensemble of simulations with an isotopic-enabled model using iCESM1 is available for that last millennium, we were not able to test the sensitivity of our results to the selected climate model for the data assimilation. However, different climate models produce different covariance between variables and thus have different biases in this covariance. Previous works have highlighted the large sensitivity of the data assimilation-based reconstructions to the model prior, especially when the proxy network is relatively sparse as shown for those covering the full Common Era used in this thesis [King et al., 2021; Anchukaitis and Smerdon, 2022]. Therefore, it would be interesting to build multi-model priors in data assimilation, in particular from ensembles of isotope-enabled climate models, to replicate the analyses achieved in Chapters 3 and 4.

A

Supplementary to Chapter 2

A. 1: Forward model description

The equation ruling subsurface temperature evolution in the forward model is given in Eq. 1. According to the original publications, we applied different methods to determine the density profile for each borehole in the model. For WAIS and Styx, the density profiles, $\rho(z)$, were obtained by a quadratic fit to the measured bulk density data following Severinghaus et al. [2010]. For Larissa, the density profile was approximated following Salamatin [2000]. For Mill Island, because of the similarity between the density profiles at Mill Island and Law Dome [van Ommen et al., 1999], the density is described by a piecewise exponential plus linear or dual exponential according to the analysis on the Law Dome ice core density profile [van Ommen et al., 1999]. The density is considered to be constant in time in the model.

For the other parameters in the forward model, the specific heat capacity c_p is calculated by c_p = 152.5+7.122T (J kg-1 K-1) [Cuffey and Paterson, 2010, Chap. 9, Eq. 9.1 where T is the temperature]. The thermal conductivity in ice is taken from $K_{ice} = 9.828 \exp(-5.7 \times 10^{-3} T)$ (Wm-1K-1) [Cuffey and Paterson, 2010, Chap. 9, Eq. 9.2], and the thermal conductivity of the firn is calculated by Schwerdtfeger formula [Cuffey and Paterson, 2010, Chap. 9, Eq. 9.4]. The vertical velocity at the surface is simply the accumulation rate and decreases with depth as the integral of the densification process (compaction) and the strain due to ice flow divergence. The vertical velocity profile is determined by the method of Alley et al. [1990] and Cuffey et al. [1994] with a constant strain rate. For the accumulation rate, we use a constant value derived from their original publication, which is specified in the Table 3 of the main text. The bottom boundary condition is given by the basal heat flux and the basal temperature. The heat flux is determined by matching the slope of the temperature increase in the bottom section of the record. At Mill Island, this was not possible, because the data do not extend very deep with respect to the total ice thickness. A zero heat flux boundary condition

was chosen instead. The validity of this hypothesis is demonstrated in the original study of Roberts et al. [2013]. The basal temperature is determined using the lower "undisturbed" sections of the measured borehole temperature extrapolated to the bottom.

In order to save computation time, the vertical discretization of the model is not homogenous. For WAIS, which is the only very deep borehole, the vertical step is of 1 m for the upper 500 m and up to 25 m for the deepest part. For other sites where the depth of borehole is close or less than 500 m, the step is set to 1 m for the whole depth range.

Before the forward model is driven by the climate model results, it is initialized with a stationary profile, which is generated after a 20000-year model run with a constant climate history and a realistic seasonal cycle. Seasonal-scale variations are "undetectable below a depth of 20m" [Cuffey and Paterson, 2010], and its does not change throughout the run. At WAIS and Styx, the seasonal cycles are determined from weather station data; at Larissa and Mill Island, since the original studies do not give the seasonal cycle, we use a seasonal cycle amplitude of 10 °C similar to WAIS (Eq. S1). At WAIS, it includes a periodic function with annual and semi-annual components, fitted to 3 years of weather station data from WAIS Divide and Byrd station (AMRC, SSEC, UW-Madison) as follows [Orsi et al., 2012]:

$$T(t) = 10(\cos(2\pi t) + 0.3\cos(4\pi t)) \text{ (in K)} \qquad \text{(S1)}$$

At Styx, the seasonal cycle is determined by fitting a sinusoidal function to the automated weather station data as follows [Yang et al., 2018]:

$$T(t) = 10(\cos(2\pi t) + 0.35\cos(4\pi t)) \text{ (in K)} \qquad \text{(S2)}$$

Where t is time, T is the temperature.

Equations S1 and S2 for WAIS and STYX are nearly identical, so we presume the seasonal cycle is also similar at Larissa and Mill Island, where no seasonal data is available. Including a seasonal cycle wave is important because the heat capacity and thermal conductivity depend on temperature, and temperature changes a lot in the top 15m, but below that, it is of negligible effect.

A. 2: Supplementary figures

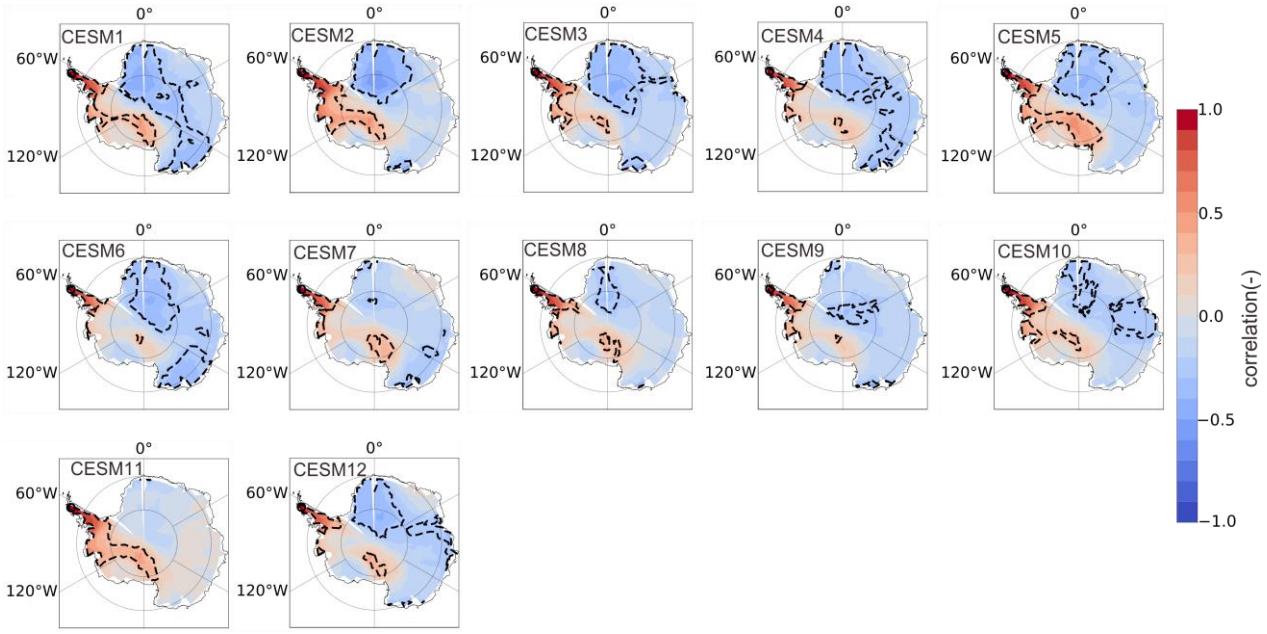

Figure A.1: *The correlation map (blue-red shading area) showing the relationship between the temperature from 1825 to 1925 CE at Larissa and other grid cells in Antarctica for each CESM member. The black dotted contour lines show a significant correlation at the 99 % significant level.*

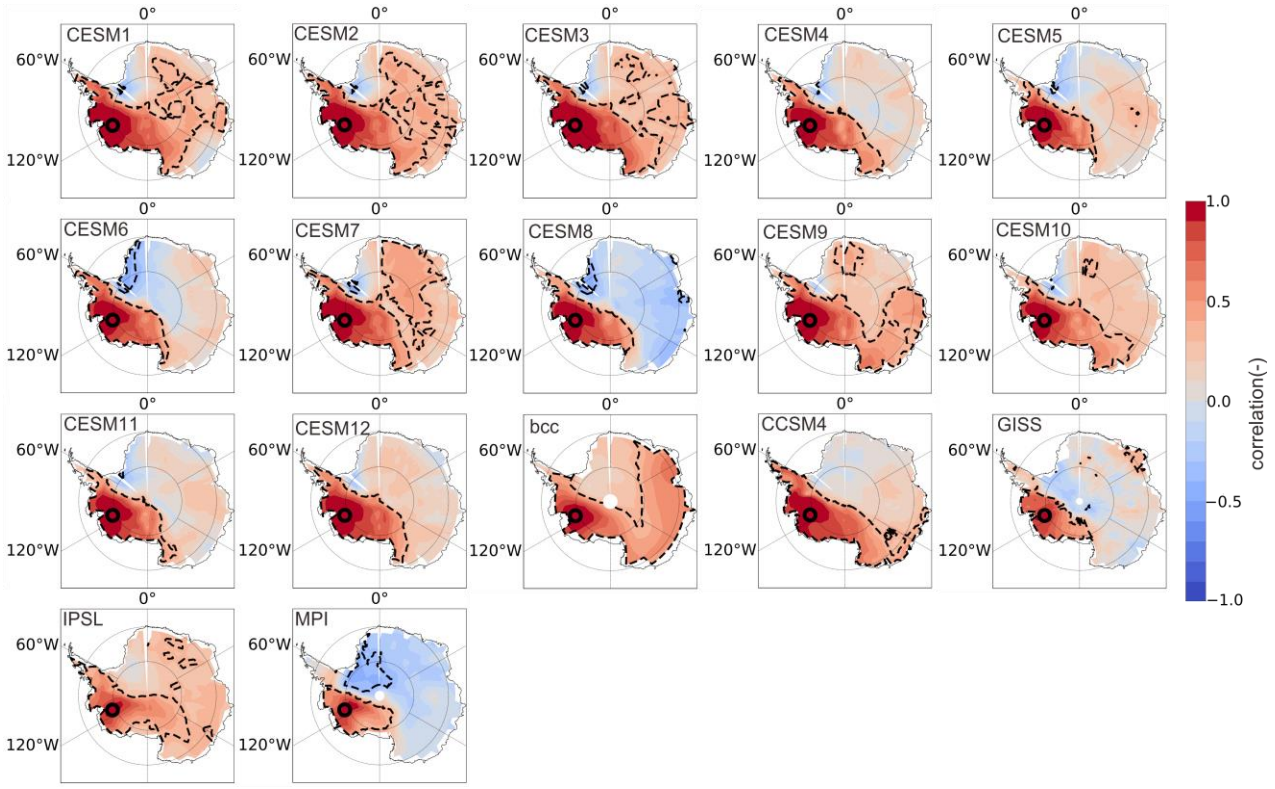

Figure A.2: *The correlation map showing the relationship between the temperature from 1950 to 2005 CE at WAIS and other grid cells for each climate models. The red dashed contour lines show a significant correlation at the 99% significant level.*

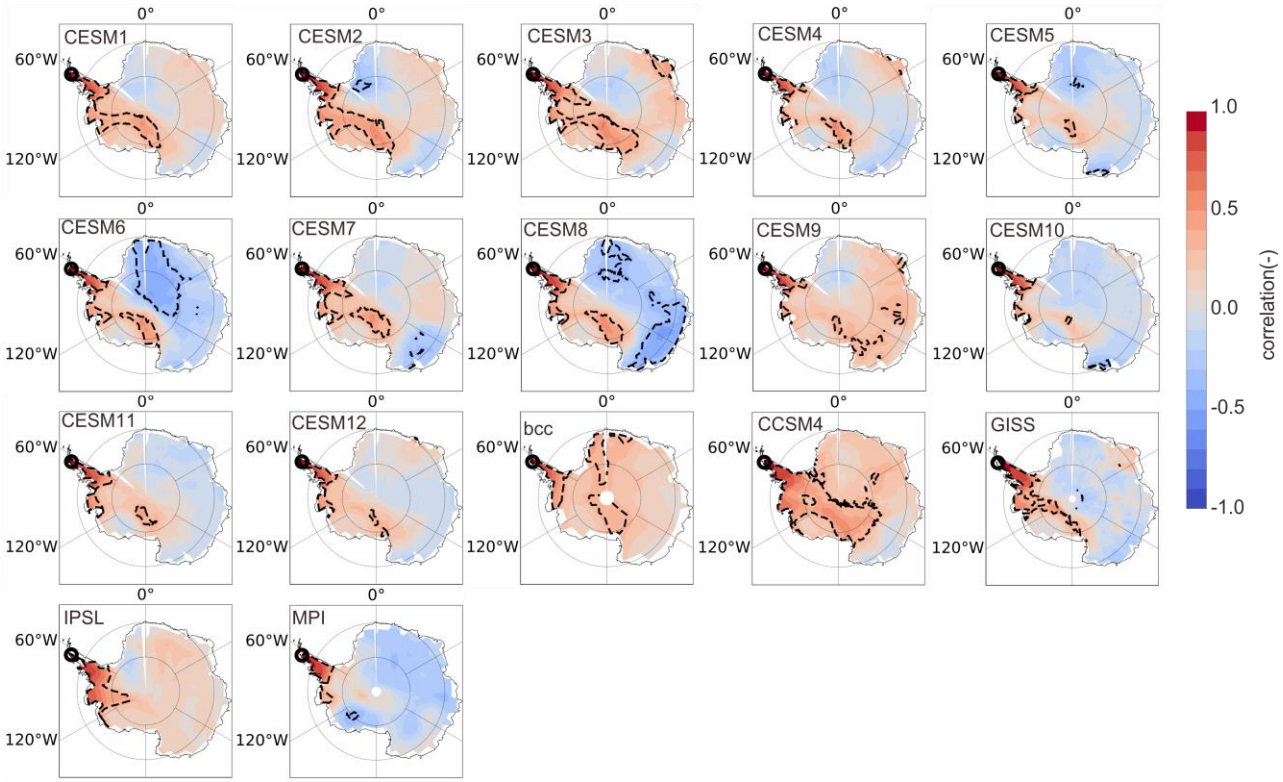

Figure A.3: *The correlation map showing the relationship between the temperature from 1950 to 2005 CE at Larissa and other grid cells for each climate models. The red dashed contour lines show a significant correlation at the 99% significant level.*

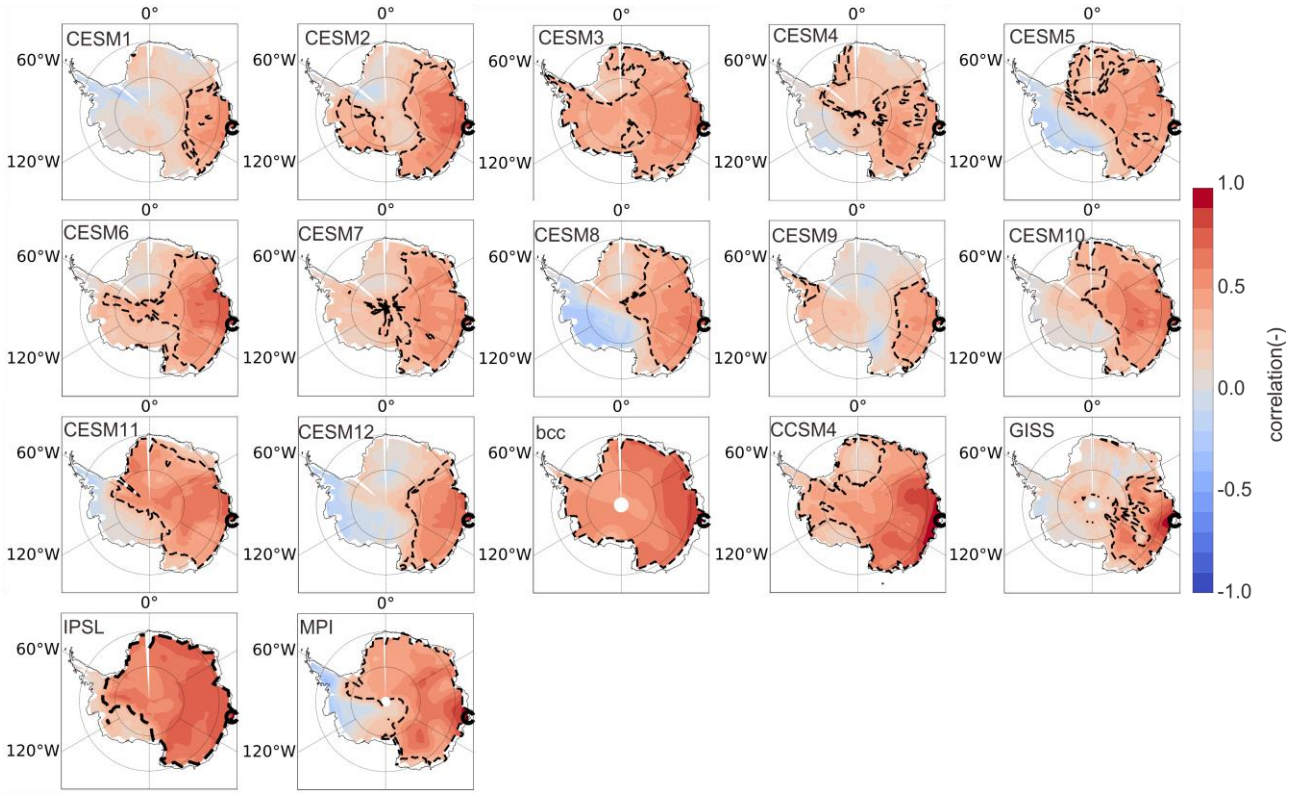

Figure A.4: *The correlation map showing the relationship between the temperature from 1950 to 2005 CE at Mill Island and other grid cells for each climate models. The red dashed contour lines show a significant correlation at the 99% significant level.*

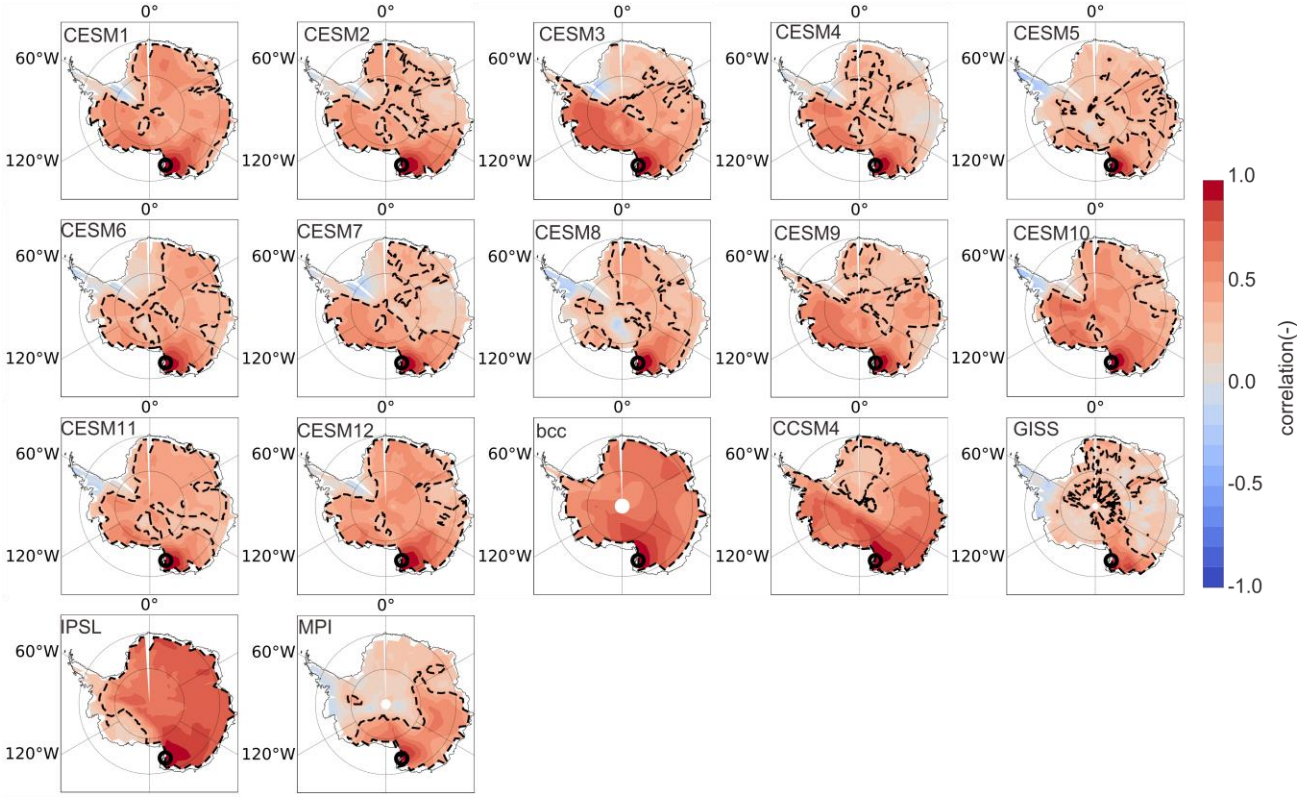

Figure A.5*: The correlation map showing the relationship between the temperature from 1950 to 2005 CE at Styx and other grid cells for each climate models. The red dashed contour lines show a significant correlation at the 99% significant level.*

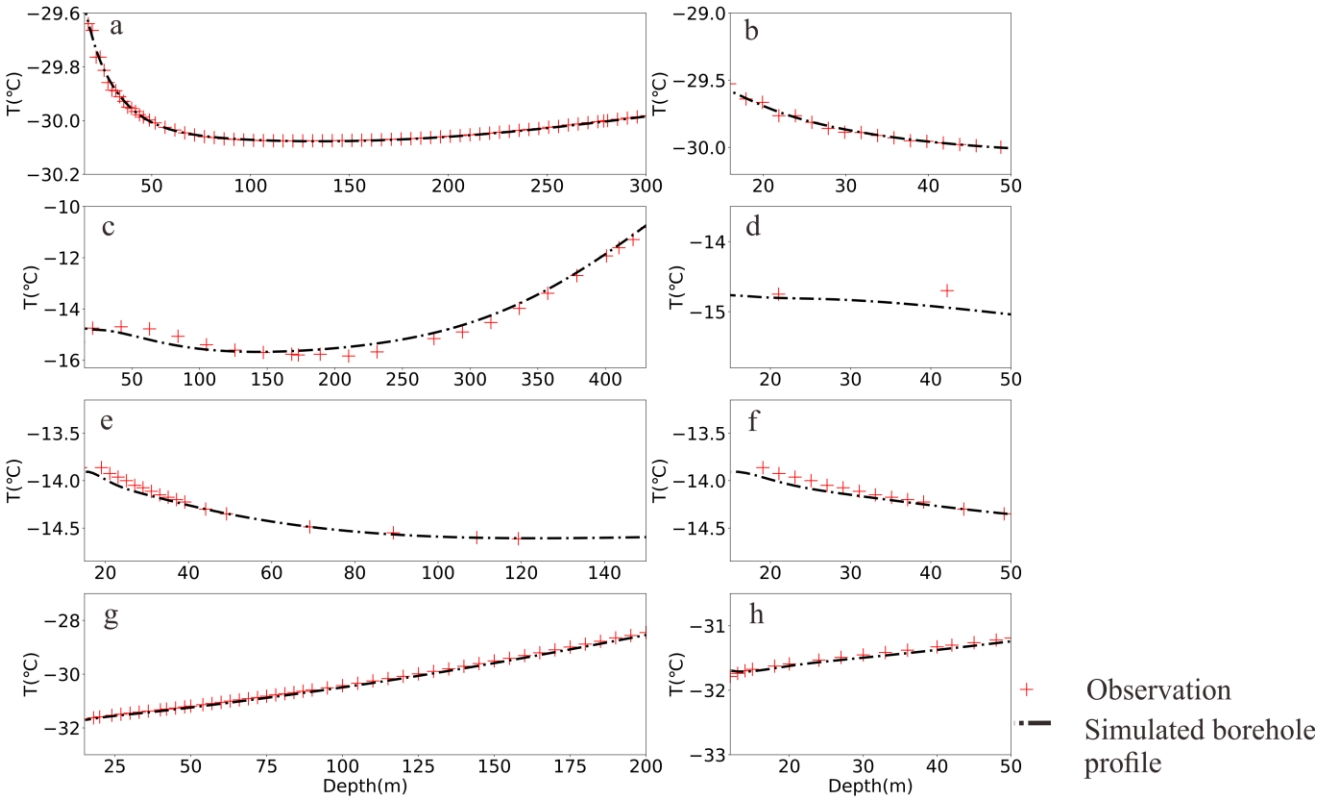

Figure A.6: *Comparison of borehole temperature profile outputs for the forward model driven by the corresponding reconstruction with the observation at each site. (a) WAIS: 15-300 m; (b) WAIS: 15-50 m; (c) Larissa: 15-430 m; (d) Larissa:15-50 m; (e) Mill Island:15-150 m; (f) Mill Island:15-50 m; (g) Styx:15-200 m; (h) Styx:15-50 m. The thick dash-dot line denotes the simulated borehole profile at each site, and red across represent the observation.*

A. 3 Observed borehole temperature distribution at WAIS.

Depth(m)	Temperature (°C)
7.96	-29.7594
9.19	-29.604
9.95	-29.5588
11.94	-29.4741
13.93	-29.4806
15.92	-29.5267
17.91	-29.6397
19.9	-29.6645
21.89	-29.7642
23.89	-29.7642
25.88	-29.8132
27.87	-29.8587
29.86	-29.8871
31.85	-29.8891
33.84	-29.9115
35.83	-29.9285
37.82	-29.9503
39.81	-29.9549
41.8	-29.9663
43.79	-29.9785
45.78	-29.9872
48.77	-29.998
51.75	-30.0089
56.73	-30.0253
61.7	-30.0352
66.68	-30.046
71.65	-30.0538
76.63	-30.0603
81.6	-30.0635

86.58	-30.0682
91.55	-30.0701
96.53	-30.0724
101.5	-30.0738
106.48	-30.0746
111.55	-30.0753
116.43	-30.0755
121.4	-30.0757
126.38	-30.0756
131.35	-30.0753
136.33	-30.0752
141.3	-30.0748
146.28	-30.0743
151.25	-30.0736
156.23	-30.0734
161.2	-30.0722
166.18	-30.0715
171.15	-30.0698
176.13	-30.0686
181.1	-30.0672
186.08	-30.0653
191.05	-30.0632
196.03	-30.0608
201	-30.0584
205.98	-30.0564
210.95	-30.0532
215.93	-30.0502
220.9	-30.0471
225.88	-30.0436
230.85	-30.0404
235.83	-30.0365

240.8	-30.0329
245.78	-30.0299
250.75	-30.0248
255.73	-30.022
260.7	-30.0165
265.68	-30.0129
270.65	-30.0078
275.63	-30.0042
278.61	-30.0017
280.6	-30.0003
285.58	-29.9954
290.55	-29.991
295.53	-29.9863
300.5	-29.9821

A. 4 Observed borehole temperature distribution at LARISSA.

Depth(m)	Temperature (°C)
8.41	-15.35
10.51	-15.3
21.02	-14.75
42.04	-14.7
63.06	-14.78
84.09	-15.07
105.11	-15.4
126.13	-15.61
147.15	-15.7
168.17	-15.77
173	-15.8
189.19	-15.77
210.21	-15.84
231.24	-15.68
273.28	-15.16
294.3	-14.9
315.32	-14.53
336.34	-13.98
357.36	-13.39
378.86	-12.7
400.77	-11.93
409.92	-11.61
420.43	-11.29
430.94	-10.82

A. 5 Observed borehole temperature distribution at Mill Island.

Depth(m)	Temperature (°C)
9.05	-14.275
14.06	-13.8625
19.07	-13.8625
21.07	-13.925
23.07	-13.9625
25.07	-14
27.07	-14.05
29.07	-14.075
31.09	-14.1125
33.09	-14.15
35.11	-14.175
37.11	-14.2
39.11	-14.225
44.125	-14.3
49.14	-14.35
69.17	-14.4875
89.24	-14.55
109.3	-14.6
119.31	-14.6125

A. 6 Observed borehole temperature distribution at Styx.

Depth(m)	Temperature (°C)
1	-29.7244
2	-32.6116
3	-33.4131
4	-33.522
5	-33.2036
6	-32.9317
7	-32.5716
8	-32.3349
9	-32.1212
10	-31.9562
11	-31.8512
12	-31.7853
13	-31.7379
14	-31.6974
15	-31.6752
18	-31.6255
20	-31.5921
24	-31.5332
27	-31.4905
30	-31.452
33	-31.4144
36	-31.3781
40	-31.3275
42	-31.3006
45	-31.2628
48	-31.2209
50	-31.1898
54	-31.1366
57	-31.0925

60	-31.0493
63	-31.0032
66	-30.9585
69	-30.9144
72	-30.8683
75	-30.82
78	-30.7722
81	-30.7296
84	-30.6835
87	-30.6367
90	-30.5892
95	-30.5113
100	-30.4264
105	-30.3411
110	-30.253
115	-30.1648
120	-30.081
125	-29.9906
130	-29.8973
135	-29.803
140	-29.7075
145	-29.6079
150	-29.5078
155	-29.412
160	-29.3098
165	-29.2065
170	-29.0968
175	-28.9922
180	-28.883
185	-28.7783
190	-28.6518

195	-28.5633
200	-28.4535
205	-28.3431
210	-28.2515

B

Supplementary to Chapter 3

Table B.1. *Information about the PMIP3-CMIP5 GCM used in this study.*

Name	Model resolution (lat × lon)	Number of simulations for 850-1850	Reference
CESM1-CAM5	96 × 144	12	Otto-Bliesner et al., (2016)
GISS-E2-R	90 × 144	1	Schmidt et al., (2014)
IPSL-CM5A-LR	96 × 96	1	Dufresne et al. (2013)
MPI-ESM-P	96 × 192	1	Stevens et al., (2013)
CCSM4	192 × 288	1	Gent et al. (2011)
BCC-CSM1-1	64 × 128	1	Wu et al., (2014)

Table B.2. *Information about the $\delta^{18}O$ records covering (nearly) 1-1000 CE.*

	Resolution(years)	Min year (CE)	Max year (CE)
EDC Dome C	15	3	1919
B32SiteDML05	1	166	1996
Plateau Remote	1	2	1986
Talos Dome	11	4	1991
DSS Law Dome	1	173	1995
James Ross Island	1	0	2007
WDC06A	0.05	-50	2005
RICE	0.14	-44	2011
Taylor Dome	1.7	-25	1939
Dome F	35	0	1950
Vostok	20	0	1950

Table B.3. *Selected terrestrial proxies over Antarctica in this study.*

Letters	Location	Longitude	Latitude	Region	Archive (Proxy type)	Reference
A	Litchfield Island	64°06′W	64°46′S	Antarctic Peninsula	Peat core (moss accumulation)	Stelling et al., (2018)
B	Elephant Island	54.824°W	61.111°	Antarctic Peninsula	Peat core (biological productivity)	Charman et al., (2018)
B	Barrientos Island	59.753°W	62.408°	Antarctic Peninsula	Peat core (biological productivity)	Charman et al., (2018)
B	Norsel Point	64.084°W	64.759°	Antarctic Peninsula	Peat core (biological productivity)	Charman et al., (2018)
B	Green Island	64.151°W	65.322°S	Antarctic Peninsula	Peat core (biological productivity)	Charman et al., (2018)
B	Leonie Island	68.343°W	67.602°S	Antarctic Peninsula	Peat core (biological productivity)	Charman et al., (2018)
C	King George Island,	58°56'W	62°12'S	Antarctic Peninsula	Lake core (GDGTs)	Roberts et al., (2017)
D	Simple Dome	148.81°W	81.65°S	WAIS	Ice core (melt layer frequency)	Das et al., (2008)
E	RICE	161.706° W	79.364° S	WAIS	Ice core (snow accumulation)	Bertler et al., (2018)
F	WDC06A	112°05′W	79°28′S	WAIS	Ice core (snow accumulation)	Fudge et al., (2016)
G	WDC06A	112°05′W	79°28′S	WAIS	Ice core (borehole temperature)	Orsi et al., (2012)
H	Kirisjes Pond Prydz Bay	76.12°E	69.43°S	Wilkes Land Coast	Lake core (diatoms)	Verleyen et al., (2004)
I	Zolotov Island Prydz Bay	77°52′E	68°39′S	Wilkes Land Coast	Penguin remains (element concentrations)	Huang et al., (2011)
J	Long Peninsula Prydz Bay	78° 15′ E	68° 33′ S	Wilkes Land Coast	Penguin remains (element concentrations)	Gao et al., (2019)
K	B40	0.07°E	75.0°S	Dronning Maud Land	Ice core (snow accumulation)	Medley et al., (2018)
L	Lützow Holm Bay	9°36.674'E	69°28.45'S	Dronning Maud Land	Lake core	Tavernier et al., (2014)

						An et al., (2021)
M	Dome A	77.37°E	80.37°S	Antarctic Plateau	Ice core (water stable isotope)	
N	South Pole	98.16°W	89.99°S	Antarctic Plateau	Ice core (water stable isotope)	Steig et al., (2021)

Table B.4. *Signal-to-noise ratio of the data used in the data assimilation process.*

Ice core $\delta^{18}O$ record	Signal noise ratio (SNR)
EDC Dome C	0.55
B32SiteDML05	11.79
Plateau Remote	3.58
Talos Dome	0.73
Law Dome	2.92
James Ross Island	2.01
WDC06A	1.80
RICE	1.84
Taylor Dome	3.16
Vostok	0.67
Dome F	1.18

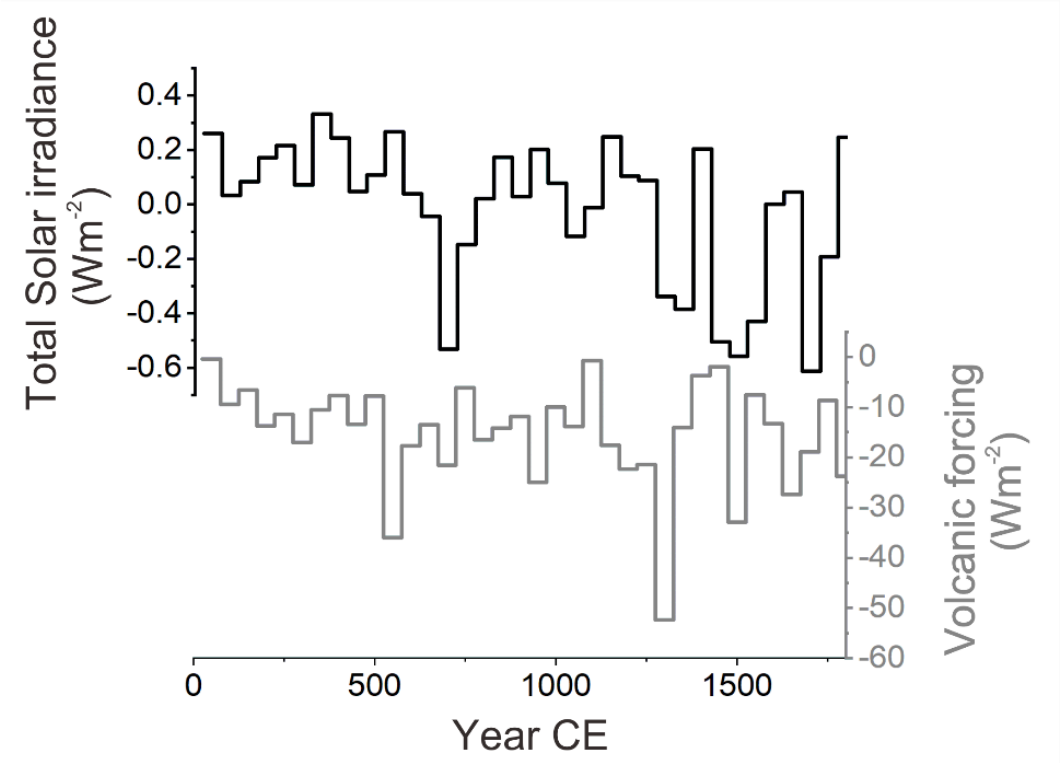

Figure B.1: *Long-term solar forcing from Steinhilber et al. (2012) (black curve) and volcanic forcing from Sigl et al. (2015) (gray curve) using 50-year averaged anomaly data. The reference period is over 1-1900 CE.*

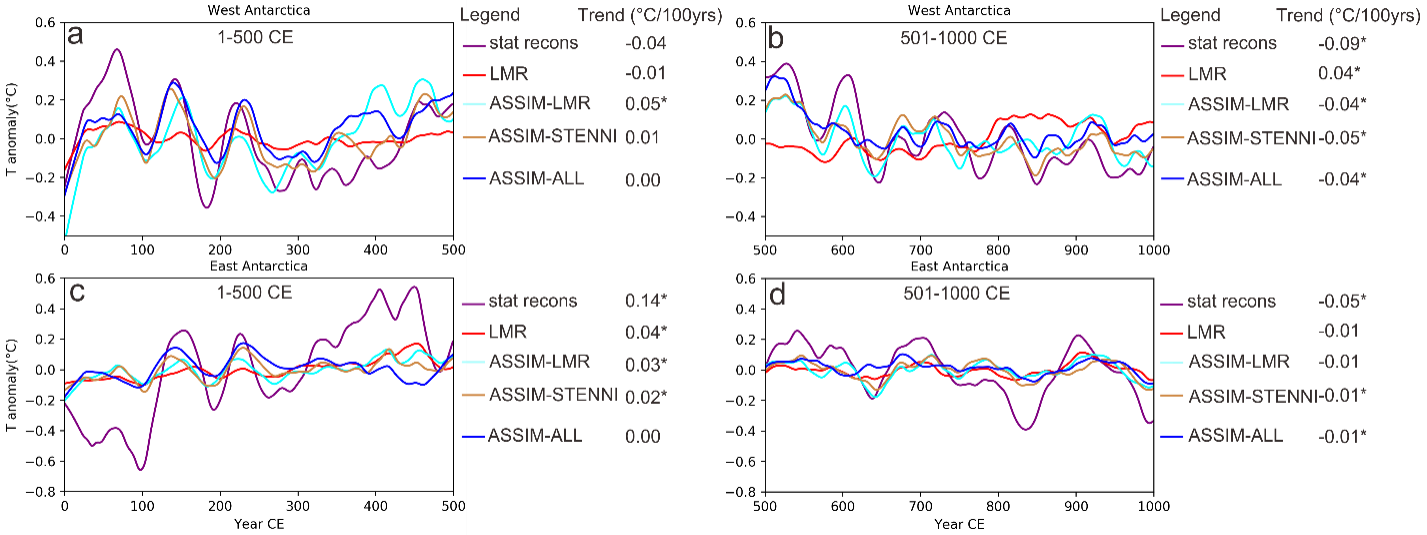

Figure B.2: *Time series and the 500-year trends over the first millennia deduced from the reconstruction of Stenni et al. (2017) (in purple), LMR (Tardif et al., 2019, in red), and three reconstructions in this study (ASSIM-LMR in cyan, ASSIM-STENNI in brown, ASSIM-ALL in blue). Statistically significant correlations (p value < 0.1) are marked by one asterisk.*

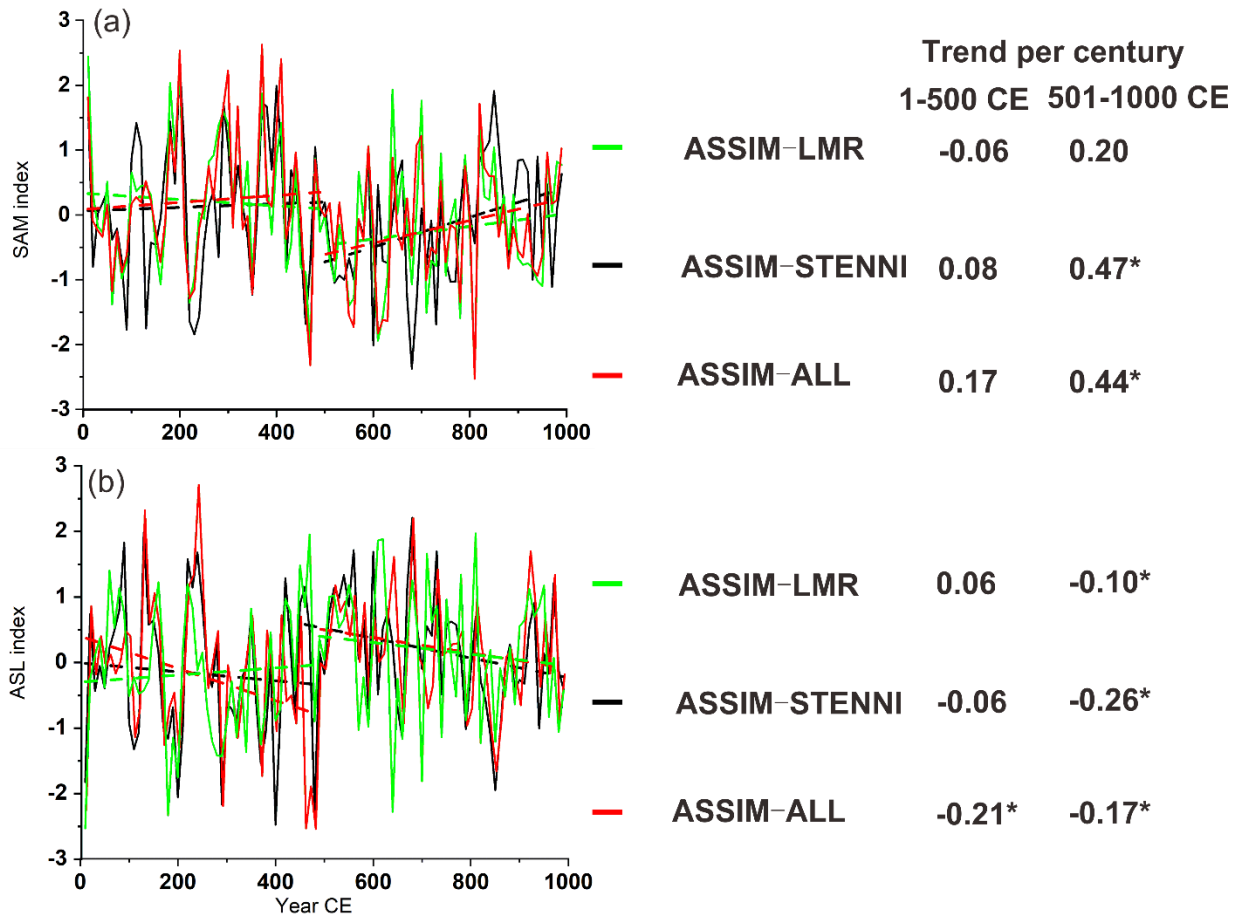

Figure B.3: *The SAM-index (a) and ASL-index (b) time series over the first millennia in three experiments. Statistically significant trends (p value < 0.1) are marked by one asterisk.*

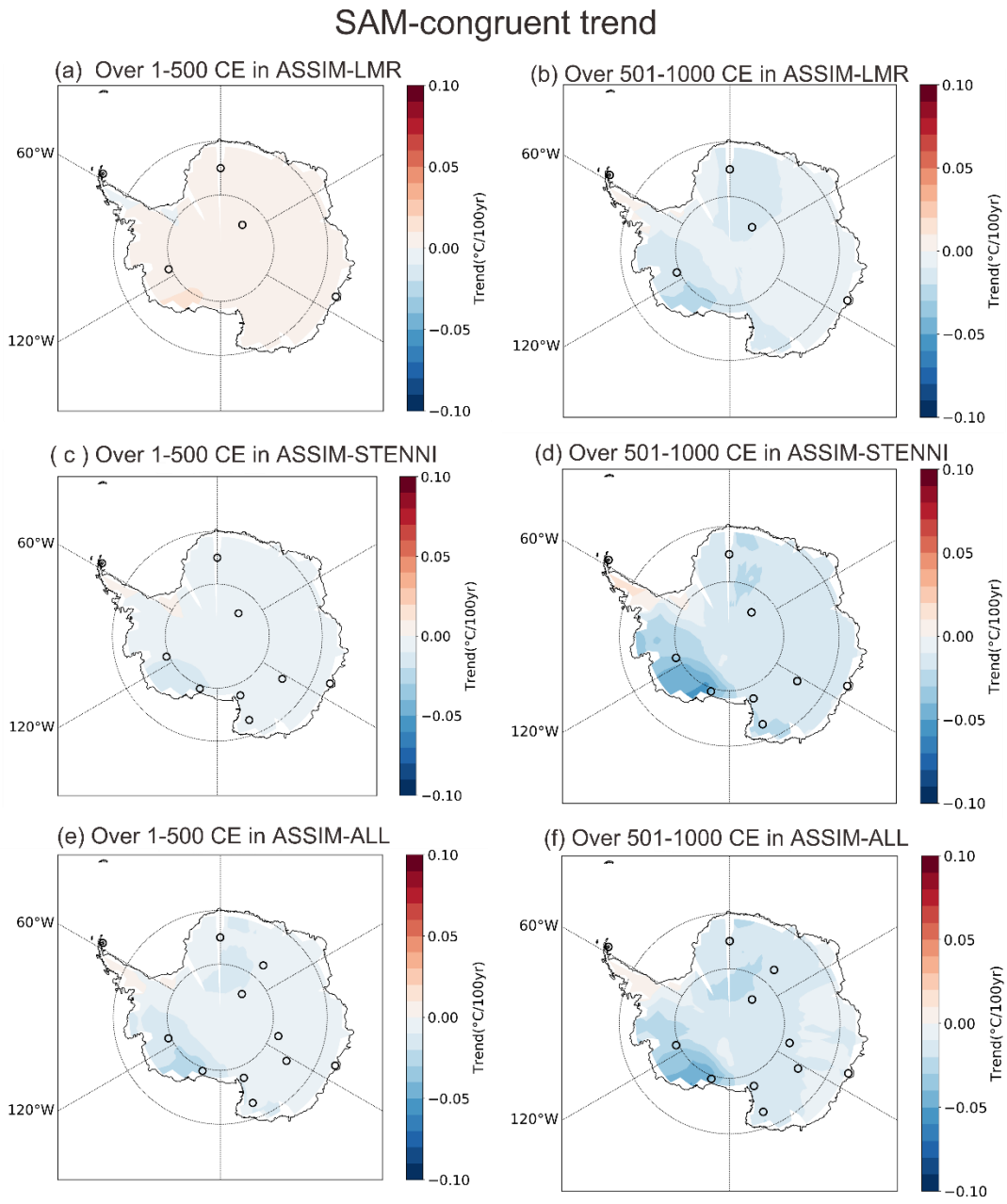

Figure B.4: *The SAM-congruent trend of SAT (°C/100yr) over 1-500 CE and 501-1000 CE in ASSIM-LMR (a, b), ASSIM-STENNI (c, d), ASSIM-ALL (e, f).*

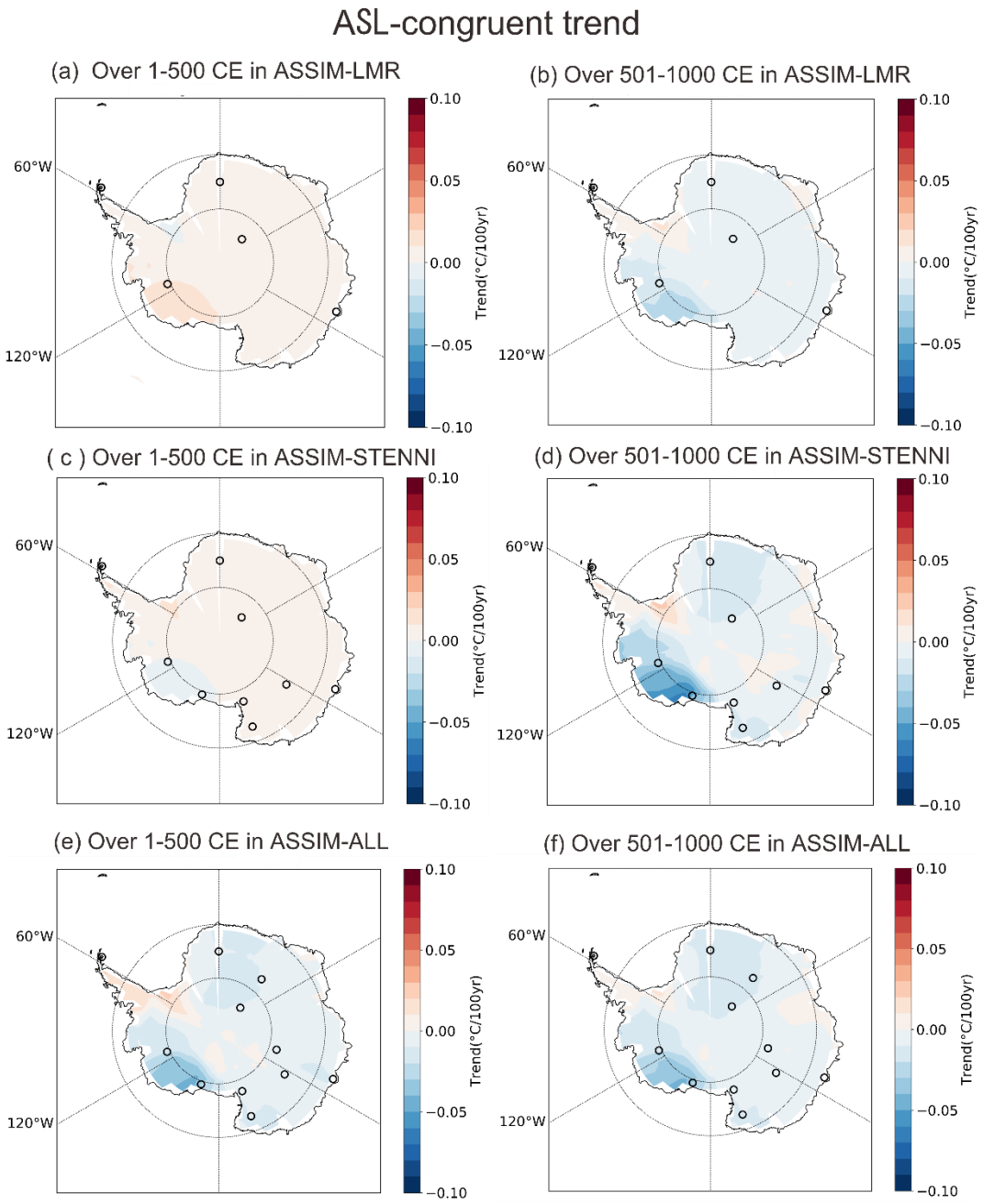

Figure B.5: *The ASL-congruent trend of SAT (°C/100yr) over 1-500 CE and 501-1000 CE in ASSIM-LMR (a, b), ASSIM-STENNI (c, d), ASSIM-ALL (e, f).*

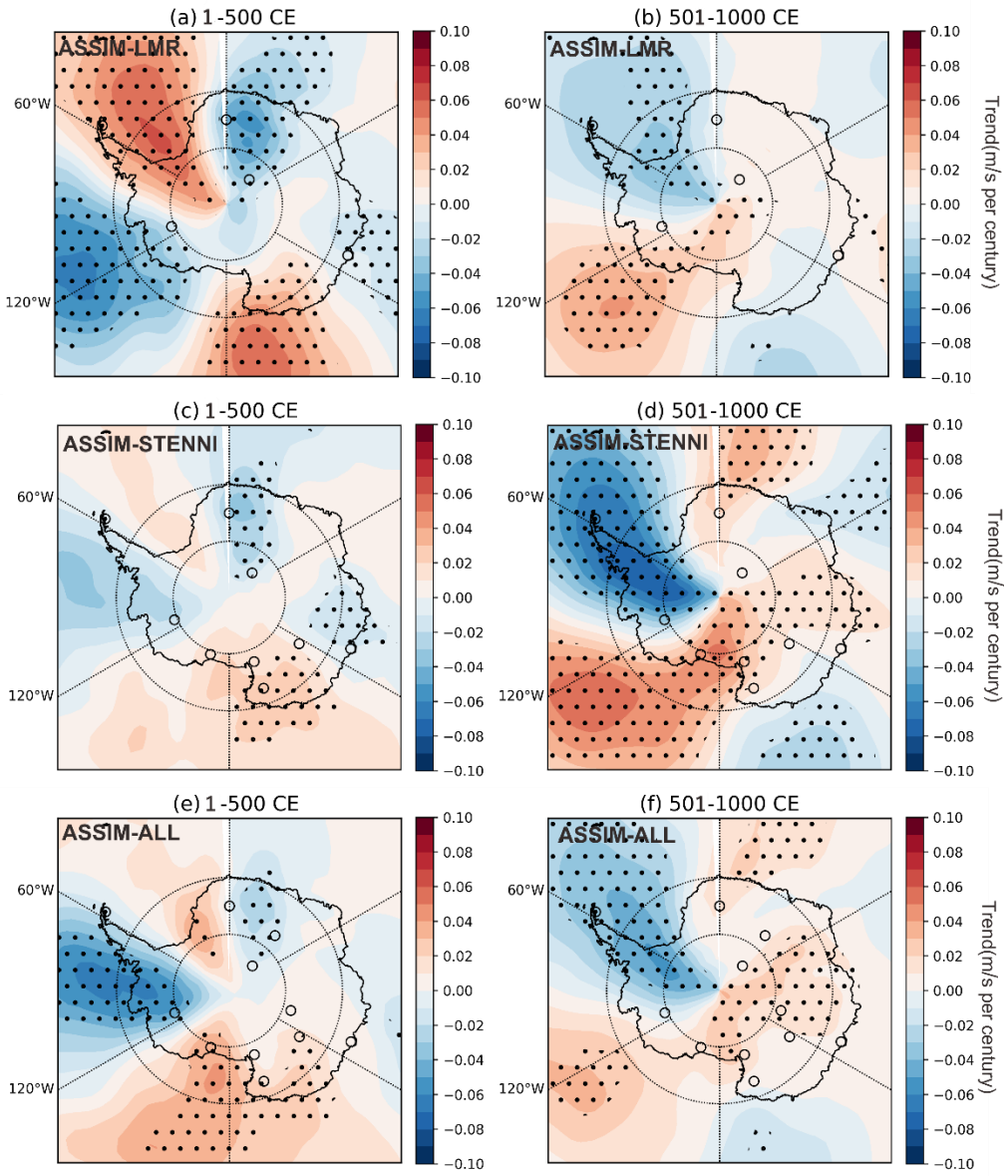

Figure B.6: *Spatial patterns of meridional wind trend (m/s per century) over 1-500 and 501-1000 CE reconstructed in ASSIM-LMR (a, b), ASSIM-STENNI (c, d), ASSIM-ALL (e, f). The position of the data assimilated in each experiment is marked by circles. The dotted area represents regions where the trend is significant at the p<0.1 level.*

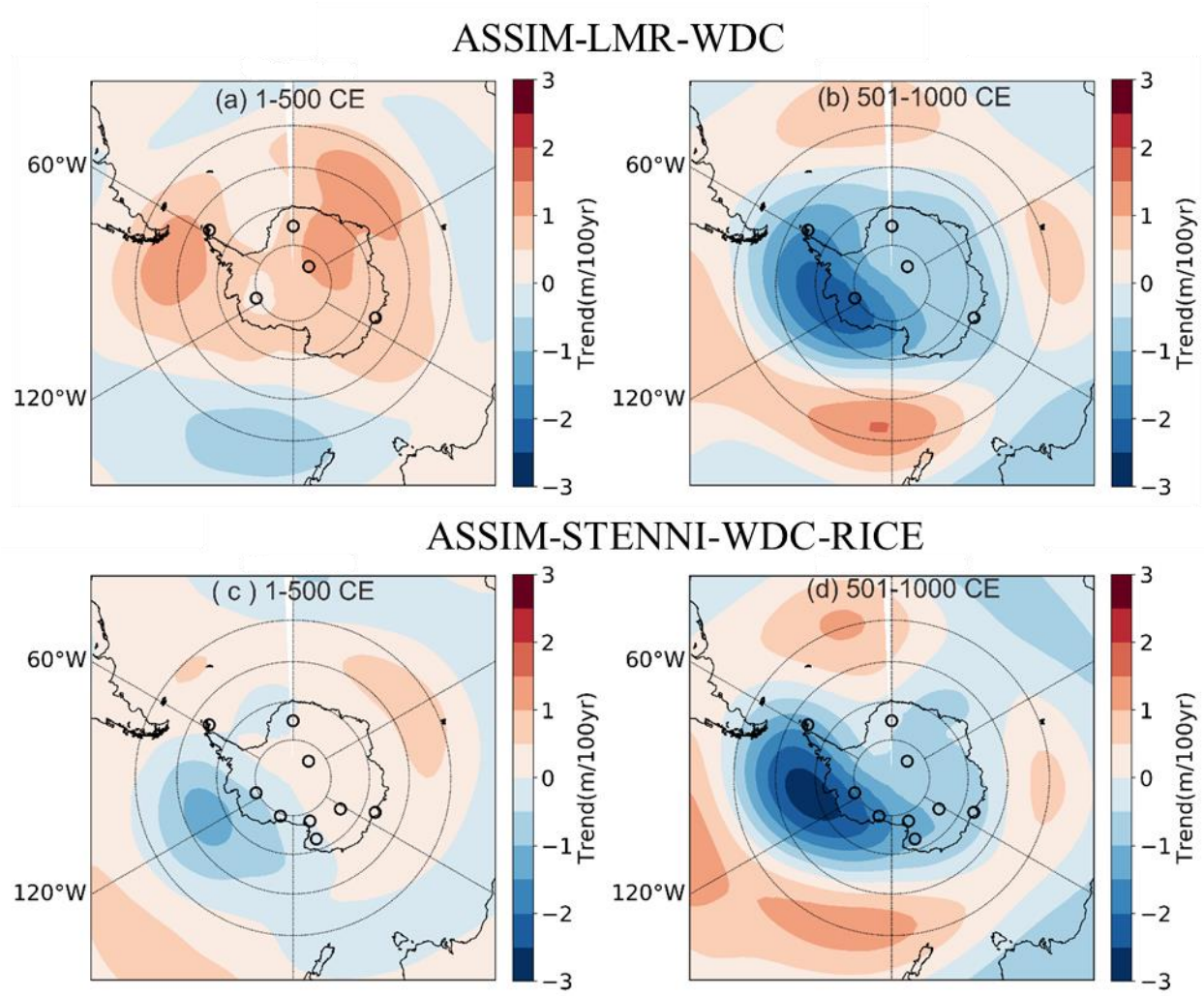

Figure B.7: *Spatial patterns of 500 hpa geopotential height trend (m/century) over 1-500 and 501-1000 CE reconstructed in ASSIM-LMR-WDC (a, b), and ASSIM-STENNI-WDC-RICE (c, d). The position of the data assimilated in each experiment is marked by circles.*

C

Supplementary to Chapter 4

C.1 Supplementary Figures

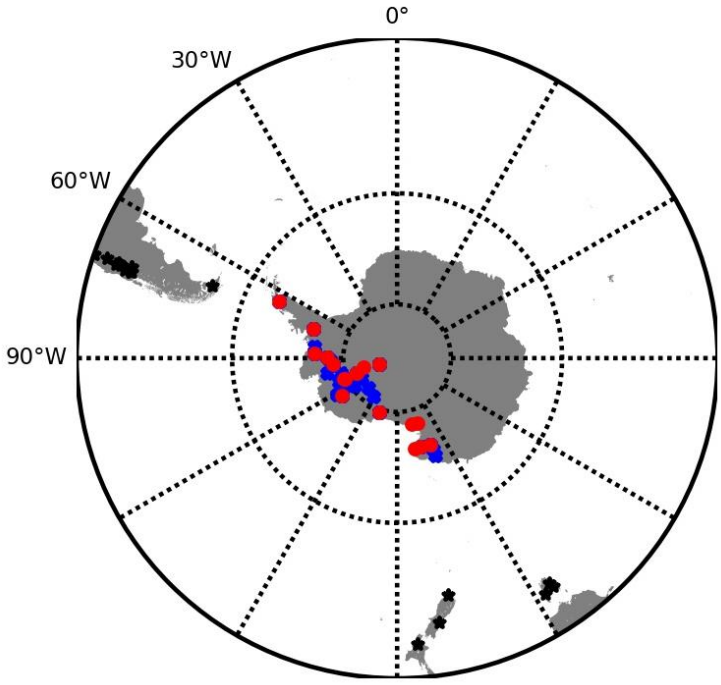

Figure C.1: *The distribution of proxy records used in ASSIM-P200-1yr and ASSIM-P200-10yr. The red circles, blue circles, and black star represents the locations of precipitation-weighted $\delta^{18}O$ records, snow accumulation records and tree-ring width records, respectively.*

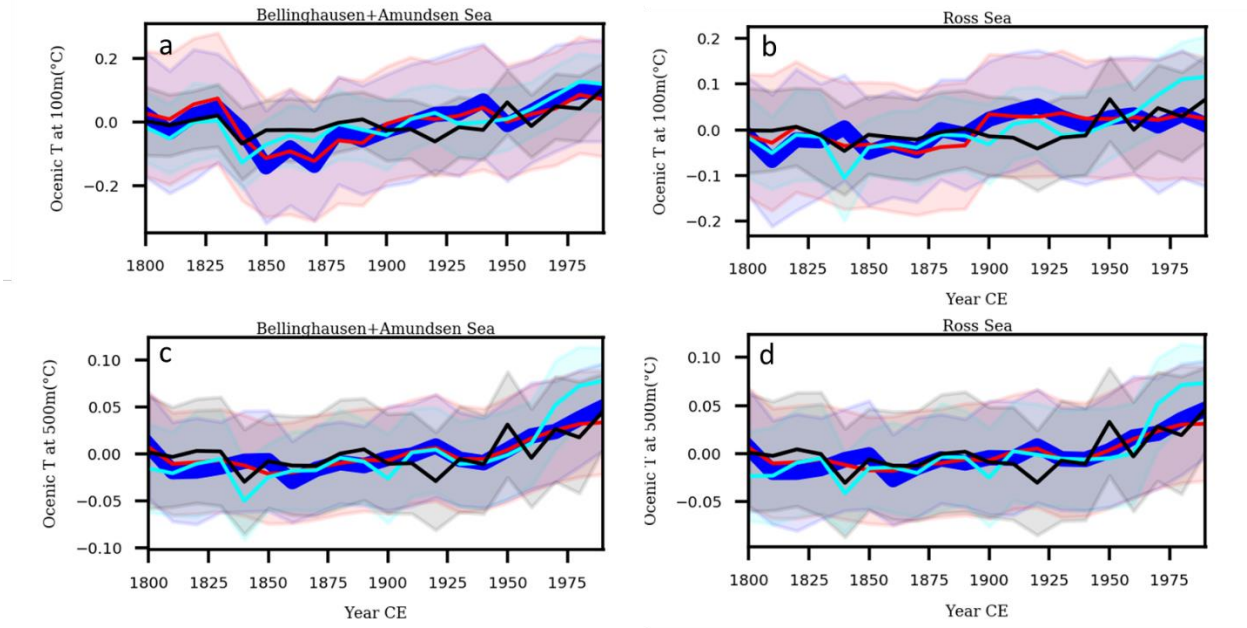

Figure C.2: *Comparisons of the oceanic temperature at 100 m (a, b) and 500 m (c, d) over the past two centuries, between various reconstructions from this study, i.e., ASSIM-P200-1yr (red), ASSIM-P200-10yr (cyan), ASSIM-P2000-ALL (black), and from Dalaiden et al. (2021, blue). All quantities are expressed in anomalies (relative to the 1800–2000 CE period). Shaded areas represent ±1 standard deviation of the DA-based reconstructions.*

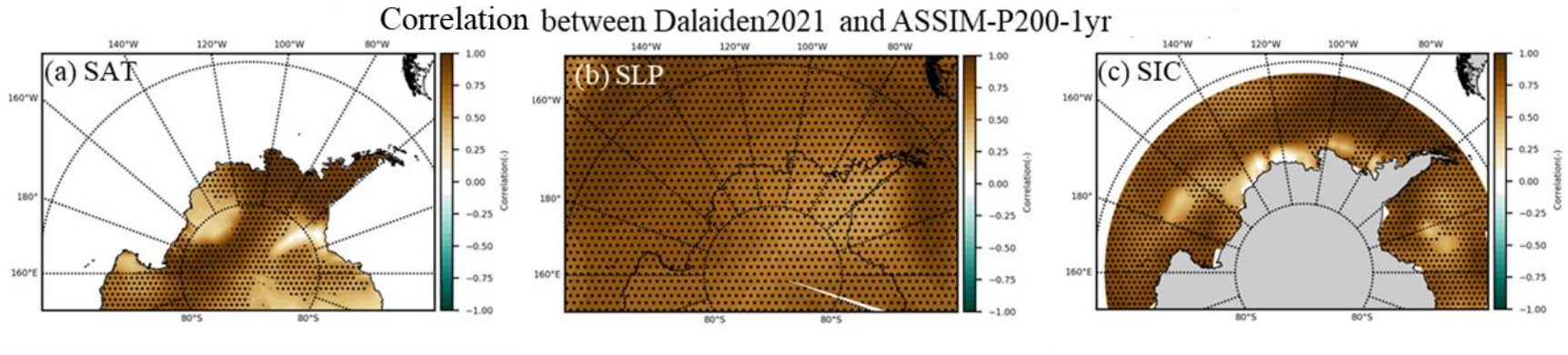

Figure C.3: *Spatial patters of the correlation coefficients for the surface air temperature (SAT), sea level pressure (SLP), and sea ice concentration (SIC) between Dalaiden et al., (2021) and ASSIM-P200-1yr. The area with stippling indicates the correlation coefficients at 95 % confidence level ($p < 0.05$).*

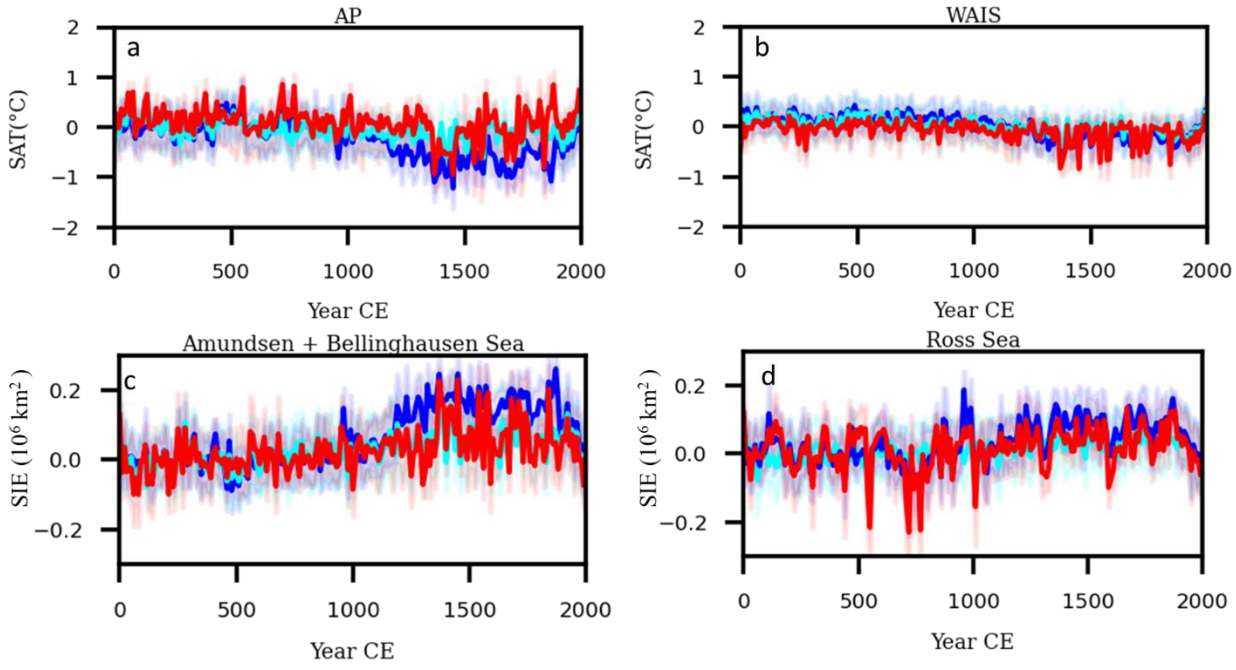

Figure C.4: *Surface air temperature (SAT) anomalies (in °C, relative to 1-2000 CE) over the Antarctic Peninsula (AP, a) and the West Antarctic Ice Sheet (WAIS, b), and sea ice extent (SIE) anomalies (in 10^6 km^2, relative to 1-2000 CE) integrated over the Amundsen/Bellingshausen Sea sector (c) and the Ross Sea sector (d) derived from the ASSIM-P2000-ALL (blue), ASSIM-P2000-CON (cyan), and the sensitivity experiment in which we consider that SST reconstructions represent summer temperature. The shaded areas represent ±1 standard deviation of the DA-based reconstructions.*

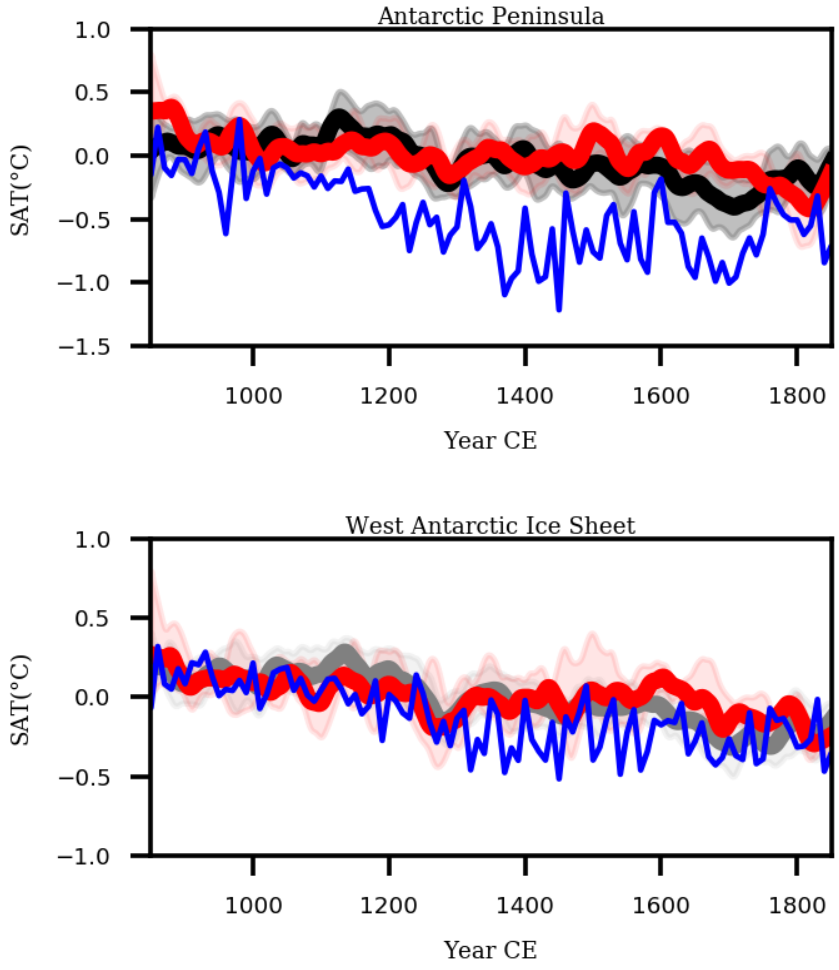

Figure C.5: *Surface air temperature in the simulations using CESM-LMR driven by all forcing (gray) and only volcanic forcing (red). The blue time series represent the reconstruction in ASSIM-P2000-ALL. The colored shading represents the mean ±1 standard deviation of the simulated ensemble. The reference period for the anomaly is 850–1850 CE.*

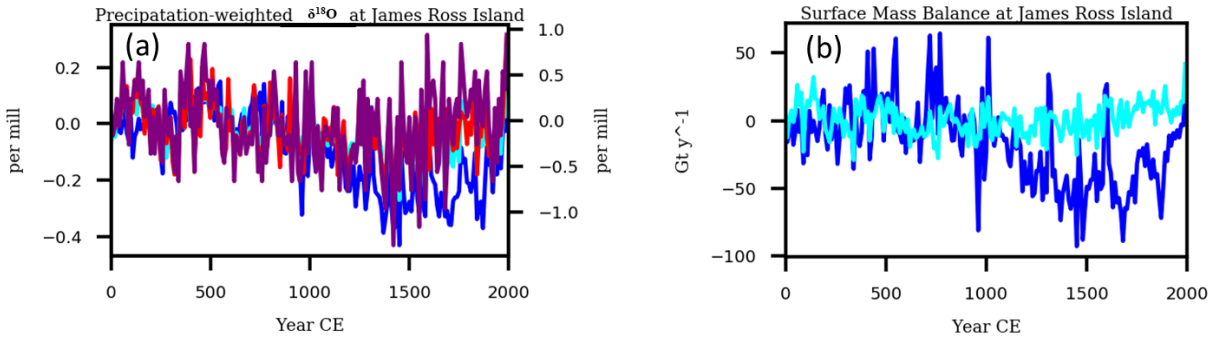

Figure C.6: *$\delta^{18}O$ (a) and surface mass balance at the James Ross Island in the original record (purple), ASSIM-P2000-CON (cyan), ASSIM-P2000-ALL (blue), and in the experiment using the same records as ASSIM-P2000-CON but using an assimilation step of one year (red). In figure a, the right axis corresponds to the original records, making the plot more readable.*

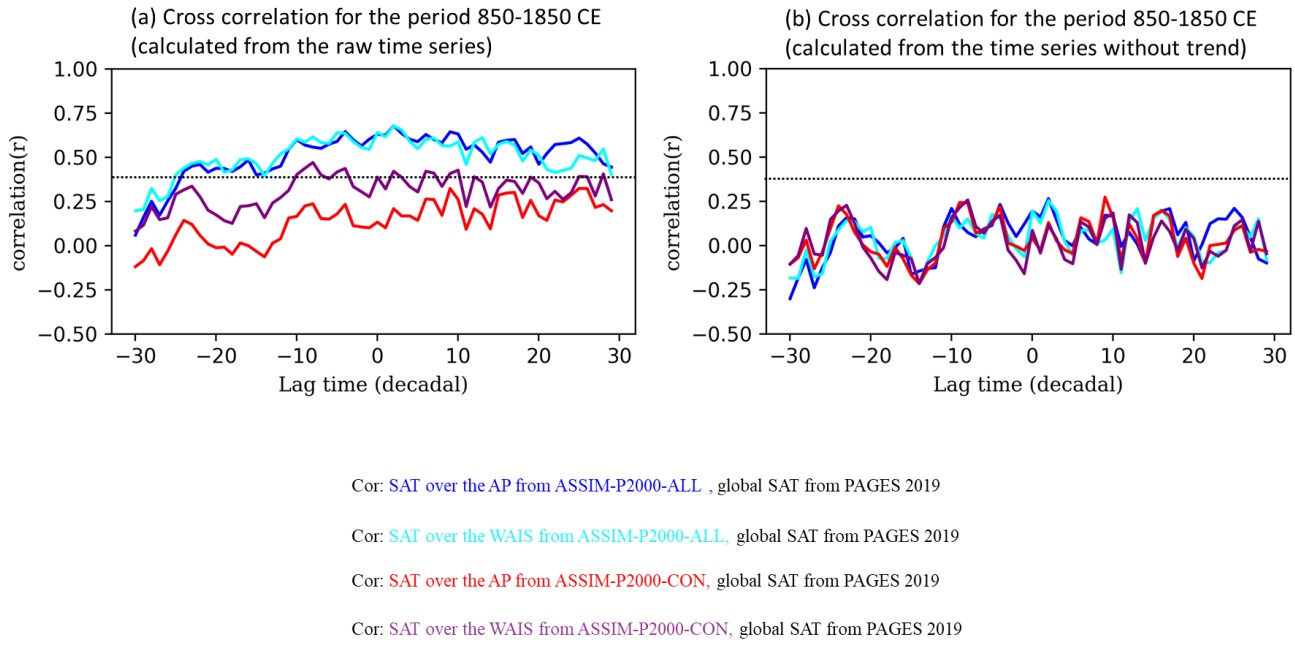

Figure C.7: *Cross-correlation between the global SAT reconstructed from Neukom et al. [2019] and the ASSIM-P2000-ALL and ASSIM-P2000-CON reconstructions, based on the raw time series (a) and the detrended time series (b). The dash line illustrates the significance of correlation at the 5% level (i.e., the significant correlations at $p < 0.05$ are beyond this dash line).*

D

Particle-filter based data assimilation in paleoclimatology

The particle-filter based data assimilation method used in the thesis is based on Bayes' theorem:

$$p(x^p|y) = \frac{p(y|x^p)p(x^p)}{p(y)} \qquad D(1)$$

Where x^p is the model state and includes all the variables of interest averaged over the assimilation period (for instance 1 or 10 years, as in the thesis). y is the available observations used to update the prior in a given time step. $p(x^p)$ is the probability density function (pdf) of all the variables of interest, also referred to as the prior. $p(y|x^p)$ is the conditional probability of the observations given the model state (or likelihood). $p(x^p|y)$ is the posterior pdf that is the probability of observing x^p given the available observations y and model constraint.

In this framework, we often assume the likelihood to be Gaussian:

$$p(y|x^p) = k^{-1} \exp\left[-\frac{1}{2}\left(y - H(x^p)\right)^T R^{-1}\left(y - H(x^p)\right)\right] \qquad D(2)$$

where k is a normalization constant; H is the observation operator which projects the model states into the observation phase space by, for instance, a proxy system model [i.e., Evans et al., 2013]. R is the error covariance of the observations. T represents the symbol for matrix transpose.

In particle filtering, a probabilistic approach is used to define the state of the climate system [Van Leeuwen, 2009]. The model prior pdf is represented in a discrete way as a set of independent model states, i.e., the particles, derived from an ensemble of model simulations. The prior pdf is defined as follows:

$$p(x^p) = \frac{1}{N}\sum_{i=1}^{N}\delta(x^p - x_i^p) \qquad D(3)$$

where N and δ correspond to the number of particles and to a kernel density, respectively.

Then the posterior pdf can be obtained by combining Eqs. D(1) and D(3):

$$p(x^p|y) = \frac{1}{N}\sum_{i=1}^{N} w_i\delta(x^p - x_i^p) \qquad D\ (4)$$

Where

$$w_i = \frac{p(y|x^p)}{\sum_{j=1}^{N} p(y|x^p)} \qquad D(5)$$

where w_i is commonly called the weight of the particle i.

Finally, for each time step of the assimilation, the posterior, i.e., the weighted mean of the sampled particles, is considered as the most likely estimate of the state of the system for that time step:

$$\overline{p(x_p)|y} = \sum_{i=1}^{N} w_i x_i^p \qquad D(6)$$

The weighted standard deviation of the sampled particles gives an estimate of the uncertainty of the reconstruction.

References

Abram, N. J., McGregor, H. V., Tierney, J. E., Evans, M. N., McKay, N. P., & Kaufman, D. S. (2016). Early onset of industrial era warming across the oceans and continents. Nature, 536(7617), 411-418.

Abram, N. J., Wolff, E. W., & Curran, M. A. (2013). A review of sea ice proxy information from polar ice cores. Quaternary Science Reviews, 79, 168-183.

Allen, C. S., & Weich, Z. C. (2022). Variety and distribution of diatom-based sea ice proxies in Antarctic marine sediments of the Past 2000 Years. Geosciences, 12(8), 282.

Alley, R. B., & Koci, B. R. (1990). Recent warming in central Greenland? Annals of Glaciology, 14, 6-8.

An, C., Hou, S., Jiang, S., Li, Y., Ma, T., Curran, M. A., ... & Sun, B. The long term cooling trend in East Antarctic Plateau over the past 2000 years is only robust between 550 and 1550 CE. Geophysical Research Letters, 2021GL092923.

Anchukaitis, K. J., Wilson, R., Briffa, K. R., Büntgen, U., Cook, E. R., D'Arrigo, R., ... & Zorita, E. (2017). Last millennium Northern Hemisphere summer temperatures from tree rings: Part II, spatially resolved reconstructions. Quaternary Science Reviews, 163, 1-22.

Atwood, A. R., Wu, E., Frierson, D. M. W., Battisti, D. S., & Sachs, J. P. (2016). Quantifying climate forcings and feedbacks over the last millennium in the CMIP5-PMIP3 models. Journal of Climate, 29(3), 1161-1178.

Banta, J. R., McConnell, J. R., Frey, M. M., Bales, R. C., & Taylor, K. (2008). Spatial and temporal variability in snow accumulation at the West Antarctic Ice Sheet Divide over recent centuries. Journal of Geophysical Research: Atmospheres, 113(D23).

Barbara, L., Crosta, X., Schmidt, S., & Massé, G. (2013). Diatoms and biomarkers evidence for major changes in sea ice conditions prior the instrumental period in Antarctic Peninsula. Quaternary Science Reviews, 79, 99-110.

Bárcena, M. A., Gersonde, R., Ledesma, S., Fabrés, J., Calafat, A. M., Canals, M., ... & Flores, J. A. (1998). Record of Holocene glacial oscillations in Bransfield Basin as revealed by siliceous microfossil assemblages. Antarctic Science, 10(3), 269-285.

Bárcena, M. Á., Isla, E., Plaza, A., Flores, J. A., Sierro, F. J., Masqué, P., ... & Palanques, A. (2002). Bioaccumulation record and paleoclimatic significance in the Western Bransfield Strait. The last 2000 years. Deep Sea Research Part II: Topicael

Barrett, B. E., Nicholls, K. W., Murray, T., Smith, A. M., & Vaughan, D. G. (2009). Rapid recent warming on Rutford Ice Stream, West Antarctica, from borehole thermometry. Geophysical Research Letters, 36(2).

Beltrami, H., Ferguson, G., & Harris, R. N. (2005). Long-term tracking of climate change by underground temperatures. Geophysical Research Letters, 32(19).

Beltrami, H., González-Rouco, J. F., & Stevens, M. B. (2006). Subsurface temperatures during the last millennium: Model and observation. Geophysical research letters, 33(9).

Bertler, N. A., Conway, H., Dahl-Jensen, D., Emanuelsson, D. B., Winstrup, M., Vallelonga, P. T., ... & Zhang, X. (2018). The Ross Sea Dipole-temperature, snow accumulation and sea ice variability in the Ross Sea region, Antarctica, over the past 2700 years. Climate of the Past, 14(2), 193-214.

Bodri, Louise, and Vladimir Cermak. Borehole climatology: a new method how to reconstruct climate. Elsevier, 2011.

Bova, S., Rosenthal, Y., Liu, Z., Godad, S. P., & Yan, M. (2021). Seasonal origin of the thermal maxima at the Holocene and the last interglacial. Nature, 589(7843), 548-553.

Bracegirdle, T. J., Holmes, C. R., Hosking, J. S., Marshall, G. J., Osman, M., Patterson, M., & Rackow, T. (2020). Improvements in circumpolar Southern Hemisphere extratropical atmospheric circulation in CMIP6 compared to CMIP5. Earth and Space Science, 7(6), e2019EA001065.

Braconnot, P., Harrison, S. P., Kageyama, M., Bartlein, P. J., Masson-Delmotte, V., Abe-Ouchi, A., ... & Zhao, Y. (2012). Evaluation of climate models using paleoclimatic data. Nature Climate Change, 2(6), 417-424.

Braconnot, P., Zhu, D., Marti, O., & Servonnat, J. (2019). Strengths and challenges for transient Mid-to Late Holocene simulations with dynamical vegetation. Climate of the Past, 15(3), 997-1024.

Bradley, R. S., Hughes, M. K., & Diaz, H. F. (2003). Climate in medieval time. Science, 302(5644), 404-405.

Bradley, R. S., Wanner, H., & Diaz, H. F. (2016). The medieval quiet period. The Holocene, 26(6), 990-993.

Brady, E., Stevenson, S., Bailey, D., Liu, Z., Noone, D., Nusbaumer, J., ... & Zhu, J. (2019). The connected isotopic water cycle in the Community Earth System Model version 1. Journal of Advances in Modeling Earth Systems, 11(8), 2547-2566.

Bromwich, D. H., & Fogt, R. L. (2004). Strong trends in the skill of the ERA-40 and NCEP-NCAR reanalysis in the high and midlatitudes of the Southern Hemisphere, 1958-2001. Journal of Climate, 17(23), 4603-4619.

Bromwich, D. H., Nicolas, J. P., Monaghan, A. J., Lazzara, M. A., Keller, L. M., Weidner, G. A., & Wilson, A. B. (2013). Central West Antarctica among the most rapidly warming regions on Earth. Nature Geoscience, 6(2), 139-145.

Caniupán, M., Lamy, F., Lange, C. B., Kaiser, J., Kilian, R., Arz, H. W., ... & Tiedemann, R. (2014). Holocene sea-surface temperature variability in the Chilean fjord region. Quaternary Research, 82(2), 342-353.

Casado, M., Münch, T., & Laepple, T. (2020). Climatic information archived in ice cores: impact of intermittency and diffusion on the recorded isotopic signal in Antarctica. Climate of the Past, 16(4), 1581-1598.

Cavitte, M. G., Dalaiden, Q., Goosse, H., Lenaerts, J., & Thomas, E. R. (2020). Reconciling the surface temperature-surface mass balance relationship in models and ice cores in Antarctica over the last 2 centuries. The Cryosphere, 14(11), 4083-4102.

Chapman, W. L., & Walsh, J. E. (2007). A synthesis of Antarctic temperatures. Journal of Climate, 20(16), 4096-4117.

Charman, D. J., Amesbury, M. J., Roland, T. P., Royles, J., Hodgson, D. A., Convey, P., & Griffiths, H. (2018). Spatially coherent late Holocene Antarctic Peninsula surface air temperature variability. Geology, 46(12), 1071-1074.

Chemke, R., & Polvani, L. M. (2020). Using multiple large ensembles to elucidate the discrepancy between the 1979-2019 modeled and observed Antarctic sea ice trends. Geophysical Research Letters, 47(15), e2020GL088339.

Clem, K. R., & Fogt, R. L. (2015). South Pacific circulation changes and their connection to the tropics and regional Antarctic warming in austral spring, 1979-2012. Journal of Geophysical Research: Atmospheres, 120(7), 2773-2792.

Clem, K. R., Fogt, R. L., Turner, J., Lintner, B. R., Marshall, G. J., Miller, J. R., & Renwick, J. A. (2020). Record warming at the South Pole during the past three decades. Nature Climate Change, 10(8), 762-770.

Clow, G. D. (1992). The extent of temporal smearing in surface-temperature histories derived from borehole temperature measurements. Global and Planetary Change, 6(2-4), 81-86.

Collins, J. A., Lamy, F., Kaiser, J., Ruggieri, N., Henkel, S., De Pol-Holz, R., ... & Arz, H. W. (2019). Centennial-scale SE Pacific sea surface temperature variability over the past 2,300 years. Paleoceanography and Paleoclimatology, 34(3), 336-352.

Crosta, X., Etourneau, J., Orme, L. C., Dalaiden, Q., Campagne, P., Swingedouw, D., ... & Ikehara, M. (2021). Multi-decadal trends in Antarctic sea-ice extent driven by ENSO-SAM over the last 2,000 years. Nature Geoscience, 14(3), 156-160.

Crosta, X., Romero, O., Armand, L. K., & Pichon, J. J. (2005). The biogeography of major diatom taxa in Southern Ocean sediments: 2. Open ocean related species. Palaeogeography, Palaeoclimatology, Palaeoecology, 223(1-2), 66-92.

Crowley, T. J., & Unterman, M. B. (2013). Technical details concerning development of a 1200 yr proxy index for global volcanism. Earth System Science Data, 5(1), 187-197.

Cuffey, K. M. (2007), Ice core methods: Borehole temperature records, in Encyclopedia of Quaternary Science, edited by S. A. Elias, pp. 1167- 1173, Elsevier, Amsterdam, doi:10.1016/B0-44-452747-/00332-X.

Cuffey, K. M., & Paterson, W. S. B. (2010). The physics of glaciers. Academic Press.

Dahl-Jensen, D., Morgan, V. I., & Elcheikh, A. (1999). Monte Carlo inverse modelling of the Law Dome (Antarctica) temperature profile. Annals of Glaciology, 29, 145-150.

Dahl-Jensen, D., Mosegaard, K., Gundestrup, N., Clow, G. D., Johnsen, S. J., Hansen, A. W., & Balling, N. (1998). Past temperatures directly from the Greenland ice sheet. Science, 282(5387), 268-271.

Dalaiden, Q., Goosse, H., Klein, F., Lenaerts, J., Holloway, M., Sime, L., & Thomas, E. R. (2020). How useful is snow accumulation in reconstructing surface air temperature in Antarctica? A study combining ice core records and climate models. The Cryosphere, 14(4), 1187-1207.

Dalaiden, Q., Goosse, H., Lenaerts, J., Cavitte, M. G., & Henderson, N. (2020). Future Antarctic snow accumulation trend is dominated by atmospheric synoptic-scale events. Communications Earth & Environment, 1(1), 1-9.

Dalaiden, Q., Goosse, H., Rezsöhazy, J., & Thomas, E. R. (2021). Reconstructing atmospheric circulation and sea-ice extent in the West Antarctic over the past 200 years using data assimilation. Climate Dynamics, 57(11), 3479-3503.

Dee, S. G., Parsons, L. A., Loope, G. R., Overpeck, J. T., Ault, T. R., & Emile-Geay, J. (2017). Improved spectral comparisons of paleoclimate models and observations via proxy system modeling: Implications for multi-decadal variability. Earth and Planetary Science Letters, 476, 34-46.

Dee, S., Emile-Geay, J., Evans, M. N., Allam, A., Steig, E. J., & Thompson, D. M. (2015). PRYSM: An open-source framework for PRoxY System Modeling, with applications to oxygen-isotope systems. Journal of Advances in Modeling Earth Systems, 7(3), 1220-1247.

Ding, Q., Steig, E. J., Battisti, D. S., & Küttel, M. (2011). Winter warming in West Antarctica caused by central tropical Pacific warming. Nature Geoscience, 4(6), 398-403.

Dubinkina, S., Goosse, H., Sallaz-Damaz, Y., Crespin, E., & Crucifix, M. (2011). Testing a particle filter to reconstruct climate changes over the past centuries. International Journal of Bifurcation and Chaos, 21(12), 3611-3618.

Dufresne, J. L., Foujols, M. A., Denvil, S., Caubel, A., Marti, O., Aumont, O., ... & Vuichard, N. (2013). Climate change projections using the IPSL-CM5 Earth System Model: from CMIP3 to CMIP5. Climate Dynamics, 40(9), 2123-2165.

Eayrs, C., Li, X., Raphael, M. N., & Holland, D. M. (2021). Rapid decline in Antarctic sea ice in recent years hints at future change. Nature Geoscience, 14(7), 460-464.

Eayrs, C., Li, X., Raphael, M. N., & Holland, D. M. (2021). Rapid decline in Antarctic sea ice in recent years hints at future change. Nature Geoscience, 14(7), 460-464.

Edwards, F., Lee, H., & Esposito, M. (2019). Risk of being killed by police use of force in the United States by age, race-ethnicity, and sex. Proceedings of the National Academy of Sciences, 116(34), 16793-16798.

Emanuelsson, B. D., Bertler, N. A., Neff, P. D., Renwick, J. A., Markle, B. R., Baisden, W. T., & Keller, E. D. (2018). The role of Amundsen-Bellingshausen Sea anticyclonic circulation in forcing marine air intrusions into West Antarctica. Climate Dynamics, 51(9), 3579-3596.

Enfield, D. B., Mestas-Nuñez, A. M., & Trimble, P. J. (2001). The Atlantic multidecadal oscillation and its relation to rainfall and river flows in the continental US. Geophysical Research Letters, 28(10), 2077-2080.

Esper, J., & Büntgen, U. (2021). The future of paleoclimate. Climate Research, 83, 57-59.

Etourneau, J., Collins, L. G., Willmott, V., Kim, J. H., Barbara, L., Leventer, A., ... & Massé, G. (2013). Holocene climate variations in the western Antarctic Peninsula: evidence for sea ice extent predominantly controlled by changes in insolation and ENSO variability. Climate of the Past, 9(4), 1431-1446.

Etourneau, J., Sgubin, G., Crosta, X., Swingedouw, D., Willmott, V., Barbara, L., ... & Kim, J. H. (2019). Ocean temperature impact on ice shelf extent in the eastern Antarctic Peninsula. Nature Communications, 10(1), 1-8.

Evans, M. N., Tolwinski-Ward, S. E., Thompson, D. M., & Anchukaitis, K. J. (2013). Applications of proxy system modeling in high resolution paleoclimatology. Quaternary Science Reviews, 76, 16-28.

Eyring, V., Bony, S., Meehl, G. A., Senior, C. A., Stevens, B., Stouffer, R. J., & Taylor, K. E. (2016). Overview of the Coupled Model Intercomparison Project Phase 6 (CMIP6) experimental design and organization. Geoscientific Model Development, 9(5), 1937-1958.

Fan, T., Deser, C., & Schneider, D. P. (2014). Recent Antarctic sea ice trends in the context of Southern Ocean surface climate variations since 1950. Geophysical Research Letters, 41(7), 2419-2426.

Ferreira, D., Marshall, J., Bitz, C. M., Solomon, S., & Plumb, A. (2015). Antarctic Ocean and sea ice response to ozone depletion: A two-time-scale problem. Journal of Climate, 28(3), 1206-1226.

Fogt, R. L., Bromwich, D. H., & Hines, K. M. (2011). Understanding the SAM influence on the South Pacific ENSO teleconnection. Climate Dynamics, 36(7-8), 1555-1576.

Fogt, R. L., Wovrosh, A. J., Langen, R. A., & Simmonds, I. (2012). The characteristic variability and connection to the underlying synoptic activity of the Amundsen-Bellingshausen Seas Low. Journal of Geophysical Research: Atmospheres, 117(D7).

Franzke, C. L., Barbosa, S., Blender, R., Fredriksen, H. B., Laepple, T., Lambert, F., ... & Yuan, N. (2020). The structure of climate variability across scales. Reviews of Geophysics, 58(2), e2019RG000657.

Fretwell, P., Pritchard, H. D., Vaughan, D. G., Bamber, J. L., Barrand, N. E., Bell, R., ... & Zirizzotti, A. (2013). Bedmap2: improved ice bed, surface and thickness datasets for Antarctica. The Cryosphere, 7(1), 375-393.

Frieler, K., Clark, P. U., He, F., Buizert, C., Reese, R., Ligtenberg, S. R., ... & Levermann, A. (2015). Consistent evidence of increasing Antarctic accumulation with warming. Nature Climate Change, 5(4), 348-352.

Fudge, T. J., Markle, B. R., Cuffey, K. M., Buizert, C., Taylor, K. C., Steig, E. J., ... & Koutnik, M. (2016). Variable relationship between accumulation and temperature in West Antarctica for the past 31,000 years. Geophysical Research Letters, 43(8), 3795-3803.

Gao, Y., Yang, L., Yang, W., Wang, Y., Xie, Z., & Sun, L. (2019). Dynamics of penguin population size and food availability at Prydz Bay, East Antarctica, during the last millennium: A solar control. Palaeogeography, Palaeoclimatology, Palaeoecology, 516, 220-231.

García-García, A., Cuesta-Valero, F. J., Beltrami, H., & Smerdon, J. E. (2016). Simulation of air and ground temperatures in PMIP3/CMIP5 last millennium simulations: implications for climate reconstructions from borehole temperature profiles. Environmental Research Letters, 11(4), 044022.

Gent, P. R., Danabasoglu, G., Donner, L. J., Holland, M. M., Hunke, E. C., Jayne, S. R., ... & Zhang, M. (2011). The community climate system model version 4. Journal of Climate, 24(19), 4973-4991.

Ghilain, N., Vannitsem, S., Dalaiden, Q., Goosse, H., De Cruz, L., & Wei, W. (2022). Large ensemble of downscaled historical daily snowfall from an earth system model to 5.5 km resolution over Dronning Maud Land, Antarctica. Earth System Science Data, 14(4), 1901-1916.

Gillett, N. P., & Fyfe, J. C. (2013). Annular mode changes in the CMIP5 simulations. Geophysical Research Letters, 40(6), 1189-1193.

Gong, D., & Wang, S. (1999). Definition of Antarctic oscillation index. Geophysical Research Letters, 26(4), 459-462.

González-Rouco, F., Von Storch, H., & Zorita, E. (2003). Deep soil temperature as proxy for surface air-temperature in a coupled model simulation of the last thousand years. Geophysical Research Letters, 30(21).

González-Rouco, J. F., Beltrami, H., Zorita, E., & Von Storch, H. (2006). Simulation and inversion of borehole temperature profiles in surrogate climates: Spatial distribution and surface coupling. Geophysical Research Letters, 33(1).

Goosse, H. (2017). Reconstructed and simulated temperature asymmetry between continents in both hemispheres over the last centuries. Climate Dynamics, 48(5), 1483-1501.

Goosse, H., Braida, M., Crosta, X., Mairesse, A., Masson-Delmotte, V., Mathiot, P., ... & Verleyen, E. (2012). Antarctic temperature changes during the last millennium: evaluation of simulations and reconstructions. Quaternary Science Reviews, 55, 75-90.

Goosse, H., Brovkin, V., Fichefet, T., Haarsma, R., Huybrechts, P., Jongma, J., ... & Weber, S. L. (2010). Description of the Earth system model of intermediate complexity LOVECLIM version 1.2. Geoscientific Model Development, 3(2), 603-633.

Goosse, H., Crespin, E., de Montety, A., Mann, M. E., Renssen, H., & Timmermann, A. (2010). Reconstructing surface temperature changes over the past 600 years using climate model simulations with data assimilation. Journal of Geophysical Research: Atmospheres, 115(D9).

Goosse, H., Crowley, T. J., Zorita, E., Ammann, C. M., Renssen, H., & Driesschaert, E. (2005). Modelling the climate of the last millennium: What causes the differences between simulations? Geophysical Research Letters, 32(6).

Goosse, H., Dalaiden, Q., Cavitte, M. G., & Zhang, L. (2021). Can we reconstruct the formation of large open-ocean polynyas in the Southern Ocean using ice core records? Climate of the Past, 17(1), 111-131.

Goosse, H., Lefebvre, W., de Montety, A., Crespin, E., & Orsi, A. H. (2009). Consistent past half-century trends in the atmosphere, the sea ice and the ocean at high southern latitudes. Climate Dynamics, 33(7), 999-1016.

Haddam, N. A., Siani, G., Michel, E., Kaiser, J., Lamy, F., Duchamp-Alphonse, S., ... & Kissel, C. (2018). Changes in latitudinal sea surface temperature gradients along the Southern Chilean margin since the last glacial., Quaternary Science Reviews, 194, 62-76.

Hakim, G. J., Emile-Geay, J., Steig, E. J., Noone, D., Anderson, D. M., Tardif, R., ... & Perkins, W. A. (2016). The last millennium climate reanalysis project: Framework and first results. Journal of Geophysical Research: Atmospheres, 121(12), 6745-6764.

Harris, R. N., & Gosnold, W. D. (1999). Comparisons of borehole temperature-depth profiles and surface air temperatures in the northern plains of the USA. Geophysical Journal International, 138(2), 541-548.

Hegerl, G. C., Zwiers, F. W., Braconnot, P., Gillett, N. P., Luo, Y., Orsini, J. A. M., ... & Planton, S. (2007). Understanding and attributing climate change.

Herbert, T. D. (2006). Alkenone Paleotemperature. The oceans and marine geochemistry, 6, 391.

Hetzinger, S., Halfar, J., Mecking, J. V., Keenlyside, N. S., Kronz, A., Steneck, R. S., ... & Lebednik, P. A. (2012). Marine proxy evidence linking decadal North Pacific and Atlantic climate. Climate Dynamics, 39(6), 1447-1455.

Hobbs, W. R., Massom, R., Stammerjohn, S., Reid, P., Williams, G., & Meier, W. (2016). A review of recent changes in Southern Ocean sea ice, their drivers and forcings. Global and Planetary Change, 143, 228-250.

Hosking, J. S., Orr, A., Marshall, G. J., Turner, J., & Phillips, T. (2013). The influence of the Amundsen-Bellingshausen Seas low on the climate of West Antarctica and its representation in coupled climate model simulations. Journal of Climate, 26(17), 6633-6648.

Huang, T., Sun, L., Wang, Y., & Kong, D. (2011). Late Holocene Adélie penguin population dynamics at Zolotov Island, Vestfold Hills, Antarctica. Journal of Paleolimnology, 45(2), 273-285.

IPCC, 2021. Climate change 2021: The physical science basis. In: Masson-Delmotte, V. P., Zhai, A., Pirani, S.L., Connors, C., Péan, S., Berger, S.N., et al. (Eds.), Contribution of Working Group I to the Sixth Assessment Report of the Intergovernmental Panel on Climate Change. Cambridge University Press, Cambridge, UK.

Jones, J. M., Gille, S. T., Goosse, H., Abram, N. J., Canziani, P. O., Charman, D. J., ... & Vance, T. R. (2016). Assessing recent trends in high-latitude Southern Hemisphere surface climate. Nature Climate Change, 6(10), 917-926.

Jones, M. E., Bromwich, D. H., Nicolas, J. P., Carrasco, J., Plavcová, E., Zou, X., & Wang, S. H. (2019). Sixty years of widespread warming in the southern middle and high latitudes (1957-2016). Journal of Climate, 32(20), 6875-6898.

Jones, M. E., Bromwich, D. H., Nicolas, J. P., Carrasco, J., Plavcová, E., Zou, X., & Wang, S. H. (2019). Sixty years of widespread warming in the southern middle and high latitudes (1957-2016). Journal of Climate, 32(20), 6875-6898.

Jones, P. D., Briffa, K. R., Osborn, T. J., Lough, J. M., van Ommen, T. D., Vinther, B. M., ... & Xoplaki, E. (2009). High-resolution palaeoclimatology of the last millennium: a review of current status and future prospects. The Holocene, 19(1), 3-49.

Jones, P. D., Osborn, T. J., & Briffa, K. R. (2001). The evolution of climate over the last millennium. Science, 292(5517), 662-667.

Jouzel, J., Masson-Delmotte, V., Cattani, O., Dreyfus, G., Falourd, S., Hoffmann, G., ... & Wolff, E. W. (2007). Orbital and millennial Antarctic climate variability over the past 800,000 years. Science, 317(5839), 793-796.

Jouzel, J., Vimeux, F., Caillon, N., Delaygue, G., Hoffmann, G., Masson-Delmotte, V., & Parrenin, F. (2003). Magnitude of isotope/temperature scaling for interpretation of central Antarctic ice cores. Journal of Geophysical Research: Atmospheres, 108(D12).

Jun, S. Y., Kim, J. H., Choi, J., Kim, S. J., Kim, B. M., & An, S. I. (2020). The internal origin of the west-east asymmetry of Antarctic climate change. Science Advances, 6(24), eaaz1490.

Jungclaus, J. H., Bard, E., Baroni, M., Braconnot, P., Cao, J., Chini, L. P., ... & Zorita, E. (2017). The PMIP4 contribution to CMIP6-Part 3: The last millennium, scientific objective, and experimental design for the PMIP4 past1000 simulations. Geoscientific Model Development, 10(11), 4005-4033.

Kalnay, E. (2003). Atmospheric modeling, data assimilation and predictability. Cambridge university press.

Kaufman, D., McKay, N., Routson, C., Erb, M., Davis, B., Heiri, O., ... & Zhilich, S. (2020). A global database of Holocene paleotemperature records. Scientific data, 7(1), 1-34.

Kim, R. A., Lee, K. E., & Bae, S. W. (2015). Sea surface temperature proxies (alkenones, foraminiferal Mg/Ca, and planktonic foraminiferal assemblage) and their implications in the Okinawa Trough. Progress in Earth and Planetary Science, 2(1), 1-16.

Kirchgaessner, A., King, J. C., & Anderson, P. S. (2021). The impact of Föhn conditions across the Antarctic Peninsula on local meteorology based on AWS measurements. Journal of Geophysical Research: Atmospheres, 126(4), e2020JD033748.

Klein, F., & Goosse, H. (2018). Reconstructing East African rainfall and Indian Ocean sea surface temperatures over the last centuries using data assimilation. Climate Dynamics, 50(11), 3909-3929.

Klein, F., Abram, N. J., Curran, M. A., Goosse, H., Goursaud, S., Masson-Delmotte, V., ... & Werner, M. (2019). Assessing the robustness of Antarctic temperature reconstructions over the past 2 millennia using pseudoproxy and data assimilation experiments. Climate of the Past, 15(2), 661-684.

Klein, F., Goosse, H., Graham, N. E., & Verschuren, D. (2016). Comparison of simulated and reconstructed variations in East African hydroclimate over the last millennium. Climate of the Past, 12(7), 1499-1518.

Kreutz, K. J., Mayewski, P. A., Pittalwala, I. I., Meeker, L. D., Twickler, M. S., & Whitlow, S. I. (2000). Sea level pressure variability in the Amundsen Sea region inferred from a West Antarctic glaciochemical record. Journal of Geophysical Research: Atmospheres, 105(D3), 4047-4059.

Kunz, T., & Laepple, T. (2021). Frequency-dependent estimation of effective spatial degrees of freedom. Journal of Climate, 34(18), 7373-7388.

Lamping, N., Müller, J., Hefter, J., Mollenhauer, G., Haas, C., Shi, X., ... & Hillenbrand, C. D. (2021). Evaluation of lipid biomarkers as proxies for sea ice and ocean temperatures along the Antarctic continental margin. Climate of the Past, 17(5), 2305-2326.

Lamy, F., Rühlemann, C., Hebbeln, D., & Wefer, G. (2002). High-and low-latitude climate control on the position of the southern Peru-Chile Current during the Holocene. Paleoceanography, 17(2), 16-1.

Lee, J., Sperber, K. R., Gleckler, P. J., Taylor, K. E., & Bonfils, C. J. (2021). Benchmarking performance changes in the simulation of extratropical modes of variability across CMIP generations. Journal of Climate, 34(17), 6945-6969.

Lefebvre, W., Goosse, H., Timmermann, R., & Fichefet, T. (2004). Influence of the Southern Annular Mode on the sea ice-ocean system. Journal of Geophysical Research: Oceans, 109(C9).

Li, X., Cai, W., Meehl, G. A., Chen, D., Yuan, X., Raphael, M., ... & Song, C. (2021). Tropical teleconnection impacts on Antarctic climate changes. Nature Reviews Earth & Environment, 2(10), 680-698.

Liu, H., Liu, Z., & Lu, F. (2017). A systematic comparison of particle filter and EnKF in assimilating time-averaged observations. Journal of Geophysical Research: Atmospheres, 122(24), 13-155.

Ljungqvist, F. C., Zhang, Q., Brattström, G., Krusic, P. J., Seim, A., Li, Q., ... & Moberg, A. (2019). Centennial-scale temperature change in last millennium simulations and proxy-based reconstructions. Journal of Climate, 32(9), 2441-2482.

Lüning, S., Gałka, M., & Vahrenholt, F. (2019). The medieval climate anomaly in Antarctica. Palaeogeography, Palaeoclimatology, Palaeoecology, 532, 109251.

Lyu, Z., Goosse, H., Dalaiden, Q., Klein, F., Shi, F., Wagner, S., & Braconnot, P. (2021). Spatial patterns of multi-centennial surface air temperature trends in Antarctica over 1-1000 CE: Insights from ice core records and modeling. Quaternary Science Reviews, 271, 107205.

MacAyeal, D. R., Firestone, J., & Waddington, E. (1991). Paleothermometry by control methods. Journal of Glaciology, 37(127), 326-338.

Manabe, S., & Wetherald, R. T. (1975). The effects of doubling the CO^2 concentration on the climate of a general circulation model. Journal of Atmospheric Sciences, 32(1), 3-15.

Mann, M. E., Steinman, B. A., & Miller, S. K. (2014). On forced temperature changes, internal variability, and the AMO. Geophysical Research Letters, 41(9), 3211-3219.

Mann, M. E., Zhang, Z., Rutherford, S., Bradley, R. S., Hughes, M. K., Shindell, D., ... & Ni, F. (2009). Global signatures and dynamical origins of the Little Ice Age and Medieval Climate Anomaly. science, 326(5957), 1256-1260.

Marshall, G. J. (2003). Trends in the Southern Annular Mode from observations and reanalyses. Journal of Climate, 16(24), 4134-4143.

Marshall, G. J. (2007). Half-century seasonal relationships between the Southern Annular Mode and Antarctic temperatures. International Journal of Climatology: A Journal of the Royal Meteorological Society, 27(3), 373-383.

Marshall, G. J. (2009). On the annual and semi-annual cycles of precipitation across Antarctica. International Journal of Climatology: A Journal of the Royal Meteorological Society, 29(15), 2298-2308.

Marshall, G. J., & Bracegirdle, T. J. (2015). An examination of the relationship between the Southern Annular Mode and Antarctic surface air temperatures in the CMIP5 historical runs. Climate Dynamics, 45, 1513-1535.

Marshall, G. J., & Thompson, D. W. (2016). The signatures of large-scale patterns of atmospheric variability in Antarctic surface temperatures. Journal of Geophysical Research: Atmospheres, 121(7), 3276-3289.

Marshall, G. J., Di Battista, S., Naik, S. S., & Thamban, M. (2011). Analysis of a regional change in the sign of the SAM-temperature relationship in Antarctica. Climate Dynamics, 36(1), 277-287.

Marshall, G. J., Orr, A., & Turner, J. (2013). A predominant reversal in the relationship between the SAM and East Antarctic temperatures during the twenty-first century. Journal of Climate, 26(14), 5196-5204.

Marshall, G. J., Stott, P. A., Turner, J., Connolley, W. M., King, J. C., & Lachlan-Cope, T. A. (2004). Causes of exceptional atmospheric circulation changes in the Southern Hemisphere. Geophysical Research Letters, 31(14).

Masson, V., Vimeux, F., Jouzel, J., Morgan, V., Delmotte, M., Ciais, P., ... & Vaikmae, R. (2000). Holocene climate variability in Antarctica based on 11 ice-core isotopic records. Quaternary Research, 54(3), 348-358.

Masson-Delmotte, V., Hou, S., Ekaykin, A., Jouzel, J., Aristarain, A., Bernardo, R. T., ... & White, J. W. C. (2008). A review of Antarctic surface snow isotopic composition: Observations, atmospheric circulation, and isotopic modeling. Journal of Climate, 21(13), 3359-3387.

Masson-Delmotte, V., Schulz, M., Abe-Ouchi, A., Beer, J., Ganopolski, A., Rouco, J. G., ... & Timmermann, A. (2013). Information from paleoclimate archives. In Climate change 2013: the physical science basis: Contribution of Working Group I to the Fifth Assessment Report of the Intergovernmental Panel on Climate Change (pp. 383-464). Cambridge University Press.

Matsikaris, A., Widmann, M., & Jungclaus, J. (2015). On-line and off-line data assimilation in palaeoclimatology: a case study. Climate of the Past, 11(1), 81-93.

McGregor, H. V., Evans, M. N., Goosse, H., Leduc, G., Martrat, B., Addison, J. A., ... & Ersek, V. (2015). Robust global ocean cooling trend for the pre-industrial Common Era. Nature Geoscience, 8(9), 671-677.

Medley, B., & Thomas, E. R. (2019). Increased snowfall over the Antarctic Ice Sheet mitigated twentieth-century sea-level rise. Nature Climate Change, 9(1), 34-39.

Medley, B., McConnell, J. R., Neumann, T. A., Reijmer, C. H., Chellman, N., Sigl, M., & Kipfstuhl, S. (2018). Temperature and snowfall in western Queen Maud Land increasing faster than climate model projections. Geophysical Research Letters, 45(3), 1472-1480.

Meehl, G. A., Arblaster, J. M., Bitz, C. M., Chung, C. T., & Teng, H. (2016). Antarctic sea-ice expansion between 2000 and 2014 driven by tropical Pacific decadal climate variability. Nature Geoscience, 9(8), 590-595.

Mezgec, K., Stenni, B., Crosta, X., Masson-Delmotte, V., Baroni, C., Braida, M., ... & Frezzotti, M. (2017). Holocene sea ice variability driven by wind and polynya efficiency in the Ross Sea. Nature Communications, 8(1), 1-12.

Mo, K. C., & Higgins, R. W. (1998). The Pacific-South American modes and tropical convection during the Southern Hemisphere winter. Monthly Weather Review, 126(6), 1581-1596.

Mohrmann, M., Heuzé, C., & Swart, S. (2021). Southern Ocean polynyas in CMIP6 models. The Cryosphere, 15(9), 4281-4313.

Morice, C. P., Kennedy, J. J., Rayner, N. A., Winn, J. P., Hogan, E., Killick, R. E., ... & Simpson, I. R. (2021). An updated assessment of near-surface temperature change from 1850: the HadCRUT5 data set. Journal of Geophysical Research: Atmospheres, 126(3), e2019JD032361.

Müller, P. J., Kirst, G., Ruhland, G., Von Storch, I., & Rosell-Melé, A. (1998). Calibration of the alkenone paleotemperature index U37K′ based on core-tops from the eastern South Atlantic and the global ocean (60 N-60 S). Geochimica et Cosmochimica Acta, 62(10), 1757-1772.

Mulvaney, R., Abram, N. J., Hindmarsh, R. C., Arrowsmith, C., Fleet, L., Triest, J., ... & Foord, S. (2012). Recent Antarctic Peninsula warming relative to Holocene climate and ice-shelf history. Nature, 489(7414), 141-144.

Münch, T., & Laepple, T. (2018). What climate signal is contained in decadal- to centennial-scale isotope variations from Antarctic ice cores? Climate of the Past, 14(12), 2053-2070.

Münch, T., Kipfstuhl, S., Freitag, J., Meyer, H., & Laepple, T. (2016). Regional climate signal vs. local noise: a two-dimensional view of water isotopes in Antarctic firn at Kohnen Station, Dronning Maud Land. Climate of the Past, 12(7), 1565-1581.

Muto, A., Scambos, T. A., Steffen, K., Slater, A. G., & Clow, G. D. (2011). Recent surface temperature trends in the interior of East Antarctica from borehole firn temperature measurements and geophysical inverse methods. Geophysical Research Letters, 38(15).

Nagornov, O. V., Konovalov, Y. V., & Tchijov, V. (2006). Temperature reconstruction for Arctic glaciers. Palaeogeography, Palaeoclimatology, Palaeoecology, 236(1-2), 125-134.

Neukom, R., Barboza, L. A., Erb, M. P., Shi, F., Emile-Geay, J., Evans, M. N., ... & von Gunten, L. (2019). Consistent multi-decadal variability in global temperature reconstructions and simulations over the Common Era. Nature Geoscience, 12(8), 643.

Neukom, R., Gergis, J., Karoly, D. J., Wanner, H., Curran, M., Elbert, J., ... & Frank, D. (2014). Inter-hemispheric temperature variability over the past millennium. Nature Climate Change, 4(5), 362-367.

Neukom, R., Steiger, N., Gómez-Navarro, J. J., Wang, J., & Werner, J. P. (2019). No evidence for globally coherent warm and cold periods over the preindustrial Common Era. Nature, 571(7766), 550-554.

Nicolas, J. P., & Bromwich, D. H. (2014). New reconstruction of Antarctic near-surface temperatures: Multidecadal trends and reliability of global reanalyses. Journal of Climate, 27(21), 8070-8093.

O'Connor, G. K., Steig, E. J., & Hakim, G. J. (2021). Strengthening Southern Hemisphere Westerlies and Amundsen Sea Low Deepening Over the 20th Century Revealed by Proxy-Data Assimilation. Geophysical Research Letters, 48(24), e2021GL095999.

Okazaki, A., Miyoshi, T., Yoshimura, K., Greybush, S. J., & Zhang, F. (2021). Revisiting online and offline data assimilation comparison for paleoclimate reconstruction: an idealized OSSE study. Journal of Geophysical Research: Atmospheres, 126(16), e2020JD034214.

Orsi, A. J., Cornuelle, B. D., & Severinghaus, J. P. (2012). Little Ice Age cold interval in West Antarctica: evidence from borehole temperature at the West Antarctic Ice Sheet (WAIS) divide. Geophysical Research Letters, 39(9).

Osborn, T. J., Jones, P. D., Lister, D. H., Morice, C. P., Simpson, I. R., Winn, J. P., ... & Harris, I. C. (2021). Land surface air temperature variations across the globe updated to 2019: The CRUTEM5 data set. Journal of Geophysical Research: Atmospheres, 126(2), e2019JD032352.

Otto-Bliesner, B. L., Brady, E. C., Fasullo, J., Jahn, A., Landrum, L., Stevenson, S., ... & Strand, G. (2016). Climate variability and change since 850 CE: An ensemble approach with the Community Earth System Model. Bulletin of the American Meteorological Society, 97(5), 735-754.

Otto-Bliesner, B. L., Joussaume, S., Braconnot, P., Harrison, S. P., & Abe-Ouchi, A. (2009). Modeling and data syntheses of past climates: paleoclimate modelling intercomparison Project Phase II Workshop; Estes Park, Colorado, 15-19 September 2008.

PAGES 2k Consortium. (2017). A global multiproxy database for temperature reconstructions of the Common Era. Scientific data, 4.

PAGES 2k Consortium. Consistent multidecadal variability in global temperature reconstructions and simulations over the Common Era. Nature Geoscience. 12, 643-649 (2019).

PAGES 2k Consortium. Continental-scale temperature variability during the past two millennia. Nature Geoscience. 6, 339-346 (2013).

PAGES 2k-PMIP3 group, 2015: Continental-scale temperature variability in PMIP3 simulations and regional temperature reconstructions over the past millennium. Climate of the Past, 11, 1673-1699.

Palerme, C., Claud, C., Dufour, A., Genthon, C., Wood, N. B., & L'Ecuyer, T. (2017). Evaluation of Antarctic snowfall in global meteorological reanalyses. Atmospheric Research, 190, 104-112.

Parkinson, C. L. (2019). A 40-y record reveals gradual Antarctic sea ice increases followed by decreases at rates far exceeding the rates seen in the Arctic. Proceedings of the National Academy of Sciences, 116(29), 14414-14423.

Pattyn, F., & Morlighem, M. (2020). The uncertain future of the Antarctic Ice Sheet. Science, 367(6484), 1331-1335.

Perkins, W. A., & Hakim, G. J. (2017). Reconstructing paleoclimate fields using online data assimilation with a linear inverse model. Climate of the Past, 13(5), 421-436.

Phipps, S. J., McGregor, H. V., Gergis, J., Gallant, A. J., Neukom, R., Stevenson, S., ... & Van Ommen, T. D. (2013). Paleoclimate data-model comparison and the role of climate forcings over the past 1500 years. Journal of Climate, 26(18), 6915-6936.

Pithan, F., & Mauritsen, T. (2014). Arctic amplification dominated by temperature feedbacks in contemporary climate models. Nature geoscience, 7(3), 181-184.

Post, E., Alley, R. B., Christensen, T. R., Macias-Fauria, M., Forbes, B. C., Gooseff, M. N., ... & Wang, M. (2019). The polar regions in a 2 °C warmer world. Science advances, 5(12), eaaw9883.

Previdi, M., & Polvani, L. M. (2016). Anthropogenic impact on Antarctic surface mass balance, currently masked by natural variability, to emerge by mid-century. Environmental Research Letters, 11(9), 094001.

Purich, A., England, M. H., Cai, W., Chikamoto, Y., Timmermann, A., Fyfe, J. C., ... & Arblaster, J. M. (2016). Tropical Pacific SST drivers of recent Antarctic sea ice trends. Journal of Climate, 29(24), 8931-8948.

Raphael, M. N., Holland, M. M., Landrum, L., & Hobbs, W. R. (2019). Links between the Amundsen Sea Low and sea ice in the Ross Sea: seasonal and interannual relationships. Climate Dynamics, 52(3), 2333-2349.

Raphael, M. N., Marshall, G. J., Turner, J., Fogt, R. L., Schneider, D., Dixon, D. A., ... & Hobbs, W. R. (2016). The Amundsen Sea Low: variability, change, and impact on Antarctic climate. Bulletin of the American Meteorological Society, 97(1), 111-121.

Rath, V., González Rouco, J. F., & Goosse, H. (2012). Impact of postglacial warming on borehole reconstructions of last millennium temperatures. Climate of the Past, 8(3), 1059-1066.

Renssen, H., Goosse, H., Fichefet, T., Masson-Delmotte, V., & Koç, N. (2005). Holocene climate evolution in the high-latitude Southern Hemisphere simulated by a coupled atmosphere-sea ice-ocean-vegetation model. The Holocene, 15(7), 951-964.

Roach, L. A., Dörr, J., Holmes, C. R., Massonnet, F., Blockley, E. W., Notz, D., ... & Bitz, C. M. (2020). Antarctic sea ice area in CMIP6. Geophysical Research Letters, 47(9), e2019GL086729.

Roberts, J. L., Moy, A. D., Van Ommen, T. D., Curran, M. A. J., Worby, A. P., Goodwin, I. D., & Inoue, M. (2013). Borehole temperatures reveal a changed energy budget at Mill Island, East Antarctica, over recent decades. The Cryosphere, 7(1), 263-273.

Roberts, S. J., Monien, P., Foster, L. C., Loftfield, J., Hocking, E. P., Schnetger, B., ... & Hodgson, D. A. (2017). Past penguin colony responses to explosive volcanism on the Antarctic Peninsula. Nature Communications, 8(1), 1-16.

Rowell, I., Mulvaney, R., Wolff, E., Pryer, H., Tetzner, D., Thomas, L., ... & Martin, C. (2022). 1000 years of climate history from a coastal West Antarctic ie site (No. EGU22-5914). Copernicus Meetings.

Schmidt, G. A., Jungclaus, J. H., Ammann, C. M., Bard, E., Braconnot, P. C. T. J. D. G., Crowley, T. J., ... & Vieira, L. E. A. (2011). Climate forcing reconstructions for use in PMIP simulations of the last millennium (v1. 0). Geoscientific Model Development, 4(1), 33-45.

Schmidt, G. A., Kelley, M., Nazarenko, L., Ruedy, R., Russell, G. L., Aleinov, I., ... & Zhang, J. (2014). Configuration and assessment of the GISS ModelE2 contributions to the CMIP5 archive. Journal of Advances in Modeling Earth Systems, 6(1), 141-184.

Schneider, D. P., Steig, E. J., van Ommen, T. D., Dixon, D. A., Mayewski, P. A., Jones, J. M., & Bitz, C. M. (2006). Antarctic temperatures over the past two centuries from ice cores. Geophysical Research Letters, 33(16).

Schurer, A. P., Tett, S. F., & Hegerl, G. C. (2014). Small influence of solar variability on climate over the past millennium. Nature Geoscience, 7(2), 104-108.

Shi, F., Lu, H., Guo, Z., Yin, Q., Wu, H., Xu, C., ... & Zhao, C. The position of the Current Warm Period in the context of the past 22,000 years of summer climate in China. Geophysical Research Letters, 2020GL091940.

Sigl, M., McConnell, J. R., Layman, L., Maselli, O., McGwire, K., Pasteris, D., ... & Kipfstuhl, S. (2013). A new bipolar ice core record of volcanism from WAIS Divide and NEEM and implications for climate forcing of the last 2000 years. Journal of Geophysical Research: Atmospheres, 118(3), 1151-1169.

Silvestri, G., Berman, A. L., De Vleeschouwer, F., & Wainer, I. (2021). Last millennium climate changes over the Antarctic Peninsula and southern Patagonia in CESM-LME simulations: Differences between Medieval Climate Anomaly and present-day temperatures. Quaternary Science Reviews, 274, 107273.

Sime, L. C., Marshall, G. J., Mulvaney, R., & Thomas, E. R. (2009). Interpreting temperature information from ice cores along the Antarctic Peninsula: ERA40 analysis. Geophysical Research Letters, 36(18).

Simms, A. R., Bentley, M. J., Simkins, L. M., Zurbuchen, J., Reynolds, L. C., DeWitt, R., & Thomas, E. R. (2021). Evidence for a “Little Ice Age” glacial advance within the Antarctic Peninsula-Examples from glacially-overrun raised beaches. Quaternary Science Reviews, 271, 107195.

Simpkins, G. R., Peings, Y., & Magnusdottir, G. (2016). Pacific influences on tropical Atlantic teleconnections to the Southern Hemisphere high latitudes. Journal of Climate, 29(18), 6425-6444.

Smith, K. L., & Polvani, L. M. (2017). Spatial patterns of recent Antarctic surface temperature trends and the importance of natural variability: lessons from multiple reconstructions and the cmip5 models. Climate Dynamics, 48(7), 2653-2670.

Steig, E. J., Ding, Q., White, J. W., Küttel, M., Rupper, S. B., Neumann, T. A., ... & Korotkikh, E. (2013). Recent climate and ice-sheet changes in West Antarctica compared with the past 2,000 years. Nature Geoscience, 6(5), 372-375.

Steig, E. J., Jones, T. R., Schauer, A. J., Kahle, E. C., Morris, V. A., Vaughn, B. H., ... & White, J. W. C. (2021). Continuous-Flow Analysis of $\delta^{17}O$, $\delta^{18}O$, and δD of H_2O on an Ice Core from the South Pole. Frontiers in Earth Science, 9, 72.

Steig, E. J., Morse, D. L., Waddington, E. D., Stuiver, M., Grootes, P. M., Mayewski, P. A., ... & Whitlow, S. I. (2000). Wisconsinan and Holocene climate history from an ice core at Taylor Dome, western Ross Embayment, Antarctica. Geografiska Annaler: Series A, Physical Geography, 82(2-3), 213-235.

Steig, E. J., Schneider, D. P., Rutherford, S. D., Mann, M. E., Comiso, J. C., & Shindell, D. T. (2009). Warming of the Antarctic ice-sheet surface since the 1957 International Geophysical Year. Nature, 457(7228), 459-462.

Steiger, N. J., Hakim, G. J., Steig, E. J., Battisti, D. S., & Roe, G. H. (2014). Assimilation of time-averaged pseudoproxies for climate reconstruction. Journal of Climate, 27(1), 426-441.

Steiger, N. J., Smerdon, J. E., Cook, E. R., & Cook, B. I. (2018). A reconstruction of global hydroclimate and dynamical variables over the Common Era. Scientific Data, 5(1), 1-15.

Steiger, N. J., Steig, E. J., Dee, S. G., Roe, G. H., & Hakim, G. J. (2017). Climate reconstruction using data assimilation of water isotope ratios from ice cores. Journal of Geophysical Research: Atmospheres, 122(3), 1545-1568.

Steiger, N., & Hakim, G. (2016). Multi-timescale data assimilation for atmosphere-ocean state estimates. Climate of the Past, 12(6), 1375-1388.

Steinhilber, F., Abreu, J. A., Beer, J., Brunner, I., Christl, M., Fischer, H., ... & Wilhelms, F. (2012). 9400 years of cosmic radiation and solar activity from ice cores and tree rings. Proceedings of the National Academy of Sciences, 109(16), 5967-5971.

Stelling, J. M., Yu, Z., Loisel, J., & Beilman, D. W. (2018). Peat bank response to late Holocene temperature and hydroclimate change in the western Antarctic Peninsula. Quaternary Science Reviews, 188, 77-89.

Stenni, B., Buiron, D., Frezzotti, M., Albani, S., Barbante, C., Bard, E., ... & Udisti, R. (2011). Expression of the bipolar see-saw in Antarctic climate records during the last deglaciation. Nature Geoscience, 4(1), 46-49.

Stenni, B., Curran, M. A., Abram, N. J., Orsi, A., Goursaud, S., Masson-Delmotte, V., ... & Frezzotti, M. (2017). Antarctic climate variability on regional and continental scales over the last 2000 years. Climate of the Past, 13(11), 1609-1634.

Stevens, B., Giorgetta, M., Esch, M., Mauritsen, T., Crueger, T., Rast, S., ... & Roeckner, E. (2013). Atmospheric component of the MPI-M Earth system model: ECHAM6. Journal of Advances in Modeling Earth Systems, 5(2), 146-172.

Stevens, M. B., González-Rouco, J. F., & Beltrami, H. (2008). North American climate of the last millennium: Underground temperatures and model comparison. Journal of Geophysical Research: Earth Surface, 113(F1).

Stevenson, S., Otto-Bliesner, B. L., Brady, E. C., Nusbaumer, J., Tabor, C., Tomas, R., ... & Liu, Z. (2019). Volcanic eruption signatures in the isotope-enabled last millennium ensemble. Paleoceanography and Paleoclimatology, 34(8), 1534-1552.

Swart, N. C., Fyfe, J. C., Gillett, N., & Marshall, G. J. (2015). Comparing trends in the southern annular mode and surface westerly jet. Journal of Climate, 28(22), 8840-8859.

Tardif, R., Hakim, G. J., & Snyder, C. (2014). Coupled atmosphere-ocean data assimilation experiments with a low-order climate model. Climate dynamics, 43(5), 1631-1643.

Tardif, R., Hakim, G. J., Perkins, W. A., Horlick, K. A., Erb, M. P., Emile-Geay, J., ... & Noone, D. (2019). Last Millennium Reanalysis with an expanded proxy database and seasonal proxy modeling. Climate of the Past, 15(4), 1251-1273.

Tavernier, I., Verleyen, E., Hodgson, D. A., Heirman, K., Roberts, S. J., Imura, S., ... & Vyverman, W. (2014). Absence of a medieval climate anomaly, little ice age and twentieth century warming in Skarvsnes, Lützow Holm Bay, East Antarctica. Antarctic Science, 26(5), 585-598.

Taylor, K. E., Stouffer, R. J., & Meehl, G. A. (2012). An overview of CMIP5 and the experiment design. Bulletin of the American meteorological Society, 93(4), 485-498.

The IMBIE Team. Mass balance of the Greenland Ice Sheet from 1992 to 2018. Nature 579, 233-239 (2020).

Thomas, E. R., Allen, C. S., Etourneau, J., King, A. C., Severi, M., Winton, V. H. L., ... & Peck, V. L. (2019). Antarctic sea ice proxies from marine and ice core archives suitable for reconstructing sea ice over the past 2000 years. Geosciences, 9(12), 506.

Thomas, E. R., Van Wessem, J. M., Roberts, J., Isaksson, E., Schlosser, E., Fudge, T. J., ... & Ekaykin, A. A. (2017). Regional Antarctic snow accumulation over the past 1000 years. Climate of the Past, 13(11), 1491-1513.

Thompson, D. W., & Solomon, S. (2002). Interpretation of recent Southern Hemisphere climate change. Science, 296(5569), 895-899.

Thompson, D. W., & Wallace, J. M. (2000). Annular modes in the extratropical circulation. Part I: Month-to-month variability. Journal of Climate, 13(5), 1000-1016.

Tierney, J. E., & Tingley, M. P. (2018). BAYSPLINE: A new calibration for the alkenone paleothermometer. Paleoceanography and Paleoclimatology, 33(3), 281-301.

Timmermans, M. L., & Marshall, J. (2020). Understanding Arctic Ocean circulation: A review of ocean dynamics in a changing climate. Journal of Geophysical Research: Oceans, 125(4), e2018JC014378.

Toohey, M., & Sigl, M. (2017). Volcanic stratospheric sulfur injections and aerosol optical depth from 500 BCE to 1900 CE. Earth System Science Data, 9(2), 809-831.

Turner, J., Colwell, S. R., Marshall, G. J., Lachlan-Cope, T. A., Carleton, A. M., Jones, P. D., ... & Iagovkina, S. (2005). Antarctic climate change during the last 50 years. International Journal of Climatology, 25(3), 279-294.

Turner, J., Lu, H., White, I., King, J. C., Phillips, T., Hosking, J. S., ... & Deb, P. (2016). Absence of 21st century warming on Antarctic Peninsula consistent with natural variability. Nature, 535(7612), 411-415.

Turner, J., Marshall, G. J., Clem, K., Colwell, S., Phillips, T., & Lu, H. (2020). Antarctic temperature variability and change from station data. International Journal of Climatology, 40(6), 2986-3007.

Turner, J., Orr, A., Gudmundsson, G. H., Jenkins, A., Bingham, R. G., Hillenbrand, C. D., & Bracegirdle, T. J. (2017). Atmosphere-ocean-ice interactions in the Amundsen Sea embayment, West Antarctica. Reviews of Geophysics, 55(1), 235-276.

Turner, J., Phillips, T., Hosking, J. S., Marshall, G. J., and Orr, A. (2013). The Amundsen sea low. International Journal of Climatology, 33(7):1818-1829.

Van Wessem, J. M., Van De Berg, W. J., Noël, B. P., Van Meijgaard, E., Amory, C., Birnbaum, G., ... & Van Den Broeke, M. R. (2018). Modelling the climate and surface mass balance of polar ice sheets using RACMO2-Part 2: Antarctica (1979-2016). The Cryosphere, 12(4), 1479-1498.

Verfaillie, D., Pelletier, C., Goosse, H., Jourdain, N. C., Bull, C., Dalaiden, Q., ... & Wille, J. D. (2022). The circum-Antarctic ice-shelves respond to a more positive Southern Annular Mode with regionally varied melting. Communications Earth & Environment, 3(1), 1-12.

Verleyen, E., Hodgson, D. A., Sabbe, K., & Vyverman, W. (2004). Late Quaternary deglaciation and climate history of the Larsemann Hills (East Antarctica). Journal of Quaternary Science, 19(4), 361-375.

Vieira, L. E. A., Solanki, S. K., Krivova, N. A., & Usoskin, I. (2011). Evolution of the solar irradiance during the Holocene. Astronomy & Astrophysics, 531, A6.

Wadham, J. L., Hawkings, J. R., Tarasov, L., Gregoire, L. J., Spencer, R. G. M., Gutjahr, M., ... & Kohfeld, K. E. (2019). Ice sheets matter for the global carbon cycle. Nature communications, 10(1), 1-17.

Widmann, M., Goosse, H., Schrier, G., Schnur, R., & Barkmeijer, J. (2010). Using data assimilation to study extratropical Northern Hemisphere climate over the last millennium. Climate of the Past, 6(5), 627-644.

Winstrup, M., Vallelonga, P., Kjær, H. A., Fudge, T. J., Lee, J. E., Riis, M. H., ... & Wheatley, S. (2019). A 2700-year annual timescale and accumulation history for an ice core from Roosevelt Island, West Antarctica. Climate of the Past, 15(2), 751-779.

Wu, T., Song, L., Li, W., Wang, Z., Zhang, H., Xin, X., ... & Zhou, M. (2014). An overview of BCC climate system model development and application for climate change studies. Journal of Meteorological Research, 28(1), 34-56.

Yang, J. W., Han, Y., Orsi, A. J., Kim, S. J., Han, H., Ryu, Y., ... & Ahn, J. (2018). Surface temperature in twentieth century at the Styx Glacier, northern Victoria Land, Antarctica, from borehole thermometry. Geophysical Research Letters, 45(18), 9834-9842.

Zagorodnov, V., Nagornov, O., Scambos, T. A., Muto, A., Mosley-Thompson, E., Pettit, E. C., & Tyuflin, S. (2012). Borehole temperatures reveal details of 20th century warming at Bruce Plateau, Antarctic Peninsula. The Cryosphere, 6(3), 675-686.

Zheng, F., Li, J., Clark, R. T., & Nnamchi, H. C. (2013). Simulation and projection of the Southern Hemisphere annular mode in CMIP5 models. Journal of Climate, 26(24), 9860-9879.

Zhong, Y., Jahn, A., Miller, G. H., & Geirsdottir, A. (2018). Asymmetric Cooling of the Atlantic and Pacific Arctic During the Past Two Millennia: A Dual Observation-Modeling Study. Geophysical Research Letters, 45(22), 12-497.

Zunz, V., Goosse, H., & Massonnet, F. (2013). How does internal variability influence the ability of CMIP5 models to reproduce the recent trend in Southern Ocean sea ice extent? The Cryosphere, 7(2), 451-468.

List of publications related to the thesis

Lyu, Z., Orsi, A. J., & Goosse, H. (2020). Comparison of observed borehole temperatures in Antarctica with simulations using a forward model driven by climate model outputs covering the past millennium. Climate of the Past, 16(4), 1411-1428 (Chapter 2)

Lyu, Z., Goosse, H., Dalaiden, Q., Klein, F., Shi, F., Wagner, S., & Braconnot, P. (2021). Spatial patterns of multi–centennial surface air temperature trends in Antarctica over 1–1000 CE: Insights from ice core records and modeling. Quaternary Science Reviews, 271, 107205. (Chapter 3)

Lyu, Z., Goosse, H., Dalaiden, Q., Crosta, X., & Etourneau, J. Widespread cooling over West Antarctica and adjacent seas over the past millennium. In preparation. (Chapter 4)